
Université d'Ottawa · University of Ottawa

# Université d'Ottawa • University of Ottawa

FACULTÉ DE ÉTUDES SUPÉRIEURES ET POSTDOCTORALES

FACULTY OF GRADUATE AND POSTDOCTORAL STUDIES

Maroun BOU KHALIL

AUTEUR DE LA THÈSE - AUTHOR OF THESIS

Ph.D. (Biochemistry)

GRADE - DEGREE

Department of Biochemistry, Microbiology and Immunology

FACULTÉ, ÉCOLE, DÉPARTEMENT - FACULTY, SCHOOL, DEPARTMENT

TITRE DE LA THÈSE - TITLE OF THE THESIS

Biophysical and Biochemical properties of the Mammalian Male Germ Cell Specific Sulfogalactosylglycerolipid (SGG) : Contribution to the Structure and Zona Pellucida Affinity of Pig Sperm Raft Membranes

N. Tanpahichitr

DIRECTEUR DE LA THÈSE - THESIS SUPERVISOR

D. Carrier

CO-DIRECTEUR DE LA THÈSE - THESIS CO-SUPERVISOR

EXAMINATEURS DE LA THÈSE - THESIS EXAMINERS

J. Bailey

H. Kaplan

J. Ngsee

Z. Yao

J.-M. De Koninck, Ph.D.

LE DOYEN DE LA FACULTÉ DES ÉTUDES SUPÉRIEURES ET POSTDOCTORALES

DEAN OF THE FACULTY OF GRADUATE AND POSTDOCTORAL STUDIES

# BIOPHYSICAL AND BIOCHEMICAL PROPERTIES OF THE MAMMALIAN MALE GERM CELL SPECIFIC SULFOGALACTOSYLGLYCEROLIPID (SGG): CONTRIBUTION TO THE STRUCTURE AND ZONA PELLUCIDA AFFINITY OF PIG SPERM RAFT MEMBRANES

by

Maroun Bou Khalil

Thesis submitted to the Faculty of Graduate and Postdoctoral Studies
in partial fulfillment of the requirements for the degree of
**Doctor of Philosophy**

Department of Biochemistry, Microbiology and Immunology
Faculty of Medicine
University of Ottawa

*Your file Votre référence*
*ISBN: 0-494-01674-4*
*Our file Notre référence*
*ISBN: 0-494-01674-4*

*This thesis is dedicated to my parents.*

## ACKNOWLEDGEMENTS

Through my research experience in the Biochemistry field, the scientific abilities acquired were very valuable because I have had direct input from fellow student colleagues and professors, especially from my supervisor Dr. N. Tanphaichitr and my co-supervisor Dr. D. Carrier.

First and foremost, I would like to thank my advisor and my co-advisor for their excellent supervision. Dr. N. Tanphaichitr and Dr. D. Carrier had made use of their extraordinary skills as scientists, professors, proofreaders, and logicians, requiring perfection of me as they co-supervised my ambitious graduate work. Prior to embarking in the Biochemistry research field, I had modest knowledge of infrared spectroscopy and biophysical methods, lipids biochemistry and cell biological techniques. This was rapidly rectified due to my co-supervisor's wealth of knowledge, unlimited patience, and talent of transforming intricate concepts into easily comprehensive ideas. I also have been very blessed to have had the privilege of working with and training in the field of lipid biochemistry under the supervision of world renowned Dr. M. Kates. Words cannot even begin to describe such a feeling and an experience. I will always be grateful to Dr. N. Tanphaichitr and Dr. D. Carrier because their high expectations of me have helped me realize what I am truly capable of. Thank your from the bottom of my heart.

I would also like to thank my thesis advisory committee members (Dr. S. Evans, Dr. H. Jarrell, and Dr. V. Mezl) for their guidance, as well as our collaborators (Dr. P.T.T. Wong, Dr. M. Buhr, Dr. T. Berger, Dr. P. Kumarathasan, Dr. M. Mbikay, and Dr. J. Mayne) for their continued support and contributions to my Ph.D. project. In addition, this work would not have been possible if it was not for the paramount help and moral support I got from past and present members of our laboratory. I will always be grateful to Dr. K. Chakrabandhu, Dr. E. Carmona, Mr. H. Xu, Mr. N. Vuong, Mr. S. Hazra, Ms. S. da Silva, Ms. A. Anupriwan, Ms. D. Dacosta Santos, Dr. W. Weerachatyanukul, Dr. J. Tantibhedhyangkul, Ms. A. Furimsky, and Mr. A. Shoushtarian. I am also very grateful for the help I received from our administrative assistant Ms. T. van Gulik, and for her friendship.

I truly have been blessed, and for that I thank my Lord and Savior Jesus Christ, my mother and father (Eva and Fouad for waiting for me to come back from work no matter how late it was, making sure that I was home safe and sound before they went to sleep), my very precious aunt and spiritual mother Labibé, my brothers (wise and talkative Georges, generous Joseph, hilarious Elie, and Tony), my sisters (thoughtful, lovable and hospitable Marie; sweet Josephine who's always been there to cheer me up, and pick me up no matter how early/late it was; wonderful Moni for her friendship, support, prayers, technical help with computers, and for her own special ways to make me laugh, and sometimes cry of laughter; and kind, hospitable Aida), my nieces (Melissa and Jessica), and last but not least my nephews (Kevin, Jason, Juliano and Danny). Also, I would like to thank all my special friends at St. Charbel Church for their support and prayers (especially, Mr. D. Aboutanos, and my guardian angels Ms. V. Elhage and Msgr. R. Hanna).

## ABSTRACT

Raft membranes are implicated in cell adhesion. Here, we demonstrated that rafts isolated from hypermotile capacitated pig sperm as low-density Triton X-100 insoluble membranes had the ability to bind specifically to homologous zonae pellucidae (ZP). This binding was dependent on pig ZP3α sulfoglycoprotein, a major player in intact sperm binding. The male germ cell specific sulfogalactosylglycerolipid (SGG) was a sperm raft component and participated in sperm raft-ZP binding, since rafts pretreated with anti-SGG IgG/Fab had decreased ability to bind to the ZP dose dependently. SGG may also partake in raft formation. Fourier transform infrared (FTIR) spectroscopic studies of mixed SGG-cholesterol liposomes revealed that the sulfoglycolipid interacted with cholesterol (a significant raft component) via intermolecular hydrogen bonding. Moreover, mixtures of SGG and cholesterol were insoluble in 1-2 % Triton X-100. Since cholesterol is significant for raft formation and since sperm capacitation is associated with cholesterol efflux, we determined whether raft levels in capacitated sperm were the same as those in control sperm. Interestingly, our results revealed an increase in raft levels in the capacitated sperm, as well as an enhanced ZP affinity of these membrane domains, compared to those of control sperm. These results corroborated the implication of rafts in cell adhesion and strongly suggested that the enhanced ZP-binding ability of capacitated sperm may be attributed to increased levels of sperm rafts, with a greater affinity for the ZP.

# CONTENTS

## LIST OF FIGURES

## LIST OF FIGURES

## LIST OF FIGURES

## LIST OF FIGURES

# LIST OF TABLES

## LIST OF ABBREVIATIONS

| | |
|---|---|
| AAG | 1-*O*-alkyl-2-*O*-acyl-*sn*-glycerol |
| AFM | Atomic force microscopy |
| AKAPs | A kinase anchoring proteins |
| AS-A | Arylsulfatase-A |
| BCR | B-cell receptor |
| BSA | Bovine serum albumin |
| BTS | Beltsville thawing solution |
| CABYR | $Ca^{2+}$-binding tyrosine phosphorylation-regulated protein |
| cAMP | Cyclic adenosine monophosphate |
| CGT | Ceramide galactosyltransferase |
| CM | Capacitation medium |
| CST | Cerebroside sulfotransferase |
| DAG | Diacylglycerol |
| DIM | Detergent insoluble membranes |
| DMAs | Dimethylacetals |
| DMPC | 1, 2-dimyristoyl-*sn*-glycerophosphorylcholine |
| DMPE | 1, 2-dimyristoyl-*sn*-glycerophosphorylethanolamine |
| DMSO | Dimethylsulfoxide |
| DOPC | 1, 2-dioleoyl-*sn*-glycerophosphorylcholine |
| DOPE | 1, 2-dioleoyl-*sn*-glycerophosphoethanolamine |
| DPPC | 1, 2-palmitoyl-*sn*-glycerophosphorylcholine |
| DSC | Differential scanning calorimetry |

| | |
|---|---|
| DTGS | Deuterated triglycine sulfate |
| ECL | Enhanced chemiluminescence |
| EDTA | Ethylenediaminetetraacetic acid |
| EGFR | Epidermal growth factor receptor |
| ELISA | Enzyme-linked immunosorbent assay |
| Endo H | Endo-*β*-*N*-acetylglucosaminidase H |
| F-actin | Filamentous actin |
| FAMEs | Fatty acid methyl esters |
| FRAP | Fluorescence recovery after photobleaching |
| FRET | Fluorescence resonance energy transfer |
| FTIR | Fourier transform infrared spectroscopy |
| $GABA_A$ | γ-aminobutyric acid type A |
| Gal | Galactose |
| GalNAc | *N*-acetyl galactosamine |
| GC | *β*-D-galactopyranosyl-1'-1-*N*-tetracosanoylsphingosine or galactosylceramide |
| GC-MS | Gas chromatography-mass spectrometry |
| GG | 1-*O*-alkyl-2-*O*-acyl[*β*-D-galactopyranosyl(1'-3)]-*sn*-glycerol or galactosylglycerolipid |
| GlcNAc | *N*-acetyl glucosamine |
| GPI | Glycosylphosphatidylinositol |
| $G_i$-R | $G_i$ subtype of the GTP binding heterotrimeric protein-receptor |
| HA | Influenza virus hemagglutinin |

| | |
|---|---|
| HFA-GC | GC containing amide linked α-hydroxylated fatty acids |
| HDL | High-density lipoproteins |
| HIV | Human immunodeficiency virus |
| HPLC | High performance liquid chromatography |
| HPTLC | High performance thin layer chromatography |
| HRP | Horseradish peroxidase |
| IIF | Indirect immunofluorescence |
| IgG | Immunoglobulin G |
| $IP_3$ | Inositol 1,4,5-trisphosphate |
| $L_\alpha$ | Liquid-crystalline or hydrocarbon chain melted phase |
| $L_\beta$ | Gel phase |
| $L_o$ | Liquid-ordered phase |
| M$\beta$CD | Methyl-$\beta$-cyclodextrin |
| MDCK | Madin-Darby canine kidney cells |
| MS | Mass spectrometry |
| NCS | *p*-nitrocatechol sulfate |
| NeuAc | *N*-acetyl neuraminic or sialic acid |
| NeuGc | *N*-glycolyl neuraminic acid |
| NFA-GC | GC containing amide linked non-hydroxylated fatty acids |
| NMR | Nuclear magnetic resonance |
| *N*-Rh-PE | *N*-rhodamine-conjugated 3-*sn*-phosphatidylethanolamine |
| NSF | *N*-ethylmaleimide-sensitive factor |
| OPD | *o*-phenylenediamine dihydrochloride |

| | |
|---|---|
| PAP | 3'-phosphoadenosine-5'-phosphate |
| PAPS | 3'-phosphoadenosine-5'-phosphosulfate |
| PBS | Phosphate-buffered saline |
| PDPC | 1-palmitoyl-2-docosahexaenoyl-*sn*-glycerophosphorylcholine (or 16:0/22:6-PC) |
| PGC | Percoll gradient centrifuged |
| PC | 3-*sn*-glycerophosphorylcholine |
| PE | 3-*sn*-glycerophosphorylethanolamine |
| PI | Propidium iodide |
| $PIP_2$ | Phosphatidylinositol bisphosphate |
| PKA | Protein kinase A |
| $PLA_2$ | Phospholipase $A_2$ |
| PLAP | Placental alkaline phosphatase |
| PLC | Phospholipase C |
| PRS | Preimmune rabbit serum |
| PS | 3-*sn*-glycerophosphorylserine |
| PTK | Protein tyrosine kinases |
| RBL-2H3 | Rat basophilic leukaemia-2H3 mast cells |
| ROS | Reactive oxygen species |
| SDS | Sodium dodecyl sulfate |
| SDS-PAGE | Sodium dodecyl sulfate-polyacrylamide gel electrophoresis |
| SGC | [$\beta$-D-(3'-sulfatoxy)galactopyranosyl]-(1'-1)]-*N*-tetracosanoylsphingosine or sulfogalactosylceramide |

| | |
|---|---|
| SGG | 1-*O*-alkyl-2-*O*-acyl [*β*-D-(3'-sulfatoxy)galactopyranosyl(1'-3)]-*sn*-glycerol or sulfogalactosylglycerolipid or seminolipid |
| SLIP | Sulfolipid immobilizing protein |
| SNARE | Soluble NSF attachment protein receptors |
| SOC | Store operated $Ca^{2+}$ channel |
| SPA | Saturated sinapinic acid |
| SPT | Single particle tracking |
| TBS | Tris-buffered saline |
| TCR | T-cell receptor |
| TESP5 | Testicular serine protease 5 |
| TKR | Tyrosine kinase receptor |
| TLC | Thin layer chromatography |
| TLCK | *N*α-p-tosyl-L-lysine chloromethyl ketone |
| $T_m$ | Phase transition or melting temperature |
| TNE | 10 mM Tris-HCl, 0.15 M NaCl, and 5 mM EDTA, pH 7.5 |
| TNF | Tumor necrosis factor |
| Trp | Transient receptor potential protein channels |
| UDP | Uridine diphosphate |
| UDP-Gal | Uridine diphosphate galactose |
| VCP/p97 | Valosin-containing protein |
| ZKR | Zona kinase receptor |
| ZP | Zona(e) pellucida(e) sulfoglycoproteins |

# CHAPTER ONE

# INTRODUCTION

## 1.1. Overall Rationale of Studies Performed on Sulfogalactosylglycerolipid and Pig Sperm Rafts

Evidence has accumulated for the organization of cellular membranes into lipid-based microdomains (termed rafts), enriched in glycolipids, cholesterol and saturated phospholipids. In addition, lipids and proteins involved in cell adhesion and signaling partition into rafts isolated from somatic cells (reviews: Brown and London, 1998, 2000; Simons and Toomre, 2000; van der Goot and Harder, 2001; Horejsi, 2003). As a result, rafts have been implicated in cell adhesion and signaling, and isolated rafts are ideal cell-free systems to study integrative mechanisms associated with these events. In contrast to somatic cell rafts, reports on mammalian sperm rafts are limited. Sea urchin sperm rafts bind to the 350-kDa sperm binding protein of the egg vitelline layer, and their lipids, i.e., sialyated gangliosides and sulfogalactosylceramide (SGC), play an important role in this binding (Ohta *et al.*, 1999a, b; Maehashi *et al.*, 2003). Mammalian sperm rafts house proteins involved in sperm binding to the egg extracellular matrix of sulfoglycoproteins, i.e., the zona(e) pellucida(e) (ZP), and to the egg plasma membrane (Nishimura *et al.*, 2001). In this thesis, we hypothesize that mammalian sperm rafts contain the ZP binding domains, and their direct binding to the ZP is investigated for the first time.

To acquire fertilizing competence, sperm must undergo capacitation in the female reproductive tract. Capacitation leads to the exposure of the ZP binding molecules on the sperm surface, and sperm-ZP binding is the first gamete union step leading to

fertilization. However, capacitation is associated with cholesterol efflux from the sperm plasma membrane (Flesch *et al.*, 2001 reviews: Visconti and Kopf, 1998; Visconti *et al.*, 2002). Since cholesterol is an important structural component of rafts (Simons and Toomre, 2000; Silvius, 2003), it was of interest to determine whether the release of cholesterol from the sperm plasma membrane affects the integrity and levels of rafts in capacitated sperm. If sperm rafts house the ZP binding domains, the question whether rafts isolated from capacitated sperm exhibit higher ZP binding ability than rafts isolated from non-capacitated sperm would also be addressed. Mammalian sperm contain a male germ cell specific sulfogalactosylglycerolipid (SGG), a structural analog of SGC, a component of sea urchin sperm rafts (Ohta *et al.*, 1999; Maehashi *et al.*, 2003). The hydrocarbon chains of SGG are saturated and pack tightly in the bilayer matrix. The sulfated galactosyl head group of SGG imparts further stability to SGG bilayers by participating in interfacial hydrogen bonding (Tupper *et al.*, 1994; Attar *et al.*, 2000). SGG is also a ZP adhesion molecule (White *et al.*, 2000; Weerachatyanukul *et al.*, 2001). All these properties suggest that SGG is a component of mammalian sperm rafts, and that the sulfoglycolipid may partake in their formation and in sperm raft-ZP binding.

## 1.2. Production and Maturation of Sperm

The mammalian testicular seminiferous epithelium is composed of a proliferative population of germ cells, and a non-proliferating population of supporting Sertoli cells (Figure 1.1A). In the seminiferous tubules, sperm are produced from spermatogonial stem cells via spermatogenesis, which is composed of three distinct phases of cellular and molecular changes. *1*) Mitosis is the proliferation of type A spermatogonia, some of

**Figure 1.1.** (**A**) Drawing of the seminiferous epithelium showing the relation of Sertoli cells and germ cells (After Dym, 1977). (**B**) General features of mammalian sperm. The head and midpiece of the flagellum are joined by the connecting piece. The midpiece contains the mitochondrial sheath surrounding the cytoskeletal structure of the flagellum, (i.e., the axoneme, which is located at the center of the flagellum throughout its full length). The principal piece is defined by the fibrous sheath, which underlies the sperm plasma membrane (After Moss and Gerton, 2001).

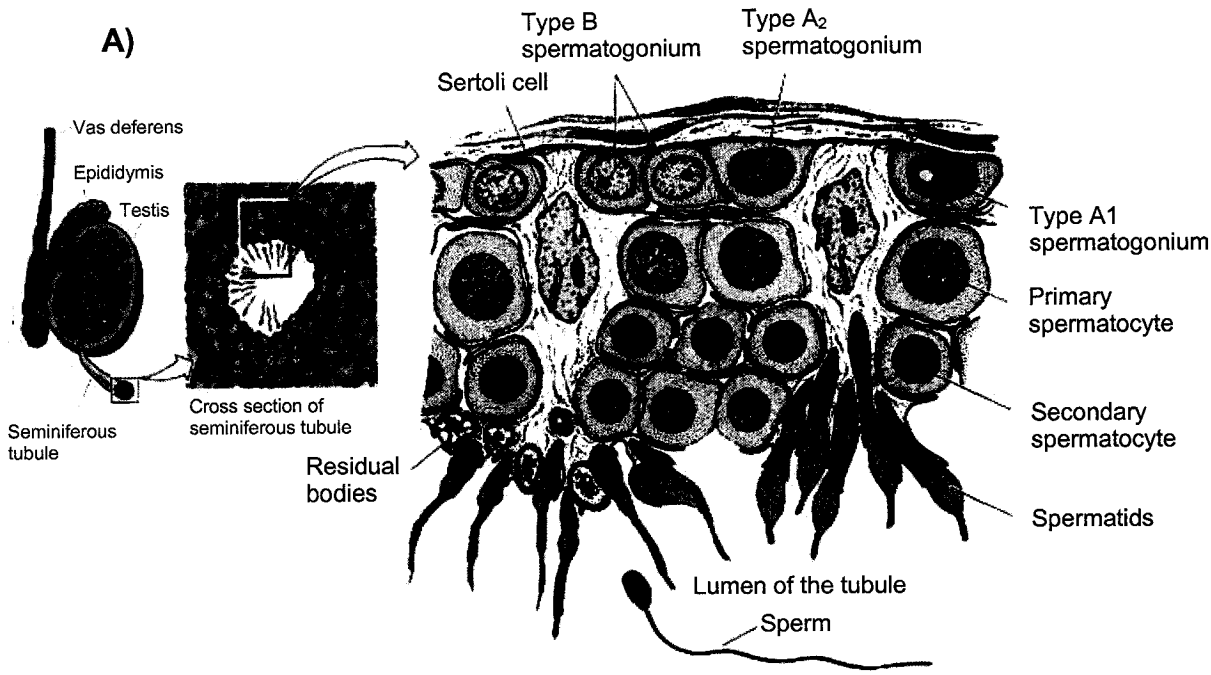
A)
Type B spermatogonium
Type A2 spermatogonium
Sertoli cell
Vas deferens
Epididymis
Testis
Seminiferous tubule
Cross section of seminiferous tubule
Residual bodies
Type A1 spermatogonium
Primary spermatocyte
Secondary spermatocyte
Spermatids
Lumen of the tubule
Sperm

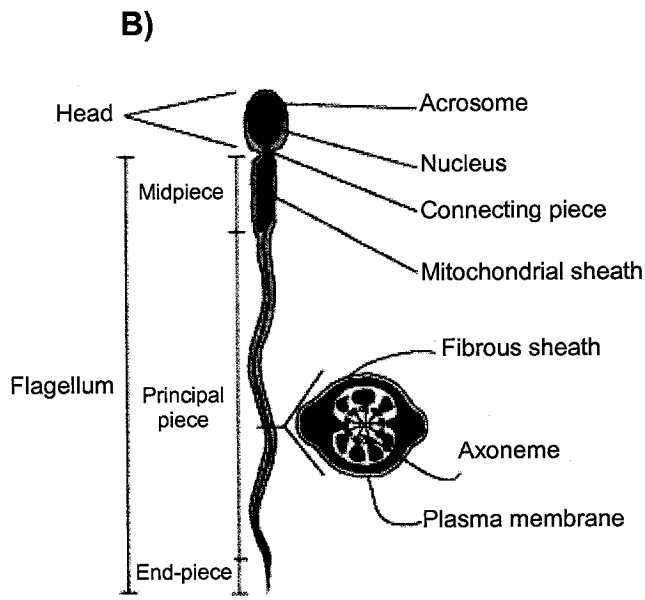
B)
Head
Acrosome
Nucleus
Midpiece
Connecting piece
Mitochondrial sheath
Fibrous sheath
Flagellum
Principal piece
Axoneme
Plasma membrane
End-piece

which will differentiate into type B spermatogonia. In rodents, four successive generations of type A spermatogonia have been described ($A_1$, $A_2$, $A_3$ and $A_4$). The type $A_1$ cells divide by mitosis to give rise to type $A_2$; the type $A_2$ in turn yields type $A_3$, which finally produce type $A_4$ spermatogonia. The type $A_4$ cells divide and give rise to type B spermatogonia. These cells are the differentiated elements committed to the production of preleptotene and leptotene primary spermatocytes, which traverse the blood-testis barrier to enter the adluminal compartment. *2*) The meiotic phase is when primary spermatocytes divide and differentiate into secondary spermatocytes and haploid spermatids. *3*) Spermiogenesis is the morphogenesis of spermatids into spermatozoa. The successive generations of spermatogenic cells have precise cellular associations, and are arranged in well-defined concentric layers. These consist of, from the basement membrane to the lumen of the seminferous tubule, spermatogonia, spermatocytes, and immature and mature spermatids. Mature or elongated spermatids impregnate themselves into the Sertoli cell cytoplasm for final development into testicular spermatozoa, which are then ejected into the lumen (reviews: Dym, 1977; Cheng and Mruk, 2002).

The well-developed sperm are highly differentiated and polarized cells, consisting of the sperm head, the interaction site of the egg ZP, and the flagellum, housing the motility apparatus (Figure 1.1B) (Yanagimachi, 1994; Eddy and O'Brien, 1994; Eddy *et al.*, 2003). The sperm head consists of a highly compact nucleus, containing the male genome, very little cytoplasm and the acrosome (Eddy and O'Brien, 1994). The acrosome is a membrane bound, cap-like structure located on the anterior portion of the sperm head and containing a large array of hydrolytic enzymes. The acrosome is believed to be mostly derived from the Golgi apparatus of round spermatids (Yanagimachi, 1994; Eddy

and O'Brien, 1994; Yoshinaga and Toshimori, 2003). Along the outer acrosomal membrane and the inner sperm plasma membrane, a filamentous actin (F-actin) network is assembled to stabilize both membranes and to prevent their premature fusion or acrosomal exocytosis (review: Breitbart and Spungin, 1997).

The sperm flagellum consists of the connecting piece, the midpiece, the principal piece, and the end piece (Eddy and O'Brien, 1994; Eddy *et al.*, 2003). The midpiece contains the mitochondrial sheath surrounding the cytoskeletal structure of the flagellum (i.e., the axoneme, which is located at the center of the flagellum throughout its full length). The principal piece is defined by the fibrous sheath, which underlies the plasma membrane, and functions as a scaffold for signaling proteins that might play a role in sperm capacitation and hyperactivated motility (Eddy *et al.*, 2003).

Testicular sperm migrate from the caput to the cauda epididymis, where they undergo maturation and acquire the potential for forward motility and fertility by the action of epithelial cell secretions and constituents of luminal fluids (Yanagimachi, 1994; De Lamirande *et al.*, 1997). These include ZP-binding ligands such as $\beta$-galactosidase, P26h, and arylsulfatase-A (AS-A) (Weerachatyanukul *et al.*, 2003; review: Hermo *et al.*, 2002), which get adsorbed onto the sperm surface. In addition, sperm membrane fluidity increases due to the enrichment of phospholipids containing polyunsaturated fatty acyl chains (Cooper and Yeung, 1997; Flesch and Gadella, 2000). However, fertilizing ability of epididymal sperm is suppressed due to the masking of the ZP binding ligands, and probably due to the overall rigidity of their plasma membrane because of their high cholesterol to phospholipid molar ratio (Yanagimachi, 1994).

## 1.3. Sperm-ZP Interaction

Following ejaculation, spermatozoa undergo capacitation in the female reproductive tract to acquire optimal fertilization properties. Capacitation leads to the exposure of ZP binding ligands on the sperm surface. Sperm also acquire hyperactivated motility. This allows sperm to swim in the viscous fluids of the oviduct, and aids capacitated sperm in the penetration of the cumulus cell barrier around ovulated eggs (Figure 1.2). Capacitated and acrosome intact sperm bind to the ZP via the interaction of multiple sperm surface molecules with the ZP, resulting in the aggregation of ZP receptors on the sperm surface. Signaling cascades are thus initiated leading to acrosomal exocytosis, which is characterized by multiple-point fusions between the outer acrosomal membrane and the overlying plasma membrane. This results in membrane vesiculation and in the release of acrosomal contents consisting of proteases (e.g., acrosin, and testicular serine protease 5, TESP5), esterases, acid phosphatases, glycohydrolases, and arylsulfatases (Tulsiani *et al.*, 1998; Honda *et al.*, 2002; review: Yoshinaga and Toshimori, 2003). Acrosomal contents play an important role in digesting the ZP, and paving the way for sperm penetration of this matrix. Acrosomal exocytosis occurs at a slow rate, since the exposed inner acrosomal membrane also participates in secondary sperm-ZP binding (Kim *et al.*, 2001). Acrosome reacted sperm enter the perivitelline space, the extracellular space between the ZP and egg plasma membrane, and bind to the egg plasma membrane at the equatorial segment. Finally one acrosome reacted sperm is incorporated into the egg proper, signifying that fertilization has occurred (Yanagimachi, 1994; reviews: Wassarman, 1999; Wassarman and Litscher, 2001; Primakoff and Myles, 2002; Diekman, 2003).

**Figure 1.2.** Sperm-egg interaction in mammals. **A.** Sperm are produced in testis and migrate from the caput to the cauda epididymis, where they mature and acquire the ability to move actively, although they still lack fertilizing competence. **B.** Epididymal sperm acquire optimal fertilizing ability in the female reproductive tract following capacitation, which involves biochemical and physiological changes in both the sperm head and flagellum. As a result, the ZP binding ligands are exposed on the sperm surface. Sperm also acquire hyperactivated motility, thus allowing them to reach the egg, and penetrate the cumulus cell barrier surrounding ovulated eggs. **C.** Capacitated and acrosome intact sperm bind to the egg ZP. Initial (primary) binding of sperm to the ZP initiates acrosomal exocytosis. Morphological features of mammalian sperm associated with acrosomal exocytosis are outlined from I-IV. (I) Acrosome intact sperm head. (II) Fusion between the outer acrosomal membrane and overlying plasma membrane at the anterior region of the sperm head occurs at the ZP surface. (III, IV) Release of acrosomal contents, mainly hydrolytic enzymes, as well as hybrid membrane vesicles consisting of plasma and outer acrosomal membranes. **D.** The released acrosomal contents digest the ZP, and allow sperm penetration of this matrix, which enables secondary binding between the exposed inner acrosomal membrane and the ZP. Acrosome reacted sperm enter the perivitelline space, and the equatorial segment of sperm binds to and fuses with the egg plasma membrane. Ultimately, one acrosome reacted sperm is incorporated into the egg proper, signifying that fertilization has occurred. *Abbreviations*: pm, plasma membrane; am, acrosomal membrane (**C, D** After Wassarman, 1999).

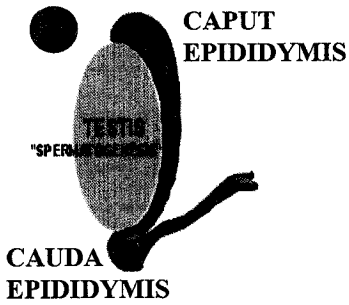


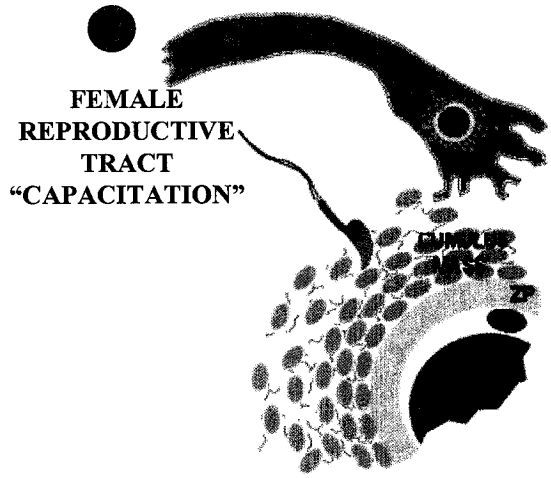


## SPERM-ZP BINDING "ACROSOMAL EXOCYTOSIS"


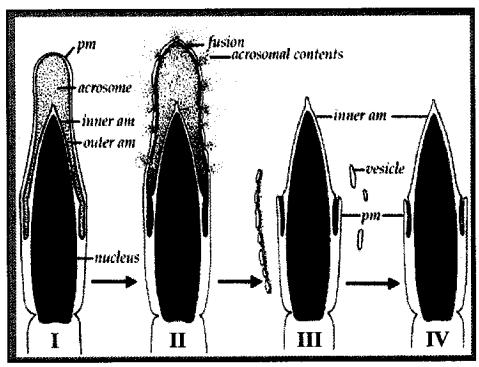


## SPERM-EGG PLASMA MEMBRANE BINDING AND FUSION

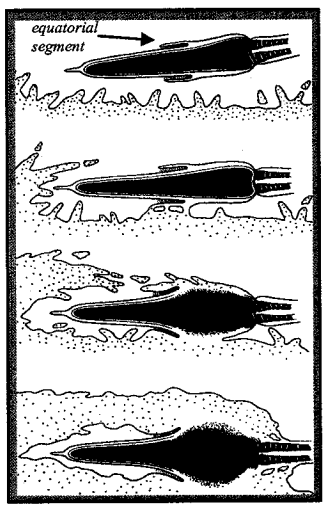

### *1.3.1. Sperm Capacitation: A Key Event for ZP Binding and Acrosomal Exocytosis*

Capacitation defines the biochemical and physiological changes occurring in the sperm head and flagellum during sperm residence in the female reproductive tract. Capacitation can be reproduced *in vitro* by incubating cauda epididymal or ejaculated sperm in chemically defined media containing albumin (cholesterol releasing agent), bicarbonate, $Ca^{2+}$ and energy substrates such as glucose, pyruvate or lactate (reviews: Aitken, 1997; De Lamirande *et al.*, 1997; Flesch and Gadella, 2000; Visconti *et al.*, 2002; Harrison, 1997).

A major event coupled with capacitation (Figure 1.3) is cholesterol efflux from the sperm plasma membrane (Cross, 1998; Visconti *et al.*, 1999a, b; Langlais *et al.*, 1988; Benoff, 1993), which is facilitated by the action of serum albumin (Cross, 1996, 1998). *In vitro* capacitation can also be induced by $\beta$-cyclodextrins (Visconti *et al.*, 1999a; Cross, 1999) and high-density lipoproteins (HDL) (Visconti *et al.*, 1999b). Cholesterol efflux may account for increased membrane fluidity during capacitation (Cross, 1998). Sterol loss from the sperm plasma membrane during capacitation results in a decrease in the steady state fluorescence anisotropy of a fluorescent lipid probe, indicative of increased lipid disorder or "membrane fluidity" (Cross, 2003). A flow cytometric study of the movement of a fluorescent phospholipid analog across the pig sperm plasma membrane reveals an increase in lipid disorder during capacitation (Gadella and Harrison, 2000). Subsequently, it was concluded that phospholipid scrambling may induce the formation of an apical membrane domain/raft in the sperm head surface that enables albumin-mediated cholesterol efflux, and thus an increase in membrane fluidity during *in vitro* capacitation (Flesch *et al.*, 2001a).

**Figure 1.3.** Signaling pathways associated with sperm capacitation. Capacitation is accompanied by cholesterol efflux from the sperm plasma membrane, which is facilitated by the action of serum albumin. Capacitation is also accompanied by hyperpolarization of the sperm plasma membrane, i.e., an increase in the intracellular negative charges, compared to the extracellular milieu, due to the activation of $Na^+/HCO_3^-$ cotransporter. An increased permeability to $K^+$ and cholesterol efflux may also contribute to hyperpolarization. $HCO_3^-$ may be one of the main initiators of signaling events associated with capacitation. Accumulating evidence also supports the presence of an oxidase, which is not yet characterized, on the sperm plasma membrane, and its activation during capacitation. This activation results in the generation of ROS. $HCO_3^-$ stimulates the production of cAMP through the activation of sperm adenylyl cyclase. This results in increased levels of cAMP, which in turn stimulates PKA. Subsequently, PKA induces serine/threonine phosphorylation of sperm proteins, and activates PTK. This results in downstream tyrosine phosphorylation of various sperm proteins. ROS have also been reported to play a role in downstream tyrosine phosphorylation during sperm capacitation. Notably, TKR exhibits an intrinsic tyrosine kinase activity, and may become primed for ZP interaction following its autophosphorylation on tyrosine residues. The intracellular free $Ca^{2+}$ concentrations increase slightly during capacitation, and this may also be maintained by the inhibition of $Ca^{2+}$-ATPases on the sperm and acrosomal membrane. $Ca^{2+}$ stimulates protein tyrosine phosphorylation and sperm hyperactivated motility. *Abbreviations:* cAMP, cyclic adenosine monophosphate; PKA, protein kinase A; PTK, protein tyrosine kinase; ROS, reactive oxygen species; TKR, tyrosine kinase receptor.

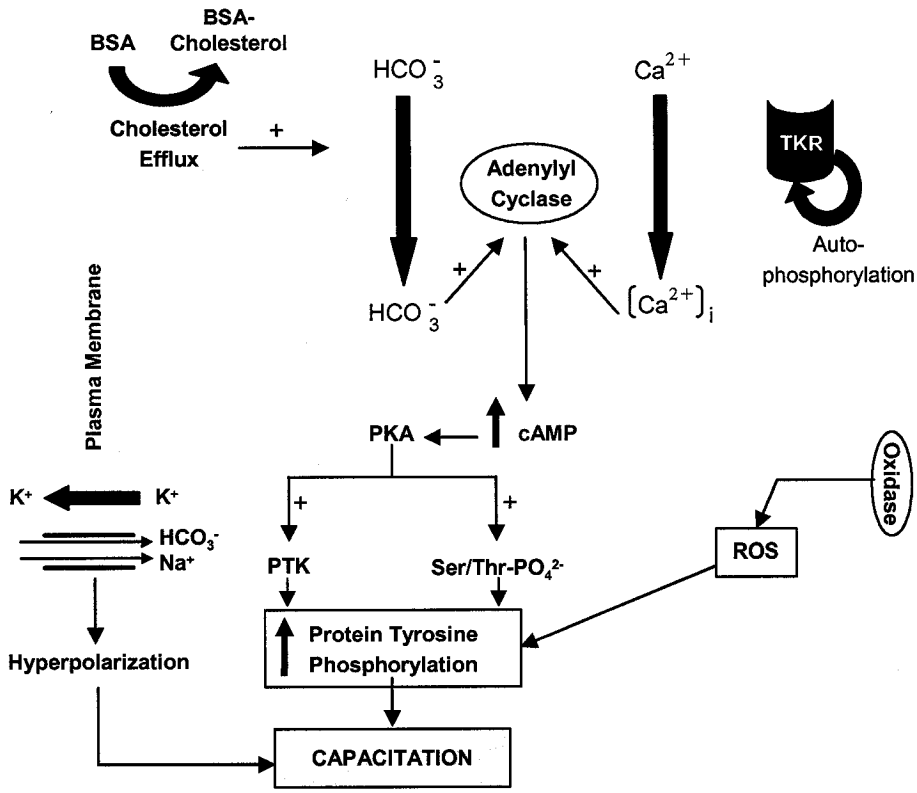
BSA
BSA-Cholesterol
Cholesterol Efflux
+
HCO3-
Ca2+
Adenylyl Cyclase
TKR
Auto-phosphorylation
HCO3-
+
+
[Ca2+]i
Plasma Membrane
PKA
cAMP
K+
K+
HCO3-
Na+
+
+
PTK
Ser/Thr-PO4 2-
Oxidase
ROS
Protein Tyrosine Phosphorylation
Hyperpolarization
CAPACITATION

Capacitation is accompanied by hyperpolarization of the sperm plasma membrane (Figure 1.3), i.e., an increase in the intracellular negative charges, compared to the extracellular milieu. Cholesterol efflux, increased $K^+$ permeability, and activation of a $Na^+/HCO_3^-$ cotransporter have been reported to induce hyperpolarization. Numerous studies reveal that $HCO_3^-$ is a main initiator of signaling events associated with capacitation (Zeng *et al.*, 1995; Demarco *et al.*, 2003; review: Visconti *et al.*, 2002). Accumulating evidence also supports the presence of an oxidase, which is not yet characterized, on the sperm plasma membrane, and its activation during capacitation (Figure 1.3). This activation results in the generation of reactive oxygen species (ROS), and these have reported to play a role in downstream tyrosine phosphorylation (see below, reviews: De Lamirande *et al.*, 1997; Aitken, 1997).

$HCO_3^-$ induces phospholipid scrambling (Gadella and Harrison, 2000), leading to cholesterol redistribution in the sperm plasma membrane and to increased membrane fluidity (discussed above, Flesch *et al.*, 2001). $HCO_3^-$ also stimulates sperm adenylyl cyclase (Visconti *et al.*, 1995a, b; Harrison *et al.*, 1996; reviews: De Lamirande *et al.*, 1997; Aitken, 1997), which may be the soluble adenylyl cyclase identified in the testis and shown to translocate from the cytoplasm to the membrane during spermatogenesis (Chen *et al.*, 2000; review: Visconti *et al.*, 2002). The activation of adenylyl cyclase results in increased levels of cAMP, which in turn stimulates protein kinase A (PKA). Subsequently, PKA induces serine/threonine phosphorylation of sperm proteins, and activates protein tyrosine kinases (PTK) (Figure 1.3). This results in downstream tyrosine phosphorylation of various sperm proteins (Table 1.1) (reviews: De Lamirande *et al.*, 1997; Visconti *et al.*, 2002).

**Table 1.1. Tyrosine Phosphorylated Proteins during Sperm Capacitation**

| Proteins | Comments |
|---|---|
| **AKAP-3 and AKAP-4** | A kinase anchoring proteins (AKAPs) represent a family of scaffolding proteins that function to tether the regulatory subunits of PKA to subcellular sites, such as the sperm fibrous sheath and head (Moss and Gerton, 2001). AKAPs participate in acrosomal exocytosis (Harrison and Miller, 2000). Tyrosine phosphorylation of AKAPs (Ficarro *et al.*, 2003) may contribute to the regulation of sperm hyperactivated motility and acrosomal exocytosis. |
| **VCP/p97** | Valosin-containing protein VCP/p97 is a homolog of NSF (N-ethylmaleimide-sensitive factor), which interacts with membrane fusion proteins, e.g., SNARE (soluble NSF attachment protein receptors). VCP localizes to sperm neck and sperm head anterior before and after capacitation, respectively. Tyrosine phosphorylation of VCP/p97 may be a link between capacitation and acrosomal exocytosis, with VCP/p97 acting as a chaperone to bring relevant membrane fusion proteins to the site of acrosomal exocytosis (Ficarro *et al.*, 2003). |
| **CABYR** | $Ca^{2+}$-binding tyrosine phosphorylation-regulated protein (CABYR) localizes to the principal piece of the human sperm flagellum in association with the fibrous sheath, and gains $Ca^{2+}$ binding capacity when phosphorylated during capacitation. Thus, CABYR may play a role in the acquisition of sperm hyperactivated motility (Naaby-Hansen *et al.*, 2002). |
| **PLC** | Following tyrosine phosphorylation, phospholipase C (PLC) is attached to the F-actin network at sites where it can participate in acrosomal exocytosis (Breitbart and Spungin, 1997). |
| **p32** | Pig sperm tyrosine phosphorylated protein. Immunoprecipitation experiments show that p32 is different from tyrosine kinase 32. Tyrosine phosphorylated proteins redistribute to the acrosome during pig sperm capacitation (Tardif *et al.*, 2001, 2003; Flesch *et al.*, 2001), implicating a role for these proteins in acrosomal exocytosis. |
| **p95 zona kinase receptor (ZKR)** | A ZP receptor with intrinsic tyrosine kinase activity in mouse and human sperm (Leyton and Saling, 1989; Leyton *et al.*, 1992; Burks *et al.*, 1995). It was reported that p95 is identical to c-*mer* tyrosine kinase (Bork, 1996; Tsai and Silver, 1996). In mouse sperm, a 95-kDa phosphotyrosine-containing protein was identified with properties of a hexokinase (Kalab *et al.*, 1994). Tyrosine phosphorylation of p95 may prime this receptor for ZP interaction (Leyton and Saling, 1989; Leyton *et al.*, 1992). |

A slight increase in intracellular free $Ca^{2+}$ concentrations occurs during capacitation (Garcia and Meizel, 1999b; review: Baldi *et al.*, 2002). This may also be maintained by the inhibition of $Ca^{2+}$-ATPases on the sperm and acrosomal membrane (Dorval *et al.*, 2002). $Ca^{2+}$ stimulates protein tyrosine phosphorylation (Figure 1.3) in mouse sperm (Visconti *et al.*, 1995a, b) and human sperm (Dorval *et al.*, 2002). $Ca^{2+}$ also induces sperm hyperactivated motility, which is characterized by vigorous, wide amplitude flagellar bends, asymmetrical flagellar beating, and high beat frequency (Suarez and Ho, 2003). An inositol 1,4,5-trisphosphate ($IP_3$)-receptor-gated $Ca^{2+}$ store and receptors for $IP_3$, which releases $Ca^{2+}$ from intracellular stores, are localized to the base of the flagellum of bull sperm (Ho and Suarez, 2001, 2003). In addition, a protein associated with sperm fibrous sheath (i.e., CABYR, Table 1.1) undergoes tyrosine phosphorylation, and gains $Ca^{2+}$ binding ability during capacitation (Naaby-Hansen *et al.*, 2002). $Ca^{2+}$ may be directly released to the axoneme to trigger sperm hyperactivated motility, presumably through the activation of CABYR.

Capacitation culminates with the acquisition of sperm hyperactivated motility, which is required for sperm to reach the egg (Suarez, 1996; Suarez and Ho, 2003). It also correlates with the exposure of the ZP binding ligands on the sperm surface. The ability of capacitated sperm to bind to the ZP, and undergo subsequent acrosomal exocytosis is considered as an endpoint of capacitation (review: Visconti *et al.*, 2002).

### *1.3.2. The Zona(e) Pellucida(e)*

The ZP is a shell-like extracellular matrix of sulfoglycoproteins around the egg. The ZP provides docking sites for species-specific sperm attachment, induces capacitated

sperm to undergo acrosomal exocytosis, and prevents post fertilization polyspermy (Yanagimachi, 1994). Sperm-ZP binding occurs via the interaction of one or two ZP sulfoglycoproteins with multiple sperm surface ZP binding ligands (Table 1.2). These may act as backup for each other, and synergistically or sequentially during ZP binding.

In most mammals, the ZP consists of a few sulfoglycoproteins encoded by three conserved gene families (Dunbar *et al.*, 2001; Harris *et al.*, 1994). The biochemical and functional properties of the mouse ZP (reviews: Wassarman, 1999; Dell *et al.*, 1999; Wassarman and Litscher, 2001) and pig ZP (Mori *et al.*, 2000; Nakano and Yonezawa, 2001; Takasaki *et al.*, 1999; Tulsiani and Abou-Haila, 2001) have been extensively studied. In mice, Bleil and Wassarman (1988) identified by SDS-PAGE three ZP sulfoglycoproteins, which were named ZP1, ZP2, and ZP3 from highest to lowest apparent molecular weight, respectively. However, ZP sulfoglycoproteins exhibit heterogeneity across species due to extensive post-translational modifications, including glycosylation and sulfation (Wassarman, 1988; Dunbar *et al.*, 2001). Because of these modifications, the nomenclature of ZP sulfoglycoproteins from different species based on electrophoretic mobility has been confusing. As the cDNAs and genes encoding the different ZP sulfoglycoproteins have been isolated and sequenced, it was possible to relate these sulfoglycoproteins according to gene families. A unified system of nomenclature was proposed (Harris *et al.*, 1994), in which ZP genes were named in order of the length of their encoded protein sequence, from longest to shortest (Table 1.3). Under these criteria, the mouse ZP genes fall in the order ZP2, ZP1, then ZP3, and a new letter based system was introduced to avoid confusion (i.e., ZPA, ZPB, and ZPC, respectively).

**Table 1.2. Sperm-Associated Molecules Involved in ZP Binding**

| Molecules | Function |
|---|---|
| **β-galactosyltransferase** | Binds specifically to terminal *N*-acetylglucosamine on mouse ZP3, and participates in acrosomal exocytosis (Miller *et al.*, 1992a; Lu and Shur, 1997; Shur *et al.*, 1998). |
| **Arylsulfatase-A (AS-A)** | Preincubation of sperm with anti-AS-A IgG/Fab inhibits sperm-ZP binding. Exogenously added AS-A induces premature acrosomal exocytosis in mouse and human sperm, and decreases sperm-ZP binding and *in vivo* fertilization (Carmona *et al.*, 2002; Tantibhedhyangkul *et al.*, 2002). |
| **Spermadhesins** | Proteins originating from seminal vesicles, which get adsorbed onto ejaculated sperm. They exhibit carbohydrate binding activity (Dostalova *et al.*, 1995). |
| **Zonadhesin** | Binds to ZP (Hardy and Garbers, 1995; Gao and Garbers, 1998). |
| **PH-20** | A GPI-anchored protein involved in secondary ZP binding of acrosome reacted sperm (Myles and Primakoff, 1997). |
| **p95, zona kinase receptor (ZKR)** | Binds to mouse ZP3 (Leyton and Saling, 1989). Synthetic peptides corresponding to regions of the extracellular domain of p95 inhibit sperm-ZP binding in humans (Burks *et al.*, 1995). |
| **SGG** | Anti-SGG IgG/Fab inhibit ZP binding to mouse and human sperm. Coincubation of sperm and eggs with SGG liposomes also inhibits sperm-ZP binding (White *et al.*, 2000; Weerachatyanukul *et al.*, 2001). |
| **Mannose binding protein** | α-D-mannosidase that binds to mannose residues on the ZP (Cornwall *et al.*, 1991). |
| **Proacrosin** | An acrosomal protein involved in secondary ZP binding. Its affinity to polysulfated glycans implicates proacrosin in ZP binding. The cDNA clone and recombinant protein have been produced; site directed mutagenesis implicates the basic amino acids of proacrosin in ZP binding (Richardson *et al.*, 1994; Richardson and O'Rand, 1994; Moreno *et al.*, 2002). |
| **Sperm protein-56 (sp56)** | The cDNA sequence has been described. It binds to *O*-linked glycans of the ZP (Bleil and Wassarman, 1990; Bookbinder *et al.*, 1995). Recently, sp56 has been shown to be present in the acrosomal matrix, indicating that sp56 may bind to the ZP during acrosomal exocytosis (Foster *et al.*, 1997). |
| **P26h (hamster) and P34h (human)** | Highly identical to carbonic reductase. It is synthesized in the testis and secreted into the lumen to be adsorbed onto the sperm surface in the epididymis via its GPI-linkage. Its levels in sperm correlate with male fertility (Boue *et al.*, 1994; Boue and Sullivan, 1996). |
| **$PLA_2$** | Its inhibitors and antibodies impede fertilization (Riffo and Parraga, 1996). |

**Table 1.3. Nomenclature and Function of ZP Sulfoglycoproteins***

| ZP Family[a] | Species | Nomenclature | Function |
|---|---|---|---|
| **ZP1**[b] | Mouse | ZP1 | Cross links ZP2 and ZP3 (Wassarman, 1999; Wassarman and Litscher, 2001). |
| | Human[c] | ZP1/ZPB[d] | Existence was described by molecular cloning. |
| | Pig | ZP3α/ZPB | Forms a complex with ZP3β. Sperm receptor: it binds to acrosome intact sperm (Yurewicz *et al.*, 1998). |
| **ZP2** | Mouse | ZP2 | Secondary sperm receptor: binds to acrosome reacted sperm during migration through the ZP matrix (Wassarman, 1999; Wassarman and Litscher, 2001). |
| | Human | ZP2/ZPA | Recombinant human ZP2 expressed by *E. coli* binds only to acrosome reacted human sperm. |
| | Pig | ZP1/ZPA | A minor component of pig ZP. |
| **ZP3** | Mouse | ZP3 | Primary sperm receptor: binds to acrosome intact sperm, and induces acrosomal exocytosis (Wassarman, 1999; Wassarman and Litscher, 2001). |
| | Human | ZP3/ZPC | Recombinant human ZP3 induces acrosomal exocytosis (Van Duin *et al.*, 1994; Dong *et al.*, 2001; Bray *et al.*, 2002), inhibits the binding of capacitated human sperm to the ZP (Dong *et al.*, 2001), and binds to the sperm head with a $K_d$ of 172 μM (review: Tanphaichitr *et al.*, 2003a), a value comparable to that of mouse sperm binding to native mouse ZP3 (Kerr *et al.*, 2002). Thus, human ZP3 may be the primary sperm receptor. |
| | Pig | ZP3β/ZPC | Forms a complex with ZP3α: it assists ZP3α in sperm binding (Yurewicz *et al.*, 1998). |

* Adapted from Prasad *et al.* (2000), Dunbar *et al.* (2001), and Tanphaichitr *et al.* (2003a).

[a] Based on polypeptide homology.

[b] Based on mouse ZP nomenclature.

[c] In humans, the ZP cannot be obtained in quantity, and the discernment of the identity of human ZP sulfoglycoproteins was achieved through molecular cloning (Harris *et al.*, 1994; Chamberlin and Dean, 1990; Liang and Dean, 1993) using corresponding mouse cDNA probes.

[d] Nomenclature proposed by Harris *et al.* (1994).

Despite genetic similarities in their DNA sequences, the mammalian ZP sulfoglycoproteins exhibit functional heterogeneity, and different gene products mediate species-specific sperm-ZP binding in mice/humans and pigs (Table 1.3). In pigs, the three ZP sulfoglycoproteins appear on non-reducing SDS gels as two diffuse bands; ZP1 runs at $M_r$ 90,000, whereas ZP3α and ZP3β co-migrate at $M_r$ 55,000. ZP3α and ZP3β are orthologs of mouse ZP1 and ZP3, respectively. ZP3α and ZP3β can be separated by reverse phase high performance liquid chromatography (HPLC) following pretreatment with endo-β-galactosidase, with ZP3α being the major component and containing small amounts (5-10%) of ZP3β contaminant (Yurewicz *et al.*, 1987). ZP3α-ZP3β complexes participate in sperm binding (Sacco *et al.*, 1989; Berger *et al.*, 1989), and stimulate acrosomal exocytosis in capacitated pig sperm (Berger *et al.*, 1989). Initially, it was reported that ZP3α, but not ZP3β, is involved in binding to pig sperm (Sacco *et al.*, 1989; Yonezawa *et al.*, 1995) and to isolated pig sperm membrane vesicles (Yurewicz *et al.*, 1993). However, highly purified ZP3α preparations were recently reported, and it was demonstrated that ZP3α-ZP3β heterocomplexes are required in the binding to isolated pig sperm plasma membrane vesicles. Thus, it was suggested that minor amounts of putative ZP3α-ZP3β complexes could account for the binding activity of previous ZP3α preparations (Yurewicz *et al.*, 1998).

The polypeptide sequences of the ZP sulfoglycoproteins are conserved across species. Therefore, species specificity of sperm-egg interaction should not be governed by the polypeptide entity of the ZP sulfoglycoproteins, but rather by their carbohydrate moieties, the overall structures of which differ across animal species (reviews: Dell *et al.*, 1999; Oehninger, 2001; Wassarman and Litscher, 2001). In mice, *N*-linked

oligosaccharides are primarily high mannose ($Man_5GlcNAc_2$) and biantennary complex glycans terminated with Gal$\beta$1-4GlcNAc, NeuAc$\alpha$2-3Gal$\beta$1-4GlcNAc, NeuGc$\alpha$2-3Gal$\beta$1-4GlcNAc, NeuAc$\alpha$2-3[GalNAc$\beta$1-4]Gal$\beta$1-4GlcNAc, NeuGc$\alpha$2-3[GalNAc$\beta$1-4]Gal$\beta$1-4GlcNAc), and terminal GlcNAc. Polylactosamine sequences and terminal $\alpha$-galactose are also detected on a subset of the antenae. The majority of the *O*-glycans are core 2 structures (Gal$\beta$1-4GlcNAc$\beta$1-6[Gal$\beta$1-3]GalNAc) terminated with one or two *N*-acetyl or *N*-glycolyl neuraminic acid residues (Easton *et al.*, 2000). In pigs, the majority of the *N*- and *O*-linked oligosaccharides express extended polylactosamine chains highly substituted with sulfate groups and sialic acids at their terminal ends (Yurewicz *et al.*, 1991; Takasaki *et al.*, 1999).

In mice, ZP3 glycopeptides produced by extensive proteolysis of the sulfoglycoprotein retain activity as a sperm receptor. Chemical or enzymatic removal of all ZP3 oligosaccharides (*N*- and *O*-linked) results in complete inactivation of ZP3 as a sperm receptor in mice. *O*-linked oligosaccharides of mouse ZP3 inhibit sperm-egg binding *in vitro*, and the removal of *N*-linked glycans from intact mouse eggs results in decreased sperm binding (reviews: Wassarman, 1999; Dell *et al.*, 1999). In pigs, both *O*-linked (Yurewicz *et al.*, 1991) and *N*-linked oligosaccharides (Noguchi *et al.*, 1992; Noguchi and Nakano, 1992; Yonezawa *et al.*, 1995) block porcine sperm-egg binding. In addition, ZP sulfated glycans are implicated in sperm-ZP binding in various species (Takasaki *et al.*, 1999; review: Diekman, 2003). These observations indicate that species-specific sperm-ZP binding in mammals is a carbohydrate-mediated event (reviews: Dell *et al.*, 1999; Diekman, 2003; Talbot *et al.*, 2003).

### *1.3.3. Acrosomal Exocytosis; A Consequence of Sperm-ZP Binding*

Following sperm interaction with the ZP, signaling events are initiated and acrosomal exocytosis occurs on the surface of the ZP. In mice and humans, ZP3 is the natural agonist that initiates acrosomal exocytosis upon binding to acrosome-intact sperm (Bleil and Wassarman, 1983; Ward and Kopf, 1993). This binding leads to the activation of $G_i$-protein receptor ($G_i$-R, $G_i$ subtype of the GTP binding heterotrimeric protein) linked to PLC pathway (Figure 1.4). This in turn induces a transient $Ca^{2+}$ influx into the sperm (Florman *et al.*, 1989) through T-type voltage-dependent $Ca^{2+}$ channels in the sperm plasma membrane (Arnoult *et al.*, 1996; Patrat *et al.*, 2000; Darszon *et al.*, 2001), as well as a rise in cytosolic pH presumably due the activation of a $Na^+/H^+$ exchanger. A tyrosine kinase receptor (TKR) linked to PLCγ may also be activated during ZP3 binding (Patrat *et al.*, 2000; reviews: Breitbart and Spungin, 1997; Breitbart, 2002a, b) (Figure 1.4). The TKR exhibits an intrinsic tyrosine kinase activity, and may become primed for ZP interaction following its autophosphorylation (Leyton and Saling, 1989; Leyton *et al.*, 1992; Burks *et al.*, 1995).

The ZP-induced activation of $G_i$-R stimulates adenylyl cyclase, and subsequent cAMP production (Leclerc and Kopf, 1995, 1999). This results in PKA activation (Visconti *et al.*, 1997), and in downstream tyrosine phosphorylation of sperm proteins, including PLCγ (reviews: Breitbart and Spungin, 1997; Breitbart, 2002a, b) and Src-related cytoplasmic tyrosine kinases (e.g., c-Yes, Leclerc and Goupil, 2002) (Figure 1.4). PLCγ is then activated, resulting in the hydrolysis of phosphatidylinositol bisphosphate ($PIP_2$) to generate diacylglycerol (DAG) and $IP_3$. DAG activates phospholipase $A_2$ ($PLA_2$), which hydrolyzes membrane phospholipids to produce arachidonic acid and

**Figure 1.4.** Signaling pathways associated with sperm acrosomal exocytosis. In mice and humans, ZP3 initiates acrosomal exocytosis upon binding to acrosome-intact sperm. This binding leads to the activation of $G_i$-R ($G_i$ subtype of the GTP binding heterotrimeric protein) coupled to PLC, which induces a transient $Ca^{2+}$ influx into the sperm through T-type voltage-dependent $Ca^{2+}$ channels in the sperm plasma membrane, as well as a rise in cytoplasmic pH presumably due the activation of a $Na^+/H^+$ exchanger. In addition, a TKR coupled to PLCγ may be activated during ZP3 binding. TKR exhibits an intrinsic tyrosine kinase activity, and may become primed for ZP interaction following its tyrosine phosphorylation. The ZP-induced activation of $G_i$-R stimulates adenylyl cyclase, which leads to increased cAMP levels, PKA activation, and downstream protein tyrosine phosphorylation. PLCγ and Src-related cytoplasmic tyrosine kinases, including c-Yes, undergo tyrosine phosphorylation following sperm-ZP3 interaction. PLCγ is then activated, resulting in the hydrolysis of $PIP_2$ to generate DAG and $IP_3$. DAG activates $PLA_2$, which hydrolyzes membrane phospholipids to produce arachidonic acid and lysophopholipids (fusogenic lipids). $IP_3$ may interact with its receptor on the outer acrosomal membrane, resulting in the mobilization of intracellular $Ca^{2+}$ from the acrosome. Acrosomal $Ca^{2+}$ release may also be due to PKA-induced activation of voltage-dependent $Ca^{2+}$ channels on the outer acrosomal membrane. The increase in intracellular $Ca^{2+}$ promotes a subsequent sustained $Ca^{2+}$ influx via SOC. Intracellular $Ca^{2+}$ concentrations increase to supramicromolar levels. This induces depolymerization of F-actin and subsequent acrosomal exocytosis. *Abbreviations:* AC, adenylyl cyclase; cAMP, cyclic adenosine monophosphate; DAG, diacylglycerol; $G_i$-R, $G_i$-protein receptor; $IP_3$, inositol trisphosphate; $PIP_2$, phosphatidylinositol bisphosphate; PKA, protein kinase A; $PLA_2$, Phospholipase $A_2$; PL, phospholipids; PLC, Phospholipase C; SOC, store operated $Ca^{2+}$ channels; TKR, tyrosine kinase receptor; ZP, zona(e) pellucida(e).

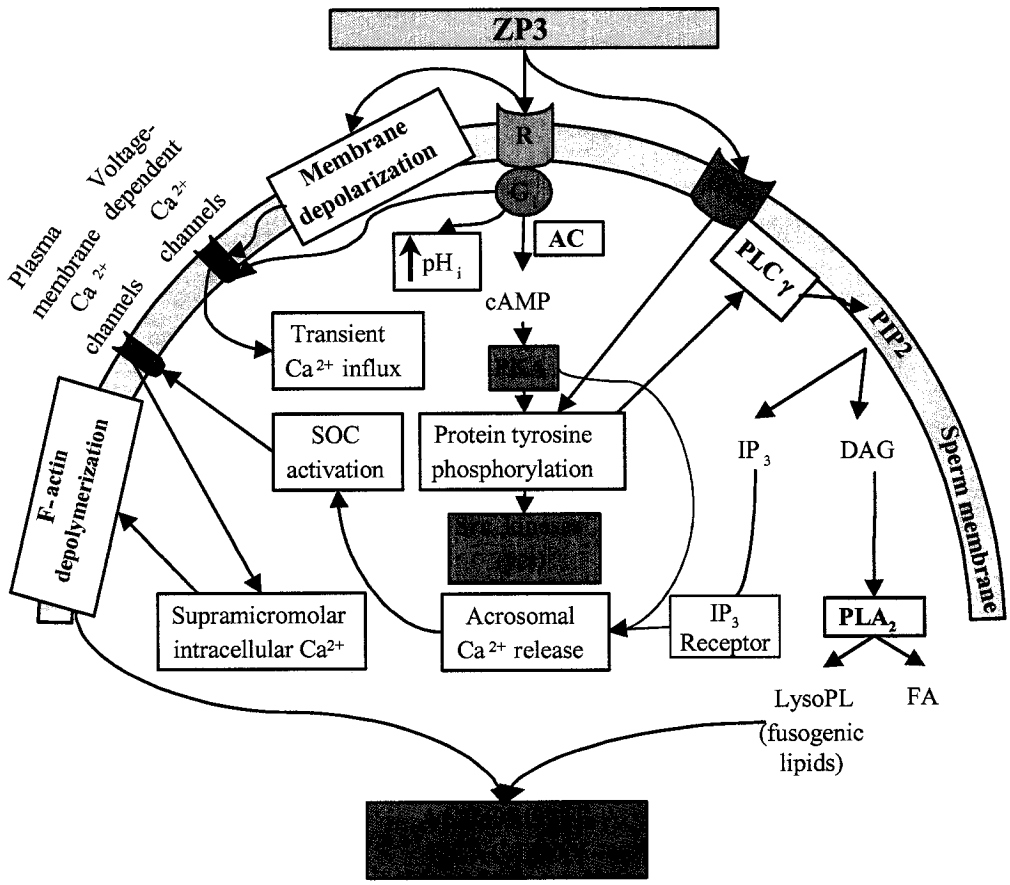
ZP3
R
G
Membrane depolarization
Voltage-dependent Ca2+ channels
Plasma membrane Ca2+ channels
pHi
AC
cAMP
PLCγ
PIP2
Sperm membrane
Transient Ca2+ influx
SOC activation
Protein tyrosine phosphorylation
IP3
DAG
F-actin depolymerization
Supramicromolar intracellular Ca2+
Acrosomal Ca2+ release
IP3 Receptor
PLA2
LysoPL
FA
(fusogenic lipids)

lysophopholipids (fusogenic lipids) (Yuan *et al.*, 2003). $IP_3$ may interact with its receptor on the outer acrosomal membrane (Walensky and Snyder, 1995; Naaby-Hansen *et al.*, 2001), resulting in the mobilization of intracellular $Ca^{2+}$ from the acrosome. PKA-induced activation of voltage-dependent $Ca^{2+}$ channels on the outer acrosomal membrane may also account for acrosomal $Ca^{2+}$ release (review: Breitbart and Spungin, 1997). The increase in intracellular $Ca^{2+}$ promotes a subsequent sustained $Ca^{2+}$ influx into sperm via store operated $Ca^{2+}$ channels (SOC). Recent studies reveal that transient receptor potential protein channels 1, 2, 3, and 6 (Trp1, Trp2, Trp3, and Trp6), all putative $Ca^{2+}$-permeant SOC, are expressed in sperm (Trevino *et al.*, 2001), and Trp2 participates in the ZP3-induced acrosomal exocytosis in mouse sperm (Jungnickel *et al.*, 2001). $Ca^{2+}$ imaging of single mouse sperm reveals that $PLC_{\delta 4}$ is required for $Ca^{2+}$ mobilization from the acrosome, and for the sustained increase in intracellular $Ca^{2+}$ concentrations through SOC (Fukami *et al.*, 2003). Intracellular $Ca^{2+}$ concentrations are elevated to supramicromolar levels, thus inducing F-actin depolymerization and subsequent acrosomal exocytosis (Figure 1.4) (reviews: Breitbart and Spungin, 1997; Breitbart, 2002a, b).

In addition to the ZP, progesterone released from the cumulus cells also triggers acrosomal exocytosis (Roldan *et al.*, 1994; Meizel, 1997; Forti *et al.*, 1999; Blackmore, 1999; Patrat *et al.*, 2000; Kirkman-Brown *et al.*, 2002). Progesterone-induced acrosomal exocytosis is dependent on extracellular $Ca^{2+}$. However, it is not clear whether T-type voltage-dependent $Ca^{2+}$ channels play a role in this event (review: Garcia and Meizel, 1999). Progesterone acts on γ-aminobutyric acid type A ($GABA_A$)-like receptor with $Cl^-$ channel activity to activate acrosomal exocytosis (Roldan *et al.*, 1994; Shi and Roldan,

1995; review: Meizel, 1997). Subsequently, PKA and AKAP (Harrison *et al.*, 2000), PKC (O'Toole *et al.*, 1996) and PTK (Murase and Roldan, 1996) are activated, indicating that protein phosphorylation is important for this event. Progesterone stimulates DAG formation via the activation of PLC (Roldan *et al.*, 1994; Murase and Roldan, 1996), and the steroid also activates $PLA_2$ (Roldan and Vazquez, 1996; Calogero *et al.*, 2000). Although progesterone and the ZP activate different signaling pathways (Murase and Roldan, 1996), cross talk between these pathways is possible, and physiologically, progesterone may play a priming role in the initiation of the ZP-induced acrosomal exocytosis, as suggested by Roldan *et al.* (1994).

## 1.4. The Mammalian Male Germ Cell Specific Sulfogalactosylglycerolipid

Sulfogalactosylglycerolipid (SGG) was initially described as the major glycolipid of rat testis (Kornblatt *et al.*, 1972). Subsequently, SGG was found to be the major glycolipid of testes and sperm of all mammalian species examined (Ishizuka *et al.*, 1973; Suzuki *et al.*, 1973; Kornblatt *et al.*, 1974). Using silicic acid column chromatography, SGG was separated from total lipids following elution with acetone, and thin layer chromatography (TLC) revealed a unique $R_f$ of SGG (Ishizuka *et al.*, 1973). SGG stained positively for a sugar moiety, and reacted with sulfate recognizing dyes, such as Azure A (Ishizuka *et al.*, 1973) and rhodizonate (Kornblatt *et al.*, 1972). Infrared spectroscopy and nuclear magnetic resonance (NMR) demonstrated the presence of (*a*) a sulfate ester at the 3'-equatorial galactosyl hydroxyl group, and (*b*) a galactopyranoside with a $\beta$-anomeric configuration in SGG (Ishizuka *et al.*, 1973). In addition, the injection of $Na_2{}^{35}SO_4$ into adult rat testis resulted in the incorporation of $^{35}S$ radiolabel into SGG (Kornblatt *et al.*,

1974). Following chemical degradation, SGG consists of a galactosyl moiety, a sulfate group, a chimyl alcohol (1-*O*-hexadecyl glycerol) and palmitic acid (2-*O*-hexadecanoyl glycerol) in equimolar stoichiometry (Kornblatt *et al.*, 1972). Thus, the structure of SGG was deduced to be 1-*O*-alkyl-2-*O*-acyl [β-D-(3'-sulfatoxy)galactopyranosyl(1'-3)]-*sn*-glycerol (Figure 1.5). SGG was also isolated from bovine (Alvarez *et al.*, 1990) and ram (Tupper *et al.*, 1994; Attar *et al.*, 2000) testes, and was shown by gas chromatography (GC), mass spectrometry (MS), NMR and FTIR spectroscopy to have the same chemical structure as that described above.

SGG constitutes ~12 mol% of total sperm lipids or ~20 mol% of the sperm head plasma membrane lipids (Ishizuka, 1997; Murray and Narasimhan, 1990; Furimsky *et al.*, 2002; Flesch *et al.*, 2001a). SGG is a structural analog of sulfogalactosylceramide (SGC, [β-D-(3'-sulfatoxy)galactopyranosyl]-(1'-1)]-*N*-tetracosanoylsphingosine) (Figure 1.5). SGC is the major sulfoglycolipid in myelin (4-7 mol% of total lipids) (Ishizuka, 1997; Murray and Narasimhan, 1990; Norton and Cammer, 1984), and SGC is also expressed in the cytoplasm and nuclear membrane of neurons and astrocytes of adult rat brain (Pernber *et al.*, 2002). Both SGC and SGG are present in brain white and gray matter (Pernber *et al.*, 2002; Murray and Narasimhan, 1990; Han *et al.*, 2002). SGC is also found in lower vertebrate and invertebrate male germ cells (Ishizuka, 1997; Murray and Narasimhan, 1990; Vos *et al.*, 1994). Due to structural similarity between SGG and SGC, antibodies generated against either SGC or SGG cross-react with both sulfoglycolipids (Lingwood *et al.*, 1980; Eddy *et al.*, 1985; Crook *et al.*, 1987; Fredman *et al.*, 1988; Gadella *et al.*, 1994; White *et al.*, 2000). SGC and its precursor galactosylceramide (GC, β-D-galactopyranosyl-1'-1-*N*-tetracosanoylsphingosine, Figure 1.5), which comprises 20 wt%

**Figure 1.5.** Chemical structure of SGG (**A**), SGC (**B**), GG (**C**) and GC (**D**). *Abbreviations:* GC, [*β*-D-galactopyranosyl]-1'-1-*N*-tetracosanoylsphingosine; GG, 1-*O*-hexadecyl-2-*O*-hexadecanoyl-*β*-D-galactopyranosyl(1'-3)]-*sn*-glycerol; SGC, [*β*-D-(3'-sulfatoxy)galactopyranosyl]-1'-1-*N*-tetracosanoylsphingosine; SGG, 1-*O*-hexadecyl-2-*O*-hexadecanoyl-*β*-D-(3'-sulfatoxy)galacto-pyranosyl(1'-3)]-*sn*-glycerol.

**A)**

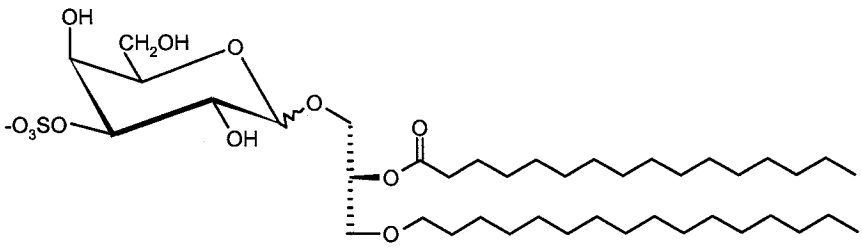
OH
CH2OH
O
-O3SO
OH
O
O
O
O

**B)**

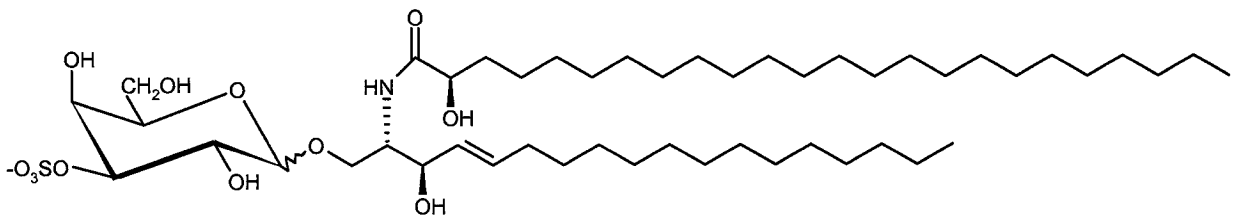
OH
CH2OH
O
-O3SO
OH
O
HN
O
OH
OH

**C)**

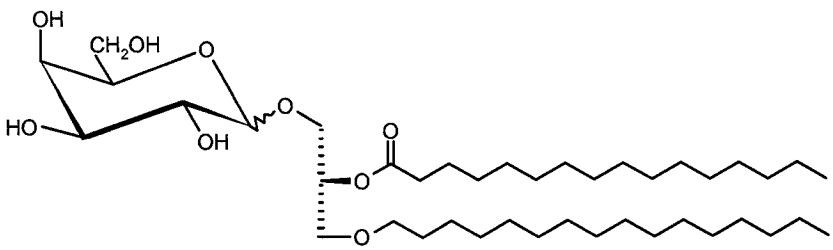
OH
CH2OH
O
HO
OH
O
O
O
O

**D)**

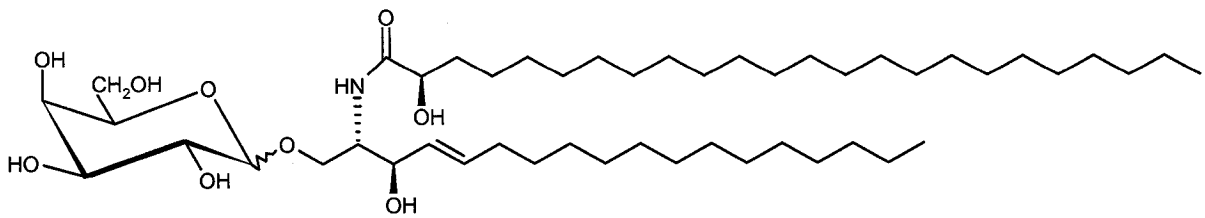
OH
CH2OH
O
HO
OH
O
HN
O
OH
OH

of total myelin lipids, occur naturally as non-hydroxylated and α-hydroxylated species (Vos *et al.*, 1994; Norton and Cammer, 1984). The hydroxyl group may increase the hydrogen bonding potential of SGC (Boggs *et al.*, 1988a) and GC (Pascher and Sundell, 1977; Lee *et al.*, 1986), thus imparting further stability to biological membranes.

Both SGG and SGC engage in cell-cell/extracellular protein interactions (reviews: Brockhausen and Kuhns, 1997; Flesch and Gadella, 2000). SGG and SGC bind *in vitro* to cell adhesion proteins, including L-selectin, fibronectin, laminin, thrombospondin, von Willebrand factor, and malaria sporozoite surface proteins (Suzuki *et al.*, 1993; Roberts and Ginsburg, 1988; Pancake *et al.*, 1993; review: Ishizuka, 1997). SGG also binds *in vitro* to the surface glycoprotein of the human immunodeficiency virus (HIV-1) gp120 (Harouse *et al.*, 1991; Gadella *et al.*, 1998; Piomboni and Baccetti, 2000), and infertility-related mycoplasmas (Lingwood *et al.*, 1990). Significantly, the binding of these pathogens to SGG on the sperm surface may decrease sperm-egg interaction, as well as transmit these microorganisms into the female reproductive tract following intercourse. All of these findings suggest that sperm SGG may participate in cell-cell/extracellular matrix interactions during mammalian fertilization (see below).

### *1.4.1. Biosynthesis of SGG*

During the isolation procedure of SGG, a less polar compound was found in boar sperm and testis (Ishizuka *et al.*, 1973), and in guinea pig testis (Suzuki *et al.*, 1973) and rat testis (Hsu *et al.*, 1983; Knapp *et al.*, 1973). The structure of this compound was considered as desulfated SGG (i.e., 1-*O*-alkyl-2-*O*-acyl[β-D-galactopyranosyl(1'-3)]-*sn*-

glycerol, Figure 1.5), also known as galactosylglycerolipid (GG). The injection of [$^{14}$C]palmitate, [$^{14}$C]cetyl alcohol and [$^{14}$C]galactose into adult rat testes results in the formation of radioactive GG and SGG, with the radioactivity peak of GG preceding that of SGG (Hsu *et al.*, 1983). Rat testis extracts contain a sulfotransferase activity, catalyzing the transfer of a sulfate group from 3'-phosphoadenosine-5'-phosphosulfate (PAPS) to GG and GC, resulting in the formation of SGG and SGC, respectively (Knapp *et al.*, 1973). Testicular sulfotransferases (Knapp *et al.*, 1973; Kornblatt *et al.*, 1974; Handa *et al.*, 1974; Sakac *et al.*, 1992), and human renal cancer cell sulfotransferases (Honke *et al.*, 1996; Honke *et al.*, 1997) also catalyze the sulfation reaction of both GG and GC. Recent data reveal that testicular sulfotransferase is encoded by the same cerebroside sulfotransferase (*Cst*) gene, present in brain and kidney. The testis and brain of *Cst* knockout mice are genetically depleted of SGG and SGC, respectively, with GG accumulation in the testis of these mice. All these results affirmed that SGG synthesis occurs via sulfation of GG (Figure 1.6) (Honke *et al.*, 2002).

Coetzee *et al.* (1996) and Fujimoto *et al.* (2000) generated mice genetically depleted of ceramide galactosyltransferase (CGT), which catalyzes the production of GC from ceramide in the presence of UDP-galactose (Morell and Radin, 1969). The brain and testis of *Cgt* knockout mice are depleted of GG (Fujimoto *et al.*, 2000; Coetzee *et al.*, 1996). Since small amounts of 1-*O*-alkyl-2-*O*-acyl-*sn*-glycerol (AAG) are present in the rat testis (Hsu *et al.*, 1983), CGT may catalyze the synthesis of GG in the testis via galactosylation of AAG in the presence of UDP-galactose, similarly to GC synthesis from ceramide (Figure 1.6) (Kates, 1990).

**Figure 1.6.** Biosynthetic pathway of SGG and SGC. *Abbreviations:* AAG, 1-*O*-alkyl-2-*O*-acyl-*sn*-glycerol CST, cerebroside sulfotransferase; CGT, ceramide galactosyltransferase; GC, galactosylceramide; GG, galactosylglycerolipid; PAP, 3'-phosphoadenosine-5'-phosphate; PAPS, 3'-phosphoadenosine-5'-phosphosulfate; SGC, sulfogalactosylceramide; SGG, sulfogalactosylglycerolipid; UDP, uridine diphosphate; UDP-Gal, uridine diphosphate galactose.

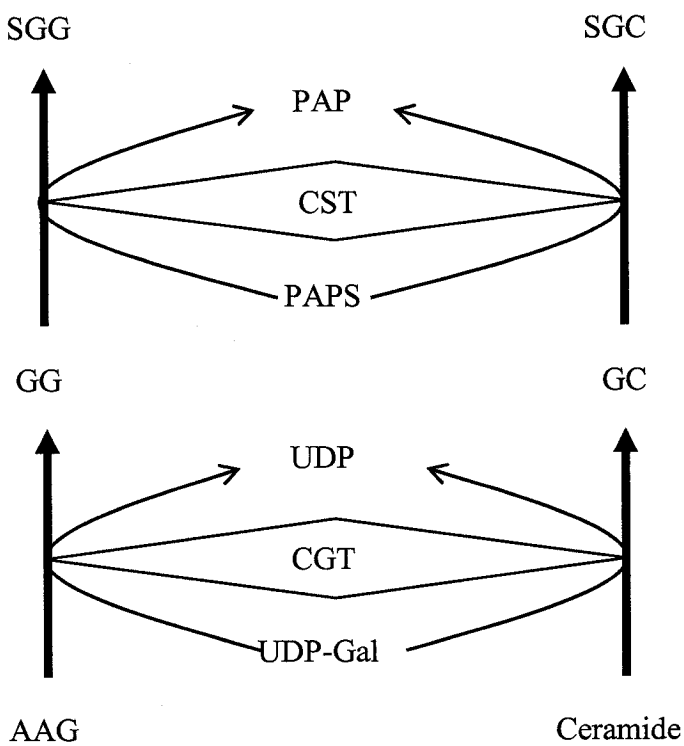
SGG
SGC
PAP
CST
PAPS
GG
GC
UDP
CGT
UDP-Gal
AAG
Ceramide

Biosynthesis of SGG occurs in the Golgi bodies of early primary spermatocytes during spermatogenesis (Kornblatt *et al.*, 1974; Letts *et al.*, 1978; Kornblatt, 1979; Lingwood, 1985), and SGG is presumably transferred to the outer leaflet of the germ cell plasma membrane via vesicular transport (Vos *et al.*, 1994). Once synthesized, SGG remains stable throughout spermatogenesis and sperm epididymal transit (Kornblatt, 1979). These results corroborate the finding that degradation products of SGG are either found at very low amounts (e.g., GG) or totally absent (e.g., lysoSGG and lysoGG) in testes of fertile adult animals (Murray and Narasimhan, 1990). Moreover, SGG is the only glycolipid of freshly ejaculated pig sperm (Gadella *et al.*, 1993), and the sulfoglycolipid is stable during the initial phase of in vitro capacitation of epididymal mouse sperm. However, SGG becomes desulfated (~15%) following prolonged incubation in capacitation medium, at which time sperm undergo spontaneous acrosomal exocytosis (Tanphaichitr *et al.*, 1990). The physiological relationship between the desulfation of SGG and ZP-induced acrosomal exocytosis remains to be elucidated.

### *1.4.2. Role of SGG in Spermatogenesis*

SGG plays a vital role in the development of spermatogenic cells into sperm. This is deduced from the observation that the development of spermatogenic cells is arrested at the pachytene spermatocyte stage *in Cst* and *Cgt* knockout mice. These mice are infertile, and their testes are depleted of SGG. Although GG accumulates in the testes of the *Cst* knockout mice, GG does not compensate for the lack of SGG, nor does it rescue spermatogenesis. Pachytene spermatocytes undergo apoptosis, whereas

spermatogonia and Sertoli cells appear to be normal in the *Cgt* and *Cst* knockout mice (Fujimoto *et al.*, 2000; Honke *et al.*, 2002). These findings implicate a role for SGG in spermatogenesis and cell survival. However, the mechanism and extent of the involvement of SGG in this process remain to be determined. Interactions between layers of developing germ cells, and those of germ cells with Sertoli cells in the testicular seminiferous tubules are important for spermatogenesis (Sharpe, 1994). Since L-selectin is present in Sertoli cells (Freeman *et al.*, 2002), and since SGG binds specifically to L-selectin (review: Brockhausen and Kuhns, 1997), it is possible that SGG may mediate germ cell-Sertoli cell adhesion by binding to L-selectin. This interaction may be essential for the maintenance of the spermatogenic cell cycle.

### *1.4.3. Cellular Localization of SGG in the Mammalian Male Germ Cell*

It was initially reported that, amongst various tissues of adult male rats, the testis is the only synthesis site of SGG (Lingwood *et al.*, 1981). However, the brain was subsequently shown to synthesize SGG (Burkatt *et al.*, 1983), and characterization of brain lipids reveals the presence of small amounts of SGG in this tissue (Murray and Narasimhan, 1990; Pernber *et al.*, 2002). Indirect immunofluorescence (IIF) of frozen rat testis sections, using non-affinity purified rabbit anti-SGG IgG, reveal patchy staining patterns of SGG in fixed pachytene spermatocytes, and spermatids, but not in spermatogonia and Sertoli cells (Lingwood, 1981). Similar results are also described with loose spermatogenic cells released from minced rat testis (Lingwood *et al.*, 1981). Subsequently, Lingwood (1986) reported SGG immunofluorescent staining in the rat

epididymal sperm head. Using affinity purified rabbit polyclonal anti-SGG IgG antibody, patchy fluorescent staining patterns of SGG have been described in live mouse primary spermatocytes, round and elongated spermatids, as well as in testicular and epididymal sperm (Weerachatyanukul *et al.*, 2003; Tanphaichitr *et al.*, 2003b). Since SGG is present in isolated plasma membranes of rat spermatogenic cells (Shirley and Schachter, 1980), and since an antibody cannot cross the plasma membrane of live cells, SGG is likely localized to the outer leaflet of the plasma membrane of spermatogenic cells and sperm (Tanphaichitr *et al.*, 2003b). In fact, in mature mouse sperm (White *et al.*, 2000), human sperm (Weerachatyanukul *et al.*, 2001), SGG exists exclusively on the sperm head anterior plasma membrane overlying the acrosomal ridge and postacrosome. Furthermore, SGG localizes to the inner acrosomal membrane and postacrosome following acrosomal exocytosis (Tanphaichitr and Cyr, unpublished results). Biochemical studies demonstrate that SGG is present in isolated head anterior plasma membranes of pig, bull, stallion, and rooster sperm at appreciable amounts (i.e., < 10 mole% of total lipids, Parks and Lynch, 1992). Since the sperm head anterior is the ZP binding site (Yanagimachi, 1994; Chen and Cardullo, 1994; Kerr *et al.*, 2002), both IIF and biochemical results implicate a role for SGG in sperm-ZP binding.

### *1.4.4. Role of SGG in Sperm-Egg Interaction*

*In vitro* gamete binding assays reveal that SGG is a ZP adhesion molecule. Pretreatment of capacitated mouse sperm (White *et al.*, 2000) and human sperm (Weerachatyanukul *et al.*, 2001) with anti-SGG IgG or Fab inhibits sperm-ZP binding.

This binding is also inhibited following incubation of sperm and eggs with liposomes of SGG (isolated from ram testis), but not with liposomes consisting of GG or 3-*sn*-glycerophosphorylserine (PS) (negatively charged like SGG). In addition, SGG liposomes fluorescently labeled with *N*-rhodamine-conjugated 3-*sn*-phosphatidylethanol-amine (*N*-Rh-PE) bind directly to the ZP of intact mouse eggs and to isolated mouse ZP, in contrast to GG and PS liposomes. SGG-ZP binding is specific to unfertilized eggs, since this binding is not observed in fertilized mouse eggs (White *et al.*, 2000). All of these observations indicate that sperm surface SGG, specifically its sulfate group, plays a crucial role in sperm-ZP binding. Corroborating these results is the enrichment of SGG in Percoll-gradient centrifuged (PGC) mouse sperm (Furimsky, 2001), having high ZP affinity (Furimsky, 2001) and egg penetration ability (*mouse*: Tanphaichitr *et al.*, 1988; *pig*: Matas *et al.*, 2003). SGG also participates in sperm-egg plasma membrane binding, since mouse sperm pretreated with anti-SGG IgG/Fab have reduced ability to bind to the plasma membrane of ZP-free eggs (Ahnonkitpanit *et al.*, 1999). The significance of SGG in fertilization substantiates previous findings that development of anti-SGG antibodies in women is a cause of infertility (Tsuji *et al.*, 1992).

### *1.4.5. Arylsulfatase-A/P68, an SGG Binding Protein*

In spermatogenic cells and sperm, SGG coexists with sulfolipid immobilizing protein 1 (SLIP1) (Lingwood, 1985a; Lingwood, 1986). Purified SLIP1 (68 kDa) exhibits affinity to SGG and ATP (Law *et al.*, 1988; Lingwood and Nutikka, 1991) and to the ZP of intact eggs (Tanphaichitr *et al.*, 1993). SLIP1 consists of three proteins, a ZP

binding component, heat shock protein 70 (Hsp70), and albumin (Tanphaichitr *et al.*, 1998a, b, 1999; Carmona *et al.*, 2002a; Boulanger *et al.*, 1995). The ZP binding component of SLIP1 was initially termed P68. However, immunoblotting, tryptic peptide sequencing, and molecular cloning indicate that P68 is AS-A. Immunolocalization at both the light and electron microscopic levels reveals that AS-A binds to the mature mouse sperm head at sites where SGG is localized. Pretreatment of sperm with anti-SGG IgG/Fab inhibits the observed binding (Carmona *et al.*, 2002b). These results are astonishing since AS-A catalyzes the removal of the sulfate group of SGG in the presence of saposin B, i.e., physiological detergent required to solubilize SGG to access the active site of AS-A. To date, saposin B has not been found in the male reproductive tract or seminal plasma. It is therefore not surprising that AS-A and SGG colocalize to the same sperm head regions, and that SGG remains sulfated.

Characterization of the enzymatic properties of pig sperm surface AS-A reveals that the enzyme desulfates a small artificial substrate (*p*-nitrocatechol sulfate, NCS) and detergent solubilized SGG/SGC, at an optimum pH of 5. The $K_M$ values of sperm AS-A for these three substrates are very similar to those of human liver AS-A, although $V_{max}$ of purified sperm surface AS-A are consistently much lower. These findings indicate that AS-A is an active peripheral plasma membrane enzyme (Carmona *et al.*, 2002a). Given the low $V_{max}$ and high $K_M$ (90 μM) of SGG, desulfation of SGG should only occur when a high number of SGG molecules surround AS-A. Analysis of the three-dimensional structure of AS-A reveals that AS-A contains numerous positively charged amino acids on its surface (Lukatela *et al.*, 1998). This suggests that AS-A can bind to SGG non-enzymatically via electrostatic interactions. In fact, purified pig sperm AS-A binds to

SGG (isolated from ram testis) monolayers with a $K_d$ of 9 nM (Carmona *et al.*, 2002b), and this binding does not induce SGG desulfation. Structural modeling suggests that amino acids outside the active site pocket of AS-A are crucial for SGG binding: Arg143 and Phe204 of AS-A interact with the sulfate group and hydrophobic moiety of SGG, respectively (Tanphaichitr and Nyholm, unpublished results).

AS-A is known as a lysosomal enzyme in somatic cells (Hart *et al.*, 1987; Fujii *et al.*, 1992; Schierau *et al.*, 1999), and as an acrosomal enzyme in sperm (Dudkiewicz, 1984; Brandon *et al.*, 1997). Therefore, the presence of AS-A on the mature sperm head surface is unique (Tantibhedhyangkul *et al.*, 2002; Carmona *et al.*, 2002a). Recent results demonstrate that sperm surface AS-A originates from the epididymal fluid, and that AS-A is deposited onto the sperm surface via its high affinity to SGG (Weerachatyanukul *et al.*, 2003). Hsp70 is also present in the epididymal fluid (Miller *et al.*, 1992b), and it is presumably deposited via the same mechanism onto the sperm surface, as shown by immunogold labeling studies (Boulanger *et al.*, 1995). SGG on the sperm surface may be crucial for epididymal maturation, and SGG may function in capturing proteins that are beneficial for sperm fertilizing competence.

Accumulating evidence indicates that sperm surface AS-A is the ZP binding component of SLIP1 (Tantibhedhyangkul *et al.*, 2002; Carmona *et al.*, 2002a). Incubation of sperm with anti-AS-A IgG/Fab inhibits sperm-ZP binding. Purified P68 competitively inhibits sperm-ZP binding to minimal levels at very low concentrations (i.e., 10 nM) (Tanphaichitr *et al.*, 1998a). On the other hand, recombinant Hsp70 inhibits this binding at higher concentrations (>50 μM), with maximal inhibition accounting for only 50% of control values (Tanphaichitr *et al.*, 2003b). AS-A also binds directly and

specifically to mouse and pig ZP with a $K_d$ of 0.2 μM and 0.5 μM, respectively (Tantibhedhyangkul *et al.*, 2002; Carmona *et al.*, 2002a). The $K_d$ of AS-A binding to the ZP is higher than that described for mouse sperm-ZP binding (0.05-0.07 μM) (Thaler and Cardullo, 1996; Kerr *et al.*, 2001). This indicates that sperm-ZP binding is not only dependent on AS-A, and that AS-A and other ZP binding molecules on the sperm surface, including SGG, may participate in this binding event. In fact, AS-A binds with high affinity to SGG/SGC monolayers (Carmona *et al.*, 2002a), and fluorescently-labeled AS-A binds to sperm with a $K_d$ of 0.05 μM, in an SGG dependent manner (Weerachatyanukul *et al.*, 2003). Thus, SGG and AS-A may act as complexes in ZP binding due to their mutual high affinity. Sperm surface AS-A may first bind to the sulfated sugar residues of the ZP glycans. This will bring the ZP glycans next to the sperm surface to interact with SGG via carbohydrate-carbohydrate mediated interactions. Although these interactions are not as strong as protein-carbohydrate interactions, they may be stabilized by the multiplicity of SGG molecules. This postulated function of SGG in sperm-ZP binding is analogous to the involvement of gangliosides in cell adhesion events (Hakomori, 2000a, b), including trout sperm-egg interaction (Yu *et al.*, 2002). The $K_d$ of SGG-ZP binding will be determined for the first time in my thesis.

### *1.4.6. Biophysical Properties of SGG and Structurally Related Glycolipids*

Besides cell surface recognition (Hakomori, 1984, 1990), glycolipids are also implicated in membrane stabilization, shape determination, as well as ion binding for the negatively charged glycolipids (Curatolo, 1987a, b). Being commercially available, GC

and SGC have been extensively studied by differential scanning calorimetry (DSC), X-ray diffraction, FTIR spectroscopy, and atomic force microscopy (AFM) (Tupper *et al.*, 1992; Haas and Shipley, 1995; Nabet *et al.*, 1996; Attar *et al.*, 1998; Ohler *et al.*, 2001; Graf *et al.*, 2002), and thus served as structural analogs of SGG and GG. The structural properties of GC were first explored by X-ray crystallography, revealing that the galactose headgroup of GC is oriented parallel to the bilayer plane. This conformation involves extensive lateral interactions via hydrogen bonding between the amide groups of the ceramide backbone of GC and its galactosyl hydroxyl groups, thus imparting greater bilayer stability. The α-hydroxyl fatty acid in GC increases hydrogen bonding, and gives rise to a locked/shovel conformation of GC with respect to the hydrocarbon chain axis (Pascher and Sundell, 1977; Nyholm *et al.*, 1990; Bunow and Levin, 1980).

GC exhibits a complex phase behavior, characterized by very high hydrocarbon chain melting temperatures and by conversions between metastable and stable crystal-like bilayer phases, en route to the liquid-disordered phase (Larsson and Karlsson, 1972; Ruocco *et al.*, 1981; Curatolo, 1982; Curatolo and Jungalwala, 1985; Reed and Shipley, 1987, 1989; Haas and Shipley, 1995; Saxena *et al.*, 1999). GC also forms bilayer cylinders, tubules and ribbon-like, helically twisted structures, and the glycosphingolipid may help maintain myelin sheath stability by contributing to its curvature and cylindrical shape (Ohler *et al.*, 2001; Kulkarni *et al.*, 1995, 1999; Curatolo and Neuringer, 1986). In addition, the galactosyl headgroups of α-hydroxylated GC (HFA-GC) protrude at the air-water interface. This may confer additional stability to myelin sheath by offering multiple binding sites for complexation with ions or by favoring hydrogen bonding with apposed binding surfaces within myelin (Graf *et al.*, 2002). In fact, FTIR spectroscopy reveals

that GC and SGC play a role in adhesion between apposing extracellular surfaces of myelin, and in its stability and function via carbohydrate-carbohydrate mediated interactions (Koshy and Boggs, 1996; Koshy *et al.*, 1999; Boggs *et al.*, 2000). The role of GC/SGC in myelin maintenance is further strengthened by the finding that mice incapable of synthesizing these glycosphingolipids show myelin structural abnormalities (Bosio *et al.*, 1998; Coetzee *et al.*, 1998; Honke *et al.*, 2002).

Pressure tuning FTIR spectroscopy reveals extensive hydrogen bonding of SGG and SGC (Tupper *et al.*, 1992, 1994). SGG forms interdigitated bilayers, i.e., the hydrocarbon chains couple the outer leaflet to the inner leaflet of the bilayer, and interdigitation was reported to result in the formation of crystal-like bilayer structures of SGC (Nabet *et al.*, 1996) and GC (Bunow and Levin, 1980). SGG (Attar *et al.*, 2000) and SGC (Attar *et al.*, 1998; Boggs *et al.*, 1984, 1988a, b; Stevenson *et al.*, 1992) exhibit high phase transition temperatures, and both glycolipids increase the stability of DMPC model membranes, and form homogeneous bilayers with the saturated phospholipid (Attar *et al.*, 1998, 2000; Nabet *et al.*, 1996).

SGC and SGG may also participate in cation transport into cells (Hakomori, 1981; Karlsson *et al.*, 1974). Pressure tuning FTIR spectroscopy reveals that $Ca^{2+}$ binds to the sulfate moiety of SGC and SGG, most likely cross-linking neighboring molecules (Tupper *et al.*, 1992, 1994). The interactions of $Ca^{2+}$ with α-hydroxylated SGC induce conformational changes in the galactosyl headgroups of SGC, and this may be beneficial for interactions with other ligands at the cell surface (Menikh *et al.*, 1997). $Ca^{2+}$ is present on the sperm surface (Ruknudin, 1989) and in the female reproductive tract fluid. $Ca^{2+}$ is also required for capacitation (Kaul *et al.*, 1997; Fraser, 1998), sperm

hyperactivated motility (Yanagimachi, 1994; Suarez *et al.*, 1993; Suarez and Ho, 2003), acrosomal exocytosis (Fraser, 1993; De Blas *et al.*, 2002), sperm-ZP binding (Saling *et al.*, 1978), and sperm fusion with the egg plasma membrane (Yanagimachi, 1994; Fraser, 1987). The binding of SGG to $Ca^{2+}$ ions abolishes the interdigitated state of SGG bilayers, thus increasing the orientational disorder of their hydrocarbon chains (Tupper *et al.*, 1994). Such a phenomenon may result in increased bilayer disorder or "fluidity", proven relevant to fertilization-related events, e.g., capacitation and acrosomal exocytosis (Wolf *et al.*, 1986; review: Gadella and Harrison, 2000).

## 1.5. Raft Microdomains in Cellular Membranes

The Singer-Nicholson fluid mosaic model envisions cellular membranes as a fluid sea of lipids facilitating protein diffusion (Singer and Nicolson, 1972). Biophysical and cell biological approaches reveal that specific lipid species and proteins form segregate domains in the membrane, termed rafts (Figure 1.7). Rafts contain significant proportions of glycolipids, sphingolipids, cholesterol, and saturated phospholipids. Rafts also house GPI-anchored proteins, and cell adhesion and signaling molecules. As a result, rafts have been implicated in cell adhesion, signal transduction, and pathogenic invasion (reviews: Brown and London, 1998a, b, 2000; Simons and Ikonen, 1997; Simons and Toomre, 2000; van der Goot and Harder, 2001). The following sections summarize the biophysical and cell biological studies that came together to create and expand the raft concept.

**Figure 1.7.** Proposed organization of lipid microdomains (rafts) in the plane of the plasma membrane. In these diagrams, lipids in the liquid-ordered phase have black, bold acyl tails; the normal bilayer is in liquid-disordered phase, where lipids are depicted as having grey acyl chains. Cholesterol distribution reflects only a relative enrichment in the liquid-ordered phase; molecules are not drawn to scale. (**a**) Molecules are randomly distributed or clustered in such small microdomains, comprising just a few molecules (dashed boxes), that no appreciable FRET occurs between labelled raft components. Such domains would be too small to mediate a biological function. (**b**) Upper panel: rafts of intermediate size (~100 nm) in which the lipids might be in a liquid-ordered phase that is enriched in cholesterol. One such domain could accommodate up to a maximum of ~600 proteins, assuming a molecular mass of 50 kDa. Lower panel: raft size could be modulated by antibody-induced cross-linking (here, for simplicity, depicted as mediated by a single layer of bivalent antibodies against GPI-anchored proteins). (**c**) Upper panel: 'macrorafts' of the order of >500 nm in dimension in which the lipids might be in a liquid-ordered phase that is enriched in cholesterol. The membrane skeleton 'fence' might regulate the extent of raft development. Lower panel: model scenario in which the membrane skeleton fence confines laterally mobile intermediate-sized rafts to small regions of the plasma membrane defined by the effective mesh size of the fence (of the order of 500 nm). *Abbreviations:* FRET, fluorescence resonance energy transfer; GSL, glycosphingolipid (After Jacobson and Dietrich, 2001).

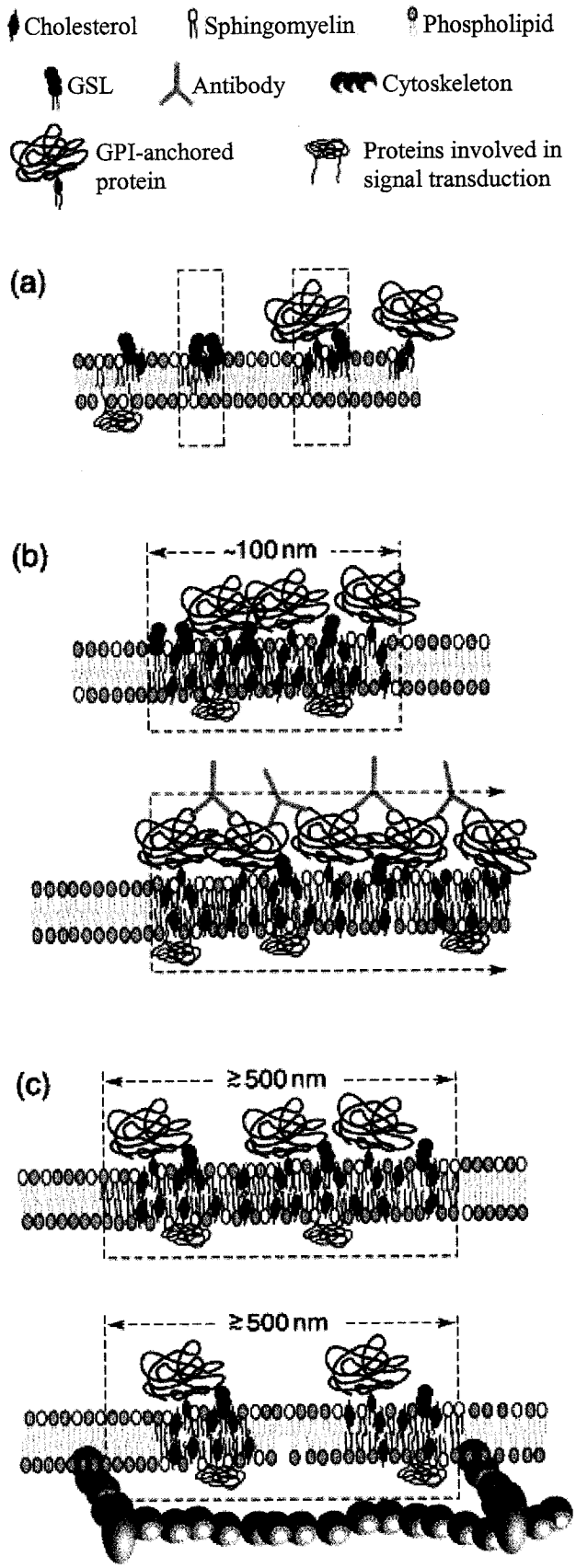
Cholesterol
Sphingomyelin
Phospholipid
GSL
Antibody
Cytoskeleton
GPI-anchored protein
Proteins involved in signal transduction
(a)
(b)
~100 nm
(c)
≥500 nm
≥500 nm

### *1.5.1. Role of Cholesterol and Glycolipids in Raft Formation*

In aqueous systems, lipids form various lamellar structures, depending on lipid species and composition, as well as temperature (Marsh, 1991; Tate *et al.*, 1991). The lamellar phases are biologically relevant; they consist of bilayer sheets of lipids separated by layers of water (Shinitzky, 1984). The various lamellar phases of lipid bilayers represent physical states that differ in the packing, the degree of hydrocarbon chain order/disorder, and the mobility of their lipid components (Marsh, 1991; Rietveld and Simons, 1998; Brown and London, 1998b). The two common phases of lipids are the "quasi-solid" gel phase ($L_\beta$) at low temperatures, and the "fluid" liquid-crystalline ($L_\alpha$) or liquid-disordered phase at high temperatures (Figure 1.8). In the gel phase, the hydrocarbon chains of lipids are in the all-*trans*, extended conformation. Lipids are highly ordered, densely packed and have reduced mobility in the bilayer plane. In the liquid-crystalline phase, the lipid hydrocarbon chains adopt non-extended conformations due to *trans-gauche* isomerization at their C–C bonds. In this phase, lipids exhibit high rotational and lateral mobility, and the bilayers are highly "fluid". Natural phospholipids generally contain polyunsaturated fatty acids, the kinked structure of which impedes straightening and tight packing of the hydrocarbon chains, thus promoting "fluid" phases (Kates, 1990). En route to the liquid-crystalline phase, lipids can also adopt a "crystal-like" ($L_c$) phase (Figure 1.8). The hydrocarbon chains are extended and tightly packed in this phase, and rotation about their long axes is severely restricted. In addition, the polar headgroup of lipids is poorly hydrated, and its motion strictly limited (Heller *et al.*, 1993).

In the presence of cholesterol, phospholipids and glycolipids adopt the liquid-ordered ($L_o$) phase, i.e., a state of intermediate fluidity between the gel phase and the

**Figure 1.8.** Lamellar phases adopted by phospholipids in aqueous systems: the gel ($L_\beta$) phase (**A**), liquid-crystalline ($L_\alpha$) or liquid-disordered phase (**B**), and crystal-like ($L_c$) phase (**C**). The cross-sectional area per polar headgroup is close to that of the hydrocarbon chains of the lipid in the lamellar phases. In the gel phase, the bilayer exhibits a structure where the hydrocarbon chains are rigid and planar. En route to the liquid-disordered state, lipids can also exist in the crystal-like phase. This phase is partially dehydrated, and the movement of the lipid hydrocarbon chains and the polar headgroups are severely restricted. In the liquid crystalline phase the hydrocarbon chains in the bilayer interior are highly disordered, undergoing motional fluctuations (Figure by Eric Martz with RasMol, and by Roger Sayle, available on line).

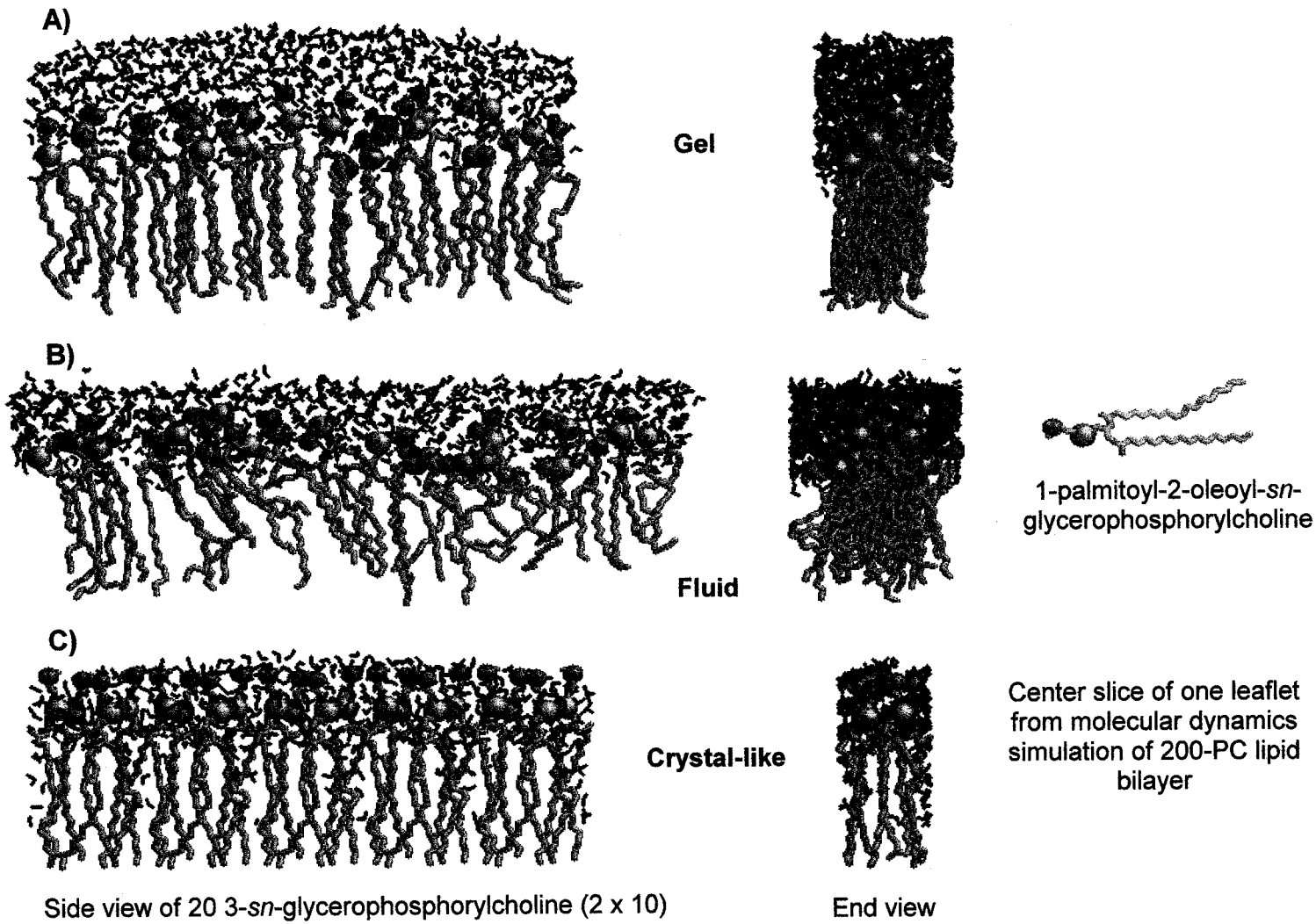
A)
Gel
B)
Fluid
1-palmitoyl-2-oleoyl-*sn*-glycerophosphorylcholine
C)
Crystal-like
Center slice of one leaflet from molecular dynamics simulation of 200-PC lipid bilayer
Side view of 20 3-*sn*-glycerophosphorylcholine (2 x 10)
End view
Water
Nitrogen
Phosphorus
Other atoms in phospholipids

liquid-crystalline "fluid" phase. In the bilayer matrix, cholesterol intercalates its rigid and planar hydrophobic steroid ring structure between the hydrocarbon chains of phospholipids and glycolipids, with its hydroxyl group oriented towards the water phase. As a result, the hydrocarbon chains of these lipids are extended and tightly packed with cholesterol in the liquid-ordered phase, similar to those in the gel phase, but nevertheless laterally diffuse and exhibit rotational mobility in the plane of the membrane (Ipsen *et al.*, 1987, 1989; Sankaram and Thompson, 1990, 1991; Vist and Davis, 1990).

The liquid-ordered and liquid-crystalline phases can coexist within a single bilayer. Fluorescence quenching measurements, which monitor lipid lateral distribution at the nanometer scale, reveal that cholesterol and saturated lipids form laterally segregated liquid-ordered domains in a bilayer matrix of unsaturated phospholipids (Silvius *et al.*, 1996; Ahmed *et al.*, 1997; Xu and London, 2000; Xu *et al.*, 2001). In addition, saturated acylated proteins selectively partition into liquid-ordered domains (Wang and Silvius, 2000, 2001; Wang *et al.*, 2000, 2001). This indicates that the saturated character of lipids/proteins plays a crucial role in their preferential partitioning into liquid-ordered domains. However, monounsaturated phospholipids still exhibit an affinity for liquid-ordered domains (Wang *et al.*, 2000; Fridriksson *et al.*, 1999). Freeze-etch electron microscopy (Rock *et al.*, 1990) and fluorescence microscopy (Spiegel *et al.*, 1984) reveal the formation of glycosphingolipid clusters in PC bilayers and lymphocytes, respectively. Fluorescence spectroscopy using non-perturbing lipid probes also show that sphingolipids form separate domains in unsaturated PC bilayers (Silvius, 1992). In this aspect, the high hydrocarbon chain melting temperature of sphingolipids and the hydrogen bonding of glycosphingolipids, compared with glycerolipids, reveals

differences in the physical properties that could play a role in the formation of separate domains in the plasma membrane. Accordingly, it was suggested that cholesterol and glycolipids/saturated phospholipids form segregate domains, termed rafts, existing in a liquid-ordered phase in the liquid-disordered/"fluid" cellular membrane (reviews: Simons and Ikonen, 1997; Simons and Toomre, 2000; Brown and London, 1998a, b, 2000).

### *1.5.2. The Raft Hypothesis Stems from Studies on Polarized Epithelial Cells*

Epithelial cells are morphologically and functionally polarized, consisting of apical and basolateral compartments. Each epithelial cell layer is linked to its neighbors by intracellular junctions, including tight junctions that form the permeability barrier between epithelial cells. Experiments using different probes show that tight junctions also form a fence that prevents lipid molecules in the outer leaflets from diffusing across the boundary between the apical and basolateral membranes (van Meer and Simons, 1986; Spiegel *et al.*, 1985). As a result, the apical membrane of epithelial cells is chemically and functionally distinct from the basolateral membrane (review: Simons and van Meer, 1988). Lipid analyses on viruses budding through either the apical or basolateral membranes of infected host epithelial cells (van Meer and Simons, 1982, 1986) reveal that the apical membrane is enriched, relative to the basolateral membrane, in glycosphingolipids at the expense of 3-*sn*-glycerophosphorylcholine (PC). In addition, the cholesterol to phospholipid ratio is higher in the apical plasma membrane of intestinal epithelial cells (review: Simons and van Meer, 1988). It was postulated that the

difference in composition of the apical and basolateral membranes is due to the sorting of proteins and lipids in the Golgi complex and *trans*-Golgi membranes.

Sphingolipids are synthesized in endoplasmic reticuli (ER) and Golgi bodies. The ER and Golgi are connected via anterograde and retrograde vesicular pathways. The enrichment of sphingolipids in the apical membrane is explained by lateral segregation from phospholipids in the Golgi membrane, and exclusion from retrograde transport vesicles. The newly reported tight connection between the trans cisternae of the Golgi and ER may allow cholesterol to pass from the ER directly into the trans Golgi, where it might induce or stabilize lateral phase segregation (reviews: van Meer, 1989, 2000; van Meer and Lisman, 2002). Ceramide destined for sphingolipids synthesis may also enter the Golgi by this direct pathway, as its route is different from the ER–Golgi vesicular pathway (Fukasawa *et al.*, 1999). Glycosphingolipids exhibit strong hydrogen bonding networks (Pascher, 1976; Tupper *et al.*, 1992) and form clusters in model and native membranes (Rock *et al.*, 1990; Thompson and Tillack, 1985). In addition, glycosylphosphatidylinositol (GPI)-anchored proteins are also selectively found at the apical surface of epithelial cells both *in vivo* and *in vitro* (Lisanti *et al.*, 1989). Therefore, glycosphingolipids/cholesterol-rich clusters or rafts may form in the Golgi, and that these microdomains may act as platforms to target GPI-anchored proteins to the apical plasma membrane (reviews: Simons and van Meer, 1988; van Meer and Lisman, 2002). This concept gained experimental credibility by the recent finding that rafts, containing GPI-anchored proteins and glycosphingolipids, cycle rapidly between the cell surface and the Golgi complex (Nichols *et al.*, 2001).

### *1.5.3. Biochemical Isolation of Rafts and Their Components*

Sphingolipids (Hagmann and Fishman, 1982; review: Anderson, 1998) and GPI-anchored proteins (Hoessli and Rungger-Brandle, 1985; Hooper and Turner, 1988) are insoluble in Triton X-100 in the presence of cholesterol. In a landmark paper, Brown and Rose (1992) used this insolubility criterion and pulse-chase experiments to track the biosynthetic transport of the GPI-anchored protein alkaline phosphatase from the ER to the apical cell surface. This protein becomes insoluble in 1% Triton X-100 at 4°C during biosynthetic transport. Moreover, ninety percent of nascent alkaline phosphatase acquires resistance to Triton X-100 and endo-$\beta$-*N*-acetylglucosaminidase H (endo H) by the time their *N*-oligosaccharide chains matured. This indicates that this protein becomes detergent insoluble in the Golgi apparatus. Following sucrose density gradient ultracentrifugation of the Triton X-100 cell extracts, mature alkaline phosphatase was found in lipid-rich, low-density membrane fractions. These are vesicles of varied sizes, but typically hundreds of nanometers in diameter. Relative to whole cell lipids, the vesicles were enriched in cholesterol and sphingolipids. The molar ratio of phospholipids:sphingolipids:cholesterol was 1:1:1, and this ratio has become the canonical "lipid raft" mixture used for model membrane studies (Brown and Rose, 1992; review: Edidin, 2003). Combined together, these findings suggest that the GPI-anchored protein alkaline phosphatase becomes detergent-insoluble upon association with lipid microdomains in the Golgi on its way to the apical cell surface. These observations corroborate the "raft concept" put forth by Simons and colleagues (reviews: Simons and van Meer, 1988; van Meer *et al.*, 1987), and reveal that detergent insolubility at low temperatures, combined with flotation in a density gradient (Brown and Rose, 1992),

provides a useful means to gain further insight into the biological significance of rafts. This isolation procedure is widely used to biochemically analyze rafts from living cells, with the terms detergent insoluble membranes (DIM) and rafts being used interchangeably (review: Brown and London, 2000).

Rafts are not "aggregation artifacts" formed due to selective solubilization of membrane lipids by the detergent at low temperatures. Rafts were isolated from a mixture of two cell populations: one isotopically labeled with amino acids, and the other treated with cholesterol-binding molecules to disrupt rafts. The isolated rafts only contained the radiolabeled proteins (Foster *et al.*, 2003). Rafts were also isolated at 37°C using the detergent Brij98 (Drevot *et al.*, 2002; Braccia *et al.*, 2003), and this method generated rafts with similar lipid and protein composition to those isolated with Triton X-100 at 4°C. Combined together, these findings exclude the possibility that low-temperature solubilization induces lipid phase transitions to artificially create detergent-insoluble protein-lipid complexes.

Initially, rafts were considered identical to caveolae, flask shaped membrane invaginations in endothelial and epithelial cells. This was based on the finding that caveolae and rafts are insoluble in 1% Triton X-100 at 4°C, and both membrane domains contain sphingolipids, cholesterol, and caveolin-1, a cholesterol binding protein and caveolae marker (reviews: Smart *et al.*, 1999; Simons and Toomre, 2000). However, rafts have been separated from caveolin-enriched membrane domains in mouse melanoma cells (Iwabuchi *et al.*, 1998a). Rafts have also been isolated from cells containing no caveolae (Fra *et al.*, 1994), indicating that rafts are distinct and caveolae-independent membrane domains.

To date, rafts have been isolated as DIM from cells of vertebrates, invertebrates, plants, and fungi. Consistently, these isolated rafts contain glycolipids, sphingolipids and cholesterol, and in some cases sterols other than cholesterol (Iwabuchi *et al.*, 1998a, b; Fra *et al.*, 1994; Kubler *et al.*, 1996; Rietveld and Simons, 1998; Rietveld *et al.*, 1999; review: Simons and Toomre, 2000). Another criterion used to isolate rafts is based on their resistance to high pH/carbonate. However, this method is not widely, compared with detergent insolubility at low temperatures. Specifically, signature raft molecules, e.g., glycosphingolipids, cholesterol, and GPI-anchored proteins, are obtained with both methods (Iwabuchi *et al.*, 1998a, b; Foster *et al.*, 2003). The enrichment of cholesterol and glycosphingolipids in rafts suggests that these molecules play an important role in the formation and stabilization of rafts. In fact, cholesterol sequestration and depletion by treating cells with filipin and M$\beta$CD, respectively, disrupts raft integrity. In addition, inhibition of cholesterol biosynthesis with lovastatin reduces raft formation (review: Simons and Toomre, 2000). However, cholesterol removal from living cells is reported to induce large-scale domain segregation (Hao *et al.*, 2001). Cholesterol-independent rafts exist in fibrosarcoma and epidermoid carcinoma cell lines (Claas *et al.*, 2001; Berditchevski, 2001), and in microvillar membranes of enterocytes (Braccia *et al.*, 2003b; Hansen *et al.*, 2001). Rafts also exist in cells deficient in glycosphingolipid synthesis; this mutant cell line exhibits an upregulation of sphingomyelin presumably to compensate for the lack of glycosphingolipids (Ostermeyer *et al.*, 1999). In addition, monosialogangliosides $GM_1$ and $GM_3$ reside in two distinct types of rafts in T-cells (Gomez-Mouton *et al.*, 2001). All of these findings indicate that various types of rafts, with different lipid and protein composition, may exist in a given cell.

While most raft lipids are important for the structural integrity of these membrane domains, raft proteins are implicated in the biological functions of rafts (Table 1.4). Given the small size of elementary raft units (see below), a given raft can only contain a low number of proteins. In the first functional proteomic analysis of rafts, quantitative high-resolution mass spectrometry was used to specifically detect raft proteins. These results reveal a set of 241 authentic raft component proteins, including a large proportion of signaling molecules, which were enriched in rafts versus total membranes (Foster *et al.*, 2003). Raft components include cell adhesion molecules, GPI-anchored proteins, and doubly acylated cytoplasmic signaling proteins, e.g., specific members of the Src-family kinases, and $G_{\alpha}$ subunits of heterotrimeric GTPases. Some transmembrane and integral membrane proteins are also present in rafts (Foster *et al.*, 2003; reviews: Simons and Toomre, 2000; van der Goot and Harder, 2001). It was recently reported that these proteins are targeted to rafts via a cholesterol/sphingolipid-rich "lipid shell", which defines the molecular address for raft-destined proteins. Theoretically these shells have an estimated diameter of 7 nm, and contain about 80 lipid molecules that act as a local solvent for the single protein they harbor (review: Anderson and Jacobson, 2002). Cross-linking of the GPI-anchored protein CD59 or $GM_1$ in lymphoid cells results in the accumulation of F-actin in these patches (Harder and Simons, 1999). Rafts also selectively house $PIP_2$, which binds to actin. This suggests that $PIP_2$ may promote actin recruitment into rafts. In addition, $PLC_{\gamma 1}$ is also present in rafts, indicating that rafts may be the sites of $PIP_2$ hydrolysis by $PLC_{\gamma 1}$ (Harder and Simons, 1999; review: Caroni, 2001).

**Table 1.4. Raft Associated Molecules**

| Type | Specific Molecules | References |
|---|---|---|
| **Cell adhesion molecules** | Monosialoganglioside $GM_1$ and $GM_3$;<br>Transient axonal glycoprotein (TAG-1);<br>Contactin | Dietrich *et al.*, 2001; Yamamura *et al.*, 1997; Iwabuchi *et al.*, 1998; Harder and Simons, 1999; Moffett *et al.*, 2000; Faivre-Sarrailh *et al.*, 2000; Kasahara *et al.*, 2000. |
| **GPI-anchored proteins**[a] | Placental alkaline phosphatase (PLAP);<br>Thy-1; Ly-6; CD55; CD59 | Brown and Rose, 1992; Harder *et al.*, 1998; Harder and Simons, 1999; Dietrich *et al.*, 2001; review: Horejsi, 2003. |
| **Transmembrane and integral membrane proteins** | Influenza virus hemagglutinin (HA);<br>Transmembrane adaptor proteins LAT;<br>Galectin; Tetraspanin proteins; Caveolins; Flotilins;<br>Several members of the tumor necrosis factor (TNF)-receptor family;<br>$G_i$-protein coupled receptors family;<br>Tyrosine kinases receptors;<br>Low-density lipoproteins (LDL) receptor family | Claas *et al.*, 2001; Berditchevski, 2001; Schlegel and Lisanti, 2001; Foster *et al.*, 2003; reviews: Smart *et al.*, 1999; Horejsi, 2003; Pike, 2003. |
| **Cytoplasmic signaling molecules** | Src-family tyrosine kinases[b], i.e., Fyn, Lck, Yes, and Lyn; Syk tyrosine kinases; Regulatory subunits of heterotrimeric G proteins[b]; Small GTP-binding proteins, e.g., Ras, Rab, Rho, Arf;<br>$PIP_2$; $PLC_{\gamma 1}$ | Foster *et al.*, 2003; Gupta and DeFranco, 2003; reviews: Caroni, 2001; van der Goot and Harder, 2001; Horejsi, 2003 |
| **Cytoskeletal components** | F-actin | Harder and Simons, 1999; review: Caroni, 2001. |

[a] The hydrocarbon chains of GPI-anchored proteins are generally saturated in line with their affinity for ordered membrane domains or rafts (McConville and Ferguson, 1993).

[b] These doubly acylated proteins may anchor in the cytoplasmic leaflet of rafts via their saturated acyl chains, most likely palmitic and myristic acid (review: van der Goot and Harder, 2001).

Although DIM analysis is invaluable to identify raft components, and to determine parameters that affect partitioning of proteins and lipids into rafts, caution is required when using detergent solubilization of membranes. Membrane lipids or proteins with a weak affinity for liquid-ordered phases may not be detected in DIM (reviews: Brown and London, 1998b; van der Goot and Harder, 2001). Preparation of DIM may also affect the structural organization of native membranes, and thus provoke coalescence of different raft domains (Mayor and Maxfield, 1995). Particularly, co-fractionation of two proteins in DIM does not imply that these two proteins reside in the same membrane domain.

### *1.5.4. Rafts are Liquid-Ordered Domains*

Schroeder *et al.* (1994) demonstrated that, following treatment of lipid mixtures with Triton X-100 at 4°C, cholesterol, sphingolipids and GPI-anchored proteins partition in the insoluble fraction, and unsaturated phospholipids in the detergent-soluble fraction. The high phase transition temperature of sphingolipids, and the interactions between the saturated hydrocarbon chains promote the formation of Triton X-100 insoluble lipid-protein mixtures in the presence of cholesterol. Fluorescence depolarization of cholesterol and sphingolipid containing liposomes, using the fluorescent probe diphenyl-hexatriene, reveals that these liposomes were about as fluid as DPPC-cholesterol liposomes, but much less fluid than 1, 2-dioleoyl-*sn*-glycerophosphorylcholine (DOPC) liposomes or DOPC-cholesterol liposomes. This indicated that cholesterol/sphingolipid-rich liposomes exist in the liquid-ordered phase (Schroeder *et al.*, 1994). Using fluorescent lipid analogs, fluorescence microscopy reveals that cholesterol/sphingolipid-

rich domains coexist with fluid lipid regions in planar-supported monolayers/bilayers composed of phospholipids-cholesterol-sphingomyelin (equimolar ratio) or extracted brush border membrane lipids. These cholesterol/sphingolipid-rich domains are resistant to Triton X-100 extraction, and exhibit characteristics of the liquid-ordered phase (i.e., they are fluid-like), although diffusion of the fluorescent probes in these domains is slower than in the coexisting fluid regions (Dietrich *et al.*, 2001a). Interestingly, rafts isolated from cells as DIM form rat basophilic leukemia (RBL)-2H3 mast cells also exhibit typical signatures of liquid-ordered phases, i.e., high degree of acyl chain order, but substantial rotational and lateral mobility (Ge *et al.*, 1999). These studies indicate that rafts may exist in the liquid-ordered phase in cellular membranes (reviews: Brown and London, 1998b, 2000; Silvius, 2003).

### *1.5.5. Detection and Dynamics of Rafts in Cells*

To probe the dynamics and size of rafts in cellular membranes, the local diffusion of single raft components and proximity measurements between these components have been assessed. Photonic force microscopy reveals that raft components, i.e., GPI-anchored proteins and influenza virus HA, have restricted diffusion in fibroblasts, and are stably associated to a basic cholesterol-dependent raft-like lipid assembly with an average diameter of 26 ± 13 nm (Pralle *et al.*, 2000). Other single particle tracking studies define relatively large (350 nm diameter) confinement zones for GPI-anchored proteins in fibroblasts (Sheets *et al.*, 1997). Tracing the movement of single fluorescent lipid analogs on smooth muscle cells also reveals that a saturated raft lipid probe (i.e., 1, 2-

dimyristoyl-*sn*-glycerophosphorylethanolamine, DMPE), was confined to large domains (0.2-2 μm). In contrast, a monounsaturated non-raft lipid probe (i.e., 1, 2-dioleoyl-*sn*-glycerophospho-ethanolamine, DOPE), shows very little confinement (Schutz *et al.*, 2000). Further evidence for the existence of rafts in cellular membranes stems from FRET measurements (Varma and Mayor, 1998) and chemical cross-linking (Friedrichson and Kurzchalia, 1998; Harder *et al.*, 1998; Janes *et al.*, 1999). These studies reveal that the distance between GPI-anchored proteins is unaffected by their level of expression, and the coupling between these proteins is sensitive to cholesterol depletion. This strongly indicates that GPI-anchored proteins are clustered in small microdomains. All these findings reveal that specific classes of lipids and proteins are confined within cholesterol-dependent raft domains physically separated from the bulk membrane. To date, the dimensions of rafts vary from 50 nm to more than 1 μm, depending on the cell type and the methods employed (review: Anderson and Jacobson, 2002).

Recent diffusion measurements used a laser trap to confine molecules labeled with beads to small areas (<100 nm diameter), and then followed the motion of the beads around their position. These results show that rafts diffuse in the membrane plane, and that GPI-anchored proteins remain raft-bound up to 10 min (Pralle *et al.*, 2000). Another group measuring diffusion of raft markers in cellular membranes was unable to detect diffusion of the raft entities, as opposed to individual components of rafts (Kenworthy *et al.*, 2000). Single particle tracking was also employed to compare the movement of the GPI-linked protein, CD59, and 1, 2-dioleoyl-*sn*-glycerophosphorylcholine (DOPC), which is typically excluded from rafts. With a time resolution of 25 μs, both GPI-anchored proteins and DOPC visit frequently (every 25 ms) cellular compartments (110

nm). From the identical behavior of the two classes of molecules, it was concluded that, at steady state, these core lipid rafts consist of only a few molecules and persist for 1 ms or less. However, when CD59 is cross-linked with antibody or its native ligand, larger rafts developed with a diffusion coefficient about eightfold smaller than that of core rafts. Cross-linked CD59 is frequently immobilized, and the immobilized rafts were associated with actin and signaling kinases (Suzuki *et al.*, 2002; Fujiwara *et al.*, 2002).

Rafts diffuse freely in the cell membrane and coalesce into larger functional structures when their constituents are ligated and oligomerized (GPI-anchored proteins) (reviews: Edidin, 2003; Subczynski and Kusumi, 2003). Rafts may be further stabilized by components of the cytoskeleton. F-actin accumulates in clusters of GPI-anchored proteins and $GM_1$ (Harder and Simons, 1999), and $PIP_2$ serves as an attachment site for F-actin in cells (reviews: van der Goot and Harder, 2001; Caroni, 2001). In fact, fluorescence microscopy reveals that membrane rafts are assembled following association with the actin cytoskeleton (Rodgers and Zavzavadjian, 2001). This association may also result in the recruitment of signaling molecules (Gupta and DeFranco, 2003; review: Caroni, 2001).

### *1.5.6. Biological Significance of Rafts and their Functions*

Because DIM house adhesion and signaling molecules, rafts have been implicated in cell-cell adhesion and signal transduction. In addition, cholesterol depletion disrupts rafts formation, reduces the segregation of signaling molecules into rafts, and affects signaling events (reviews: Simons and Ikonen, 1997; Brown and London, 1998a; Simons

and Toomre, 2000). Cross-linking of GPI-anchored proteins and glycolipids by antibodies or ligands may induce redistribution or clustering of G proteins and Src-family kinases on the cytoplasmic side, thus initiating signaling cascades (Moffett *et al.*, 2000; review: Horejsi, 2003). In fact, cross-linking of GPI-anchored proteins and glycolipids in lymphoid cells results in the formation of raft patches, which accumulate the Src-family tyrosine kinase Lck and F-actin. The accumulation of F-actin in these raft membrane patches requires tyrosine phosphorylation. It was suggested that, under physiological conditions, F-actin may stabilize rafts on the cytoplasmic side, and organize an architecture allowing different components of the signaling machinery to interact with each other (Harder and Simons, 1999). Rafts are implicated in signaling events associated with immunoreceptors. The T- cell antigen receptor (TCR), the B-cell antigen receptor (BCR), and Fc receptors, as well as crucial components of their respective signaling pathways, associate with rafts following ligand binding in mouse thymocytes and splenic T-lymphocytes, and RBL-2H3 cells (Holowka *et al.*, 2000; Drevot *et al.*, 2002; Gupta and DeFranco, 2003; review: Langlet *et al.*, 2000). The TCR promotes coalescence of rafts in the membrane, and induces the segregation of raft lipids and key signaling effectors (e.g., Fyn and Lck Src-kinases) through a mechanism involving reorganization of the actin cytoskeleton in Jurkat T-cells (Valensin *et al.*, 2002). In addition, the dynamics of rafts and early events associated with BCR signaling are visualized microscopically on primary mouse splenic B-lymphocytes and mature mouse B-cell line Bal 17. Rafts colocalize with the BCR, and the tyrosine kinase Syk, and these units laterally diffuse at the cell surface, and coalesce into larger patches. Stimulation of the BCR induces the formation of long, thread like filopodial projections, rich in lipid

rafts and F-actin. Rafts were thus suggested to play a role in communication and/or transportation of signaling molecules in B-cells during an immune response (Gupta and DeFranco, 2003).

Over the last years, it has become apparent that many pathogens (bacteria, parasites, and viruses) and toxins utilize rafts to interact with their target cell. The Gag protein of HIV-1 binds to rafts in HeLa cells, and cholesterol depletion disrupts this binding, and inhibits virus particle production and infectivity. This indicates that the binding of Gag to rafts is an important step in HIV-1 replication (Ono and Freed, 2001). Treatment of COS-1 cells with unsaturated fatty acids, which does not alter intracellular protein trafficking nor cell viability, results in the exclusion of Gag from rafts, and inhibits HIV assembly in host cells (Lindwasser and Resh, 2002). Interestingly, a common sphingolipid-binding domain was identified in the V3 loop of the HIV-1 surface envelope glycoprotein gp120, Alzheimer $\beta$-amyloid peptide, and human prion protein (Mahfoud *et al.*, 2002). This suggests that these proteins bind to sphingolipids in rafts. Rafts isolated from insects are (*a*) enriched in several receptors of Cry1A, the major protein of parasporal crystals produced by *Bacillus thuringiensis*, as well as (*b*) involved in Cry1A toxin binding to the midgut epithelium and subsequent pore formation (Zhuang *et al.*, 2002). Rafts also act as portals for entry of bacterial toxins, such as cholera toxin, the B subunit of which binds to the lipid-raft $GM_1$ (Wolf *et al.*, 2002). All these findings underscore the role of rafts as a site of pathogenic attacks. These units may concentrate receptors for certain pathogens/toxins, thereby either increasing binding affinity or promoting toxin oligomerization. In addition, certain pathogens/toxins may exploit the signaling capacity of raft domains by binding to, and probably clustering, raft-associated

receptors. These signaling patches may provide entry pathways for these organisms/proteins into the cell, possibly by utilizing the ability of rafts to accumulate F-actin. From the cytoplasmic side of the plasma membrane, rafts may provide sites for assembly and budding of these viruses (review: van der Goot and Harder, 2001).

### *1.5.7. Current State of Knowledge about Rafts in Gametes*

The insolubility of raft membranes in 1% Triton X-100 at 4°C has also been used as a criterion for the isolation of rafts from gametes (Ohta *et al.*, 1999a, b, 2000; Luria *et al.*, 2002; Travis *et al.*, 2001; Nishimura *et al.*, 2001; Honda *et al.*, 2002; Sato *et al.*, 2002). Ohta *et al.* (1999a) isolated rafts from sea urchin sperm. These rafts contain cholesterol and more than 50% of the total amounts of glycosphingolipids (including gangliosides and SGC) in sea urchin sperm. Sea urchin sperm rafts house egg binding ligands (e.g., 80 kDa speract receptor and 210 kDa REJ-1) and cell signaling proteins (e.g. adenylyl cyclase, guanylyl cyclase, $G_{s\alpha}$ and PKA), and these microdomains bind to egg rafts via carbohydrate-carbohydrate mediated interactions (Ohta *et al.*, 1999b, 2000). Sea urchin sperm rafts also bind to the 350-kDa sperm binding protein of the egg vitelline layer, and their lipids, i.e., sialyated gangliosides and SGC, play an important role in this binding (Maehashi *et al.*, 2003). These results implicated a role for rafts in cell-cell adhesion and subsequent signaling events during fertilization. Rafts were also isolated form mature mouse and guinea pig sperm, and shown to contain caveolin-1. Since immunofluorescence reveals that caveolin-1 was localized to regions of the acrosome and flagellum in both mouse and guinea pig sperm, it was suggested that rafts and caveolin-1

may play a role in signaling cascades associated with capacitation, flagellar motility, and acrosomal exocytosis (Travis *et al.*, 2001). In addition, proteins encoding $Ca^{2+}$ channels for sperm capacitation (i.e., trp 1-7) were also present in mouse sperm rafts, also implicating a possible role of rafts during capacitation (Trevino *et al.*, 2001). Mouse sperm rafts have also been reported to house ZP-binding proteins (e.g., GPI-linked PH-20) and egg plasma membrane binding proteins (e.g., fertilin α and cyritestin) (Nishimura *et al.*, 2001). All of these findings suggested that sperm rafts may represent a platform of molecules involved in the sequential events of fertilization.

Rafts were also isolated from *Xenopus* eggs, and shown to contain cholesterol, $GM_1$ monosialoganglioside, and signaling molecules (e.g., *Xenopus* egg Src (Xyk), Gqα, Ras, integrin β1 and CD9). Fertilization of *Xenopus* eggs stimulated tyrosine phosphorylation of Xyk and other raft proteins *in vitro*. Pretreatment of eggs with MβCD reduces cholesterol levels, and inhibits raft formation and sperm-induced tyrosine phosphorylation in *Xenopus* egg rafts. These findings suggest that rafts are required for signalling in *Xenopus* egg during fertilization (Sato *et al.*, 2002). Interestingly, membrane domains were isolated from *Xenopus* eggs without the use of a detergent, and shown to have similar protein and lipid composition to DIM or rafts (Luria *et al.*, 2002). These results suggested that rafts isolated from *Xenopus* eggs are not "low-temperature Triton X-100 artefacts", thus further strengthening the existence of rafts *in situ*.

Conclusively, the existence of rafts in gamete cells, as well as the presence of adhesion and signaling proteins in these membrane domains (Ohta *et al.*, 2000; Nishimura *et al.*, 2001; Sato *et al.*, 2002) indicates that gamete rafts share common characteristics with rafts isolated from somatic cells. This also suggests that gamete rafts

may participate in cell-cell interaction and subsequent signal transduction events. Although mammalian sperm rafts house ZP and egg plasma membrane binding molecules (Nishimura *et al.*, 2001), a direct involvement of these membrane domains in ZP binding remains to be elucidated.

## 1.6. Research Hypotheses

In this thesis, we hypothesize that mammalian sperm rafts contain the ZP binding domains. Cholesterol is an important structural component of rafts (Simons and Toomre, 2000; Silvius, 2003). However, cholesterol efflux from the sperm plasma membrane during capacitation (Flesch *et al.*, 2001 review: Visconti *et al.*, 2002) raises the question whether the integrity and levels of rafts are affected in capacitated sperm. The question whether rafts isolated from capacitated sperm exhibit higher ZP binding ability than rafts isolated from non-capacitated sperm should also be addressed.

Intermolecular hydrogen bonding between glycolipids (reviews: Simons and Toomre, 2000; Hakomori, 2000), and interactions between the saturated hydrocarbon chains of lipids (Schroeder *et al.*, 1994; Ahmed *et al.*, 1997; reviews: Brown and London, 1998b, 2000) play a key role in the formation of rafts in cellular membranes. The sperm plasma membrane contains appreciable levels of the male germ cell specific sulfoglycolipid SGG (Murray and Narasimhan, 1990; Ishizuka, 1997), and significant amounts of polyunsaturated phospholipids (Cooper and Yeung, 1997; Flesch and Gadella, 2000). SGG is predominantly saturated, and the sulfoglycolipid exhibits strong intermolecular hydrogen bonding networks (Tupper *et al.*, 1994; Attar *et al.*, 2000). SGG is also a ZP adhesion molecule, and the sulfoglycolipid participates in sperm-ZP binding

(White *et al.*, 2000; Weerachatyanukul *et al.*, 2001). All these properties suggest that SGG is a component of mammalian sperm rafts; SGG may partake in sperm rafts formation by interacting preferentially with cholesterol and saturated phospholipids, two components found in common in raft membranes, via strong hydrogen bonding and van der Waals interactions, respectively. Being a ZP adhesion molecule, SGG may also contribute to sperm raft-ZP binding.

## 1.7. Research Objectives

The following specific aims were undertaken to verify our hypothesis. (*a*) The biophysical properties of SGG and its structural analogs (i.e., SGC and GC), and the interaction of SGG with raft lipids, i.e., cholesterol and saturated phospholipids, was investigated by FTIR spectroscopy to gain further insight into the contribution of SGG to the formation of sperm rafts. (*b*) Rafts were characterized from pig sperm since it can be obtained in quantity, and since all pig ZP sulfoglycoproteins involved in sperm binding have been characterized (Mori *et al.*, 2000; Nakano and Yonezawa, 2001; Takasaki *et al.*, 1999; Tulsiani and Abou-Haila, 2001), and can also be prepared in quantity as well. The binding of sperm rafts to fluorescently labeled homologous ZP (Alexa-430 ZP) was investigated using the microtiter plate assay. The dependence of this binding on pig ZP3 sulfoglycoproteins (i.e., ZP3α and ZP3β, shown to play a role in ZP binding, Sacco *et al.*, 1989; Yurewicz *et al.*, 1993, 1998) was also studied by including various amounts of unlabeled ZP sulfoglycoproteins in the sperm rafts-Alexa-430 ZP co-incubates. (*c*) If SGG is a sperm raft component, the role of this ZP adhesion molecule in sperm raft-ZP binding will be assessed following pretreatment of sperm rafts with anti-SGG IgG/Fab.

# CHAPTER TWO

## MATERIALS AND METHODS

### Materials

The enhanced chemiluminescence (ECL) Western blotting detection kit was obtained from Amersham Pharmacia Biotech (Piscataway, NJ, USA). Perdeuterated DMPC ($DMPC_{d54}$) and DPPC ($DPPC_{d62}$), and 1-palmitoyl-2-docosahexaenoyl-*sn*-glycerophosphorylcholine (16:0/22:6-PC or PDPC) were purchased from Avanti Polar Lipids (Alabaster, AL, USA), and used without further purification. Sodium chloride, acetic acid, acetone, $CHCl_3$, MeOH, and heptane were purchased from BDH (Toronto, ON, Canada). Acetone, $CHCl_3$, and MeOH were glass distilled before use (Kates, 1986). Ultra-clear™ ultracentrifuge tubes (14 x 95 mm, 344060) were obtained from Beckman (Palo Alto, CA, USA). Bio-Rad protein assay dye reagent concentrate, Coomassie brilliant blue G-250, goat anti-rabbit IgG conjugated with horseradish peroxidase (HRP), nitrocellulose membranes (0.45 μm), sodium dodecyl sulfate (SDS), tris(hydroxymethyl)-aminomethane (Tris) and Triton X-100 were purchased from Bio-Rad Laboratories (Hercules, CA, USA). Pig ovary ZP was either purchased from Calbiochem (San Diego, CA, USA) or kindly provided by Dr. T. Berger (University of California, Davis, CA, USA, see Appendix 2). Anhydrous EtOH was bought from Commercial Alcohols (Brampton, ON, Canada). Polystyrene 96-well flat-bottom black (CS003915) and clear (CS003370) microtiter plates were obtained from Corning (New York, NY, USA). Phospholipid and neutral lipid standards (PC, PE, sphingomyelin, cholesterol, DAG, and $PIP_2$) were purchased from Doosan Serdary Research Laboratories (Englewood Cliffs,

NJ, USA), and used without further purification. Microcon YM-30 was obtained from Millipore (Bedford, MA, USA). Amplex™ Red, Alexa Fluor®-430 and 488, goat anti-rabbit IgG conjugated to Alexa-488, and propidium iodide (PI) were purchased from Molecular Probes (Eugene, OR, USA). Immuno Pure Immobilized Protein A Affinity Pak Column, and Immuno Pure Fab Preparation kit were purchased from Pierce (Rockford, IL, USA). Ammonium molybdate, azure A, Bio-Sil A silica (100-200 mesh, bead size 150-300 μm), bovine brain SGC (containing both α-hydroxylated and non-hydroxylated fatty acids; major cations were 1.72% $Na^+$, 1.07% $Ca^{2+}$), and GC (HFA-GC and NFA-GC containing 98% α-hydroxylated and non-hydroxylated fatty acids, respectively), bovine serum albumin (BSA, essentially fatty acid free), calcium chloride, cholesterol, cholesterol oxidase, cholic acid-sodium salt, *cis*-4,7,10,13,16,19-docosahexaenoic acid methyl ester, *cis*-7,10,13,16,19-docosapentaenoic acid methyl ester, dihydrostreptomycin, dimethyl-sulfoxide (DMSO), ethylenediaminetetracetic acid (EDTA), filipin III, glucose, Hepes, $H_2O_2$, HRP, ovalbumin, potassium chloride, magnesium chloride, magnesium nitrate, malachite green, methyl-β-cyclodextrin (MβCD), Nα-p-tosyl-L-lysine chloromethyl ketone (TLCK), *o*-phenylenediamine dihydrochloride (OPD), orcinol, potassium phosphate, pyruvic acid, sodium bicarbonate, sodium carbonate, sodium citrate, sodium hydroxyde, sodium phosphate, and sucrose were purchased from Sigma (St. Louis, MO, USA). Fatty acid methyl ester mix standard was obtained from Supelco (Bellefonte, PA, USA). Durex™ borosilicate glass disposable culture tubes (12 x 75 mm, 47729-570), and glass columns (3 cm inner diameter x 40 cm, 250ml) with a stopcock were purchased from VWR Scientific Products (Montréal, Québec, Canada). HPK silica gel high performance thin layer chromatography

(HPTLC) plates (60 Å, 10 μm pore size, 200 μm thickness, 10 x 10 cm), and K6 silica gel TLC plates (60 Å, 10 μm pore size, 250 μm thickness, 20 x 20 cm) were obtained from Whatman (Clifton, NJ, USA). Percoll was purchased from Pharmacia (Uppsala, Sweden). $^2H_2O$ (99.9 atom%) was purchased from Merck Sharp and Dohme/Isotopes (Pointe Claire, Québec, Canada). Ram testes (~350 g each, wet wt) were obtained from a local slaughterhouse, and frozen in small pieces at -80°C.

**Anti-SGG IgG/Fab**

Rabbit polyclonal anti-SGG/SGC IgG was generated in our laboratory according to the method of Zalc *et al.* (1997), which involved direct intravenous immunization of SGC-containing liposomes without any adjuvant into the ear vein of New Zealand white female rabbits, as described previously (White *et al.*, 2000). The IgG fraction of the antiserum from the immunized rabbits was further purified using the Immuno Pure Immobolized Protein A Affinity Pak Column, according to the manufacturer's instructions. White *et al.* (2000) demonstrated by the TLC-overlay technique that the anti-SGG/SGC IgG antibody reacts specifically with SGG and SGC, but not with cholesterol sulfate, phospholipids or monogalactosyldiacylglycerol. Since antibodies generated against either SGC or SGG show cross-reactivity with both glycolipids (White *et al.*, 2000), SGC liposomes were used for affinity purification of anti-SGG/SGC IgG. Specifically, 100 μl of anti-SGG/SGC IgG (0.007 μmoles) were co-incubated (room temperature, 1h) with 100-fold mole concentration of multilamellar SGC liposomes (0.7 μmoles, prepared in PBS, 10 mM sodium phosphate, 150 mM NaCl, pH 7, as described in section 2.2), followed by ultracentrifugation (200,000 g, 4°C, 1 h) (New, 1997) using a

Beckman (Chaska, MN, USA) TLA 120.2 rotor. The pellet was then resuspended in 400 µl 1 M potassium iodide (Boulanger *et al.*, 1994), and left overnight at 4°C to dissociate the bound anti-SGG/SGC IgG from the SGC liposomes. Subsequently, the mixture was diluted with 1 ml PBS, and ultracentrifuged as described in the previous step. The supernatant, containing the affinity-purified anti-SGG/SGC IgG, was washed free of KI by Microcon YM-30 centrifugation (4,000 g, 4°C) in PBS (0.5-1 ml). This Microcon YM-30 was pretreated with 1% BSA to block non-specific binding sites. Subsequently, the affinity purified anti-SGG/SGC IgG was resuspended in PBS (10 µg/µl). Fab fragments were generated from the affinity-purified anti-SGG/SGC IgG following papain digestion using the Immuno Pure Fab Preparation kit, according to the manufacturer's instructions. Preimmune rabbit serum (PRS) IgG and Fab were prepared as described above (Harlow and Lane, 1988; White *et al.*, 2000), and served as a negative control.

The immunoactivity of non-affinity purified and affinity-purified anti-SGG/SGC IgG/Fab, as well as that of PRS IgG/Fab was determined by the enzyme-linked immunosorbent assay (ELISA) (White *et al.*, 2000), with minor modifications. SGG/SGC was dissolved in $CHCl_3$:MeOH (1:1, v/v), dried under a stream of $N_2$ at 37°C, and then resuspended in EtOH at a final concentration of 10 µg/ml. Following sonication, SGG/SGC (1 µg) was coated into each well of a Corning 96-well flat-bottom clear microtiter plate, which was then dried in a dessicator overnight, at room temperature. After blocking (1 h, room temperature) non-specific binding sites with 1% BSA in TBS (20 mM Tris-HCl, 137 mM NaCl, pH 7.4), the plate was washed five times with TBS-0.05% Tween-20. The SGC-coated wells were then exposed (1 h, room temperature) to the primary antibody (100 µl), followed by washing for five times with

TBS-0.05% Tween-20 to remove unbound primary antibodies. Subsequently, each well was incubated (30 min, room temperature) with 100 µl of goat anti-rabbit IgG conjugated with HRP (1:3,000 in TBS), and washed five times with TBS-0.05% Tween-20 to remove unreacted secondary antibodies. Bound antibodies were then detected calorimetrically using an HRP substrate, OPD, following the manufacturer's instructions. The intensity of the color product was measured at 490 nm. PRS IgG and secondary antibody alone were used as negative controls.

## 2.1. Extraction and Purification of Sulfogalactosylglycerolipid

Total lipids were extracted from ram testis according to the Bligh and Dyer (1959) procedure, as modified by Kates (1986). Ram testes were decapsulated by removing the *tuniea albuginea*, i.e., the enveloping connective tissue of each testis, and then cut into small pieces. One hundred gram portions of testes tissue were homogenized in 150 ml $CHCl_3$:MeOH (1:2, v/v) in a Waring blender for 3 min at maximum speed at room temperature. The homogenate was then suction-filtered on glass wool using a Buchner funnel. The ratio of $CHCl_3$: MeOH:$H_2O$ in this single phase filtrate was close to 1:2:0.8 (v/v), assuming 85% water content in the tissue. Equal volumes of $CHCl_3$ and $H_2O$ were added to the single phase filtrate to give a two phased system with a final ratio of MeOH:$CHCl_3$:$H_20$ (1:1:0.9 v/v). The two phased system was gently mixed, then transferred into a separatory funnel and left overnight at room temperature to allow complete separation of the two phases. The lower $CHCl_3$ phase containing the lipids was transferred to a round bottom flask, diluted with benzene and concentrated almost to dryness using a rotary evaporator. The concentrated $CHCl_3$ phase (5 ml) was transferred

to a centrifuge tube and diluted with ten volumes of acetone (45 ml), and left overnight at -20°C. The precipitate of glycolipids and phospholipids was centrifuged briefly at low speed. The supernatant (containing neutral lipids) was removed with a Pasteur pipette, and the pellet was washed once with 0.5 ml acetone, and then dried under an $N_2$ stream and brought up in $CHCl_3$. The extracted lipids in $CHCl_3$ were fractionated by column chromatography using Bio-Sil A silica (100-200 mesh, 60 g/column) (Kates, 1986; Tupper *et al.*, 1994; Attar *et al.*, 2000). The resin was first activated at 100°C for 2 h, and then 180 ml of $CHCl_3$ were added to make a slurry, which was packed into a glass column (2 cm inner diameter x 20 cm, 80 ml) column, and allowed to equilibrate overnight at room temperature. Subsequently, the Bio-Sil A silica was washed with two column volumes (60 ml ea.) of $CHCl_3$, and then the extracted testicular lipids, concentrated to ~5 ml under a stream of $N_2$, were loaded on top of the silica. The column was eluted in succession with 1 column volume each of $CHCl_3$ and $CHCl_3$:acetone (1:1, v/v) (traces of neutral lipids), 15 column volumes of acetone (glycolipids), and 10 column volumes of MeOH (phospholipids). The organic solvents were delivered onto the column through a separatory funnel (500 ml). The lipid composition of each fraction was detected by TLC using the solvent system $CHCl_3$:MeOH:$H_2O$ (65:25:4, v/v) (Ishizuka *et al.*, 1973), followed by orcinol staining (section 2.15).

The eluted acetone fractions, containing SGG, were pooled and then brought to dryness in a rotary evaporator, and the SGG residue was dissolved in a small volume of $CHCl_3$. SGG was then precipitated with the addition of acetone to the final acetone:$CHCl_3$ ratio of 9:1 (v/v). The SGG precipitate was centrifuged (350 g, 4°C, 5 min), and further purified by preparative TLC using the solvent system

$CHCl_3$:MeOH:$H_2O$ (65:25:4, v/v) (Ishizuka *et al.*, 1973), with SGG standards co-chromatographed on the side of the TLC plate. Following iodine vapor staining, the band corresponding to SGG was scraped off, and the silica was extracted with $CHCl_3$:MeOH:$H_2O$ (1:2:0.8, v/v). To remove endogenous cations, SGG extracts were diluted with $CHCl_3$ and 0.6 N HCl to form the two phased acidic Bligh and Dyer system ($CHCl_3$:MeOH:0.33 N HCl, 1:1:0.9, v/v). This step was carried out at a fast pace to prevent SGG hydrolysis. SGG was retrieved in the $CHCl_3$ phase, and immediately neutralized with 1 N methanolic NaOH, and concentrated to a small volume under $N_2$. The $Na^+$ form of SGG was isolated by acetone precipitation (Kates, 1986; Tupper *et al.*, 1994; Attar *et al.*, 2000), and used for FTIR spectroscopic and cell biological experiments.

## 2.2. Preparation of Multilamellar Bilayers

Multilamellar bilayers of SGG, SGC, NFA-GC, HFA-GC, $DPPC_{d62}$ and PDPC, as well as equimolar mixtures of SGG:cholesterol, DPPC:cholesterol, SGG:$DPPC_{d62}$ and SGG:PDPC were generated as follows. For FTIR spectroscopic studies, the dried lipids (2 mg) were resuspended in 38 $\mu$l of $^2H_2O$ buffered with 50 mM Tris-HCl ($p^2H$ 7.05) in Teflon-lined screw capped glass vials. The obtained dispersions (5 wt%) were then subjected to four freeze-thaw cycles to obtain homogeneous bilayers (Mayer *et al.*, 1985; Kulkarni and Brown, 1998). During each cycle, the lipids were brought to 90°C (20 s) and vortex-mixed for complete dispersion. The lipid dispersions were then immediately frozen by plunging the glass vial into liquid nitrogen (-215°C, 20 s). After the final thawing, the dispersion was left to equilibrate to room temperature (23°C) for 1 h. For

the affinity purification of anti-SGG/SGC IgG, SGC dispersions (1 mg/ml) were prepared in PBS, and treated as described above.

## 2.3. Fourier Transform Infrared Spectroscopic Analysis

FTIR measurements were conducted on a Digilab FTS-40A spectrometer equipped with a deuterated triglycine sulfate (DTGS) detector. Aqueous dispersions (10 $\mu$l) of the lipid or lipid mixtures under investigation were placed between two $CaF_2$ windows separated by a 6-$\mu$m spacer in a thermostated cell mount. Temperatures were varied at 1°C/min with a water circulation bath. Heating and cooling mode FTIR spectra were recorded between 0 and 90°C, in increments of 3°C. The spectra were derived from 128 scans collected at a spectral resolution of 2 $cm^{-1}$, signal-averaged, Fourier transformed and ratioed against a background interferogram. Each spectrum was recorded in ~ 5 min, after a waiting period of 7 min. To determine whether the polymorphism of SGG, SGC, HFA-GC and NFA-GC can also be driven in a time dependent manner, these glycolipids were heated to a temperature that favors the formation of the first observed polymorph (5°C for SGG, 32°C for SGC, 38°C for HFA-GC and NFA-GC), and maintained at that temperature for 96 h. In a different set of experiments, these bilayers were heated to liquid-disordered temperatures (90°C), cooled to 38°C, and maintained at that temperature for 96 h. For NFA-GC, additional incubation experiments were conducted at 65°C following cooling from liquid-disordered temperatures. To prepare dehydrated SGG, SGC and NFA-GC and HFA-GC bilayers, the lipid dispersions (5%, w/v) were prepared as described above, and left in the open

transmission cell in the sample compartment of the infrared spectrophotometer for 96 h. The instrument was under continuous dry air purge to eliminate atmospheric water vapor.

To assess the polymorphism of SGG, SGC, and GC, the phase behavior of these glycolipids was monitored by following changes of the $CH_2$ (2846-2854 $cm^{-1}$) symmetric stretching vibration as a function of temperature. In addition, the phase behavior of $DPPC_{d62}$ and PDPC was monitored by following changes of the $CD_2$ (2088-2099 $cm^{-1}$) symmetric stretching vibration as a function of temperature. Below the phase transition temperature ($T_m$), most of the hydrocarbon chains are in the all-*trans* conformation, whereas at the $T_m$, the progressive *trans-gauche* isomerization results in lateral area expansion of the bilayer and in a shift to higher frequencies in the chain melted state (Casal and Mantsch, 1984). The contribution of hydrogen bonding to the polymorphism of SGG and SGC/GC was determined by monitoring the ester C=O (1680-1780 $cm^{-1}$) and amide I (1580-1680 $cm^{-1}$) stretching vibrations, respectively, as a function of temperature. To assess hydrogen bonding interactions of SGG and DPPC with cholesterol, the ester C=O stretching band was monitored in equimolar mixtures of SGG-cholesterol and DPPC-cholesterol. The interaction of SGG with saturated and unsaturated phospholipids was determined by monitoring the $CH_2/CD_2$ symmetric stretching band in equimolar mixtures of SGG-$DPPC_{d62}$, SGG-PDPC, and $DPPC_{d62}$-PDPC as a function of temperature. Data processing was performed using GplotC and RAMOP programs (Moffatt *et al.*, 1986). Band frequencies were determined from 3$^{rd}$ order derivative spectra with a breakpoint of 0.3 and 0.95 for the $CH_2$ and ester C=O/amide I stretching bands, respectively (Cameron and Moffatt, 1987).

## 2.4. Triton X-100 Insolubility Experiments

Multilamellar lipid vesicles of SGG-cholesterol and DPPC-cholesterol were prepared with various molar ratios (9:1, 4:1, 2:1 and 1:1) of SGG or DPPC to cholesterol as described in section 2.2). Multilamellar bilayers of SGG-cholesterol-DPPC were generated with a molar ratio mimicking that of capacitated sperm rafts (i.e., 1.0:2.0:3.4, see Results). To assess changes of lipid insolubility in Triton X-100, multilamellar bilayers consisting of 0.2 μmoles of single lipids (i.e., SGG or DPPC) or mixed lipids (i.e., SGG-cholesterol or DPPC-cholesterol) were resuspended in 900 μl of 10 mM Tris-HCl, 0.15 M NaCl and 5 mM EDTA, pH 7.5 (TNE), and the lipid dispersions were vortex-mixed and measured for light scattering at 400 nm, using an Ultrospec 2000 (Pharmacia). Subsequently, 100 μl of 5 to 20% Triton X-100 in TNE of various concentrations was added to the lipid dispersions to give a final concentration of 0.5 to 2%. The lipid dispersions were then vortex-mixed, incubated at 23°C for 1 h, and remeasured for light scattering at 400 nm. Relative insolubility of the lipid dispersions was expressed as a percentage of the ratio of $A_{400}$ after Triton X-100 incubation to $A_{400}$ of the original lipid dispersions, i.e., before Triton X-100 addition (Xu and London, 2000; Xu *et al.*, 2001).

## 2.5. Pig Sperm Preparation and Capacitation

Semen was obtained from three mature, fertile boars at the Department of Animal and Poultry Science, University of Guelph (through collaboration with Dr. Mary Buhr). The sperm rich fraction was collected from boars by the gloved hand technique (King and Macpherson, 1973) through a layer of gauze into an insulated thermos bottle maintained

at 35°C. The sperm rich fraction was diluted in Beltsville Thawing Solution (BTS: 0.2 M glucose, 20 mM sodium citrate, 15 mM $NaHCO_3$, 3.36 mM $Na_2EDTA$, 10 mM KCl, 8 mM $Na_2HPO_4$, 2 mM $NaH_2PO_4$, and 1 mg/ml dihydrostreptomycin, pH 7.4) (Flesch *et al.*, 1998; Pursel and Johnson, 1975), and shipped overnight from Guelph in an insulated box (18°C). The diluted semen was washed free of seminal plasma by centrifugation (350 g, 28°C, 10 min). Sperm samples were then divided into two groups: one subjected to simple washing and the other to Percoll gradient centrifugation. For the first procedure, seminal plasma free sperm were washed with non-capacitation medium (NCM: 0.1 M NaCl, 0.36 mM $NaH_2PO_4$, 8.6 mM KCl, 0.5 mM $MgCl_2$, 11 mM glucose, 23 mM Hepes, pH 7.6) (Melendrez *et al.*, 1994) by centrifugation (350 g, 28°C, 10 min). The resultant sperm pellet was named **washed sperm**. For the second procedure, seminal plasma free sperm were layered on a discontinuous Percoll density gradient of 35% and 70%, and centrifuged (first at 300 g, 28°C, 5 min, then at 750 g, 28°C, 25 min) (Harrison *et al.*, 1993). The obtained sperm pellet was named **PGC sperm**. Washed sperm and PGC sperm were resuspended to a concentration of 20 x $10^6$ cells/ml in capacitation medium (CM: 0.1 M NaCl, 0.36 mM $NaH_2PO_4$, 8.6 mM KCl, 0.5 mM $MgCl_2$, 11 mM glucose, 23 mM Hepes, supplemented with 10 mM $NaHCO_3$, 2 mM $CaCl_2$, 5 mM pyruvate and 0.3% BSA, pH 7.6) (Melendrez *et al.*, 1994), and incubated (39°C, 5% $CO_2$, 3 h) to undergo capacitation. Capacitated pig sperm were then washed free of BSA with NCM by centrifugation (350 g, 28°C, 10 min).

## 2.6. Isolation of Pig Sperm Tails

PGC-capacitated pig sperm suspended in NCM were sonicated to separate heads from tails, as described previously by Shao *et al.* (1997). The suspension was washed twice with TBS by centrifugation (350 g, 28°C, 10 min), and the final pellet was resuspended in TBS containing 80% (w/v) sucrose, followed by centrifugation (280,000 g, 4°C, 1 h) using a Beckman 70 Ti rotor. The sperm tail pellet obtained on the inside of the tube (centripetal side) was then washed twice with TBS by ultracentrifugation (285,000 g, 4°C, 70 min) using a Beckman 70 Ti rotor.

## 2.7. SDS-PAGE and Western Blotting

To validate the capacitation status of pig sperm, we separated proteins by SDS-PAGE (12% polyacrylamide), and transferred them electrophoretically (250 mA, 30 min) onto nitrocellulose membranes (0.45 μm) (Laemmli 1970; Towbin and Gordon, 1984). Non-specific binding sites on the membrane were blocked (1 h, room temperature) with 5% dry non-fat milk in TBS. Sperm proteins immobilized onto nitrocellulose membranes were incubated (overnight, 4°C) with mouse monoclonal anti-phosphotyrosine IgG (4G10, Upstate, Lake Placid, NY) at 2 μg/ml in TBS containing 3% non-fat powdered milk. To remove unbound primary antibody, the blot was washed (3 times, 10 min ea.) in TBS-0.05% Tween 20. Subsequently, the blot was incubated (1 h, room temperature) with goat anti-mouse IgG conjugated with HRP (1:2,000 dilution in TBS), and washed (3 times, 10 min ea.) with TBS-0.05% Tween 20 to remove unreacted secondary antibody. Protein-antibody recognition was detected using an ECL Western blotting detection kit, according to the manufacturer's instructions. The membrane was soaked briefly in the

detection reagent. This elicited the HRP-catalyzed oxidation of luminol in the presence of chemical enhancers (e.g., phenols), resulting in enhanced chemiluminescence. The emitted (428 nm) light, where the HRP labeled protein is bound to the membrane, was detected on blue light sensitive autoradiography film, Hyperfilm™ ECL™.

## 2.8 Immunolocalization of SGG on Live Pig Sperm

Indirect immunofluorescence (IIF) using anti-SGG IgG was employed for the localization of SGG on live washed and PGC pig sperm before and after capacitation. In another experiment, washed sperm and PGC sperm were resuspended to a concentration of 2 x $10^7$ cells/ml in CM, containing 3 mM M$\beta$CD (Visconti *et al.*, 1999) instead of 0.3% BSA. These sperm samples were incubated (39°C, 5% $CO_2$, 3 h), and then washed free of M$\beta$CD with NCM by centrifugation (350 g, 28°C, 10 min). Approximately 500,000 sperm were co-incubated (39°C, 5% $CO_2$, 30 min) with affinity-purified anti-SGG IgG (50 μg/ml) or PRS IgG (negative control). The unbound antibody was washed with NCM by centrifugation (350 g, 28°C, 10 min). Sperm were then incubated (39°C, 5% $CO_2$, 30 min) with goat anti-rabbit IgG conjugated to Alexa-488 (50 μg/ml). After 25 min of incubation with the secondary antibody, PI (0.5 μg/ml) was added to assess sperm viability. Following two washes (350 g, 28°C for 10 min) with NCM to remove unbound secondary antibody and unincorporated PI. The sperm suspension was placed onto a glass slide, and then viewed under a Zeiss-IM35 epifluorescent inverted microscope (Carl Zeiss Canada, Toronto, ON, Canada) (fluorescein and rhodamine filters were used for anti-SGG IgG and PI staining, respectively). Phase contrast and fluorescence images of

sperm were captured under 400X magnification with a Spot Junior CCD camera (Carl Zeiss, Canada), and processed using Corel PhotoPaint software for Windows.

## 2.9 Visualization of Cholesterol on Live Pig Sperm by Filipin Labeling

Filipin is an antibiotic that aggregates non-esterified membrane sterols into complexes. Live washed and PGC pig sperm before and after capacitation (~ 500,000 sperm) were resuspended in NCM containing 25 μM filipin (10 mM DMSO stock solution). To determine whether the observed staining pattern of filipin-cholesterol complexes on the pig sperm surface did in fact reflect the existence of free cholesterol, sperm were treated with M$\beta$CD as described in section 2.8. Sperm samples treated with similar DMSO concentrations without filipin served as negative controls. Sperm were incubated (39°C, 5% $CO_2$, 30 min) in the dark. To assess sperm viability, PI (0.5 μg/ml) was added 5 min before the end of the incubation period. Sperm samples were washed (350 g, 28°C, 10 min) with NCM to remove the unbound filipin and unincorporated PI, mounted onto a glass slide, and fluorescence patterns of filipin-cholesterol complexes were viewed as described in section 2.9 (Hoechst and rhodamine filters were used for filipin and PI staining, respectively).

## 2.10 Binding of SGG to Pig ZP

The binding of solubilized pig ZP to SGG-containing liposomes was determined as follows. Multilamellar bilayers (5%, w/v) of SGG-cholesterol-DPPC, having a molar ratio mimicking that of capacitated sperm rafts (i.e., 1.0:2.0:3.4, see Results), were prepared in TBS as described in section 2.2. The SGG-containing liposomes were

transferred to 5 different Eppendorf tubes (2 μg/tube; the 2 μg represent the amount of total lipids, assayed as described in section 2.14, present in 0.5 μg raft proteins used in the sperm raft-ZP binding assay, section 2.18). The liposomes were incubated (1 h, room temperature) with 1% BSA in TBS to block non-specific binding, and then ultracentrifuged (100,000 g, 4°C, 1 h) (New, 1997) using a Beckman (Chaska, MN, USA) TLA 120.2 rotor to remove unbound BSA. Subsequently, the SGG-cholesterol-DPPC liposomes were incubated (1 h, room temperature) with various concentrations (0-0.4 μM) of Alexa-430 ZP. In an alternative experiment, these SGG-containing liposomes were incubated with Alexa-430 ZP in the presence of 100-fold excess of unlabeled ZP to establish the level of non-specific binding. The liposomes were ultracentrifuged (100,000 g, 4°C, 1 h) to remove unbound Alexa-430 ZP/unlabeled ZP, and the pellet (i.e., SGG-cholesterol-DPPC + Alexa-430 ZP) was resuspended in 100 μl TBS and then transferred into the wells of a black polystyrene 96-well microtiter plate. Fluorescence intensity was measured using a Spectramax GeminiXS spectrofluorometer (Molecular Devices) at excitation and emission wavelengths of 425 and 520 nm, respectively. The amount of Alexa-430 ZP bound to SGG in each well was determined from the Alexa-430 ZP standard curve.

## 2.11. Isolation of Pig Sperm Rafts

Washed, washed-capacitated, PGC, and PGC-capacitated sperm, as well as washed-capacitated sperm tail preparations, prepared as described above, were lysed, homogenized, and subjected to sucrose density gradient centrifugation to isolate the low density, light-scattering membrane fraction containing the rafts. Briefly, sperm were

centrifuged (350 g, 28°C, 10 min), and resuspended to a final concentration of $1x10^9$ sperm/ml in lysis buffer consisting of TNE, 1% Triton X-100 and 0.2 mM TLCK. The mixture was kept on ice for 2 h, and then homogenized with 30 strokes by a Dounce homogenizer. After removal of the sperm pellet by centrifugation (1300 g, 4°C, 10 min), the supernatant (lysate) was mixed with an equal volume of 85% (w/v) sucrose in TNE. Two ml of the supernatant (lysate) in 42.5% (w/v) sucrose was placed into ultraclear ultracentrifuge tubes (14 x 95 mm, 344060, Beckman), and 6 ml of 30% (w/v) sucrose in TNE and 3.5 ml of 5% (w/v) sucrose in TNE were layered successively on top of the sperm lysate-42.5% (w/v) sucrose mixture. These sucrose gradient tubes were then ultracentrifuged (200,000 g, 18 h, 4°C) using a Beckman SW 40 Ti rotor. After ultracentrifugation, 1 ml fractions were collected from top to bottom of the tube. The insolubility of each fraction in Triton X-100 was measured by $A_{400}$ (Xu *et al.*, 2001). The sucrose density gradient fractions were also analyzed calorimetrically for total protein content by the Bradford dye-binding procedure (Bradford, 1976) using the Bio-Rad protein assay. Cholesterol content in each fraction was quantified fluorometrically using the Amplex Red (Molecular Probes) cholesterol assay, according to the manufacturer's instructions (see below). Fractions 4-6 (light scattering band, indicative of the formation of Triton X-100 insoluble membranes or rafts) were pooled. These fractions were ultracentrifuged (285,000 g, 4°C, 70 min) using a Beckman 70 Ti rotor to pellet raft membranes. The lipid and protein content of pig sperm rafts were characterized, and the binding ability of these membrane domains to the egg ZP was also investigated for the first time in my thesis.

## 2.12. Lipid Extraction

Lipids were extracted from non-capacitated and capacitated pig sperm, as well as from their corresponding rafts by the modified (Kates, 1986) Bligh and Dyer (1959) method. The organic solvents used throughout this study were glass distilled to prevent contamination (Kates, 1986). $CHCl_3$ and MeOH were added to the aqueous sperm/raft sample to give a one-phase system of $CHCl_3$:MeOH:$H_2O$ (1:2:0.8, v/v). To this system, equal amounts of $CHCl_3$ and $H_2O$ were added to yield a two-phased system of $CHCl_3$:MeOH:$H_2O$ (1:1:0.9, v/v), consisting of a lower $CHCl_3$ phase (containing lipids) and an upper MeOH:$H_2O$ phase (containing water soluble contaminants). The mixture was left in a funnel overnight at 4°C. Subsequently, the lower $CHCl_3$ phase was collected, and the sample was concentrated under a stream of $N_2$ in the presence of benzene to remove small/trace amounts of water.

## 2.13. Thin Layer Chromatography

Thin layer chromatography plates (either TLC or HPTLC plates) were washed twice in the same direction in $CHCl_3$:MeOH (1:1, v/v), and then activated by heating in an oven at 100°C for 2 h. Lipids in $CHCl_3$ (ram testis total lipids, SGG, neutral lipids, and total phospholipids, as well as total lipids isolated from pig non-capacitated and capacitated sperm and their corresponding rafts) were spotted as a 0.75 cm band on the plate, along with lipid standards, i.e., SGG, PC, PE, sphingomyelin, cholesterol, DAG, and $PIP_2$. The TLC plate was developed in a glass TLC tank lined with filter paper and pre-equilibrated (2 h) with the solvent system $CHCl_3$:MeOH:$H_2O$ (65:32:4, v/v/v), which effectively separates glycolipids from other lipids. Subsequently, the plate was air dried

and then stained with 0.2% orcinol in 75% $H_2SO_4$, followed by heating at 120°C for color development (Kates, 1986); glycolipids (e.g., SGG and GG) became violet-purple, whereas phospholipids and cholesterol turned light brown and red, respectively. In other experiments, the TLC plates were also stained with 0.03% Coomassie blue in 30% MeOH:100 mM NaCl for 30 min, under continuous gentle shaking conditions. The plate was then destained in 30% MeOH:100 mM NaCl for 5 min, under continuous gentle stirring conditions (Nakamura and Handa, 1984). Following destaining, the plate was removed and gently blotted with filter paper to remove excess liquid. All lipid bands stained blue.

## 2.14. Lipid Composition of Pig Sperm and their Corresponding Rafts

Lipids were extracted from non-capacitated and capacitated sperm and from their corresponding rafts, as well as from sperm tail rafts, as described in section 2.14. The lipid composition of whole sperm and their rafts, as well as that of sperm tail rafts was first characterized by HPTLC using the solvent system $CHCl_3$:MeOH:$H_2O$ (65:32:4, v/v/v). HPTLC plates were stained either with orcinol, specific for glycolipids, or with Coomassie blue. The quantitation of the major lipids (i.e., SGG, cholesterol, and total phospholipids) in pig sperm and their corresponding rafts, prepared from three pig sperm ejaculates, proceeded as follows.

### *2.14.1. Sulfolipid Assay*

The concentration of SGG in sperm/raft lipids was determined using the method of Kean (1968), with the reaction volume reduced to ~ 0.33 ml. This assay was based on

the formation of a colored complex between the cationic Azure A dye and the sulfate group of sulfolipids. Since cholesterol sulfate, which is present in mammalian sperm (Lalumière *et al.*, 1976; Langlais and Roberts, 1985), is found at relatively low concentrations in epididymal pig sperm (Nikolopoulou *et al.*, 1985), quantitation of sulfolipids by this calorimetric method predominantly represents the levels of SGG in pig sperm and their corresponding rafts. Sperm/raft lipids in $CHCl_3$, extracted from about 30-60 x $10^6$ sperm, were brought to dryness under a stream of $N_2$. To the dried lipids, 1.5 ml $CHCl_3$:MeOH (1:1, v/v), 1.5 ml 0.05 N $H_2SO_4$ and 0.3 ml Azure A solution (1.4 mM in 0.0025 N $H_2SO_4$) were added to each sample, followed by vortex-mixing for 30 sec. The sperm/raft lipid samples were centrifuged at 300 g, 4°C, 15 min, and the lower $CHCl_3$ phase, containing SGG, was collected. A standard curve was constructed using SGG (1-5 μg) purified from ram testis (Attar *et al.*, 2000), and treated as described above for the lipid samples. Absorbance was read at 635 nm using 0.5 ml quartz cuvette.

### *2.14.2. Phospholipid Assay*

The phospholipid content of sperm/raft lipids was quantitated according to the method described by Duck-Chong (1979), as modified by Tanphaichitr *et al.* (1996). Sperm/raft lipids in $CHCl_3$ (obtained from 0.5-1.5 x $10^6$ sperm) were mixed with 30 μl of magnesium nitrate (10% w/v, in MeOH) in borosilicate glass disposable culture tubes (12 x 75 mm), and then evaporated to dryness by heating in a water bath at 85-100°C. The dried sperm/raft lipid extract was heated in the top portion of a Bunsen flame for 15 s. The presence of magnesium nitrate and the high temperature resulted in the conversion of phospholipid-esterified phosphate to inorganic phosphate, which was detected

colorimetrically as follows. After brief cooling, 300 µl of HCl (1 M) were added to the lipid samples, which were heated at 90-95°C for 15 min; samples were covered with glass marbles to minimize evaporation during the heating process. Subsequently, the tubes were cooled, and 10 µl of 1% Triton X-100 and 600 µl of acidic ammonium molybdate-malachite green color reagent was added to each tube, followed by vortex-mixing. The color reagent was prepared by mixing ammonium molybdate (4.2%, w/v, in 4.5 M HCl) and malachite green (0.3%, w/v) in a 1:3 volumetric ratio, followed by filtering through a Whatman No.1 filter paper. A standard curve corresponding to 0.02-0.1 µg phosphorus was constructed with $KH_2PO_4$ (4.4 µg $KH_2PO_4$/ml MeOH, which is equivalent to 1 µg phosphorus/ml MeOH), and treated the same way as the sperm/raft lipid samples. Absorbance was measured colorimetrically at 650 nm after an incubation period of 5 min at room temperature.

### *2.14.3. Cholesterol Assay*

The cholesterol content of sperm/raft lipids was quantitated fluormetrically by the Amplex Red (Molecular Probes) cholesterol assay, according to the manufacturer's instructions. Cholesterol was oxidized by cholesterol oxidase to yield $H_2O_2$ and 4-cholestene-3-one. In the presence of HRP, the Amplex Red reagent (10-acetyl-3,7-dihydroxy-phenoxazine) reacted with $H_2O_2$ in a 1:1 stoichiometry, resulting in the formation of highly fluorescent resorufin. In this study, the Amplex Red assay was used to determine cholesterol concentrations in biological samples, i.e., sperm, rafts and the sucrose density gradient fractions, as well as in extracted sperm/raft lipids. For the sucrose gradient fractions (1-13) of the Triton X-100 sperm extract, the reaction was

conducted in the cholesterol assay reaction buffer (100 mM $KH_2PO_4$, pH 7.4, 50 mM NaCl, 5 mM cholic acid, and 0.1% Triton X-100), containing 0.3 mM Amplex Red reagent, 2 U/ml cholesterol oxidase, and 2 U/ml HRP; Amplex Red Reagent (20 mM) was prepared in DMSO, whereas $H_2O_2$ (20 mM), cholesterol oxidase (200 U/ml) and HRP (200 U/ml) were made in the reaction buffer. On the other hand, cholesterol assay was carried out in MeOH and the reaction buffer for sperm/raft lipids, as outlined below.

To determine the cholesterol content of the sucrose gradient fractions (1-13) of the Triton X-100 sperm extract, 50 µl of fractions 1-3, 5 µl of fractions 4-6, and 25 µl of fractions 7-13 were added in triplicates into separate wells of a black 96-well microtiter plate. When the volume was smaller than 50 µl, the volume was adjusted to 50 µl with the reaction buffer. For this experiment, the cholesterol standard curve (0.1-0.5 µg) was constructed in the reaction buffer. To ensure that endogenous components in the sucrose gradient fractions of the Triton X-100 sperm extract did not interfere with the assay, sperm was included as an internal standard in the cholesterol standard curve. The cholesterol content of total lipids isolated from non-capacitated and capacitated pig sperm and their corresponding rafts was also determined. Sperm/raft total lipids in $CHCl_3$ were dried under $N_2$, and resuspended in MeOH. Subsequently, aliquots of 50 µl, containing lipids extracted from ~0.5 x $10^6$ sperm, were added in triplicates into separate wells of a black 96-well microtiter plate. The cholesterol standard curve (0.1-0.5 µg) was constructed in MeOH for this experiment (Tanphaichitr *et al.*, 1996). The reaction was initiated by adding 50 µl of the reaction buffer. The reactions were incubated for 30 min at 37°C, protected from light, then fluorescence of the reaction product (i.e., resorufin) was measured using a fluorescence microtiter plate reader, SpectraMAX GeminiXS

fluorometer (Molecular Devices, Sunnyvale, CA, USA) at excitation and emission wavelengths of 563 and 587 nm, respectively.

## 2.15. Preparation of Fatty Acyl Methyl Esters and Dimethylacetals

Preparative TLC (Kates, 1986) was used to purify PC and PE from total lipids isolated from non-capacitated and capacitated pig sperm and their corresponding rafts. The extracted lipids (from ~ 1 x $10^8$ sperm) were applied to the TLC plate as a thin band (15 cm), along with PC, PE and sphingomyelin standards on both sides of the plate. Subsequently, the plate was developed in $CHCl_3$:MeOH:acetic acid:$H_2O$ (50:37.5:3.5:2, v/v/v/v) (Holub and Watson, 1996). The plate was removed from the TLC chamber, and excess solvent was allowed to evaporate (15-30 min) in a tank flushed with $N_2$. The plate was then immersed in 0.0012% rhodamine 6G solution. The bands corresponding to PC and PE were viewed under UV light (366 nm), marked with a pencil, and gently scraped off the plate. PC/PE were extracted from the scraped silica powder by adding 4.5 ml of 0.6 N methanolic HCl to the powder, followed by heating 95°C for 4 h. Mammalian sperm are enriched in plasmalogens (Alvarez *et al.*, 1987). The *sn*-1 and *sn*-2 hydrocarbon chains of plasmalogens are linked to the glycerol backbone of phospholipids via an alk-1-enyl ether group and an ester C=O group, respectively. Therefore, acid methanolysis of a sperm/raft lipids, which contained appreciable amounts of plasmalogens, resulted in the generation of dimethylacetals (DMAs) and fatty acid methyl esters (FAMEs) from the *sn*-1 and *sn*-2 hydrocarbon chains, respectively (Kates, 1986). After the hydrolysis reaction, the tubes containing FAMEs and DMAs generated from PC and PE were placed at -20°C for 30 min. All subsequent steps were performed on ice to

prevent hydrolysis of FAMEs and DMAs. To the reaction mixture, cold water (0.5 ml) was added, followed by the addition of three 5 ml portions of petroleum ether. The reaction mixture was centrifuged at 300 g, 4°C for 1 min, to generate a two-phased solution. FAMEs and DMAs of sperm/raft PC and PE were collected from the upper petroleum ether layer and pooled, brought to dryness under a stream of $N_2$, and resuspended in 1 ml of heptane for gas chromatography-mass spectrometry (GC-MS) analysis.

A Varian 3400 GC instrument equipped with an autosampler (CTC Model A-200S) was operated using the Magnum software system 2.40 (Varian, San Jose, CA). The GC column was a DB-5 narrow bore capillary column (30 m long, 0.25 mm i.d., 0.1 $\mu$m film thickness). The GC injection port, transfer line and the detector manifold temperatures were 270, 280, and 300°C, respectively. The linear gas velocity with helium as carrier gas was 28.57 cm/s. The column temperature was initially held at 80°C for 1 min then increased at a rate of 10°C/min to 300°C where it was held for 20 min. Ionization was in the electron impact (EI) mode with an emission current of 10 $\mu$A, and the electron multiplier voltage was 1650 V. The mass range scanned was 40-650 amu with the automatic gain control setting and the total ion spectrum was obtained. The scan rate was 1 $s^{-1}$. Automated injections (1 $\mu$l of FAMEs and DMAs of sperm/raft PC and PE in heptane) were made on the GC. Linear ($R^2$ = 0.99) calibration curves were established for the FAMEs and DMAs by analysis of working standard solutions. Blanks were analyzed along with samples to verify cross contamination between analysis. DMAs of palmitaldehyde and stearic aldehyde were first characterized for their identity by injection into GC/MS. Molecular ions *(M/e)* of the DMA generated from palmitaldehyde were 255

(weak peak) and 75 (strong peak), typical of 16:0 DMA, whereas corresponding values of the DMA generated from stearic aldehyde were 283 and 75, typical of 18:0 DMA. FAME peaks were identified by both their retention times, compared to FAME standards (FAME mix (grain) standard, *cis*-4,7,10,13,16,19-docosahexaenoic acid methyl ester, and *cis*-7,10,13,16,19-docosapentaenoic acid methyl ester) and mass spectrometry, and their amounts were calculated based on the peak of an internal standard, methylhepta-decanoate.

## 2.16. Conjugation of Solubilized ZP to Alexa Fluor® Dye

Pig ZP were heat solubilized (1 h, 70°C) in 10 mM Tris-HCl, 100 mM NaCl, pH 9.5 (Burkin and Miller, 2000), and labeled with the Alexa Fluor dye, according to the manufacturer's instructions. While Alexa-488 was used for sperm-ZP binding experiments, Alexa-430 was employed for sperm rafts-ZP binding studies. Amine reactive probes, such as the Alexa Fluor® dye react with non-protonated aliphatic amine groups, i.e., ε-amino group of lysines and the terminal amino group of proteins. Therefore, the primary amine group of Tris, which was used for solubilization, would compete with the ZP for conjugation with the Alexa Fluor dye. To circumvent this problem, pig ZP was washed free of TBS by Microcon YM-30 centrifugation (4,000 g, 4°C) in PBS, as described above, and then resuspended in PBS. Since the success of the conjugation reaction is highly concentration dependent, it was recommended by the manufacturer to set the final concentration of the ZP solution in the range of 5-20 μg/μl. Therefore, Alexa-430/488 (5 μg/μl DMSO) was added to the ZP solution, and the ZP concentration used for this conjugation reaction was 20 μg/μl PBS. The reaction pH was

adjusted to 9.0 with 1 M sodium bicarbonate buffer. The reaction mixture was incubated overnight at 4°C in the dark, with continuous stirring. The unreacted dye was separated from the Alexa-430/488-ZP conjugates by Microcon YM-30 centrifugation (4,000 g, 4°C) in TBS, as described above. The degree of labeling was determined using the absorbance of the protein at 280 nm, and the absorbance of the dye at its absorbance maximum ($\lambda_{max}$), according to the manufacturer's instructions (Molecular Probes).

## 2.17. Binding of Fluorescently Labeled ZP to Live Sperm

Pig sperm were washed and capacitated as described above. Alexa-488-conjugated ZP (Alexa-488 ZP) was added to non-capacitated and capacitated sperm suspension (20 x $10^6$ sperm/ml of NCM and CM, respectively) to yield a final concentration of 5 μg/ml of Alexa-488 ZP in sperm. Alexa-488-conjugated ovalbumin (Alexa-488 ovalbumin) was used instead of Alexa-488-conjugated ZP, and served as a negative control. Sperm were incubated (39°C, 5% $CO_2$, 30 min), and at the 25$^{th}$ min of incubation, PI (0.5 μg/ml; stock solution of 50 μg/ml water) was added to each sperm sample to detect non-viable or membrane-compromised sperm. Alexa-488-protein conjugates unbound to sperm and unincorporated PI were removed by centrifugation (350 g, 28°C, 10 min). The sperm suspension was mounted onto a glass slide, and fluorescence images were captured as described in section 2.8.

## 2.18. Binding of Pig Sperm Rafts to Homologous ZP

Interactions between solubilized pig ZP and sperm rafts were investigated using a previously described solid phase binding assay (Yurewicz *et al.*, 1993) with minor

modifications. Briefly, black polystyrene 96-well microtiter plates were coated with pig sperm rafts (0.5 μg/well) in 100 mM sodium carbonate, pH 9.6, and then left at 4°C for 48 h. After blocking for 1 h at room temperature with 1% BSA in TBS, the plates were washed three times with TBS. The plates were then incubated for 1 h at room temperature with various concentrations (0-0.4 μM) of Alexa-430-conjugated ZP. Two different approaches were used to exclude non-specific binding of sperm rafts to Alexa-430-conjugated ZP. In the first experiment, the Alexa-430 ZP was substituted in the binding assay by Alexa-430 ovalbumin, previously shown not to bind to sperm (Carmona *et al.*, 2002a; Tantibhedhyangkul *et al.*, 2002; Bendahmane and Tulsiani, 2003). Since rafts isolated from whole sperm consisted of a mixture of those from the head (the interaction site of the egg, Chen and Cardullo, 1994; Kerr *et al.*, 2001; Yanagimachi, 1994) and from the tail (housing the motility apparatus and lacking ZP binding ability, Eddy and O'Brien, 1994; Yanagimachi, 1994), the binding of Alexa-430 ZP to sperm tail rafts was used as another criterion to exclude non-specific binding between sperm rafts and the ZP. In addition, the sperm tail rafts also served as a negative control of SGG-containing rafts, since the sperm tail contained very little amounts of the ZP adhesion molecule SGG (White *et al.*, 2000; Weerachatyanukul *et al.*, 2001). The plates were washed three times with TBS to remove unbound Alexa-430-protein conjugates, and fluorescence intensity was measured using a Spectramax GeminiXS spectrofluorometer (Molecular Devices) at excitation and emission wavelengths of 425 and 520 nm, respectively. The amount of Alexa-430-conjugated ZP/ovalbumin bound to sperm rafts in each well was determined from the Alexa-430-conjugated ZP/ovalbumin standard curves.

To determine whether sperm rafts employ the same ZP receptors as sperm, pig ZP, ZP3, ZP3α and ZP3β, all known to play a role in sperm-ZP interaction (Yurewicz *et al.*, 1993, 1998), were assessed for their ability to compete with Alexa-430 ZP in binding to sperm rafts. A competitive binding assay was performed by adding various concentrations (0-4 μM) of each of pig ZP3, ZP3α, ZP3β, solubilized ZP or ovalbumin (negative control) together with 0.2 μM of Alexa-430 ZP in 0.1 ml TBS to each well of the plate precoated with 0.5 μg of PGC-capacitated sperm rafts. Following incubation for 1 h at room temperature, the plate was washed, and the fluorescence intensity of Alexa-430 ZP bound to PGC-capacitated sperm rafts was measured. Competitive binding curves were plotted as percentage of the bound Alexa-430 ZP (μmoles/0.5 μg raft proteins), i.e., from incubations of Alexa-430 ZP with PGC-capacitated sperm rafts without any competitors, as a function of the molarity of the ZP competitors. Molarity of total ZP sulfoglycoproteins in solubilized ZP was calculated based on the 1:4 molar distribution of ZP1 (86 kDa) to ZP3 (55 kDa), as determined by densitometric analysis (Carmona *et al.*, 2002a). The amount of Alexa-430 ZP bound to sperm rafts in the presence and absence of the competitors was determined as described above.

To determine the $K_d$ (dissociation constant) and binding capacity ($B_{max}$) of sperm rafts to the ZP, microtiter plate wells were coated with rafts isolated from washed, washed-capacitated, PGC and PGC-capacitated sperm, and then incubated with Alexa-430 ZP in the presence of a 100-fold excess of unlabeled ZP. The plates were washed with TBS, and fluorescence intensity was measured as described above. Following subtraction of non-specific binding of Alexa-430 ZP to sperm rafts in the presence of

100-fold excess ZP, the $K_d$ and $B_{max}$ of rafts-ZP binding were determined by non-linear regression using GraFitt 4.0 software for Windows.

## 2.19. Binding of Pig Sperm Rafts Pretreated with Affinity Purified Anti-SGG IgG/Fab to Homologous ZP

To elucidate the role of SGG as a sperm raft component in ZP binding, the binding of sperm rafts to Alexa-430 ZP was evaluated following pretreatment (1 h, room temperature) of rafts with various concentrations of affinity purified anti-SGG IgG/Fab (0-16 μM), prepared as described above. These concentration ranges gave antigen-binding units corresponding to 0.5- to 2-fold of 0.7 nmoles of SGG present in sperm rafts in each well. Anti-SGG Fab was used to determine whether the observed inhibition of sperm raft-Alexa-430 ZP binding was due to specific masking of SGG molecules in sperm rafts or due to steric hindrance due to the bivalent nature of the antibody. The plates were washed three times with TBS to remove unbound anti-SGG IgG. Subsequently, 100 μl of 0.2 μM Alexa-430 ZP was added to each well of a microtiter plate coated with PGC-capacitated sperm rafts (i.e., 0.5 μg raft proteins/well). Rafts pretreated with PRS IgG/Fab, and incubated with Alexa-430 ZP served as negative controls. The microtiter plates were then washed, the amount of Alexa-430 ZP bound to PGC-capacitated sperm rafts in each well was determined, and the data obtained was analyzed as described in section 2.18.

## 2.20. Statistical Analyses

Student's *t* test and ANOVA were used to determine a significant difference between two sets of data. Specifically, the binding of sperm rafts to Alexa-430 ZP was evaluated by ANOVA, followed by linear contrasts to evaluate differences among ZP components. The ZP component (or ovalbumin) and concentration were main effects, and replicate was a random effect.

# CHAPTER THREE

# RESULTS

## 3.1. Biophysical Properties of SGG and Structurally Related Glycolipids

The understanding of the ZP adhesion function of SGG, the major sulfoglycolipid of the mammalian male germ cell, as well as SGG's contribution to the biophysical properties of the sperm plasma membrane requires knowledge of the lipid conformational behavior. Therefore, the hydrocarbon chain conformational order/disorder and interfacial hydrogen bonding of SGG was investigated by FTIR spectroscopy. Since SGC and its precursor GC are commercially available, both glycolipids served as structural analogs of SGG and its desulfated product GG, respectively, and their biophysical properties were also studied in this thesis. In particular, comparison of the conformational properties of SGC and SGG will reveal the contribution of the structural backbone and the hydrocarbon chains (Figure 1.6) to bilayer order/disorder. Since GG, i.e., the desulfated product of SGG, is not commercially available, comparison of the results obtained with SGC and GC provides information on the influence of the sulfate group on intermolecular hydrogen bonding at the bilayer surface, as well as hydrocarbon chain conformation and packing in the bilayer matrix. Current evidence does not support GG formation prior to and during fertilization-related events (Carmona *et al.*, 2002a; Tanphaichitr *et al.*, 1990). Therefore, the deduced information will be beneficial for future studies on the structural properties of GG once its physiological significance during fertilization is established.

Both DSC and FTIR spectroscopy are used to assess the phase behavior of lipids. However, FTIR spectroscopy is advantageous since it also monitors molecular vibrations

of individual structural groups of lipids (Wong *et al.*, 1988; Lewis and McElhaney, 1990). A typical FTIR spectrum of lipids forming lamellar structures in aqueous medium is shown in Figure 3.1. This spectrum reflects the contribution of many structural groups, and different spectral regions are used to probe lipid-lipid interactions (Appendix 1). In this study, the $CH_2$ and C=O stretching regions are examined to assess the conformational properties and interfacial hydrogen bonding, respectively, of SGG, SGC and GC. The $CH_2$ symmetric stretching vibration (~ 2850 $cm^{-1}$) is sensitive to temperature and related to the average number of *gauche* conformers in a system. In the gel phase, the hydrocarbon chains of lipids are in the all-*trans* conformation. As temperature increases, lipids undergo a transition from the gel to the liquid-crystalline or chain-melted state due to the introduction of *gauche* conformers, and the $CH_2$ symmetric stretching vibration shifts to higher absorption frequencies (Appendix 1). At the interfacial region of the bilayer, hydrogen bonding was assessed by examining the ester C=O (1700-1780 $cm^{-1}$) and amide I (1600-1680 $cm^{-1}$) stretching modes of SGG and SGC/GC, respectively. The frequencies of these two modes decrease proportionally with the degree of their hydrogen bonding to proton donating groups, due to the elongation of the C=O bonds. In the gel and liquid-crystalline phase, the ester C=O and amide I stretching bands are broad, representing the equilibrium between non-hydrogen bonded and hydrogen-bonded species (Wong and Mantsch, 1988). Resolution enhancement or deconvolution of the ester C=O and amide I bands reveals a low frequency component reflecting the population of hydrogen bonded lipids, and a high frequency component representing the non-hydrogenspecies. In the crystal-like phase, the ester C=O stretching band of glycosyl-diacylglycerolipids (Lewis *et al.*, 1990) and of saturated diacylglycerophospholipids

**Figure 3.1.** FTIR spectrum of lipids forming lamellar structures in aqueous medium in the region 1000-4000 $cm^{-1}$. This spectrum reflects the contribution of many structural groups, and different spectral regions are used to probe lipid-lipid interactions. For the purpose of this study, the $CH_2$ symmetric stretching vibration (~ 2850 $cm^{-1}$) was used to monitor the dynamics and molecular order of the hydrocarbon chains of lipids. At the interfacial region of the bilayer, the ester C=O (1700-1780 $cm^{-1}$) and amide I (1600-1680 $cm^{-1}$) stretching bands of lipids were used to assess hydrogen bonding of SGG and SGC/GC, respectively.

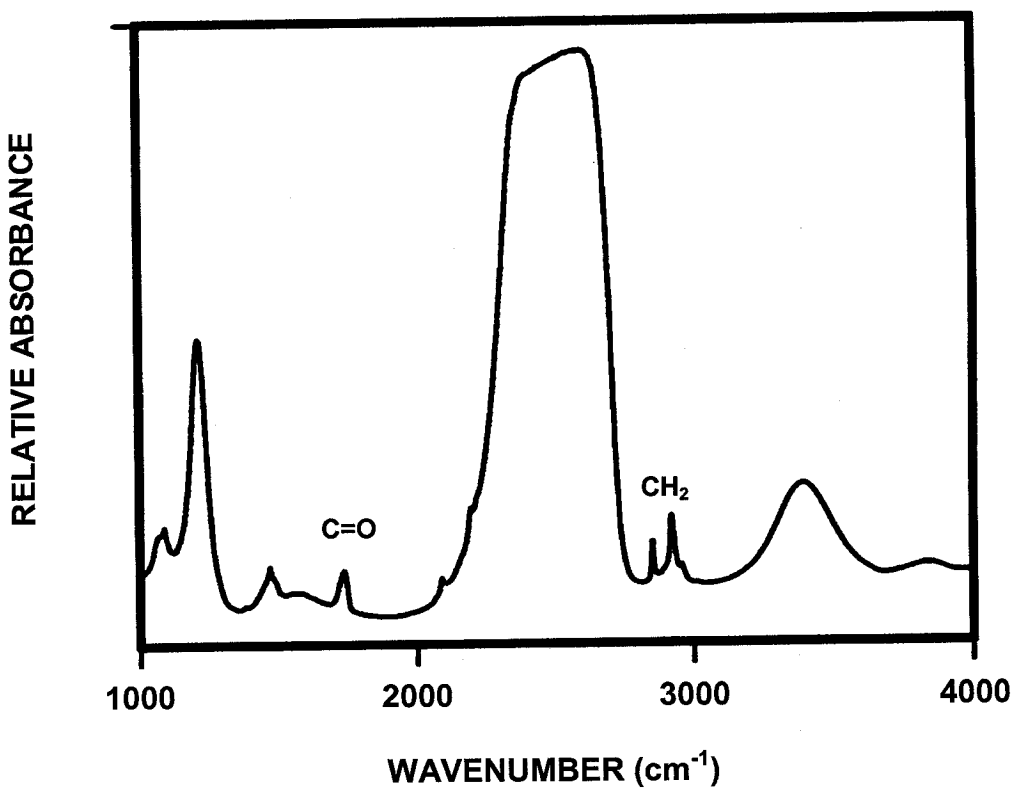
RELATIVE ABSORBANCE
C=O
CH2
1000
2000
3000
4000
WAVENUMBER (cm-1)

(Zhang *et al.*, 1997; Lewis *et al.*, 1994; McMullen *et al.*, 1999; Lewis and McElhaney, 2000) appears as a summation of several components even without any resolution enhancement of this spectral region.

DSC and X-ray diffraction reveal that GC and SGC exhibit complex polymorphic phase behavior, as well as conversions between metastable and stable bilayer structures at low temperatures during heating to the liquid-crystalline phase, and following cooling from that phase (Ruocco *et al.*, 1981; Reed and Shipley, 1987; Haas and Shipley, 1995; Saxena *et al.*, 1999). However, a diffraction pattern of the different bilayer phases was not always obtainable at various temperatures. Based on these observations, SGG and SGC may exhibit complex polymorphic phase behavior, similarly to GC. Since FTIR spectroscopy successfully probes the polymorphic phase behavior of glycosyldiacyl-glycerolipids (Lewis *et al.*, 1990), and saturated diacylglycerophospholipids (Zhang *et al.*, 1997; Lewis and McElhaney, 2000), the phase behavior of SGG, SGC, and GC bilayers was monitored by FTIR spectroscopy. The polymorphism of these glycolipids was monitored prior to hydrocarbon chain melting, and also following subsequent cooling from the chain-melted state. FTIR spectroscopic experiments were also performed as a function of time to determine whether the polymorphism of SGG, SGC, and GC was temperature, time or both temperature and time driven. The contribution of hydrocarbon chain conformation and packing, as well as hydrogen bonding to polymorphism of SGG, SGC, and GC was also examined. Since DSC and X-ray diffraction provided data suggesting that conversions between metastable and stable bilayer phases of GC were

accompanied by hydration (Ruocco *et al.*, 1981; Reed and Shipley, 1987), experiments were also conducted with dehydrated SGG, SGC and GC bilayers to gain further insight into the nature of the various polymorphs adopted by these glycolipids.

### *3.1.1. Phase Behavior of GC: Temperature-Dependent FTIR Spectroscopic Studies*

GC consists of a mixture of amide-linked non-hydroxylated and α-hydroxy fatty acyl chains (NFA-GC and HFA-GC, respectively) (Figure 1.6), with HFA-GC being 40-60% in distribution in vertebrate myelin (Norton and Cammer, 1984; Svennerholm and Stallberg-Stenhagen, 1968). Therefore, the phase behavior of both NFA-GC and HFA-GC was studied to assess the contribution of the hydroxyl group to the complex polymorphic phase behavior of GC.

#### *3.1.1.1. Hydrocarbon Chain Melting of NFA-GC*

Plots of the temperature dependence of the $CH_2$ symmetric stretching band are shown in Figure 3.2, displaying the phase behavior of NFA-GC upon heating to liquid-crystalline temperatures, and following subsequent cooling. NFA-GC bilayers underwent a main phase transition at ~80°C (Figure 3.2), in good agreement with previous results (Ruocco *et al.*, 1981; Reed and Shipley, 1987, 1989; Haas and Shipley, 1995; Saxena *et al.*, 1999; Curatolo, 1982). The abrupt increase in the frequency of the $CH_2$ band at 80°C (~4 $cm^{-1}$) represents the onset of the *trans-gauche* isomerization, and indicates an increase in the conformational disorder of the hydrocarbon chains of NFA-GC, typical of hydrocarbon chain melting in the liquid-crystalline phase. The temperature profile also exhibits another small increase in the $CH_2$ symmetric stretching frequency at ~50°C.

**Figure 3.2.** Thermotropic response of the $CH_2$ symmetric stretching frequency of hydrated NFA-GC upon heating (●) and cooling (○). NFA-GC dispersions (5%, w/v) were prepared in $^2H_2O$ buffered with 50 mM Tris-HCl (p$^2$H 7.05). The $T_m$ values were estimated from the first derivative plots of the $CH_2$ symmetric stretching vibration frequency vs. temperature. Data shown were representative of three replicate experiments.

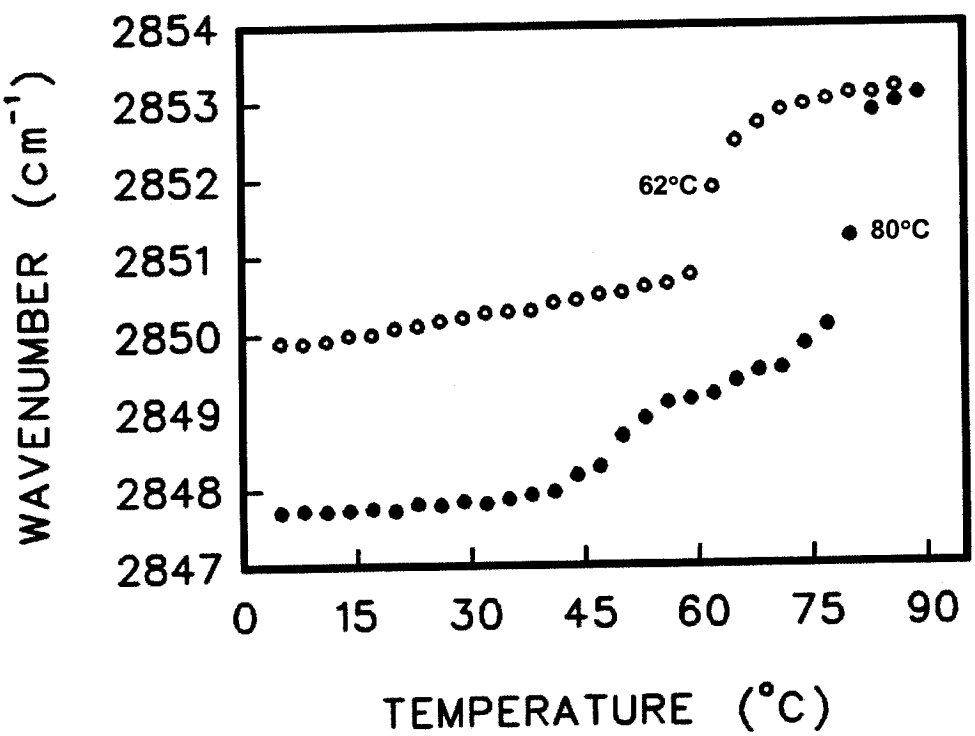
2854
2853
2852
2851
2850
2849
2848
2847
WAVENUMBER (cm$^{-1}$)
62°C
80°C
0
15
30
45
60
75
90
TEMPERATURE (°C)

Galactosylceramide (GC) was previously shown to convert between metastable and stable bilayer structures below its high temperature phase transition (Ruocco *et al.*, 1981; Reed and Shipley, 1987, 1989; Haas and Shipley, 1995; Saxena *et al.*, 1999; Curatolo, 1982). Therefore, the small transition of NFA-GC observed at 50°C presumably represents conversions between metastable and stable polymorphs prior to the main phase transition at 80°C. Upon cooling from 90°C, the hydrated NFA-GC bilayers exhibit significant hysteresis, clearly indicating a slow equilibration process, with a sharp transition shifted to 62°C (Figure 3.2). This hysteresis behavior was also observed for ceramides (Shah *et al.*, 1995), as well as for GC (Ruocco *et al.*, 1981; Reed and Shipley, 1987, 1989; Haas and Shipley, 1995; Saxena *et al.*, 1999; Curatolo, 1982). The thermotropic event observed at 50°C in the heating run of NFA-GC is not observed during the cooling process. The higher frequency of the $CH_2$ symmetric stretching band of NFA-GC upon cooling to 5°C indicates that its hydrocarbon chains are more disordered than at the beginning of the heating scan (Figure 3.2).

#### *3.1.1.2. Interfacial Hydrogen Bonding of NFA-GC*

To assess the contribution of hydrogen bonding to the metastable-stable conversions observed prior to hydrocarbon chain melting, changes in the spectral patterns of the amide I band of NFA-GC were monitored as a function of temperature upon heating and cooling (Figure 3.3). This band is the summation of several components that can be discerned even without any resolution enhancement or deconvolution. From 5 to 44°C, a major peak is observed near 1629 $cm^{-1}$, with an apparent shoulder extending from 1580 to 1620 $cm^{-1}$ (Figure 3.3A). Between 47 and 71°C, the broad shoulder becomes

**Figure 3.3.** Stacked contour plots of the amide I stretching region of the infrared spectra of hydrated NFA-GC, obtained at the temperatures indicated, upon heating (**A**) and following subsequent cooling (**B**). NFA-GC dispersions (5%, w/v) were prepared in $^2H_2O$ buffered with 50 mM Tris-HCl ($p^2H$ 7.05). Data shown were representative of three replicate experiments.

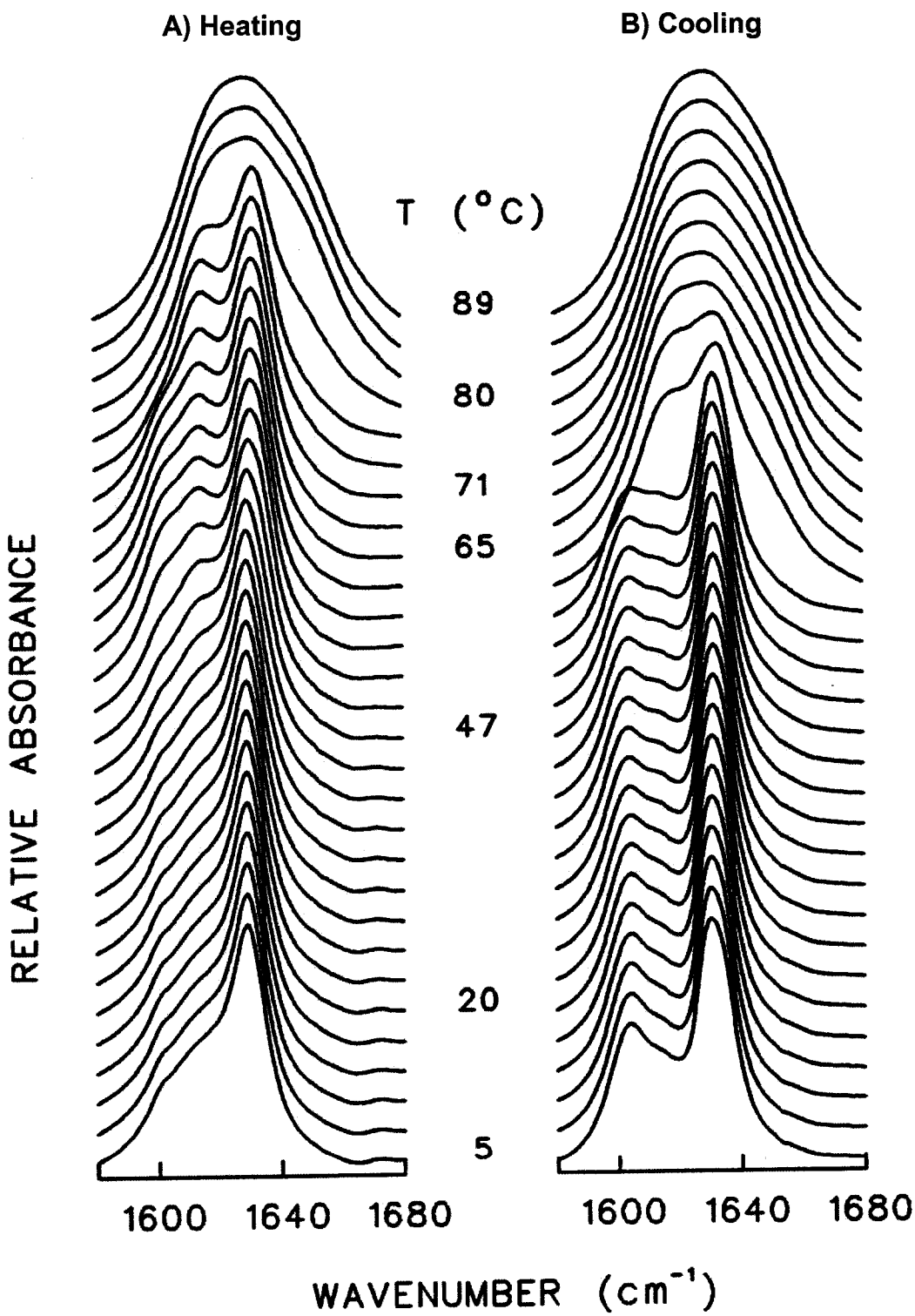
A) Heating
B) Cooling
T (°C)
89
80
71
65
47
20
5
RELATIVE ABSORBANCE
1600
1640
1680
1600
1640
1680
WAVENUMBER (cm⁻¹)

more convex, forming two discernable peaks at 1613 and 1602 $cm^{-1}$. At 74 and up to 80°C, the amide I band consists mainly of two components near 1629 and 1613 $cm^{-1}$, with the latter peak shifting to 1614 $cm^{-1}$ at 80°C. The spectral patterns of the amide I band reveal that NFA-GC adopts two crystal-like phases, en route to the chain melted state: the first (termed $L_c1$) existing between 5 and 44°C, and the second (termed $L_c2$) between 74 and 80°C (Figure 3.3A). The slow transformation of $L_c1$ into $L_c2$ starts at 47°C, with both crystal-like phases coexisting between 47 and 71°C. This transformation is completed at 74°C, at which point the spectral features of a different crystal-like phase (termed $L_c2$) were established. These results are in agreement with X-ray diffraction studies revealing that GC (Ruocco *et al.*, 1981; Reed and Shipley, 1987, 1989; Haas and Shipley, 1995; Saxena *et al.*, 1999; Curatolo, 1982) and glycosyldiacylglycerolipids (Lewis *et al.*, 1990; Sen *et al.*, 1990) form crystal structures. As the hydrocarbon chain conformational disorder of NFA-GC increased, a broad amide I band appears above 80°C (Figure 3.3A), indicative of a transformation of the bilayers into the chain-melted state. In this phase, the increased conformational disorder of the hydrocarbon chains of NFA-GC results in a lateral expansion of the lipidic network, which can compromise intermolecular hydrogen bonding between neighboring lipid molecules but allows increased hydrogen bonding with interfacial water. This also results in increased conformational heterogeneity of the amide C=O groups at the interfacial region, giving a broad amide I band in the chain melted state. The temperatures where significant changes of the amide I band of NFA-GC take place parallel those at which chain packing rearrangements and bilayer organization occur (Figure 3.2 vs. Figure 3.3A).

When NFA-GC bilayers are cooled from the chain melted state (89°C) (Figure 3.3B), the broad amide I band is maintained until 65°C, at which point a peak near 1629 $cm^{-1}$ and an adjacent shoulder at 1620 $cm^{-1}$ became apparent. This low frequency shoulder presumably represents hydrogen bonded NFA-GC molecules (Wong and Mantsch, 1988; Lee *et al.*, 1986; Jackson *et al.*, 1988). Between 65 and 62°C, the amide I spectral patterns are analogous to, although not as narrow as, those in the $L_c2$ phase. Therefore, NFA-GC bilayers presumably exist in an intermediate state corresponding to a biphasic mixture (liquid-crystalline + $L_c2$). From 59 to 5°C, the shoulder becomes more resolvable from the 1629 $cm^{-1}$ component band, and comprises two overlapping peaks near 1614 and 1603 $cm^{-1}$. This suggests a strengthened hydrogen bonding network of NFA-GC (Figure 3.3B), and the observed crystalline phase is termed $L_c3$ (due to its difference from $L_c1$ and $L_c2$). Although $L_c3$ is somewhat similar to the $L_c1$ + $L_c2$ mixture between 47 and 71°C, the amide I component bands are more separated from each other in the $L_c3$ state (Figure 3.3).

The thermal treatment of NFA-GC significantly influences its polymorphic phase behavior. When NFA-GC are heated to a temperature below its chain melting transition (80°C), conversions between metastable ($L_c1$) and stable ($L_c2$) bilayer structures are observed, as revealed by the patterns of the amide I band. Upon cooling from 80°C, $L_c2$ is stable even at 5°C, a temperature favoring the formation of $L_c1$ (results not shown). On the other hand, heating NFA-GC to 89°C, i.e., above its main chain melting transition at 80°C, and subsequent cooling results in the formation of $L_c3$ following a transition from an intermediate biphasic mixture (liquid-crystalline + $L_c2$) (Figure 3.3B). These results

indicate that, below the chain melted state, the most stable crystal-like arrangement adopted by NFA-GC is $L_c2$. However, once in the liquid-crystalline phase, conformational and orientational changes of NFA-GC may occur, leading to the generation of a stable $L_c3$ polymorph upon cooling.

The variations in the relative intensity of the 1614 and 1603 $cm^{-1}$ amide I components of NFA-GC (in the $L_c3$ phase) reflect the presence of different populations of hydrogen bonded amide C=O groups. Lewis *et al.* (1990) studied the physical properties of glycosyldiacylglycerolipids by FTIR spectroscopy and concluded that the shift of the ester C=O band to lower frequencies is possibly due to a bond to a sugar hydroxyl group. They also suggested that, as a prerequisite for strong hydrogen bonds, partial dehydration should occur at the polar/non polar interfacial region of the bilayer. By analogy, it could be proposed that $L_c3$ should possess a strong hydrogen bonding network due to a partial dehydration and/or localization of the amide C=O groups of NFA-GC in less polar environments. Therefore, dehydration experiments are conducted to gain further insight into the crystal-like structures of NFA-GC. The dehydrated bilayers exhibit no sign of a cooperative phase transition in the temperature range 0 to 90°C, as revealed by their $CH_2$ symmetric stretching band (results not shown). The spectral patterns of the amide I band of the dehydrated NFA-GC bilayers are presented in Figure 3.4. Between 5 and 77°C, the amide I band is the sum of three overlapping components at 1632, 1614 and 1602 $cm^{-1}$. The two low frequency components at 1614 and 1602 $cm^{-1}$ presumably represent two populations of hydrogen bonded amide C=O groups, which differ in the polarity of their surrounding environment and/or in the strength or degree of their hydrogen bonding interactions. While the 1632 and 1614 $cm^{-1}$ components remain detectable up to 89°C,

**Figure 3.4.** Stacked contour plots of the amide I stretching region of the infrared spectra of dehydrated NFA-GC, obtained at the temperatures indicated. NFA-GC dispersions (5%, w/v) were prepared in $^{2}H_{2}O$ buffered with 50 mM Tris-HCl ($p^{2}H$ 7.05), and left in the open transmission cell in the sample compartment of the infrared spectrophotometer for 96 h to obtain the dehydrated sample. Data shown were representative of three replicate experiments.

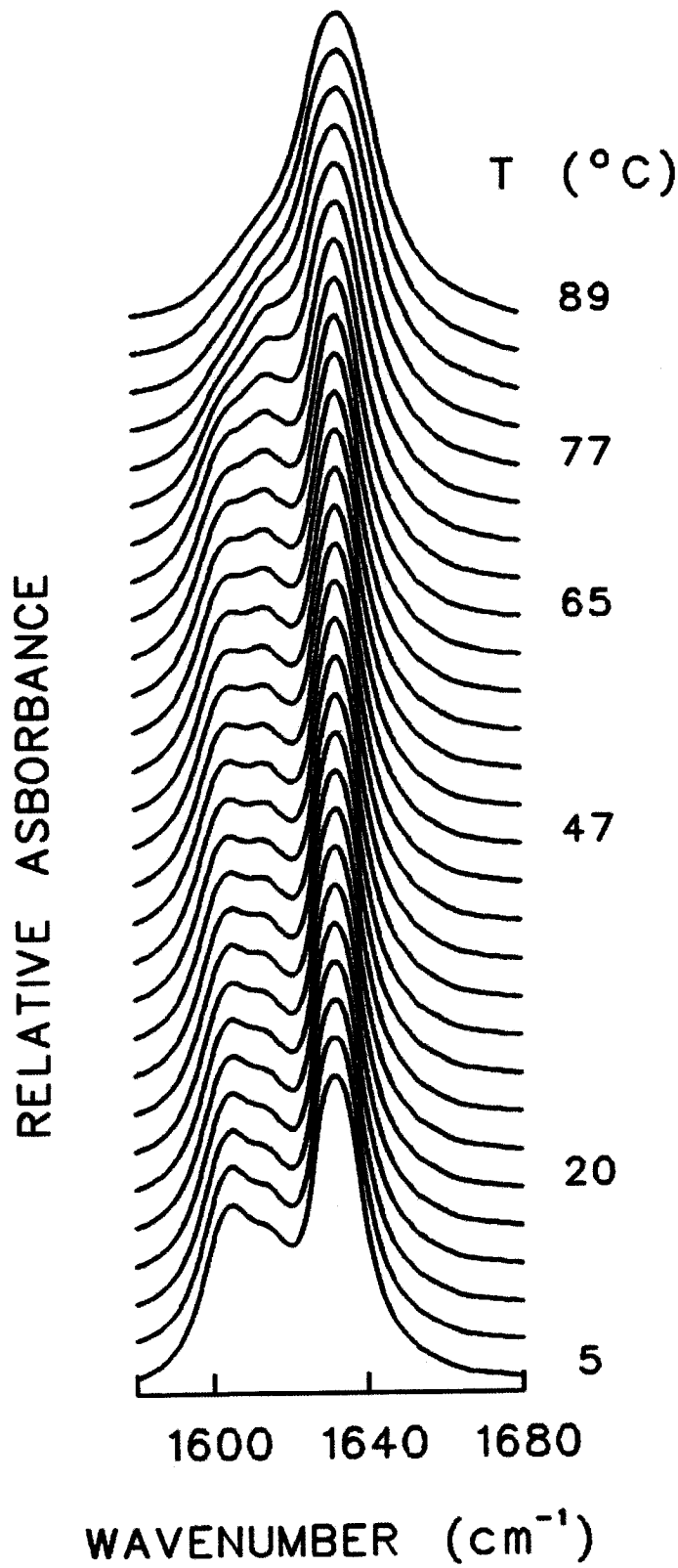
T (°C)
89
77
65
47
20
5
RELATIVE ASBORBANCE
1600
1640
1680
WAVENUMBER (cm⁻¹)

the 1602 $cm^{-1}$ peak becomes unresolvable above 77°C, indicating that the hydrogen bonding network of dehydrated NFA-GC was weakened at high temperatures. However, hydrogen bonding is not totally disrupted since the 1614 $cm^{-1}$ component band is detected even at 89°C. Upon cooling of the dehydrated NFA-GC, the 1602 $cm^{-1}$ component band is not recovered (results not shown), suggesting that heating of the dehydrated bilayers to high temperatures (89°C) induces irreversible rearrangements of the hydrogen bonding network of NFA-GC. The patterns of the amide I band in the dehydrated state (Figure 3.4) are similar to those in the $L_c3$ phase (Figure 3.3B), which suggests that this latter was poorly hydrated.

Since temperature changes are done in a timely manner, it is questionable whether the conversions between crystal-like polymorphs of NFA-GC were temperature, time or both temperature and time dependent. To investigate this, hydrated NFA-GC is first heated to 38°C to generate $L_c1$, and the bilayers are held at that temperature for 96 h (Figure 3.5A). After forty five minutes (time needed in the continuous heating experiment to increase the temperature from 38 to 47°C (Figure 3.3A), where the initiation of the transformation into $L_c2$ is apparent), the spectral patterns of $L_c1$ remain unchanged (results not shown). Following incubation of the bilayers at 38°C for 24 h, a mixture consisting of $L_c1$ + $L_c2$ was detected. The transformation of $L_c1$ into $L_c2$ is completed after 48 h, and $L_c2$ was stable up to 96 h (Figure 3.5A, top trace) at 38°C, a temperature at which only $L_c1$ is observed when the temperature is increased stepwise in the initial experiment (Figure 3.3A). These results demonstrate that the formation of $L_c1$ and $L_c2$ can be induced by either heat or time. The slow transformation of $L_c1$ into $L_c2$ at ~47°C during the heating experiment of NFA-GC (Figure 3.3A) would have probably

**Figure 3.5.** Amide I stretching region of the infrared spectra of hydrated NFA-GC. (**A**) NFA-GC dispersions were heated to 38°C, and incubated at that temperature for 96 h in the spectrophotometer compartment. (**B**) NFA-dispersions were heated to 89°C, then cooled to 38°C and left at that temperature for 96 h in the closed transmission cell inside the spectrophotometer compartment. NFA-GC dispersions (5%, w/v) were prepared in $^{2}H_2O$ buffered with 50 mM Tris-HCl ($p^{2}H$ 7.05). Data shown were representative of three replicate experiments.

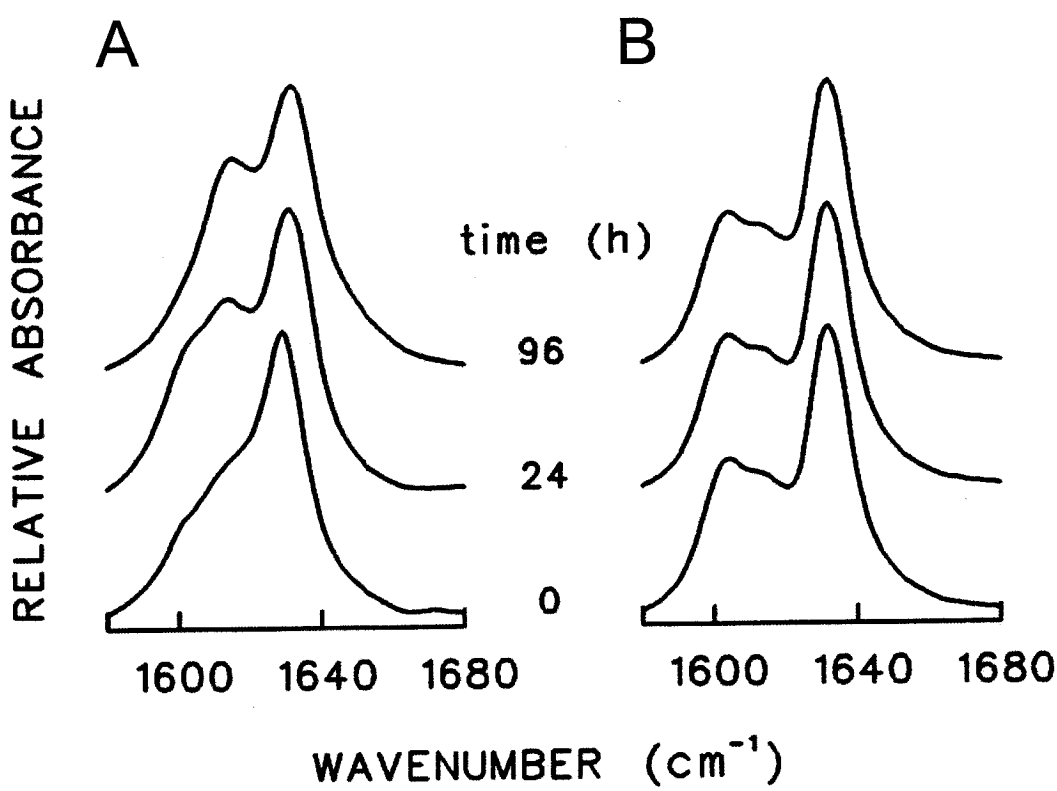
A
B
RELATIVE ABSORBANCE
time (h)
96
24
0
1600
1640
1680
1600
1640
1680
WAVENUMBER (cm$^{-1}$)

appeared at lower temperatures if the heating rate had been slower, since $L_c1$ eventually transforms into $L_c2$ at 38°C (Figure 3.5A).

In the second set of experiments, I tested whether $L_c3$, generated during the cooling experiment of NFA-GC from the liquid-crystalline phase, could be converted to $L_c1/L_c2$ or other crystal-like polymorphs. Hydrated NFA-GC bilayers are heated to 89°C, then cooled and maintained at 38°C up to 96 h. This results in the formation of $L_c3$, which is stable throughout the time course of the experiment (96 h) (Figure 3.5B). In a different experiment, when NFA-GC is cooled from 89 to 65°C, an intermediate mixture (liquid-crystalline + $L_c2$) is observed. Further incubation at 65°C results in the formation of $L_c3$ after thirty minutes (results not shown), time required for stepping down from 65 to 59°C (where $L_c3$ is first observed) in the cooling experiment (Figure 3.3B). This indicates that the formation of $L_c3$ would have occurred at 65°C if the bilayers had been cooled at a slower rate. Further cooling of the NFA-GC bilayers from 65 to 38°C reveals that once $L_c3$ is generated, it remains stable up to 96 h of incubation at 38°C. Although the hydrocarbon chain packing of NFA-GC is more disordered in the $L_c3$ phase (Figure 3.2), as evidenced by the higher frequencies of the $CH_2$ groups, its hydrogen bonding network was very stable.

### *3.1.1.3. Hydrocarbon Chain Melting of HFA-GC*

The thermotropic response of the hydrocarbon chains of HFA-GC upon heating and cooling is shown in Figure 3.6. In the heating scan, a cooperative phase transition occurs at 72°C, and a shallow feature is seen between 30 and 45°C. This peak possibly

**Figure 3.6.** Thermotropic response of the $CH_2$ symmetric stretching frequency of hydrated HFA-GC upon heating (●) and cooling (○). HFA-GC dispersions (5%, w/v) were prepared in $^2H_2O$ buffered with 50 mM Tris-HCl ($p^2H$ 7.05). The $T_m$ values were estimated from the first derivative plots of the $CH_2$ symmetric stretching vibration frequency vs. temperature. Data shown were representative of three replicate experiments.

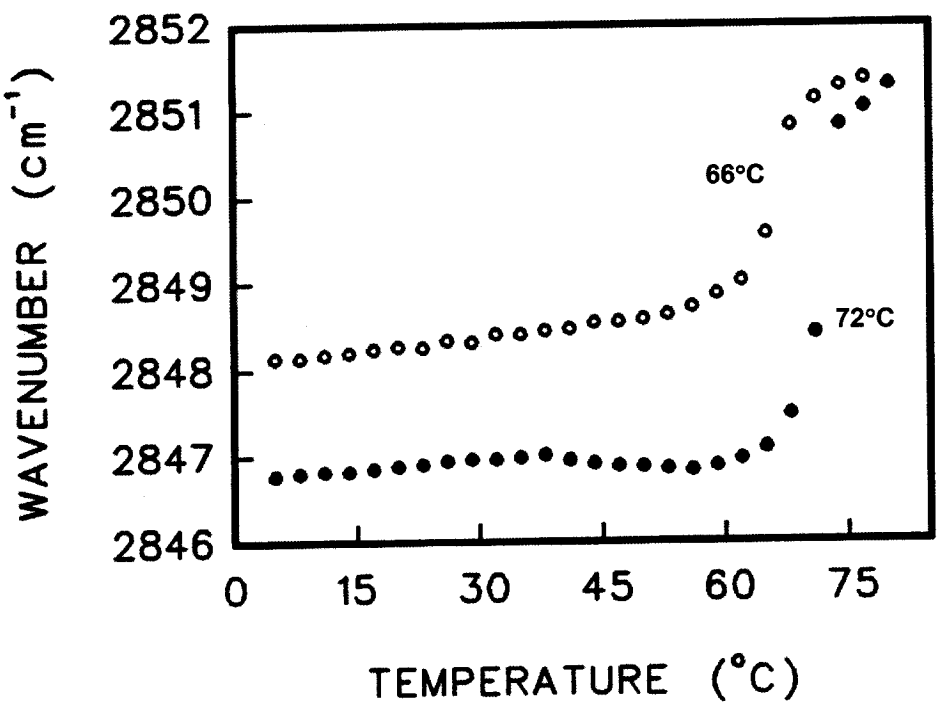
2852
2851
2850
2849
2848
2847
2846
WAVENUMBER (cm$^{-1}$)
66°C
72°C
0
15
30
45
60
75
TEMPERATURE (°C)

reflects the presence of a metastable low temperature form converting into a stable form (see below) on heating (Figure 3.6). In comparison with NFA-GC, the hydrocarbon chains of HFA-GC are more ordered, as indicated by the lower frequencies of the $CH_2$ symmetric stretching band (Figure 3.2 vs. Figure 3.6). The α-hydroxyl group may favor intermolecular hydrogen bonding between neighboring HFA-GC molecules, thus leading to increased order or stability within these bilayers. However, hydrocarbon chain melting of HFA-GC occurs at 72°C, compared to 80°C for NFA-GC. Since HFA-GC contains primarily 24:0 (Johnston and Chapman, 1988), HFA-GC may form interdigitated bilayers (Reed and Shipley, 1987), due to hydrocarbon chain asymmetry. HFA-GC may also possess a strong hydrogen bonding network, which would favor a shovel conformation of the glycosphingolipid with respect to the hydrocarbon chain axis (Pascher and Sundell, 1977; Nyholm *et al.*, 1990; Bunow and Levin, 1980). The extensive hydrogen bonding of HFA-GC may affect the interdigitated state of the hydrocarbon chains of HFA-GC, thus resulting in a lower order-disorder $T_m$, relative to NFA-GC. In fact, prevention of hydrocarbon chain interdigitation was previously reported to induce a disordering effect for different PC species (Mason *et al.*, 1981; Huang and Mason, 1986).

Upon cooling of HFA-GC from the chain-melted state, the phase transition is observed at a lower temperature (i.e., 66°C), and the frequencies of the $CH_2$ stretching band remain higher. This indicates an increase in the disorder of the hydrocarbon chains. The small peak at 38°C in the heating profile is not observed in the cooling scan (Figure 3.6).

### *3.1.1.4. Interfacial Hydrogen Bonding of HFA-GC*

The patterns of the amide I band of HFA-GC are shown in Figure 3.7. Upon heating from 5 to 38°C, the shape of the amide I band of HFA-GC is similar to that of the ester C=O band of saturated diacylglycerophospholipids in the hydrated gel phase (Zhang *et al.*, 1997). This is in accordance with X-ray diffraction and DSC studies revealing that HFA-ceramide adopts a well-ordered gel phase at 20°C (Shah *et al.*, 1995). The contours of the amide I band are asymmetric and leaning toward low frequencies, with a maximum at 1628 $cm^{-1}$ (Figure 3.7A). This presumably reflects hydrogen bonding of the amide C=O groups with interfacial water (Wong and Mantsch, 1988; Jackson *et al.*, 1988), due to the α-hydroxyl group of HFA-GC. From 44 to 71°C, two discernable peaks are detected at 1635 and 1620 $cm^{-1}$ (Figure 3.7A), representing non-hydrogen bonded and hydrogen bonded amide C=O groups, respectively. These two peaks show band narrowing, indicative of a crystal-like structure (termed $L_cI$) (Zhang *et al.*, 1997; Lewis and McElhaney, 1993). Above 71°C, the two narrow amide I components disappear: a broader band with its maximum at 1633 $cm^{-1}$ is observed, suggesting that the HFA-GC bilayers are in the liquid-crystalline phase (Figure 3.7A). Both the conformation of the hydrocarbon chains and hydrogen bonding interactions may influence the gel to crystal-like conversions of HFA-GC prior to chain melting, as suggested by Reed and Shipley (1987). Cooling of HFA-GC bilayers from 80°C results in the formation of a slightly broader amide I band, consistent with the formation of a gel phase (Figure 3.7B). The gradual shift of the amide I band from 1633 $cm^{-1}$ in the liquid-crystalline phase to 1619 $cm^{-1}$ in the gel phase suggests an increase in the hydrogen bonding potential of the amide C=O groups of HFA-GC with neighboring molecules, which is plausibly mediated by the

**Figure 3.7.** Stacked contour plots of the amide I stretching region of the infrared spectra of hydrated HFA-GC, obtained at the temperatures indicated, upon heating (**A**) and following subsequent cooling (**B**). HFA-GC dispersions (5%, w/v) were prepared in $^2H_2O$ buffered with 50 mM Tris-HCl ($p^2H$ 7.05 Data shown were representative of three replicate experiments.

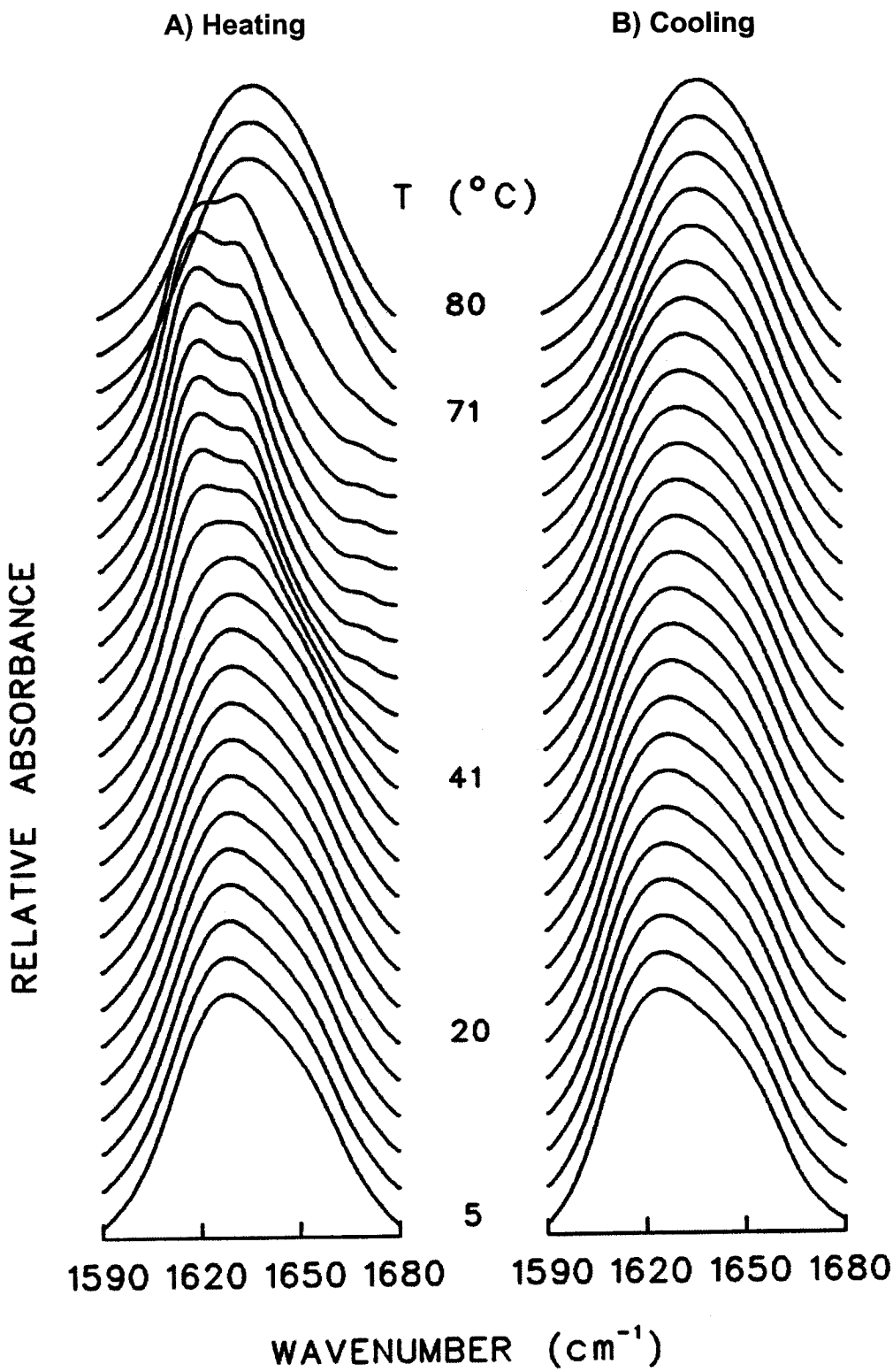
A) Heating
B) Cooling
T (°C)
80
71
41
20
5
RELATIVE ABSORBANCE
1590 1620 1650 1680
1590 1620 1650 1680
WAVENUMBER (cm⁻¹)

α-hydroxyl group of the glycosphingolipid. This would therefore stabilize the gel phase and prevent polymorphism of HFA-GC throughout the cooling process.

To further probe the polymorphic behavior of HFA-GC, as well as the nature of the crystal-like form observed on heating, dehydrated bilayers are generated and studied as a function of temperature. The dehydrated bilayers do not exhibit a phase transition from 0 to 80°C, as revealed by their $CH_2$ symmetric stretching band (results not shown). The amide I band of HFA-GC consists of a sharp peak at 1628 $cm^{-1}$, and a narrow shoulder near 1616 $cm^{-1}$ (Figure 3.8). The contours of the amide I band of HFA-GC in the dehydrated state are similar to those in the $L_cI$ state, suggesting that $L_cI$ is partially dehydrated (Figure 3.7A vs. Figure 3.8). However, the amide I components are detected near 1628 and 1616 $cm^{-1}$ in the dehydrated state, compared to 1635 and 1620 $cm^{-1}$ in the $L_cI$ state. This indicates that dehydration of HFA-GC either changed the polarity of the environment surrounding the amide C=O groups, or increased intermolecular hydrogen bonding between adjacent HFA-GC molecules, or both.

To assess whether the polymorphism of HFA-GC can also be driven by prolonged incubation of the glycosphingolipid at specific temperatures, similar to NFA-GC, HFA-GC bilayers are heated to 38°C and incubated at that temperature for 96 h (Figure 3.9A). At the beginning, the patterns of the amide I band reflect the attainment of a gel phase, as expected, and remain unchanged after forty five minutes (time required in the heating experiment to increase the temperature from 38 to 47°C (Figure 3.7A), where the transformation into $L_cI$ is observed). However, the spectrum observed after 24 h of incubation at 38°C indicates the conversion into $L_cI$, which was stable over the time course of the experiment (96 h) (Figure 3.9A). These results suggest that the formation of

**Figure 3.8.** Stacked contour plots of the amide I stretching region of the infrared spectra of dehydrated HFA-GC, obtained at the temperatures indicated. NFA-GC dispersions (5%, w/v) were prepared in $^{2}H_{2}O$ buffered with 50 mM Tris-HCl ($p^{2}H$ 7.05), and left in the open transmission cell in the sample compartment of the infrared spectrophotometer for 96 h to obtain the dehydrated sample. Data shown were representative of three replicate experiments.

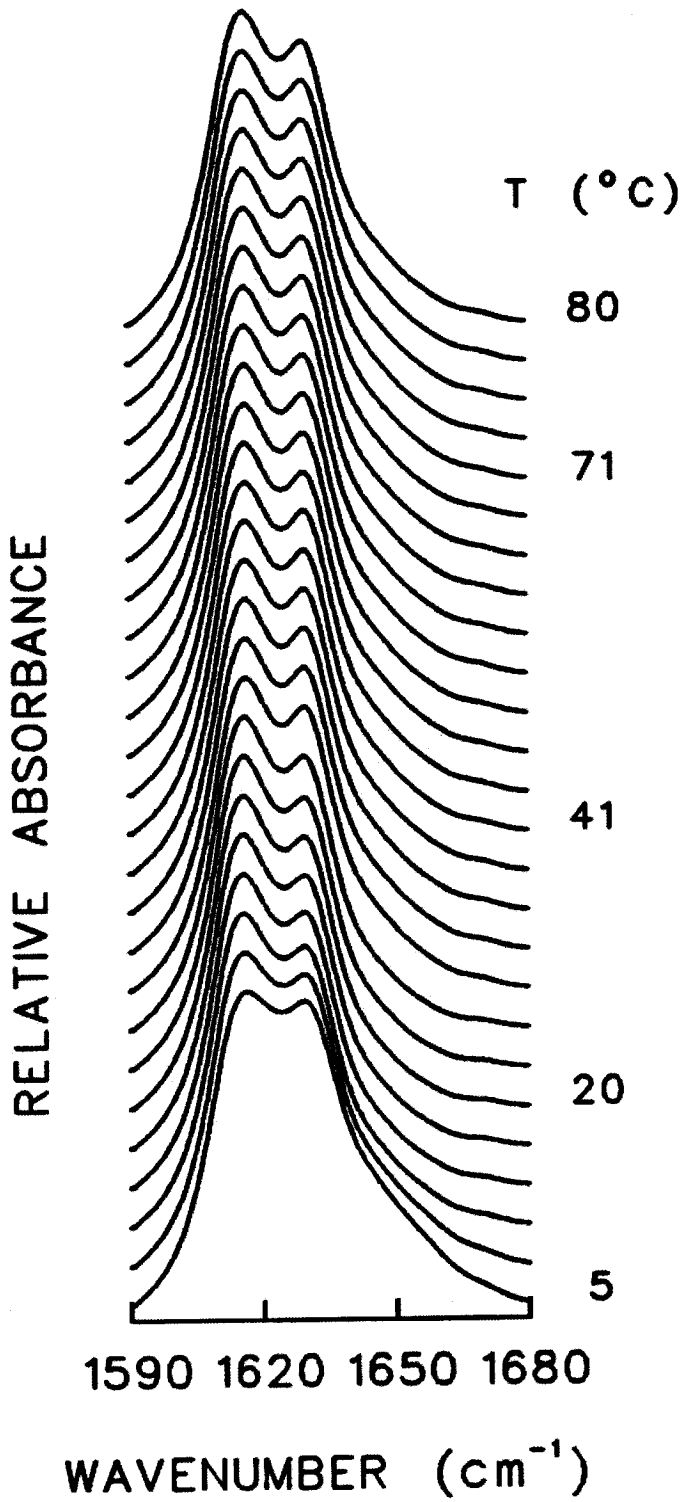
T (°C)
80
71
41
20
5
RELATIVE ABSORBANCE
1590 1620 1650 1680
WAVENUMBER (cm⁻¹)

**Figure 3.9.** Amide I stretching region of the infrared spectra of hydrated HFA-GC. (**A**) HFA-GC dispersions were heated to 38°C, and incubated at that temperature for 96 h in the spectrophotometer compartment. (**B**) HFA-dispersions were heated to 89°C, then cooled to 38°C and left at that temperature for 96 h in the closed transmission cell inside the spectrophotometer compartment. HFA-GC dispersions (5%, w/v) were prepared in $^{2}H_2O$ buffered with 50 mM Tris-HCl ($p^{2}H$ 7.05). Data shown were representative of three replicate experiments.

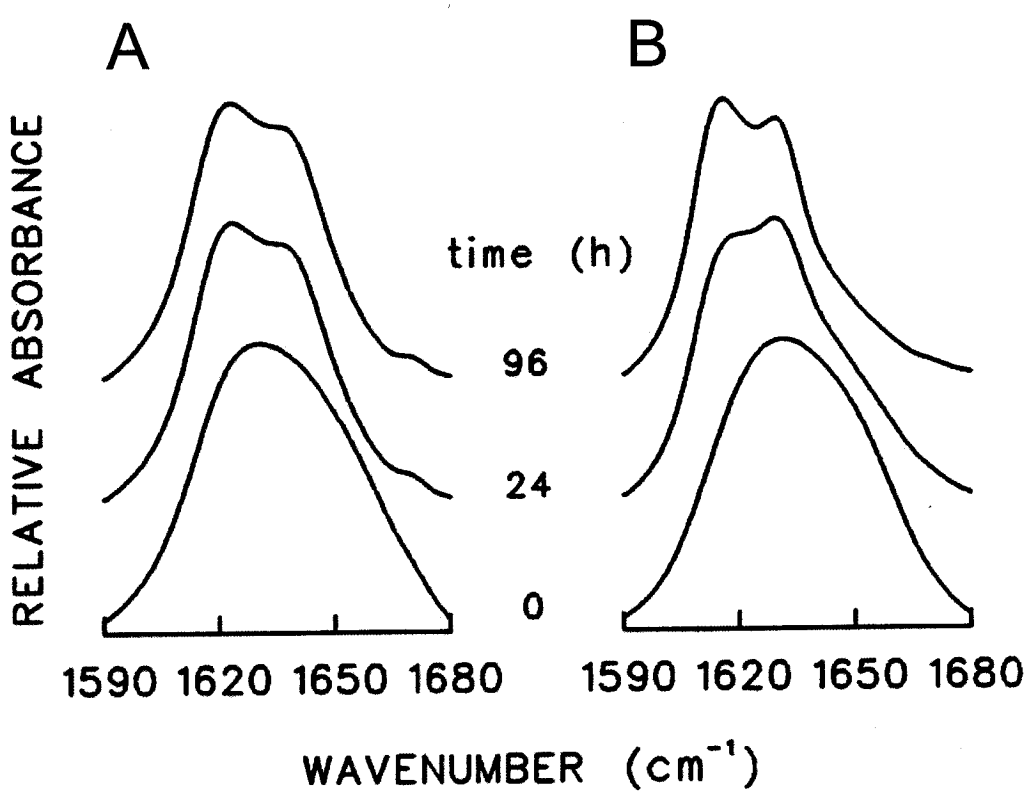
A
B
RELATIVE ABSORBANCE
time (h)
96
24
0
1590 1620 1650 1680
1590 1620 1650 1680
WAVENUMBER (cm-1)

$L_cI$ is a slow process that can be accelerated by heat. In another experiment, HFA-GC bilayers are heated to 80°C (i.e., above its chain melting transition at 72°C), followed by cooling and incubation at 38°C for 96 h (Figure 3.9B). Initially, a metastable gel phase is observed, transforming after 24 h into an intermediate biphasic mixture (gel + $L_cI$). Shortly afterwards (at the $26^{th}$ h), this mixture tranforms into a crystal-like phase whose amide I features are similar to those of $L_cI$, but more so to the dehydrated form (Figure 3.8 vs. Figure 3.9). Prolonged incubation of HFA-GC at 38°C, following cooling from the chain-melted state, is most likely accompanied by dehydration and/or by expulsion of water molecules from the interface. In addition, orientational and conformational changes of HFA-GC may have led to increased hydrogen bonding interactions, and/or localization of the amide C=O groups in less polar environments.

### *3.1.2. Phase Behavior of SGC: Temperature-Dependent FTIR Spectroscopic Studies*

#### *3.1.2.1. Hydrocarbon Chain Melting of SGC*

The thermotropic response of the hydrocarbon chains of SGC upon heating and cooling is shown in Figure 3.10. A broad phase transition of SGC bilayers occurs at 41°C. Ruocco and Shipley (1986) studied the structure and thermotropic properties of bovine brain SGC by DSC and X-ray diffraction, and showed that SGC exhibits a hydrocarbon chain melting transition over the range 32-47°C, similar to the results reported herein. SGC contains mostly 24:1 and 24:0 fatty acid species, similarly to its parental glycolipid GC (Ruocco and Shipley, 1986; Attar *et al.*, 1998; O'Brien and Rouser, 1964). However, the chain melting transition of SGC (41°C) is lower, compared to NFA-GC (80°C) and HFA-GC (72°C). The presence of the sulfate group may result in

**Figure 3.10.** Thermotropic response of the $CH_2$ symmetric stretching frequency of hydrated SGC upon heating (●) and cooling (○). SGC dispersions (5%, w/v) were prepared in $^2H_2O$ buffered with 50 mM Tris-HCl ($p^2H$ 7.05). The $T_m$ values were estimated from the first derivative plots of the $CH_2$ symmetric stretching vibration frequency vs. temperature. Data shown were representative of three replicate experiments.

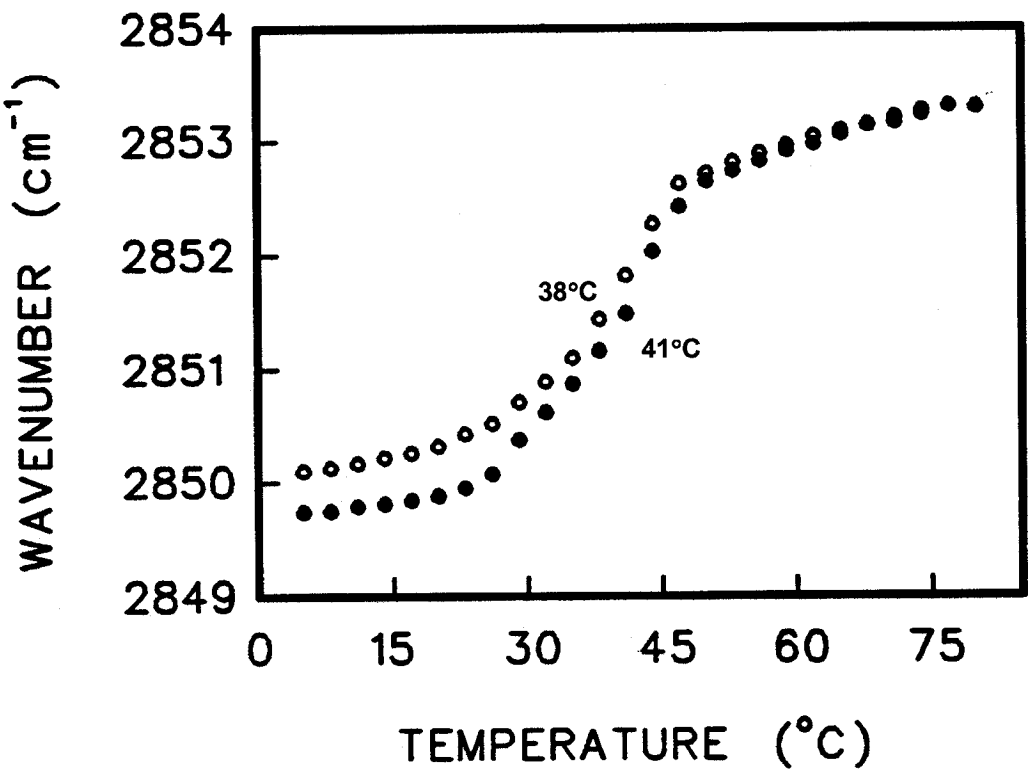
2854
2853
2852
2851
2850
2849
WAVENUMBER (cm$^{-1}$)
38°C
41°C
0
15
30
45
60
75
TEMPERATURE (°C)

charge repulsion between the negatively charged headgroups of neighboring SGC molecules. This presumably decreases hydrogen bonding and introduces conformational disorder of the hydrocarbon chains in the bilayer matrix. As a result, SGC bilayers are destabilized, which is reflected by the lower chain melting temperature, compared to NFA-GC and HFA-GC. Although SGC (Ruocco and Shipley, 1986; Attar *et al.*, 1998; O'Brien and Rouser, 1964) has the same sphingosine and hydrocarbon chain composition as sphingomyelin, the phosphorylated sphingolipid undergoes chain-melting transition at 35°C (Calhoun and Shipley, 1979; Barenholz and Thompson, 1980), a $T_m$ lower than that of SGC (41°C). Compared to the phosphorylcholine headgroup of sphingomyelin, the sulfated galactosyl moiety of SGC may increase hydrogen bonding at the interfacial region, thus resulting in the formation of ordered SGC bilayers, compared to sphingomyelin. Therefore, the long hydrocarbon chain character and the high $T_m$ of SGC, as well as its higher hydrogen bonding potential than phospholipids, suggest that SGC may impart stability to biological membranes. In fact, SGC increases the stability of DMPC model membranes (Attar *et al.*, 1998). Being a structural analog of SGC, SGG may also stabilize biological membranes by increasing the conformational order of the hydrocarbon chains in the bilayer matrix, and also by favoring interfacial hydrogen bonding (see below).

Cooling of SGC from the hydrocarbon chain melted state shifts the order-disorder $T_m$ to 38°C (Figure 3.10). This $T_m$ of SGC is slightly lower than that obtained upon heating (41°C). In addition, the frequencies of the $CH_2$ symmetric stretching band are slightly higher at the end of the cooling experiment than at the beginning of the heating

experiment. This suggests that the hydrocarbon chains of SGC are more disordered following cooling from the chain-melted state.

### *3.1.2.2. Interfacial Hydrogen Bonding of SGC*

Interfacial hydrogen bonding of SGC is also examined in this thesis for a better understanding of the contribution of hydrogen bonding to the polymorphism of SGC. The patterns of the amide I band of SGC upon heating to the chain-melted state, and following subsequent cooling from this phase are shown in Figure 3.11. Upon heating from 5 to 38°C, the contours of the amide I band of SGC are asymmetric, with a maximum at ~1625 $cm^{-1}$ and an apparent shoulder extending from 1630 to 1680 $cm^{-1}$ (Figure 3.11A). The amide I component near 1625 $cm^{-1}$ presumably reflects the hydrogen bonded population of SGC molecules (Wong and Mantsch, 1988). These spectral patterns are similar to those of glycosyldiacylglycerolipids and saturated phospholipids in the crystal-like phase (Lewis *et al.*, 1990, 1994; Lewis and McElhaney, 1993; Zhang *et al.*, 1997). Therefore, SGC bilayers are presumably in a crystal-like phase (termed $L_{c1}$) prior to hydrocarbon chain melting. These results are in agreement with the crystal structure revealed by X-ray diffraction of GC (Reed and Shipley, 1987; Saxena *et al.*, 1999) and glycosyldiacylglycerolipids (Sen *et al.*, 1981, 1990). Above 41°C (Figure 3.11A), the amide I band becomes broader, indicative of the liquid-crystalline nature of the SGC bilayers. At these temperatures, the SGC bilayers are more disordered and more hydrated. Thus, the intermolecular hydrogen bonding network may have been disturbed due to increased hydrogen bonding with interfacial water, which resulted in a broad amide I band of SGC in the liquid-crystalline phase.

**Figure 3.11.** Stacked contour plots of the amide I stretching region of the infrared spectra of hydrated SGC, obtained at the temperatures indicated, upon heating (**A**) and following subsequent cooling (**B**). SGC dispersions (5%, w/v) were prepared in $^{2}H_2O$ buffered with 50 mM Tris-HCl ($p^{2}H$ 7.05). Data shown were representative of three replicate experiments.

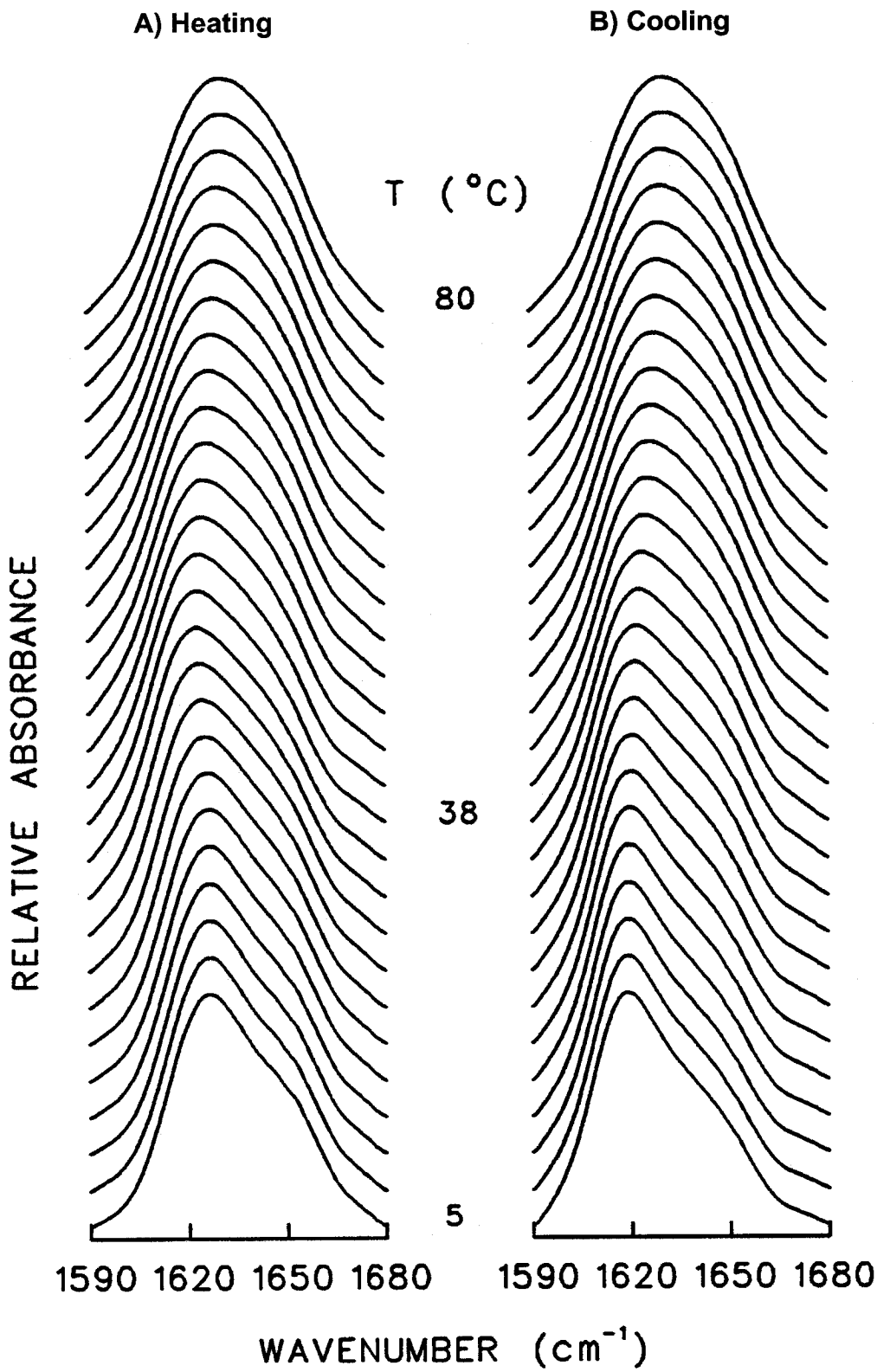
A) Heating
B) Cooling
T (°C)
80
38
5
RELATIVE ABSORBANCE
1590 1620 1650 1680
1590 1620 1650 1680
WAVENUMBER (cm⁻¹)

Upon cooling of the hydrated SGC bilayers from 80°C, the patterns of the amide I band of SGC are indicative of the formation of the $L_{c1}$ phase at 38°C, initially observed in the heating experiment (Figure 3.11). Interestingly, following cooling from the liquid-crystalline phase, the low frequency component of the amide I band of SGC is observed near 1615 $cm^{-1}$, compared to 1625 $cm^{-1}$ in the $L_{c1}$ phase upon heating (Figure 3.11). This indicates a stronger hydrogen bonding network of SGC in the $L_{c1}$ phase following cooling. Lewis *et al.* (1990) suggest that the shift of the ester C=O band of glycosyl-diacylglycerolipids to lower frequencies is possibly due to a bond to a hydroxyl group on the sugar residue. These authors also believe that strong hydrogen bonds are accompanied by partial dehydration at the interfacial region of the bilayer. Therefore, during the heating and subsequent cooling cycle from the liquid-crystalline phase, partial dehydration of the SGC bilayers may occur, thus changing the polarity of the environment surrounding the amide C=O groups, and/or increasing hydrogen bonding interactions between adjacent SGC molecules.

To further probe the polymorphic behavior and the nature of the $L_{c1}$ phase of SGC, dehydrated bilayers are generated and studied as a function of temperature. Dehydrated SGC bilayers do not exhibit a phase transition from 0 to 80°C, as revealed by their $CH_2$ symmetric stretching band (results not shown). In the dehydrated state, the amide I band of SGC (Figure 3.12) consists of two components near 1615 and 1630 $cm^{-1}$, representing the strongly and weakly hydrogen bonded amide C=O groups of SGC, respectively. The higher relative intensity of the 1615 $cm^{-1}$ amide I component of SGC reflects increased intermolecular hydrogen bonding between neighboring SGC molecules in the dehydrated state. Although the spectral contours of the amide I band of SGC in the

**Figure 3.12.** Stacked contour plots of the amide I stretching region of the infrared spectra of dehydrated SGC, obtained at the temperatures indicated. SGC dispersions (5%, w/v) were prepared in $^{2}H_{2}O$ buffered with 50 mM Tris-HCl ($p^{2}H$ 7.05), and left in the open transmission cell in the sample compartment of the infrared spectrophotometer for 96 h to obtain the dehydrated sample. Data shown were representative of three replicate experiments.

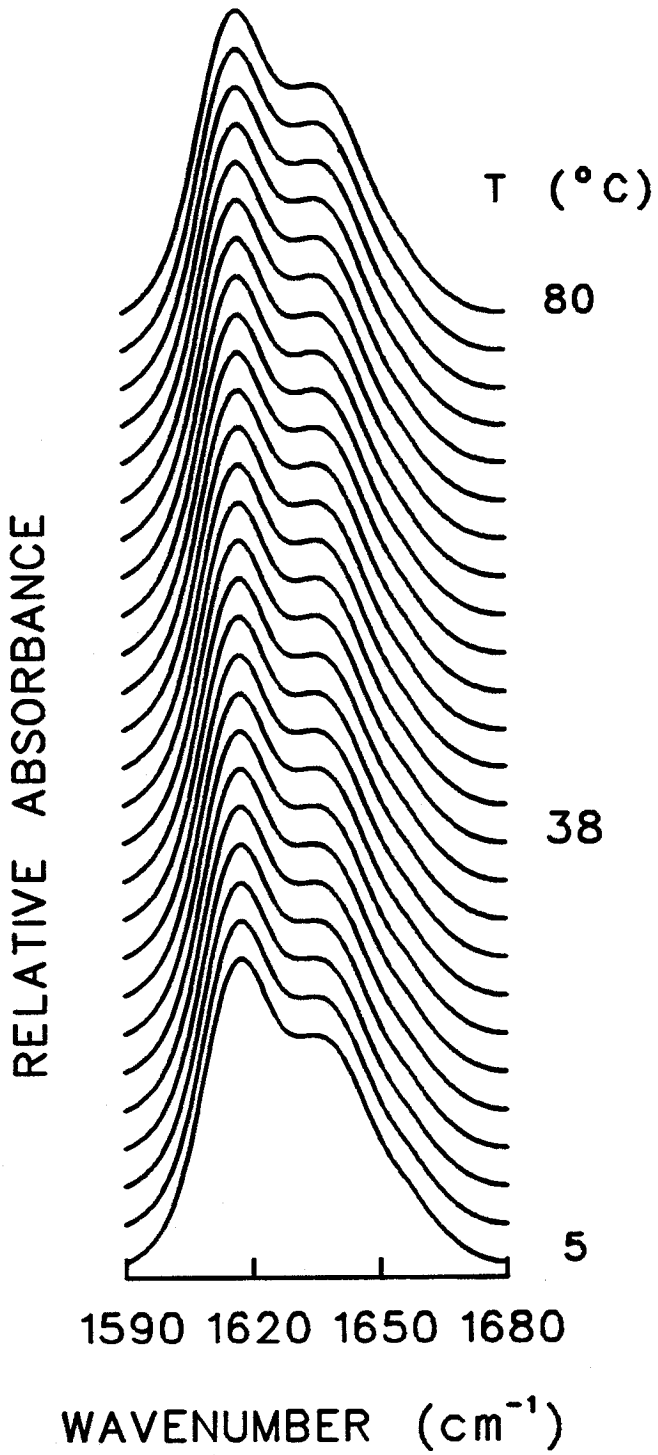
T (°C)
80
38
5
RELATIVE ABSORBANCE
1590 1620 1650 1680
WAVENUMBER (cm⁻¹)

dehydrated stated are similar to those in the $L_{c1}$ phase (Figure 3.12), the splitting between the amide I components is more evident in the dehydrated state. This suggests that the $L_{c1}$ phase is partially dehydrated (Figure 3.11 vs. Figure 3.12).

The stability of the partially dehydrated $L_{c1}$ phase of SGC is further investigated by incubating the glycosphingolipid for an extended period of time (96 h) at temperatures below the hydrocarbon chain melting transition (32°C). In the first experiment, SGC is heated to 32°C, a temperature below its main chain melting transition at 41°C, and incubated at 32°C for 96 h (Figure 3.13A). The shape of the amide I band obtained at the beginning of the incubation reflect the attainment of the $L_{c1}$ phase. In this phase, the amide I band of SGC is asymmetric, with a maximum at ~1625 $cm^{-1}$ and apparent shoulder extending from 1630 to 1680 $cm^{-1}$ (Figure 3.13A). However, this phase is metastable because additional incubation at 32°C results in its transformation into the dehydrated form after 48 h, as assessed by the patterns of the amide I band. This dehydrated crystal-like arrangement was stable over the time course of the experiment (96 h) (Figure 3.13A). In this stable polymorph, the amide I components are detected at 1615 and 1630 $cm^{-1}$. The lower frequency of the 1615 $cm^{-1}$ amide I component band of SGC in the stable dehydrated polymorph, compared to 1625 $cm^{-1}$ in the $L_{c1}$ phase, reflects stronger intermolecular hydrogen bonding between neighboring SGC molecules in the dehydrated state.

In the second experiment, hydrated SGC bilayers are heated to 80°C, cooled from that temperature and left at 32°C for 96 h (Figure 3.13B). Initially, the metastable $L_{c1}$ phase is observed, as assessed by the patterns of the amide I band of SGC. This phase transforms into the dehydrated form of SGC after 24 h, and remains stable up to 96 h

**Figure 3.13.** Amide I stretching region of the infrared spectra of hydrated SGC. **(A)** SGC dispersions were heated to 32°C, and incubated at that temperature for 96 h in the spectrophotometer compartment. **(B)** SGC dispersions were heated to 89°C, then cooled to 38°C and left at that temperature for 96 h in the closed transmission cell inside the spectrophotometer compartment. SGC dispersions (5%, w/v) were prepared in $^{2}H_{2}O$ buffered with 50 mM Tris-HCl ($p^{2}H$ 7.05). Data shown were representative of three replicate experiments.

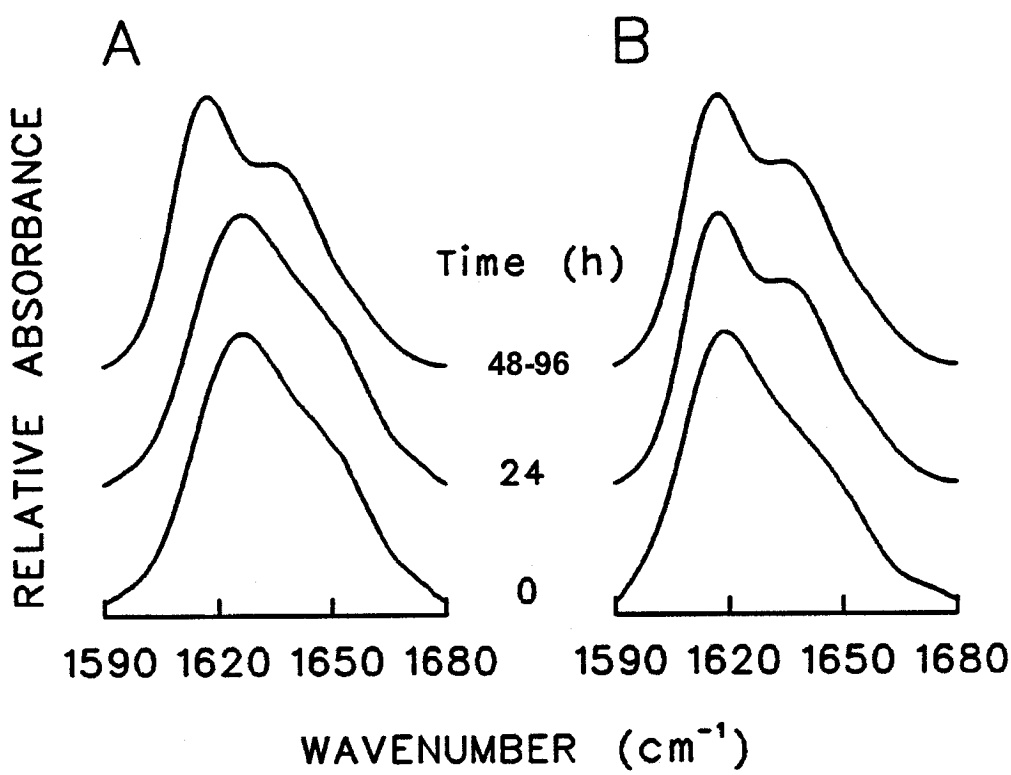
A
B
RELATIVE ABSORBANCE
Time (h)
48-96
24
0
1590 1620 1650 1680
1590 1620 1650 1680
WAVENUMBER (cm-1)

(Figure 3.13B). Prolonged incubation of SGC at 32°C, following cooling from the chain-melted state, is most likely accompanied by dehydration. In addition, orientational and conformational changes of SGC may lead to increased hydrogen bonding interactions and/or localization of the amide C=O groups in less polar environments.

### *3.1.3. Phase Behavior of SGG; Temperature-Dependent FTIR Spectroscopic Studies*

#### *3.1.3.1. Hydrocarbon Chain Melting of SGG*

Plots of the temperature dependence of the $CH_2$ symmetric stretching band of SGG upon heating and subsequent cooling are shown in Figure 3.14. Following heating, SGG bilayers undergo a main phase transition at 45°C. The temperature profile of SGG also exhibits another small increase in the frequency of the $CH_2$ symmetric stretching band between 10 and 30°C (Figure 3.14). These thermotropic events may represent conversions between metastable and stable crystal-like structures of SGG, en route to the liquid-crystalline phase. These results indicate that SGG exhibits complex polymorphic phase behavior, similar to SGC (Ruocco and Shipley, 1986; Boggs *et al.*, 1984; Nabet *et al.*, 1996), GC (Ruocco *et al.*, 1981; Curatolo, 1982; Reed and Shipley, 1987; Reed and Shipley, 1989; Haas and Shipley, 1995; Saxena *et al.*, 1999; Curatolo and Jungalwala, 1985), glycosyldiacylglycerolipids (Lewis *et al.*, 1990; Sen *et al.*, 1981, 1990; Mannock *et al.*, 1994), and saturated diacylphospholipids (Zhang *et al.*, 1997). Cooling of SGG bilayers from the liquid-crystalline state (62°C) results in a phase transition centered near 44°C (Figure 3.14). Comparison of the heating and cooling temperature profiles of SGG reveals that the thermotropic events observed between 10 and 30°C in the heating run of SGG are not observed during the cooling process.

**Figure 3.14.** Thermotropic response of the $CH_2$ symmetric stretching frequency of hydrated SGG upon heating (•) and cooling (○). SGG dispersions (5%, w/v) were prepared in $^2H_2O$ buffered with 50 mM Tris-HCl ($p^2H$ 7.05). The $T_m$ values were estimated from the first derivative plots of the $CH_2$ symmetric stretching vibration frequency vs. temperature. Data shown were representative of three replicate experiments.

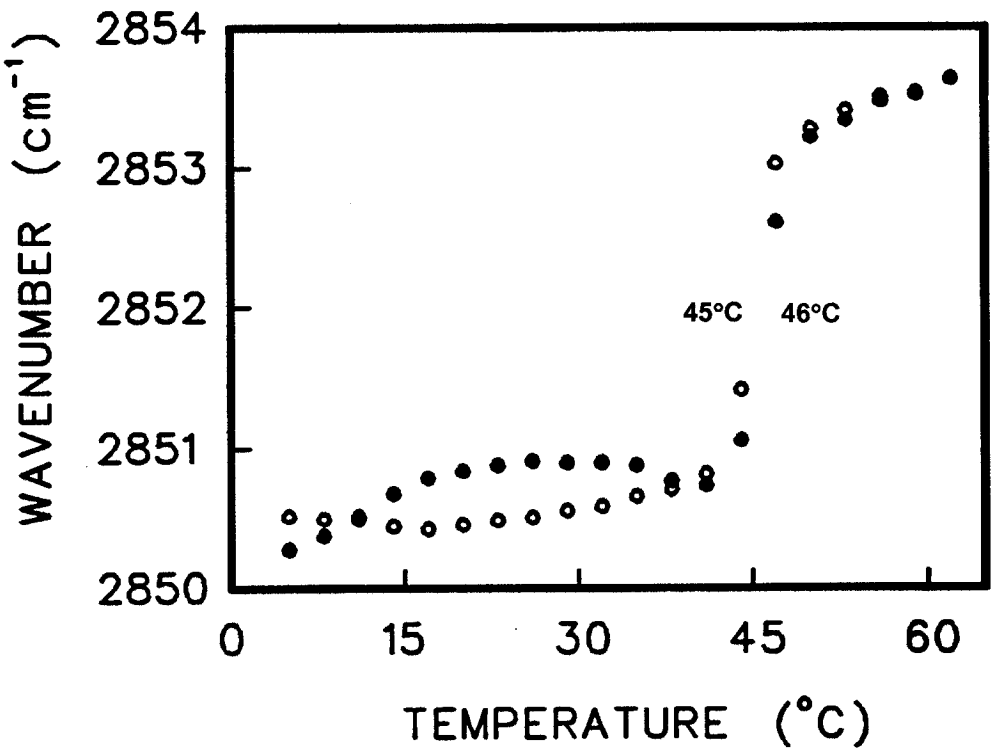
2854
2853
2852
2851
2850
WAVENUMBER (cm⁻¹)
45°C
46°C
0
15
30
45
60
TEMPERATURE (°C)

The main phase transition of SGG is sharper and occurs at higher $T_m$ (45°C), compared to SGC (41°C) (Figure 3.14 vs. Figure 3.10). While the hydrocarbon chain composition of SGC is heterogeneous (Attar *et al.*, 2000; O'Brien and Rouser, 1964), that of SGG is homogeneous and predominantly saturated, i.e., 16:0 (Tupper *et al.*, 1994; Attar *et al.*, 2000). Therefore, the sharp phase transition of SGG at 45°C reflects the homogeneity of SGG's hydrocarbon chains. Although DPPC has 16:0 hydrocarbon chains like SGG, DPPC exhibits a $T_m$ near 40°C (see below). This suggests that the sulfated galactosyl moiety of SGG partakes in hydrogen bonding at the interfacial region, and imparts further stability to the SGG bilayers. It was previously shown that SGG increased the stability of DMPC model membranes (Attar *et al.*, 2000). In addition, DSC or FTIR spectroscopy reveal that mammalian whole sperm, isolated sperm plasma membranes and sperm lipids exhibit a $T_m$ in the range of 17-26°C (Parks and Lynch, 1992; Wolf *et al.*, 1990). SGG is mostly saturated (Tupper *et al.*, 1994; Attar *et al.*, 2000). In addition, the sulfoglycolipid exhibits a high $T_m$ (45°C), compared to whole sperm membranes and lipids. Therefore, SGG may increase the hydrocarbon chain order or stability of mammalian male germ cells, which contain an appreciable amount of polyunsaturated phospholipids (Cooper and Yeung, 1997; Flesch and Gadella, 2000).

### *3.1.3.2. Interfacial Hydrogen Bonding of SGG*

The ester C=O stretching band of SGG is monitored as a function of temperature. At low temperatures (5-11°C) during the heating experiment, the ester C=O stretching band of SGG appears to be the summation of two components (Figure 3.15A). The spectral features of the ester C=O band of SGG share a striking similarity with those of

**Figure 3.15.** Stacked contour plots of the ester C=O stretching region of the infrared spectra of hydrated SGG, obtained at the temperatures indicated, upon heating (**A**) and following subsequent cooling (**B**). SGG dispersions (5%, w/v) were prepared in $^{2}H_2O$ buffered with 50 mM Tris-HCl ($p^{2}H$ 7.05). Data shown were representative of three replicate experiments.

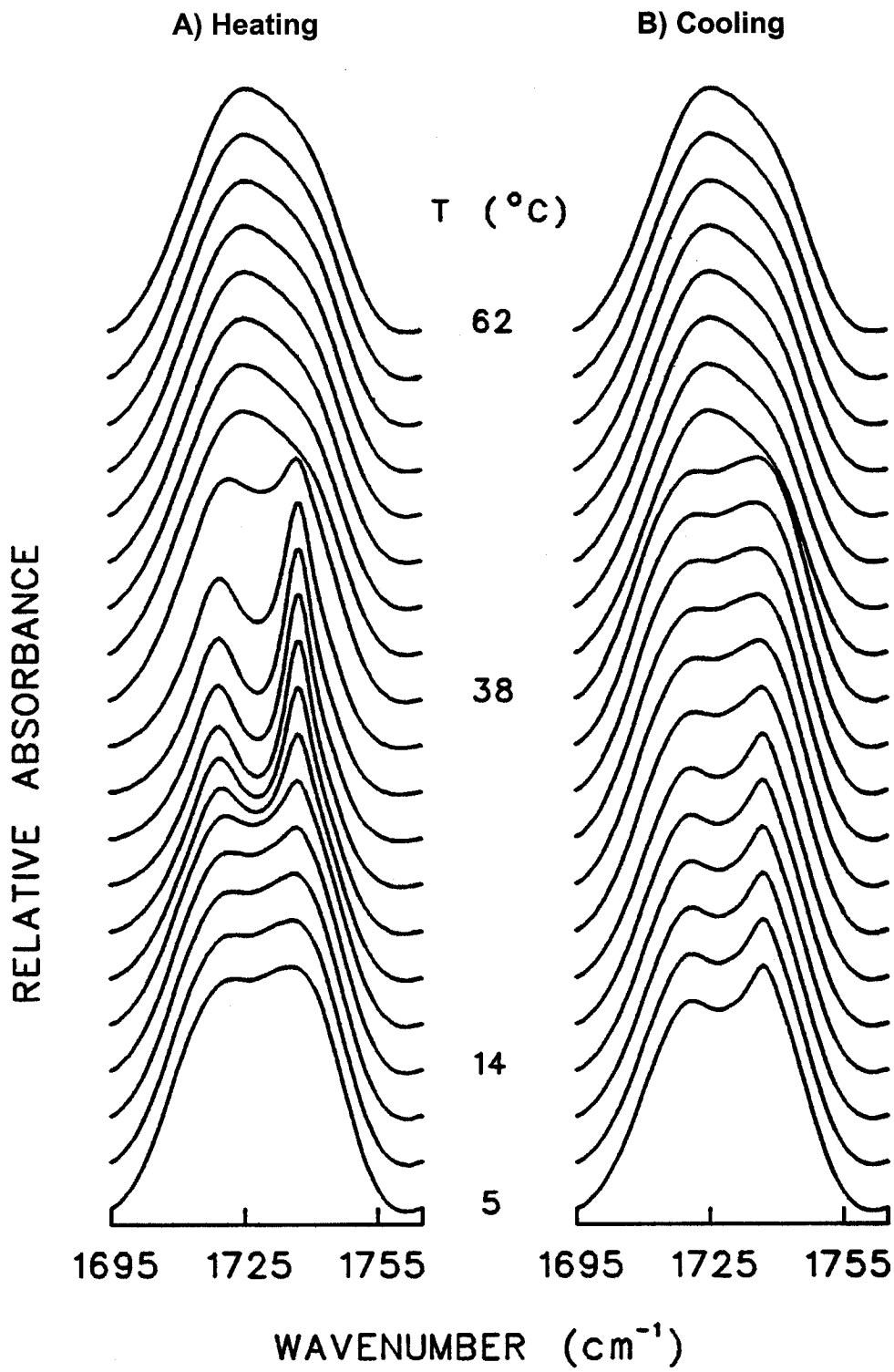
A) Heating
B) Cooling
T (°C)
62
38
14
5
RELATIVE ABSORBANCE
1695
1725
1755
1695
1725
1755
WAVENUMBER (cm⁻¹)

saturated diacylphospholipids and glycosyldiacylglycerolipids in the $L_c$ phase (Lewis *et al.*, 1990, 1994; Lewis and McElhaney, 1993; Zhang *et al.*, 1997). This suggests that SGG might adopt a metastable, crystal-like bilayer structure (termed $L_{cI}$) at low temperatures (5-11°C). At 14°C, two distinct ester C=O bands are observed near 1719 $cm^{-1}$ and 1739 $cm^{-1}$ (Figure 3.15A), representative of the hydrogen bonded and non/weakly hydrogen bonded population of the ester C=O groups of SGG, respectively (Wong and Mantsch, 1988). Studies by Mantsch *et al.* (1982) on the polymorphic phase behavior of phosphatidylsulfocholine bilayers demonstrated that general band narrowing and increased peak height of the methylene chain absorption are indicative of a reduction in the mobility of the acyl chains. Since the ester C=O band is sensitive to the geometry of the glycerol moiety and to the packing of the acyl chains (Mantsch and McElhaney, 1991), it is suggested that band narrowing and splitting of the ester C=O components of SGG may reflect a transition of the bilayers into a less mobile arrangement. Based on the spectroscopic results of saturated diacylphospholipids of Zhang *et al.* (1997), it is proposed that SGG may form a crystal-like polymorph, termed $L_{cII}$, between 14 and 38°C (Figure 3.15A) (Attar *et al.*, 2000). As the hydrocarbon chain conformational disorder increases progressively with temperature (see temperature Figure 3.14), the patterns of the ester C=O band of SGG change significantly above 38°C (Figure 3.15A). A broad, asymmetric band is observed, indicative of a liquid-crystalline phase of the SGG bilayers.

The temperatures where significant changes of the ester C=O band of SGG take place parallel those at which hydrocarbon chain conformational rearrangements and bilayer organization occurred (Figure 3.15 vs. Figure 3.14). Specifically, the thermotropic events detected in the heating experiment (Figure 3.14) may be attributed to

conversions between crystal-like phases, i.e., $L_c1$ and $L_c2$, of SGG bilayers at low temperatures, based on the patterns of the ester C=O stretching band between 5 and 38°C (Figure 3.15). Therefore, the conformation and packing of the hydrocarbon chains, as well as interfacial hydrogen bonding may induce conversions between metastable $L_c1$ and stable $L_c2$ SGG polymorphs prior to hydrocarbon chain melting.

When SGG bilayers are cooled from the hydrocarbon chain melted state, the broad SGG band is maintained from 62 to 41°C (Figure 3.15B). A peak at ~1739 $cm^{-1}$ and an adjacent shoulder at ~1719 $cm^{-1}$ become apparent at 38°C. This low frequency shoulder presumably represents hydrogen bonded species of SGG molecules (Wong and Mantsch, 1988). From 38 to 26°C, the spectral patterns of the ester C=O band of SGG are similar to those of the $L_{cI}$ phase observed in the heating experiment. Between 23 and 5°C, the splitting between the high and low frequency components of the ester C=O band of SGG becomes more apparent, and the patterns of this band are attributable to the formation of an $L_{cII}$ phase (Figure 3.15B). The ultimate transformation of $L_{cI}$ into $L_{cII}$ upon heating and following cooling from the hydrocarbon chain melted state indicates that $L_{cII}$ is the most stable crystal-like arrangement of SGG.

The increased intensity of the 1719 $cm^{-1}$ ester C=O component of SGG in the $L_{cII}$ phase, compared to the $L_{cI}$ phase, indicates that the $L_{cII}$ polymorph of SGG exhibits stronger hydrogen bonding networks. $L_c2$ possesses a strong hydrogen bonding network due to a partial dehydration and/or localization of the ester C=O groups of SGG in less polar environments (Lewis *et al.*, 1990). Therefore, dehydration experiments are conducted to gain further insight into the crystal-like structures of SGG. The dehydrated bilayers exhibit no sign of a cooperative phase transition in the temperature range 0 to

65°C, as revealed by their $CH_2$ symmetric stretching band (results not shown). The spectral patterns of the ester C=O band of dehydrated SGG bilayers are presented in Figure 3.16. Between 5 and 65°C, the ester C=O band is the sum of two components near 1739 and 1719 $cm^{-1}$, with the low frequency component representing the hydrogen bonded population of SGG molecules (Wong and Mantsch, 1988). Upon cooling of the dehydrated SGG bilayers, the features of the ester C=O band remain unchanged (results not shown). Although the patterns of the ester C=O band of SGG in the dehydrated state (Figure 3.16) are similar to those of the $L_{c\text{II}}$ phase in hydrated SGG bilayers (Figure 3.15), the separation between the low and high frequency components is more evident in the dehydrated state. This indicates that the $L_{c\text{II}}$ phase is partially dehydrated.

Since the temperature changes are performed in a time dependent manner, it is questionable whether the polymorphic phase behavior of SGG is temperature and/or time dependent. To investigate this, SGG bilayers were incubated at 5°C, a temperature favoring the formation of the $L_{c\text{I}}$ polymorph of SGG upon heating, and the bilayers were held at that temperature for 96 h (Figure 3.17). After forty minutes (time required in the continuous heating experiment to increase the temperature from 5 to 14°C, where the transformation of $L_{c\text{I}}$ to $L_{c\text{II}}$ was apparent, Figure 3.15), the spectral patterns of $L_c1$ remain unchanged (results not shown). Following incubation of the bilayers at 5°C for 24 h, the $L_{c\text{II}}$ phase is detected and stable up to 96 h (Figure 3.17), suggesting that $L_{c\text{I}}$ is metastable and that its conversion to $L_{c\text{II}}$ is induced by either heat or time. It also is probable that the slow transformation of $L_{c\text{I}}$ into $L_{c\text{II}}$ at 14°C during the heating experiment of hydrated SGG bilayers (Figure 3.15) would have appeared at lower temperatures if the heating rate had been slower, since $L_{c\text{I}}$ eventually transforms into $L_{c\text{I}}$ to $L_{c\text{II}}$ at 5°C (Figure 3.17).

**Figure 3.16.** Stacked contour plots of the ester C=O stretching region of the infrared spectra of dehydrated SGG, obtained at the temperatures indicated. SGG dispersions (5%, w/v) were prepared in $^{2}H_{2}O$ buffered with 50 mM Tris-HCl ($p^{2}H$ 7.05), and left in the open transmission cell in the sample compartment of the infrared spectrophotometer for 96 h to obtain the dehydrated sample. Data shown were representative of three replicate experiments.

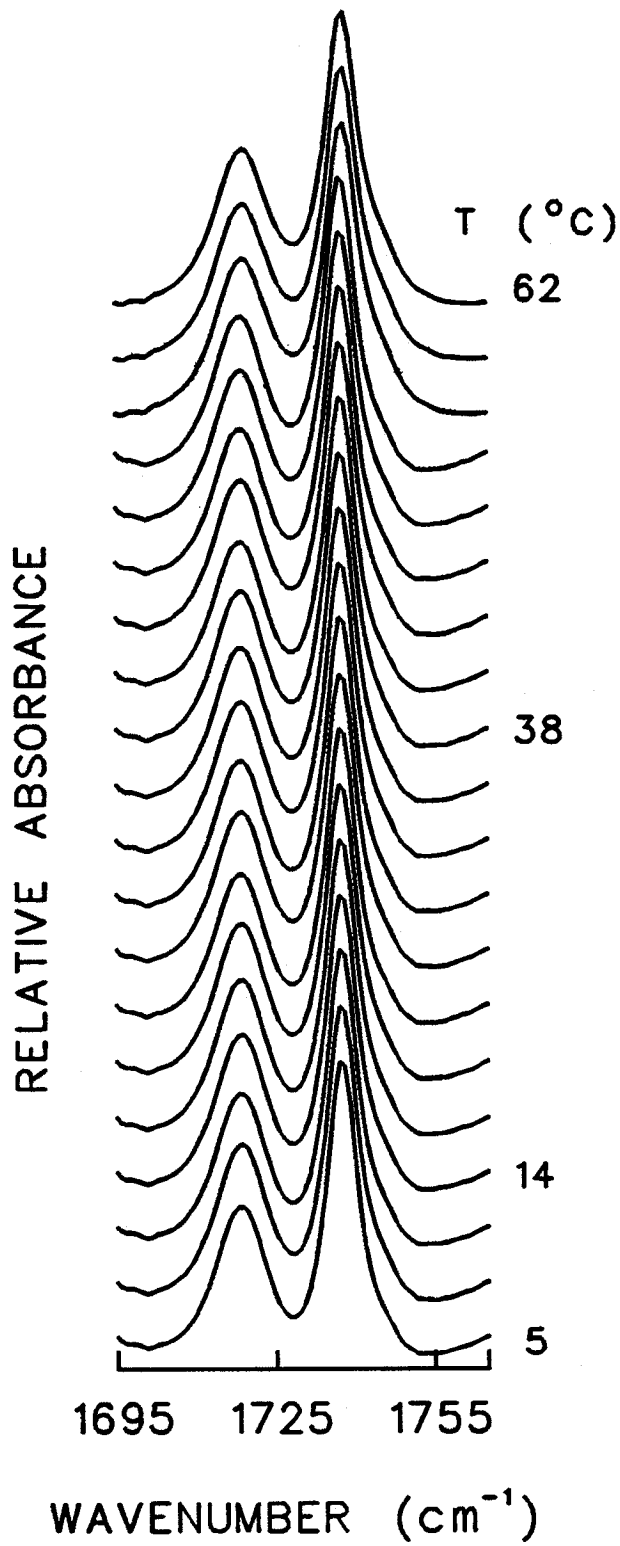
T (°C)
62
38
14
5
RELATIVE ABSORBANCE
1695
1725
1755
WAVENUMBER (cm⁻¹)

**Figure 3.17.** Ester C=O stretching region of the infrared spectra of hydrated SGG. **(A)** SGG dispersions were incubated at 5°C for 96 h in the spectrophotometer compartment. **(B)** SGG dispersions were heated to 62°C, then cooled to 5°C and left at that temperature for 96 h in the closed transmission cell inside the spectrophotometer compartment. SGG dispersions (5%, w/v) were prepared in $^{2}H_2O$ buffered with 50 mM Tris-HCl ($p^{2}H$ 7.05). Data shown were representative of three replicate experiments.

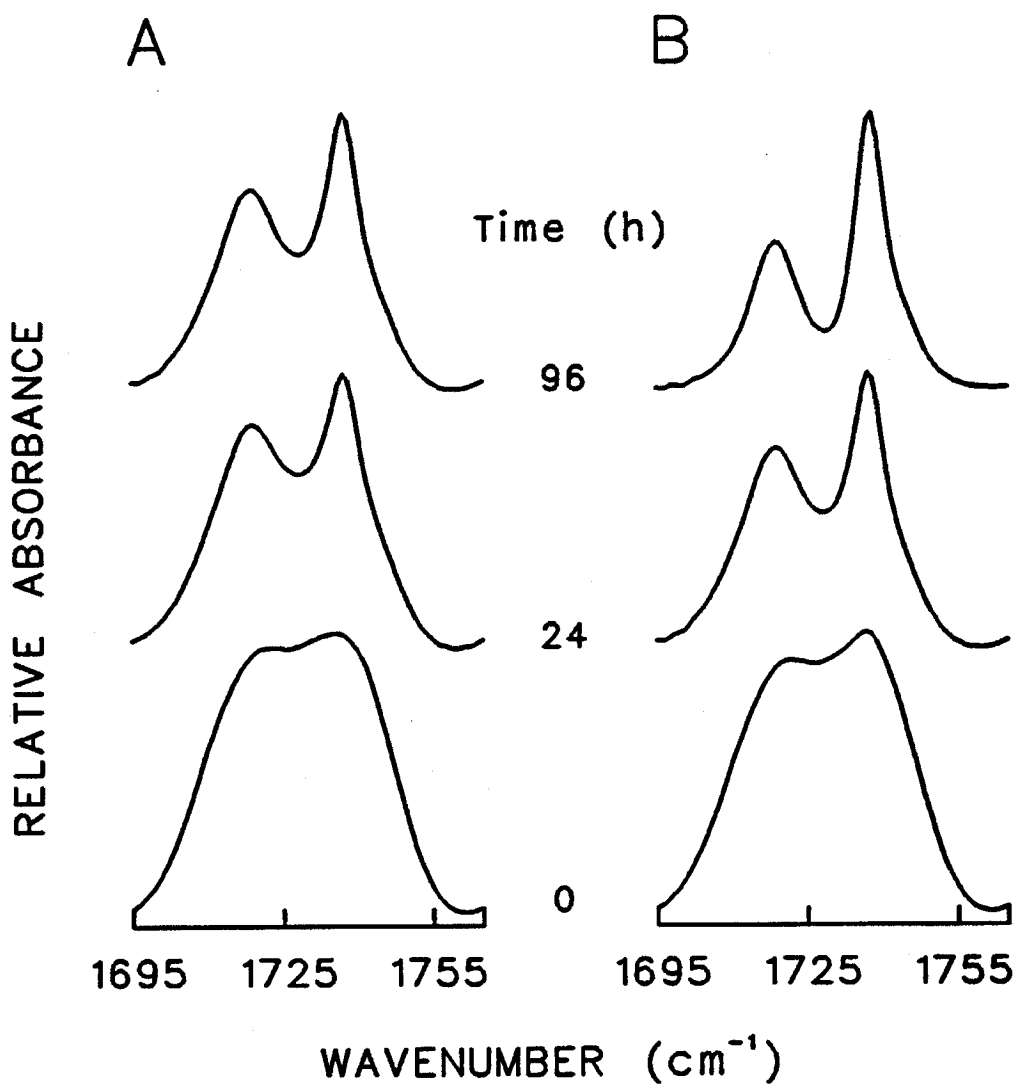
A
B
Time (h)
96
24
0
RELATIVE ABSORBANCE
1695
1725
1755
1695
1725
1755
WAVENUMBER (cm⁻¹)

In a different experiment, SGG bilayers are heated to the chain-melted state (62°C), and then cooled and maintained at 5°C up to 96 h. Cooling of the hydrated SGG bilayers from 62 to 5°C results in the formation of the $L_{c\text{II}}$ polymorph (Figure 3.17B). After incubation at 5°C for 24 h, two distinct yet still overlapping ester C=O components of SGG are detected, and the contours of the ester C=O band are strikingly similar to those in the dehydrated state. At 48 h, splitting between the ester C=O component bands is even more prominent (results not shown), suggesting that the dehydration degree was higher following cooling from the chain melted state. This dehydrated polymorph remains stable throughout the time course of the experiment (96 h) (Figure 3.17B). Prolonged incubation of SGG at 5°C, following cooling from the chain-melted state, is most likely accompanied by dehydration. In addition, orientational and conformational changes of SGG molecules may lead to increased hydrogen bonding interactions and/or localization of the ester C=O groups in less polar environments.

## 3.2. Contribution of SGG to the Formation of Sperm Rafts

Liquid-ordered domains or rafts, housing sphingolipids, cholesterol and multiple adhesion and signaling molecules, have been implicated in numerous functions in biological membranes, including membrane trafficking, as well as cell-cell adhesion and cell signaling (reviews: Simons and Toomre, 2000; Brown and London, 2000; van der Goot and Harder, 2001). It is suggested that glycosphingolipids might self-associate through intra and intermolecular hydrogen bonding to form rafts (review: Simons and Toomre, 2000). On the other hand, the interactions between saturated hydrocarbon chains of lipids have also been proposed to play a key role in raft formation (Schroeder *et*

*al.*, 1994, 1998; Ahmed *et al.*, 1997). In particular, the high hydrocarbon chain melting temperature of sphingolipids was proposed to promote phase separation in the presence of high amounts of cholesterol (review: Brown and London, 1998b). My FTIR spectroscopic data revealed that SGG formed highly ordered, crystal-like structures, characterized by a high hydrocarbon chain melting temperature, and extensive hydrogen bonding networks. These structural features of SGG may partially contribute to its ability to form segregated domains or rafts in a mammalian male germ cell containing an appreciable amount of polyunsaturated phospholipids (Cooper and Yeung, 1997; Flesch and Gadella, 2000). Therefore, I was interested in determining whether SGG contributes to the formation of sperm rafts through both or either one of the mechanisms mentioned above. As the first step to explore this possibility, I investigated by FTIR spectroscopy the interaction of SGG with cholesterol and saturated phospholipids, two lipids found in common among rafts isolated from various cells.

### *3.2.1. Interaction of SGG with Saturated and Unsaturated Phospholipids*

Since SGG is mostly saturated, i.e., 16:0 (Tupper *et al.*, 1994; Attar *et al.*, 2000), the sulfoglycolipid is likely to interact with saturated phospholipids in the sperm plasma membrane via strong van der Waals interactions between their saturated hydrocarbon chains. Therefore, its interaction with the saturated phospholipid $DPPC_{d62}$ is studied by FTIR spectroscopy in this thesis. On the other hand, the sperm plasma membrane contains appreciable amounts of the highly unsaturated phospholipid 1-palmitoyl-2-docosahexaenoyl-*sn*-glycerophosphorylcholine (16:0/22:6-PC or PDPC) (Cooper and Yeung, 1997; Flesch and Gadella, 2000). Therefore PDPC is also used to study its

interaction with SGG by FTIR spectroscopy. These experiments are performed to assess the interaction of SGG with saturated and unsaturated phospholipids, and to gain further insight into the influence of lipid-lipid interactions on the formation of sperm rafts.

The use of perdeuterated DPPC ($DPPC_{d62}$) in the mixed SGG-$DPPC_{d62}$ bilayers allows us to monitor the conformation of the lipid hydrocarbon chains of SGG (2850-2855 $cm^{-1}$) and $DPPC_{d62}$ (2090-2099 $cm^{-1}$) independently. Equimolar SGG-$DPPC_{d62}$ mixtures exhibit a $T_m$ of 42°C, in both the $CH_2$ and $CD_2$ symmetric stretching regions (Figure 3.18). The obtained $T_m$ lies between that of SGG (45°C) and $DPPC_{d62}$ (39°C). The presence of a single and cooperative phase transition is consistent with a homogeneous mixing of SGG and $DPPC_{d62}$ in the mixed bilayers, without lateral phase segregation. This is consistent with our previous results showing that SGG and $DMPC_{d54}$ form homogenous bilayers (Attar *et al.*, 2000). The saturated hydrocarbon chains of SGG, mainly 16:0 (Tupper *et al.*, 1994; Attar *et al.*, 2000), and $DPPC_{d62}$ favor the formation of tightly packed bilayers due to the strong van der Waals interaction among themselves.

On the other hand, the incorporation of SGG in PDPC bilayers results in lateral phase segregation. Plots of the temperature dependence of the $CH_2$ symmetric stretching band of SGG, PDPC and equimolar SGG-PDPC mixtures are shown in Figure 3.19. While SGG exhibits a $T_m$ near 45°C, PDPC undergoes chain melting at -10°C. Below the chain melting temperature of SGG, i.e., from 5 to 40°C, the frequency of the $CH_2$ symmetric stretching band of SGG is low (~2850-2851 $cm^{-1}$), indicating that the saturated hydrocarbon chains of SGG are ordered. In PDPC bilayers, the frequency of the $CH_2$ symmetric stretching band is relatively high (~2852-2854 $cm^{-1}$) from -20 to 20°C. This is

**Figure 3.18.** Interaction of SGG with the saturated phospholipid $DPPC_{d62}$. **(A)** Thermotropic response of the $CH_2$ symmetric stretching frequency of SGG (●), and an equimolar mixture of SGG-$DPPC_{d62}$ (○). **(B)** Thermotropic response of the $CD_2$ symmetric stretching frequency of $DPPC_{d62}$ (▽), and an equimolar mixture of SGG-$DPPC_{d62}$ (○). The samples (5%, w/v) were prepared in $^2H_2O$ buffered with 50 mM Tris-HCl ($p^2H$ 7.05). Data shown were representative of three replicate experiments.

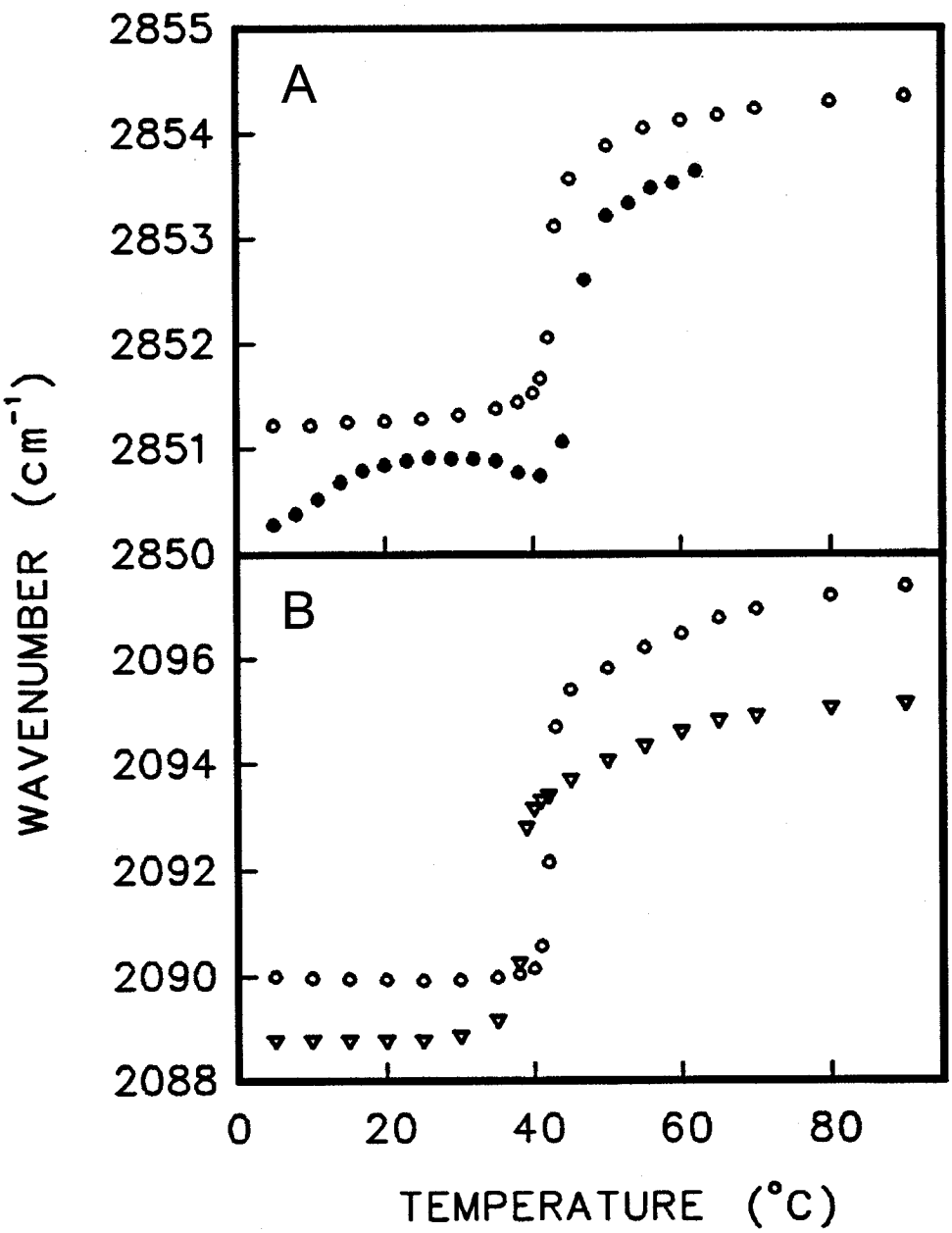
A
B
2855
2854
2853
2852
2851
2850
2096
2094
2092
2090
2088
WAVENUMBER (cm$^{-1}$)
0
20
40
60
80
TEMPERATURE (°C)

**Figure 3.19.** Interaction of SGG and $DPPC_{d62}$ with the polyunsaturated phospholipid PDPC. (**A**) Thermotropic response of the $CH_2$ symmetric stretching frequency of SGG (●), PDPC (□), and equimolar mixtures of SGG-PDPC (○) and $DPPC_{d62}$-PDPC (▼). (**B**) Thermotropic response of the $CD_2$ symmetric stretching frequency of hydrated $DPPC_{d62}$ (▽), and an equimolar mixture of $DPPC_{d62}$-PDPC (▼). The samples (5%, w/v) were prepared in $^2H_2O$ buffered with 50 mM Tris-HCl ($p^2H$ 7.05). Data shown were representative of three replicate experiments.

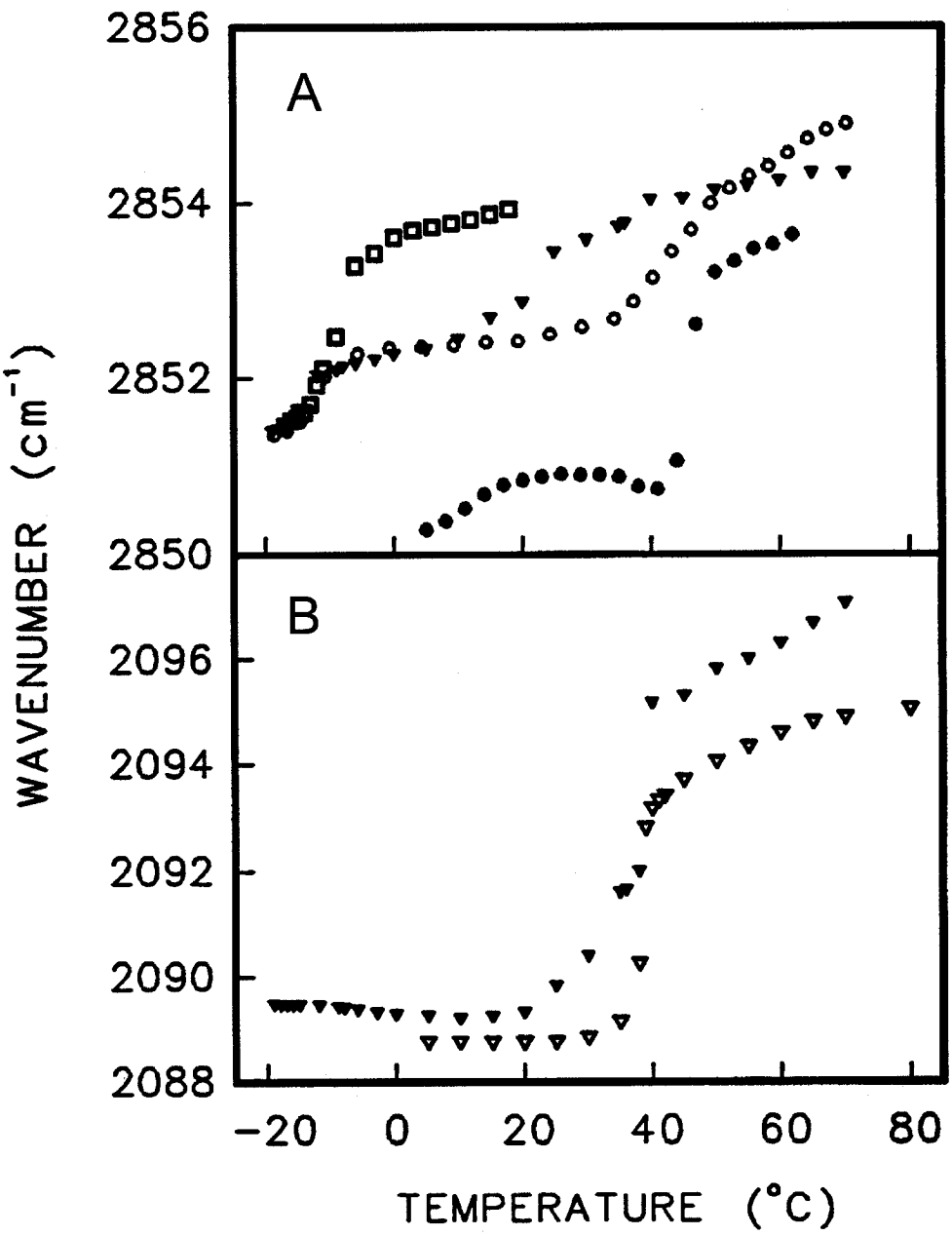
2856
2854
2852
2850
A
B
2096
2094
2092
2090
2088
WAVENUMBER (cm$^{-1}$)
−20
0
20
40
60
80
TEMPERATURE (°C)

indicative of the highly disordered hydrocarbon chains of PDPC. Combined together, these data suggest that the saturated hydrocarbon chains of SGG may favor increased order/stability, whereas the unsaturated hydrocarbon chains of PDPC may promote disorder in the sperm plasma membrane. In the equimolar SGG-PDPC mixtures, a first transition is detected between -20 and -10°C (Figure 3.19A), at exactly the same temperature as in pure PDPC. This indicates that PDPC forms segregate domains in the equimolar SGG-PDPC bilayers. However, a second broad transition is also observed in this curve at a temperature slightly lower than the $T_m$ of pure SGG, indicative of the incorporation of some PDPC molecules within SGG domains. The frequency of the $CH_2$ symmetric stretching band in the equimolar SGG-PDPC mixture is in between those of PDPC and SGG from –10 to 35°C (Figure 3.19A). This indicates that the hydrocarbon chains in the equimolar SGG-PDPC mixtures were more ordered than those of pure PDPC, but less ordered than those of pure SGG.

Since $DPPC_{d62}$ has 16:0 hydrocarbon chains like SGG, the saturated phospholipid was used instead of SGG in mixtures with PDPC to further reveal the importance of the interaction between the saturated hydrocarbon chains of lipids for the formation of segregate domains. Equimolar $DPPC_{d62}$-PDPC mixtures are generated, and the formation of separate domains was monitored in the $CD_2$ and $CH_2$ symmetric stretching regions of $DPPC_{d62}$ and PDPC, respectively. In the $CH_2$ symmetric stretching region, which reflects the contribution of the hydrocarbon chains of PDPC only, a small transition is detected in the equimolar $DDPC_{d62}$-PDPC mixtures at the same temperature as in pure PDPC (Figure 3.19A), revealing the formation of separate PDPC domains. In the $CD_2$ symmetric stretching region, pure $DPPC_{d62}$ exhibits a cooperative and sharp phase transition near

39°C. Upon comparison of the temperature profile of $DPPC_{d62}$ with that of the equimolar $DDPC_{d62}$-PDPC mixtures, it is clear that $DPPC_{d62}$ also formed distinct domains between 40 and 70°C (Figure 3.19B). From 20 to 40°C, a broad transition is observed in the chain melting curve of the equimolar $DPPC_{d62}$-PDPC mixtures, with a $T_m$ near 29°C, in both the $CH_2$ and $CD_2$ symmetric stretching regions (Figure 3.19). This suggests that the 16:0 hydrocarbon chains of PDPC interacted to a certain extent with the perdeuterated hydrocarbon chains of $DPPC_{d62}$.

Combined together, these results reveal that both DPPC and SGG show a limited miscibility with PDPC. The saturated hydrocarbon chains of SGG may favor interaction amongst each other and with saturated phospholipids, presumably promoting the formation of distinct membrane domains in a sperm plasma membrane containing significant amounts of polyunsaturated phospholipids.

### *3.2.2. Interaction of SGG with Cholesterol*

Cholesterol is a major constituent of the plasma membrane of mammalian cells (Chapman, 1988), including the mammalian male germ cell (Nikolopoulou *et al.*, 1985; Parks and Lynch, 1992). Cholesterol is also an integral component of rafts. Therefore, the interaction of SGG with cholesterol is investigated by FTIR spectroscopy for a better understanding of the contribution of SGG to the formation of sperm rafts. The effect of cholesterol is most often seen through its impact on the conformational order of the lipid hydrocarbon chains of phospholipid/glycolipid model membranes (Ipsen *et al.*, 1987; Ali *et al.*, 1994; McMullen *et al.*, 1996; review: Silvius, 2003). In fact, my FTIR spectroscopic results reveal a broadening of the phase transition curves of SGG and

DPPC, a saturated phospholipid with the same hydrocarbon chain composition as SGG, in equimolar mixtures of SGG-cholesterol and DPPC-cholesterol (Figure 3.20A). The $CH_2$ symmetric stretching band is found at lower frequencies in the mixed SGG-cholesterol and DPPC-cholesterol bilayers, compared with bilayers of SGG and DPPC, respectively. This suggests that cholesterol increases the conformational order of the hydrocarbon chains of SGG and DPPC, which may be attributed to strong van der Waals interactions between the cholesterol planar ring + side chain and the hydrocarbon chains of SGG/DPPC.

In addition to hydrophobic interactions in the bilayer matrix, FTIR spectroscopy also reveals strong intermolecular hydrogen bonding between SGG and cholesterol at the interfacial region (Figure 3.20B). In the equimolar SGG-cholesterol mixtures, the relative intensity of the high frequency component (1740 $cm^{-1}$) of SGG, representing free or weakly hydrogen bonded ester C=O groups (Wong and Mantsch, 1988), decreases significantly. On the other hand, the relative intensity of the low frequency component of SGG (1720 $cm^{-1}$) increases, indicative of strong hydrogen bonding between the ester C=O groups of SGG and the hydroxyl group of cholesterol in the equimolar SGG-cholesterol bilayers. To further reveal the importance of the sulfated galactosyl moiety of SGG in the interaction with cholesterol, SGG is substituted with DPPC in mixtures with cholesterol. The shape of the ester C=O stretching band of DPPC is very similar to that in the equimolar DPPC-cholesterol mixtures, and this band shifts to slightly lower frequencies in the mixed DPPC-cholesterol bilayers (Figure 3.20C). This indicates that DPPC, unlike SGG, does not interact strongly with cholesterol presumably due to an increased motional freedom of the headgroup of DPPC, as observed by $^2H$ NMR (Brown and Seelig, 1978).

**Figure 3.20.** Interaction of SGG and DPPC with cholesterol. (**A**) Thermotropic response of the $CH_2$ symmetric stretching frequency of SGG (●), DPPC (▼), and equimolar mixtures of SGG-cholesterol (○) and DPPC-cholesterol (▽). (**B**) Ester C=O stretching region of the infrared spectra of SGG (long dashes), and SGG-cholesterol mixtures (molar ratio 1:1) (dot-long dash). (**C**) Ester C=O stretching region of the infrared spectra of hydrated DPPC (solid line), and an equimolar mixture of DPPC-cholesterol (small dashes). The samples (5%, w/v) were prepared in $^2H_2O$ buffered with 50 mM Tris-HCl ($p^2H$ 7.05), and the spectra were collected at 37°C. Data shown were representative of three replicate experiments.

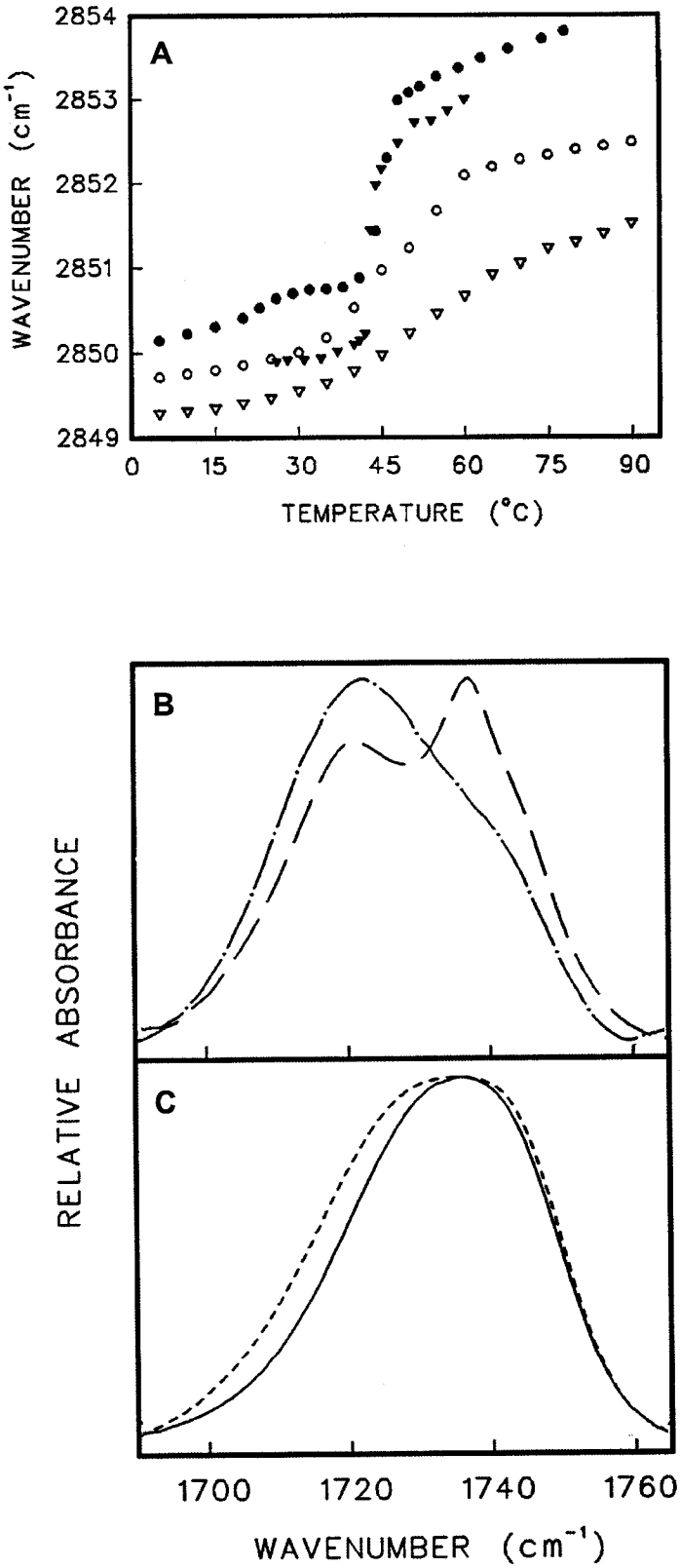
A
WAVENUMBER (cm⁻¹)
2854
2853
2852
2851
2850
2849
0
15
30
45
60
75
90
TEMPERATURE (°C)
B
C
RELATIVE ABSORBANCE
1700
1720
1740
1760
WAVENUMBER (cm⁻¹)

These results indicate that the sulfated galactosyl moiety of SGG plays an important role in the interaction with cholesterol, and that the strong intermolecular hydrogen bonding between SGG and cholesterol may be one of the driving forces behind raft formation in mammalian sperm.

### *3.2.3. Effect of SGG and Cholesterol on the Formation of Triton X-100 Insoluble Complexes*

In model membranes, the formation of rafts is correlated with the acquisition of insolubility in non-ionic detergents, such as Triton X-100, at low temperatures (Brown and Rose, 1992). Since cholesterol and sphingolipids interact preferentially with saturated phosphopholipids, leading to the formation of Triton X-100 insoluble membranes or rafts (Schroeder *et al.*, 1994; Ahmed *et al.*, 1997; Xu *et al.*, 2001; Xu and London, 2000), this thesis examines whether the same scenario holds true for SGG-cholesterol mixtures. The light scattering intensity of SGG and SGG-cholesterol mixtures (molar ratio, 9:1, 4:1, 2:1 and 1:1) at 400 nm is used to monitor the insolubility of these liposomes in the absence and presence of Triton X-100. My relative insolubility data (the degree of lipid's resistance to solubilization by Triton X-100) reveal that SGG liposomes are totally soluble at 0.5% Triton X-100 (Figure 3.21A). In contrast, ~55% of the liposomes of DPPC, having the same hydrocarbon chain composition as SGG, were insoluble in 0.5% Triton X-100. This insolubility is likely a result of tight packing of the hydrocarbon chains of DPPC (Xu *et al.*, 2001), and lipid-lipid interactions may have been stronger than lipid-detergent interactions in DPPC bilayers, compared with SGG bilayers. When the molar ratio of SGG or DPPC to cholesterol was 1:1, both SGG-cholesterol and

**Figure 3.21.** Triton X-100 insolubility of SGG and DPPC in the absence and presence of cholesterol. (**A**) Relative insolubility of SGG (●), DPPC (■), and mixed lipid dispersions of SGG-cholesterol (molar ratio 1:1, ○), DPPC-cholesterol (molar ratio 1:1, □), and SGG-cholesterol-DPPC (molar ratio 1.0:2.0:3.4, △) in 0 to 2% Triton X-100. (**B**) Relative insolubility in 1% Triton X-100 of SGG-cholesterol (○) and DPPC-cholesterol (□) liposomes prepared with different molar ratio of SGG or DPPC to cholesterol (i.e., 1:0, 9:1, 4:1, 2:1, 1:1). Relative insolubility is expressed as a percentage of the ratio of $A_{400}$ after Triton X-100 incubation to $A_{400}$ of the original lipid dispersion. The average and standard deviation of values from three different experimental days were shown.

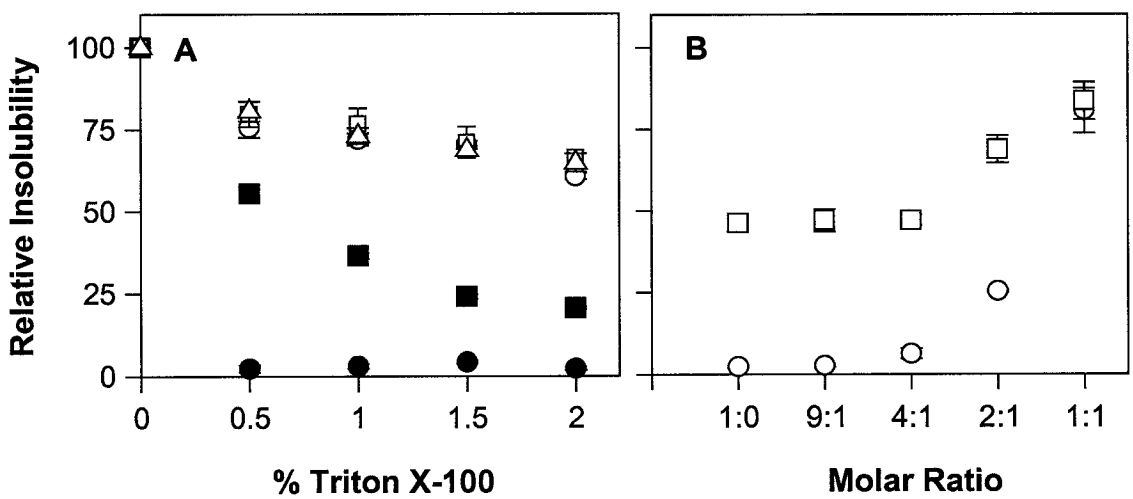
A
B
100
75
50
25
0
Relative Insolubility
0
0.5
1
1.5
2
% Triton X-100
1:0
9:1
4:1
2:1
1:1
Molar Ratio

DPPC-cholesterol complexes were equally resistant to Triton X-100 solubilization. Approximately 75% and 60% of these complexes were insoluble in 1% and 2% Triton X-100, respectively, at room temperature (Figure 3.21A). The Triton X-100 insolubility of both SGG and DPPC increased when these lipids were complexed with cholesterol with a molar ratio of 2:1 or 1:1 (Fig. 3.21B). In addition, the ternary SGG-cholesterol-DPPC mixture, with molar composition identical to that of capacitated sperm rafts (i.e., 1.0:2.0:3.4, see below), was resistant to Triton X-100 solubilization (Figure 3.21A). Therefore, the interaction between SGG/saturated phospholipids and cholesterol may account for the formation Triton X-100 insoluble microdomains or rafts in the sperm plasma membrane.

### 3.3. Properties of Capacitated Sperm rafts

The foregoing results suggest that SGG, cholesterol, and saturated phospholipids are components of mammalian sperm rafts, previously shown to house ZP and egg plasma membrane binding molecules (Nishimura *et al.*, 2001). Sperm acquire their fertilizing competence following capacitation, an event associated with the efflux of cholesterol from their plasma membrane (Flesch *et al.*, 2001 reviews: Visconti and Kopf, 1998; Visconti *et al.*, 2002). Since cholesterol is an important structural component of rafts (Simons and Toomre, 2000; Silvius, 2003), its release from the sperm plasma membrane raises the question whether the integrity and levels of rafts are affected in capacitated sperm. If rafts contain the ZP binding domains, the question whether rafts isolated from capacitated sperm exhibit higher ZP binding ability than rafts isolated from non-capacitated sperm should also be addressed. In this thesis, rafts are isolated from pig

sperm since it can be obtained in quantity, and since all ZP sulfoglycoproteins involved in sperm binding have been characterized, and can also be prepared in quantity as well.

### *3.3.1. Properties of Capacitated Pig Sperm*

Both washed sperm and PGC sperm are used in this thesis since they have been used for *in vitro* fertilization (IVF) in various mammals. Sperm preparation was performed in collaboration with Dr. K. Chakrabandhu. In comparison with washed sperm, PGC sperm consist mainly of motile sperm with normal morphology and complete chromatin condensation. In addition, PGC sperm have fewer coating vesicles around the sperm surface, and more vigorous motility patterns even in medium without albumin (Tanphaichitr *et al.*, 1988, 1990). PGC sperm also exhibit higher egg penetration ability (Tanphaichitr *et al.*, 1988; Matas *et al.*, 2003). These observations suggest better quality and higher fertilizing ability of PGC sperm. Before the isolation of non-capacitated and capacitated sperm rafts, the capacitation status of washed and PGC pig sperm is gauged by cholesterol efflux from the sperm plasma membrane, which leads to lower molar ratio of cholesterol:phospholipids, and by increased protein tyrosine phosphorylation (Tardif *et al.*, 2001, 2003; Flesch *et al.*, 2001; reviews: Visconti and Kopf, 1998; Visconti *et al.*, 2002). Since there is considerable variability from one sperm ejaculate to another in the same pig and among different pigs, and since a number of sperm ejaculates from the same and different pigs are used in our experiments, the lipid composition and protein tyrosine phosphorylation of pig sperm would also serve as quality control to ensure that the obtained results are accurate and repeatable.

### *3.3.1.1. Lipid Composition*

Cholesterol efflux from the sperm plasma membrane, induced by albumin (Langlais *et al.*, 1988; Visconti *et al.*, 1999) and by HDL and proteins originating from oviductal and follicular fluids (Ehrenwald *et al.*, 1990), is one of the main events associated with capacitation. This efflux results in a lower molar ratio of cholesterol:phospholipids, and thus leads to an increase in membrane fluidity, essential for downstream fusion-related events during capacitation (Langlais and Roberts, 1985; Langlais *et al.*, 1988; Davis, 1981; Cross, 1998). The lower molar ratio of cholesterol:phospholipids is used as a criterion to validate that the washed and PGC sperm used in this thesis had undergone capacitation following incubation in albumin containing medium. My spectrofluorometric analysis of cholesterol indicates its levels to be 0.82 ± 0.04 μmoles/$10^9$ washed sperm vs. 0.55 ± 0.04 μmoles/$10^9$ washed-capacitated sperm, and 0.49 ± 0.06 μmoles/$10^9$ PGC sperm vs. 0.27 ± 0.03 μmoles/$10^9$ PGC-capacitated sperm. These results reveal that cholesterol levels are lower in both washed and PGC sperm following capacitation, i.e., pig sperm capacitation is accompanied by cholesterol efflux from the sperm plasma membrane, consistent with previous findings (*pig*: Flesch *et al.*, 2001d; *mouse*: Visconti *et al.*, 1999a, b). Calorimetric analysis of phospholipids reveals their levels to be 2.16 ± 0.04 μmoles/$10^9$ washed sperm vs. 1.88 ± 0.03 μmoles/$10^9$ washed-capacitated sperm, and 1.00 ± 0.03 μmoles/$10^9$ PGC sperm vs. 1.01 ± 0.04 μmoles/$10^9$ PGC-capacitated sperm (Figure 3.22). While a small but significant decrease in the levels of total phospholipids is observed in washed sperm after capacitation, phospholipid levels remain unchanged in PGC sperm following incubation under capacitation conditions (Figure 3.22). The molar ratio of cholesterol:phospholipids

**Figure 3.22.** Lipid components of control and capacitated sperm. Levels of cholesterol (white bar), total phosphoplipids (black bar), and SGG (diagonal stripes bar) in washed sperm and washed-capacitated sperm (**A**), and in PGC sperm and PGC-capacitated sperm (**B**). The average and standard deviation of values obtained from three different experimental days were shown. $^{*,\times}$ Each denotes a statistical difference in the lipid value between the control and capacitated sperm samples ($P<0.01$ for cholesterol in panels **A** and **B**; $P<0.05$ for phospholipids in panel **A**, as analyzed by Student's *t* test).

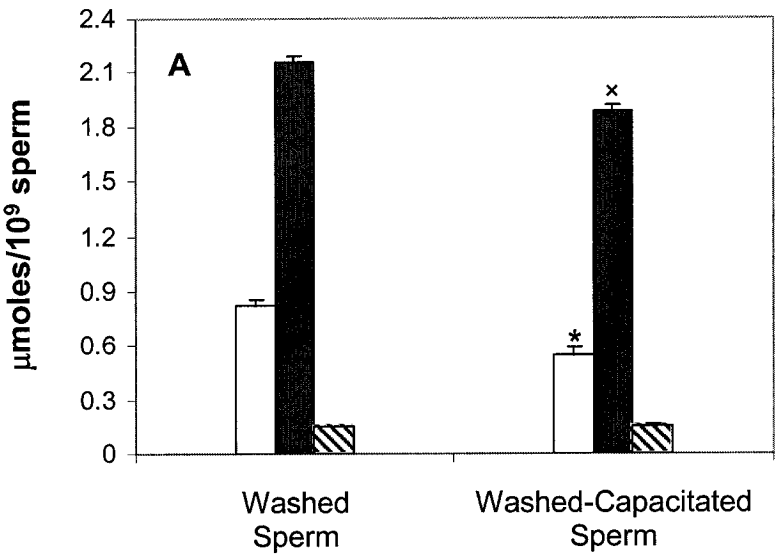
A
µmoles/10⁹ sperm
2.4
2.1
1.8
1.5
1.2
0.9
0.6
0.3
0
*
×
Washed Sperm
Washed-Capacitated Sperm

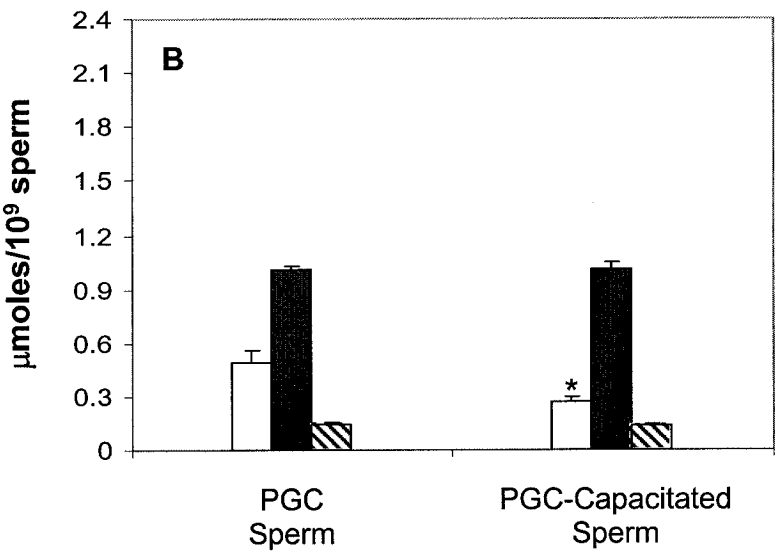
B
µmoles/10⁹ sperm
2.4
2.1
1.8
1.5
1.2
0.9
0.6
0.3
0
*
PGC Sperm
PGC-Capacitated Sperm

is lower in washed-capacitated sperm, compared with washed sperm (i.e., 0.28 vs. 0.37), as well as in PGC-capacitated sperm, relative to PGC sperm (i.e., 0.30 vs. 0.50). This is the first indication that the prepared/named "washed-capacitated" and "PGC-capacitated" pig sperm had undergone capacitation. The lower cholesterol:phospholipids molar ratio in washed sperm relative to PGC sperm is in agreement with previous results in human sperm (Sugkraroek *et al.*, 1991). This may be attributable to Percoll gradient centrifugation, which results in the removal of lipid-rich coating vesicles around the sperm plasma membrane (Tanphaichitr *et al.*, 1988, 1990).

Since SGG exists selectively in mammalian male germ cells and is involved in sperm-ZP binding (White *et al.*, 2000; Weerachatyanukul *et al.*, 2001), it is of interest to determine whether the sulfoglycolipid is affected by Percoll gradient centrifugation and/or by capacitation. Figure 3.22 shows that SGG levels remain the same in PGC sperm, compared with washed sperm, and that capacitation does not alter the levels of SGG either. This indicates that SGG is not removed from the pig sperm plasma membrane as a result of Percoll gradient centrifugation or capacitation, and this finding corroborates previous reports that SGG remains stable during the initial stages of mouse sperm capacitation (Tanphaichitr *et al.*, 1990). The distribution of SGG in washed and washed-capacitated sperm is ~6 mole% of the sperm major lipids (i.e., SGG, cholesterol, and total phospholipids). Since Percoll gradient centrifugation results in lower levels of cholesterol and phospholipids, the distribution of SGG increases to ~10 mole% of sperm major lipids in PGC and PGC-capacitated sperm. The higher proportions of the ZP adhesion molecule SGG in PGC sperm might render higher ZP binding ability to PGC sperm.

### *3.3.1.2. Protein Tyrosine Phosphorylation*

As in many mammals, sperm capacitation in pigs is associated with increased tyrosine phosphorylation of sperm proteins (Kalab *et al.*, 1998; Tardif *et al.*, 2001; Flesch *et al.*, 1999). Therefore, sperm protein tyrosine phosphorylation is used as another basis to further validate that the prepared washed and PGC sperm became capacitated upon incubation in albumin-containing medium. This is shown by immunoblotting using mouse monoclonal anti-phosphotyrosine IgG. This experiment was performed by Dr. K. Chakrabandhu. Several sperm proteins are already tyrosine phosphorylated, the major ones being p32, p42, p44, and a high molecular weight protein (> 209 kDa) (Figure 3.23), before incubation of washed and PGC sperm in CM. These results were consistent with previous findings (Tardif *et al.*, 2001, 2003). Following capacitation of washed and PGC sperm, an increased tyrosine phosphorylation of p32, p42 and a high molecular weight protein (> 209 kDa) is observed (Figure 3.23). Increased tyrosine phosphorylation of p32 was previously reported in washed-capacitated sperm, compared to washed sperm (Tardif *et al.*, 2001), as well as in isolated plasma membranes of PGC-capacitated sperm, compared to those isolated from PGC sperm (Flesch *et al.*, 1999). However, increased tyrosine phosphorylation of p42 and the high molecular weight protein (> 209 kDa) is reported for the first time in this thesis. In comparison with non-capacitated sperm, increased protein tyrosine phosphorylation in capacitated sperm (Figure 3.23), along with their lower molar ratio of cholesterol:phospholipids (Figure 3.22), reveal that the prepared "washed-capacitated" and "PGC-capacitated" pig sperm had indeed undergone the capacitation process.

**Figure 3.23.** SDS-PAGE and immunoblotting of tyrosine phosphorylated sperm proteins. Proteins obtained from 2 x $10^6$ washed sperm, washed-capacitated sperm, PGC sperm, and PGC-capacitated sperm were subjected to SDS-PAGE (12% polyacrylamide gel), and electroblotted onto a nitrocellulose membrane. Specific proteins were visualized by immunostaining using a mouse monoclonal anti-phosphotyrosine IgG. Protein patterns shown were representative of results obtained from three different experimental days.

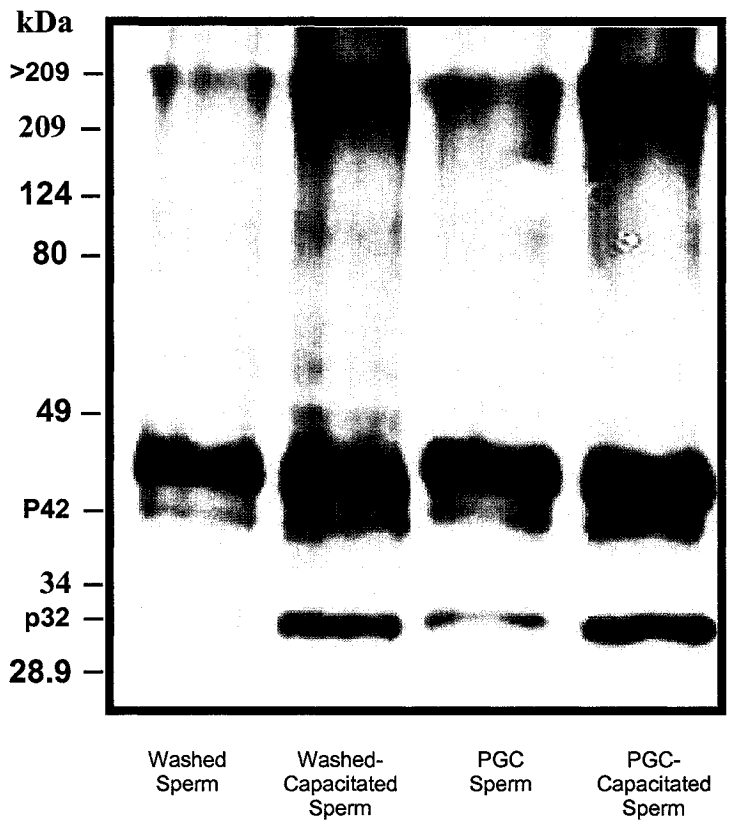
kDa
>209
209
124
80
49
P42
34
p32
28.9
Washed Sperm
Washed-Capacitated Sperm
PGC Sperm
PGC-Capacitated Sperm

### *3.3.1.3. Localization of SGG and Cholesterol in Live Sperm*

This report demonstrates that SGG interacts strongly with cholesterol via intermolecular hydrogen bonding, as revealed by FTIR spectroscopy (Figure 3.0), and mixtures of SGG with various concentrations of cholesterol are insoluble in 1% Triton X-100 at 4°C (Figure 3.21), an inherent property of rafts. Since SGG participates in ZP binding in mouse sperm (White *et al.*, 2000) and human sperm (Weerachatyanukul *et al.*, 2001), it is likely that this may hold true for pig sperm. Therefore, should SGG and cholesterol be localized to the same area on the sperm surface, both lipids may participate in the formation of rafts *in situ*. The goal of this study is to localize SGG and cholesterol in live pig sperm. Indirect immunofluorescence (IIF) using affinity purified anti-SGG/SGC IgG reveals fluorescent staining at the anterior sperm head, confined over the acrosomal ridge as a thin band, in PGC and PGC-capacitated pig sperm (Figure 3.24), as well as in washed and washed-capacitated pig sperm (results not shown), without any discernable differences. These results corroborate my biochemical analysis, revealing that SGG levels are not affected by Percoll gradient centrifugation or by capacitation (Figure 3.22). In conclusion, SGG localizes to the region participating in ZP binding (Burkin and Miller, 2000). This is in agreement with previous findings in live mouse sperm (White *et al.*, 2000) and human sperm (Weerachatyanukul *et al.*, 2001) revealing that SGG localizes to the sperm head anterior or the ZP binding site (Yanagimachi, 1994; Chen and Cardullo, 1994; Kerr *et al.*, 2002).

To localize cholesterol at the pig sperm surface, these cells are labeled with filipin (Friend, 1982). Filipin consists of a ring structure with several alternate trans double bonds (Figure 3.25A), and thus can be used as a fluorescent probe (Flesch *et al.*, 2001a).

**Figure 3.24.** Localization of SGG in live pig sperm. IIF of PGC sperm (**a, b, c**) and PGC-capacitated sperm (**d, e, f**) with 50 μg/ml affinity purified anti-SGG IgG, followed by Alexa-488 goat anti-rabbit IgG. After washing the unbound secondary antibody, sperm were viewed under a Zeiss IM35 epifluorescent microscope. Panels a, d: phase contrast micrographs; panels b, e: fluorescent micrographs showing the binding of anti-SGG IgG to the sperm head anterior; panels c, f: fluorescent micrographs showing that sperm were viable, as assessed by the lack of PI (0.5 μg/ml) staining. No labeling was detected in PGC-capacitated sperm when PRS IgG was used instead of anti-SGG IgG (**g, h, i**). Micrographs shown were representative of results obtained from three different experimental days.

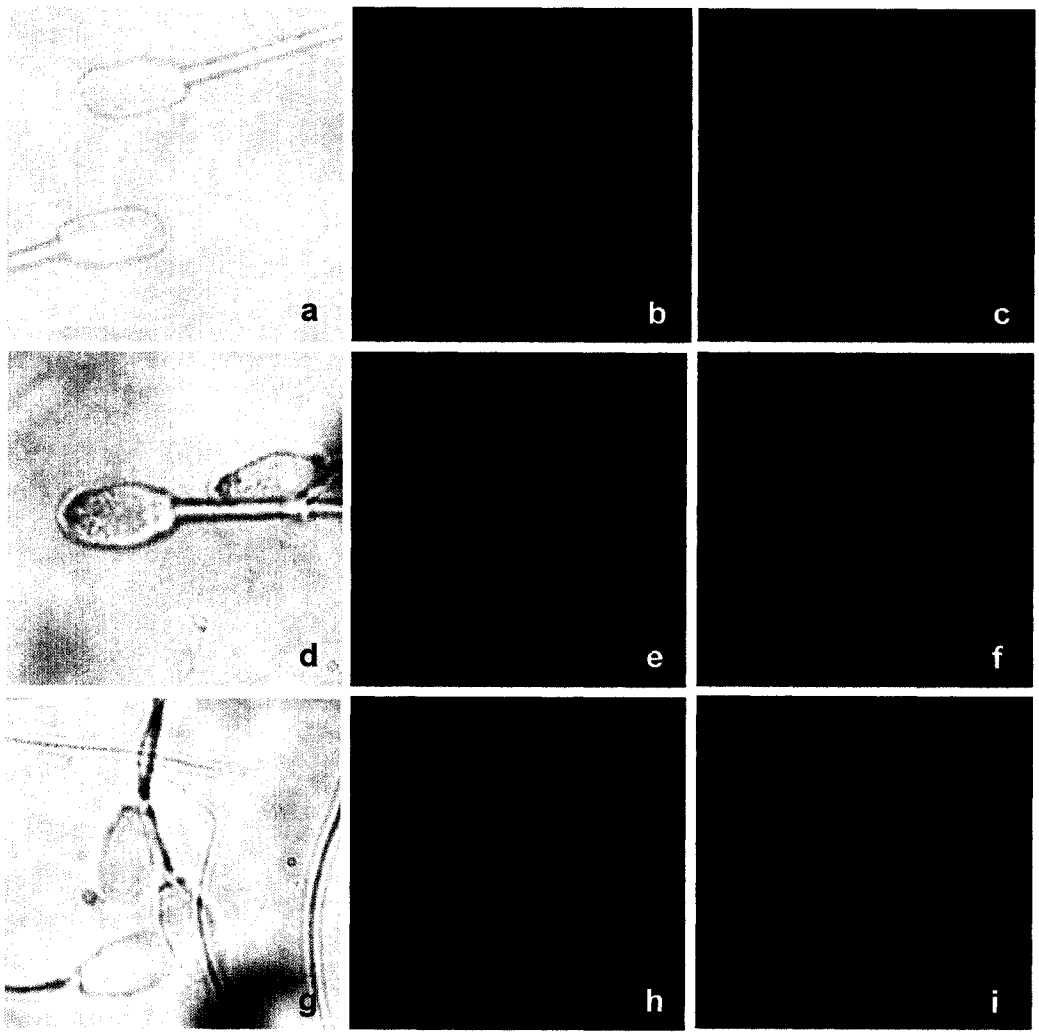
a
b
c
d
e
f
g
h
i

**Figure 3.25.** **A)** Chemical structure of filipin. **B)** Localization of cholesterol in live pig sperm. Fluorescent labeling of filipin-sterol complexes in PGC sperm (**a, b, c**) and PGC-capacitated sperm (**d, e, f**). Sperm were viewed under a Zeiss IM35 epifluorescent microscope. Panels **a, d**: phase contrast micrographs; panels **b, e**: fluorescent micrographs showing filipin labeling at the sperm head anterior; panels **c, f**: fluorescent micrographs showing that sperm were viable, as assessed by the lack of PI staining. Sperm samples were also treated with similar DMSO concentrations without filipin, and served as negative controls (**g, h, i**). Micrographs shown were representative of results obtained from three different experimental days.

A

Filipin

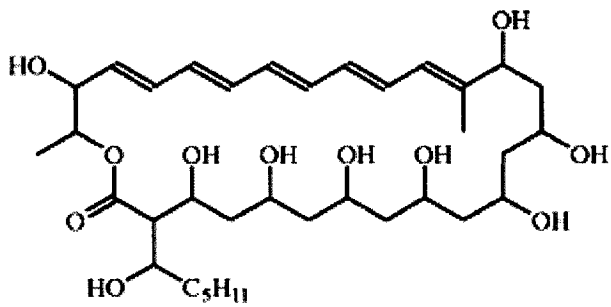


B

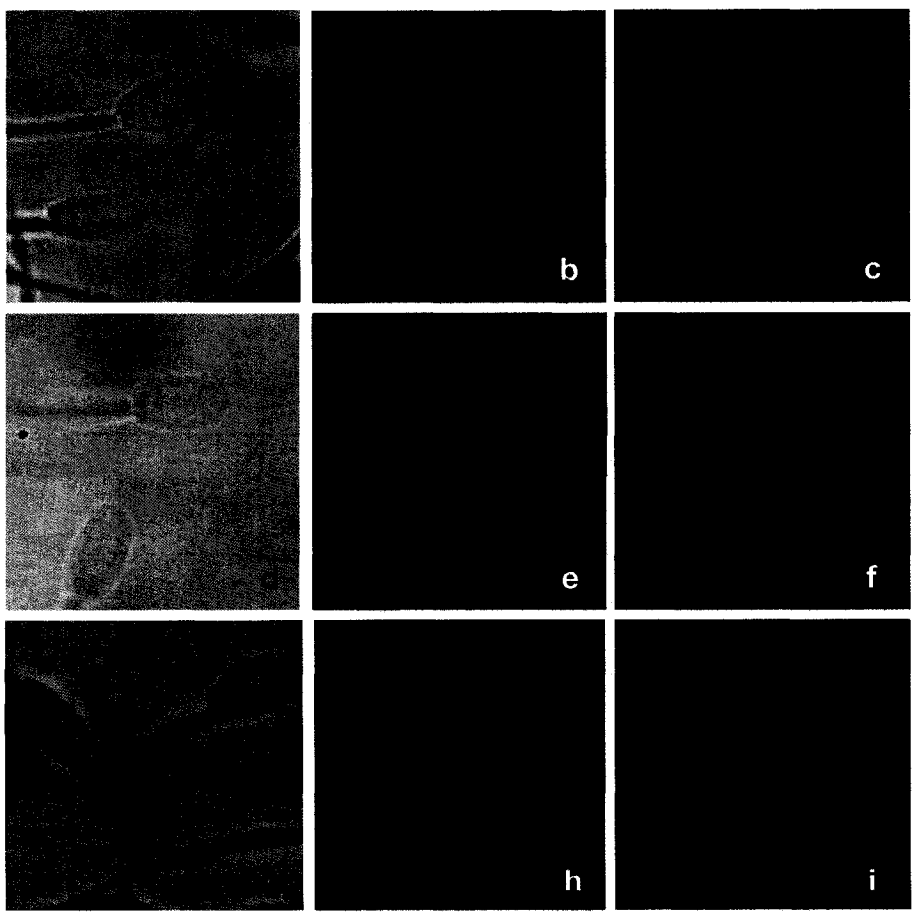

In fact, fluorescence detection of filipin-sterol complexes reveals surface labeling patterns over the sperm head anterior, specifically at the apical site, in both PGC and PGC-capacitated sperm (Figure 3.25B). Similar findings are also observed with washed and washed-capacitated pig sperm (results not shown). These results are similar to those detected in fixed PGC pig sperm by freeze fracture electron microscopy and fluorescence microscopy (Flesch *et al.*, 2001a). In addition, the coating vesicles around the sperm plasma membrane of washed sperm do not interfere with the labeling of cholesterol by filipin. Sperm samples incubated in DMSO without filipin serve as negative control, and are devoid of cholesterol-filipin aggregates (Figure 3.25B).

To demonstrate that the observed staining pattern of filipin on the pig sperm surface does in fact reflect the existence of free cholesterol, sperm are treated with 3 mM M$\beta$CD, a membrane impermeable, small cyclic oligosaccharide with a hydrophobic core that selectively extracts cholesterol from the plasma membrane (Yancey *et al.*, 1996; Kilsdonk *et al.*, 1995; Visconti *et al.*, 1999a, b). Fluorescence of filipin-cholesterol complexes is diminished in M$\beta$CD-treated sperm (Figure 3.26). Ongoing experiments in our laboratory (performed by Dr. K. Chakrabandhu) reveal that sperm treated with 3 mM M$\beta$CD still contain 30-40% of total sperm cholesterol. These results indicate that filipin staining is not sensitive enough to detect the remaining cholesterol in the plasma membrane of M$\beta$CD-treated sperm. Alternatively, filipin may pull out more cholesterol from the plasma membrane of M$\beta$CD-treated sperm, and thus account for the lack of staining in these cells. Interestingly, SGG fluorescent staining is still observed at the sperm head anterior in washed and PGC sperm treated with M$\beta$CD. In conclusion, SGG and part of cholesterol colocalize to the same site on pig sperm where ZP binding occurs.

**Figure 3.26.** Localization of SGG and cholesterol in live pig sperm pretreated with M$\beta$CD. PGC sperm pretreated with 3 mM M$\beta$CD were labeled either with filipin (**a, b, c**) or affinity purified anti-SGG IgG (**d, e, f**), and then viewed under a Zeiss IM35 epifluorescent microscope. Panels **a, d**: phase contrast micrographs; panel **b**, fluorescent micrograph showing the lack of filipin labeling at the sperm head anterior; panel **e**, fluorescent micrograph showing anti-SGG staining at the sperm head anterior; panels **c, f**: fluorescent micrographs showing that sperm were viable, as assessed by the lack of PI staining. Micrographs shown were representative of results obtained from three different experimental days.

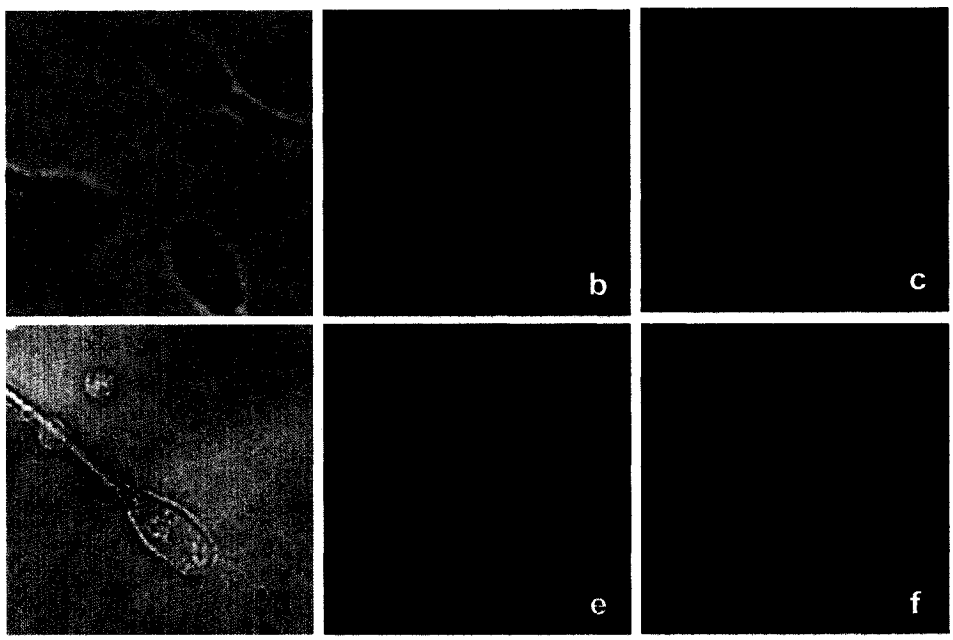
b
c
e
f

### *3.3.1.4. Binding of SGG to Pig ZP*

SGG on the sperm surface binds specifically to the ZP (White *et al.*, 2000; Weerachatyanukul *et al.*, 2001), presumably through the interaction of its sulfated galactosyl moiety with the ZP glycopeptides. In addition, sea urchin sperm rafts bind to homologous egg plasma membrane rafts via carbohydrate-carbohydrate mediated interactions between glycosphingolipids in sperm rafts an egg receptor (Ohta *et al.*, 1999b). Therefore, SGG may also bind to the pig ZP via the same mechanisms. This thesis examines for the first time the $K_d$ of SGG-ZP binding. Alexa-430 ZP binds directly and specifically to SGG-cholesterol-DPPC liposomes (having a molar ratio mimicking that of capacitated sperm rafts, i.e., 1.0:2.0:3.4, refer to section 3.3.3). The binding levels increase with Alexa-430 ZP concentrations and approach saturation (Figure 3.27). The levels of non-specific binding of Alexa-430 ZP to SGG-containing liposomes, determined by blocking the binding of the fluorescently labeled ZP with 100-fold excess of the unlabeled ligand (ZP), also rise linearly with increasing amounts of free Alexa-430 ZP, but represent only 0-30% of the total levels of the SGG-bound Alexa-430 ZP. Curves of specific binding of Alexa-430 ZP to the SGG-containing liposomes (obtained by subtracting the non-specific binding intensity from the total binding intensity of Alexa-430 ZP) reveal that the apparent $K_d$ of SGG-ZP binding is 0.092 ± 0.011 μM. The relatively low $K_d$ is indicative of a significant interaction between SGG and the pig ZP sulfoglycoproteins. These results are in accordance with previous findings in mice (White *et al.*, 2000) and humans (Weerachatyanukul *et al.*, 2001).

**Figure 3.27.** Binding of SGG to pig ZP. Various concentrations of Alexa-430 ZP were incubated (1 h, room temperature) with SGG-cholesterol-DPPC liposomes (molar ratio, 1.0:2.0:3.4, ○). Non-specific binding of Alexa-430 ZP to the SGG-containing liposomes was assessed in the presence of a 100-fold excess of unlabeled ZP (△). Specific binding of Alexa-430-conjugated ZP to the SGG-containing liposomes (●) was obtained following subtraction of non-specific binding levels from total binding levels of Alexa-430 ZP. Data shown were representative of two replicate experiments.

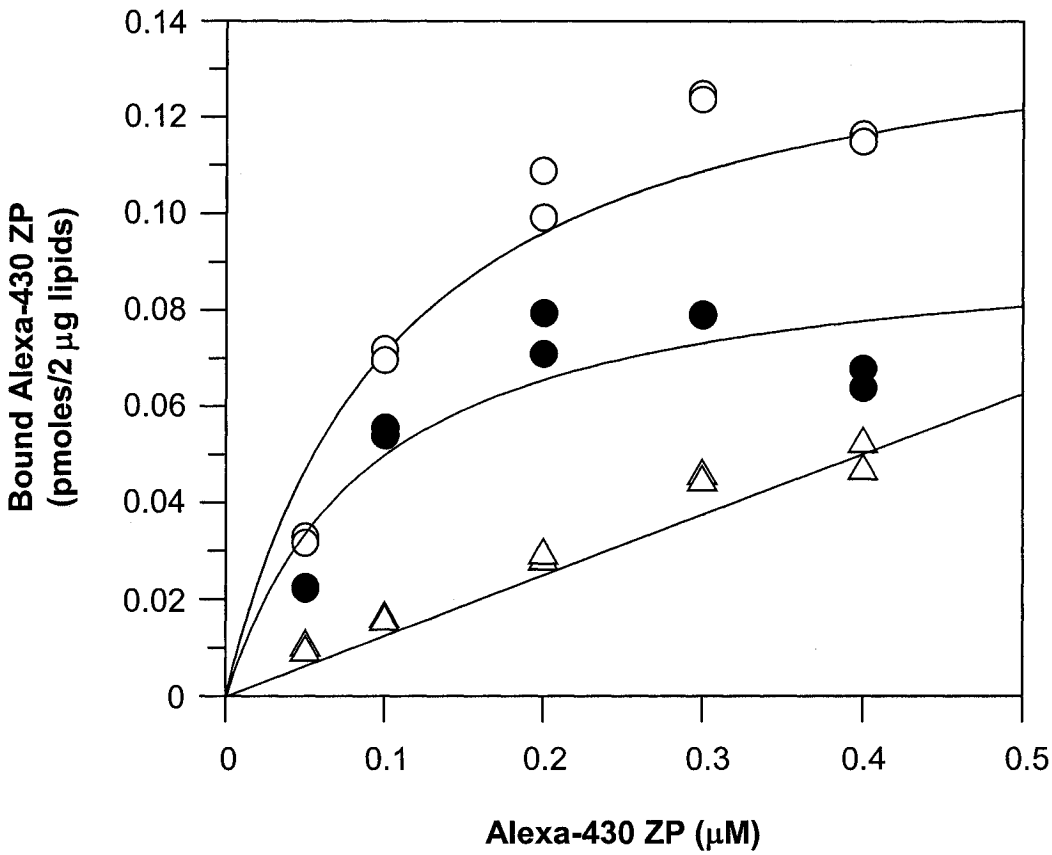
Bound Alexa-430 ZP
(pmoles/2 µg lipids)
0.14
0.12
0.10
0.08
0.06
0.04
0.02
0
0
0.1
0.2
0.3
0.4
0.5
Alexa-430 ZP (µM)

### *3.3.2. Characterization of Pig Sperm Rafts*

Insolubility of raft membranes in 1% Triton X-100 at 4°C has been used as a criterion for the isolation of rafts from cells (Brown and Rose, 1992; reviews: Brown and London, 1998b, 2000; Simons and Toomre, 2000), including gametes (Ohta *et al.*, 1999b, 2000; Luria *et al.*, 2002; Travis *et al.*, 2001; Nishimura *et al.*, 2001; Honda *et al.*, 2002; Sato *et al.*, 2002). Therefore, pig sperm rafts are isolated as low-density Triton X-100 insoluble membranes in this study. Treatment of washed and PGC non-capacitated and capacitated pig sperm with 1% Triton X-100 at 4°C, followed by sucrose gradient ultracentrifugation, results in the formation of a sharp light scattering band near the 5 and 30% sucrose interface (Figure 3.28). Fractions 4-6 of the 13 ml sucrose density gradient exhibit the highest light scattering intensity at 400 nm, i.e., highest insolubility in Triton X-100. In addition, fractions 4-6 of washed sperm (Figure 3.29) and PGC sperm (Figure 3.30) are enriched in cholesterol but not in proteins, compared with the high-density Triton X-100 soluble fractions (11-13). Conclusively, fractions 4-6 of the Triton X-100 pig sperm lysate exhibit similar properties to rafts isolated from other gametes and somatic cells, i.e., insolubility in 1% Triton X-100 at 4°C, and enrichment in cholesterol but not in proteins (Ohta *et al.*, 1999b; Sato *et al.*, 2002; Prinetti *et al.*, 1999; reviews: Simons and Toomre, 2000; Brown and London, 2000). The pooled fractions 4-6 are referred to as rafts throughout this thesis.

Significantly, the levels of rafts (measured by $A_{400}$) isolated from both washed-capacitated and PGC-capacitated sperm are higher than those isolated from control sperm (Figure 3.31). In accordance with $A_{400}$ values, capacitated sperm rafts also contain higher cholesterol levels than non-capacitated sperm rafts. Therefore, despite the lower levels of

**Figure 3.28.** Isolation of pig sperm rafts as Triton X-100 insoluble membranes. A photo of a tube after discontinuous sucrose gradient ultracentrifugation (200,000 g, 4°C for 18 h) of the Triton X-100 lysate of non-capacitated sperm (**a**) and capacitated sperm (**b**). Light scattering intensity (measured by $A_{400}$) of each of the 1 ml-fractions collected from top to bottom of the washed and washed-capacitated sperm lysates (**c**) and the PGC and PGC-capacitated sperm lysates (**d**). The average and standard deviation of values obtained from three different experimental days were shown.

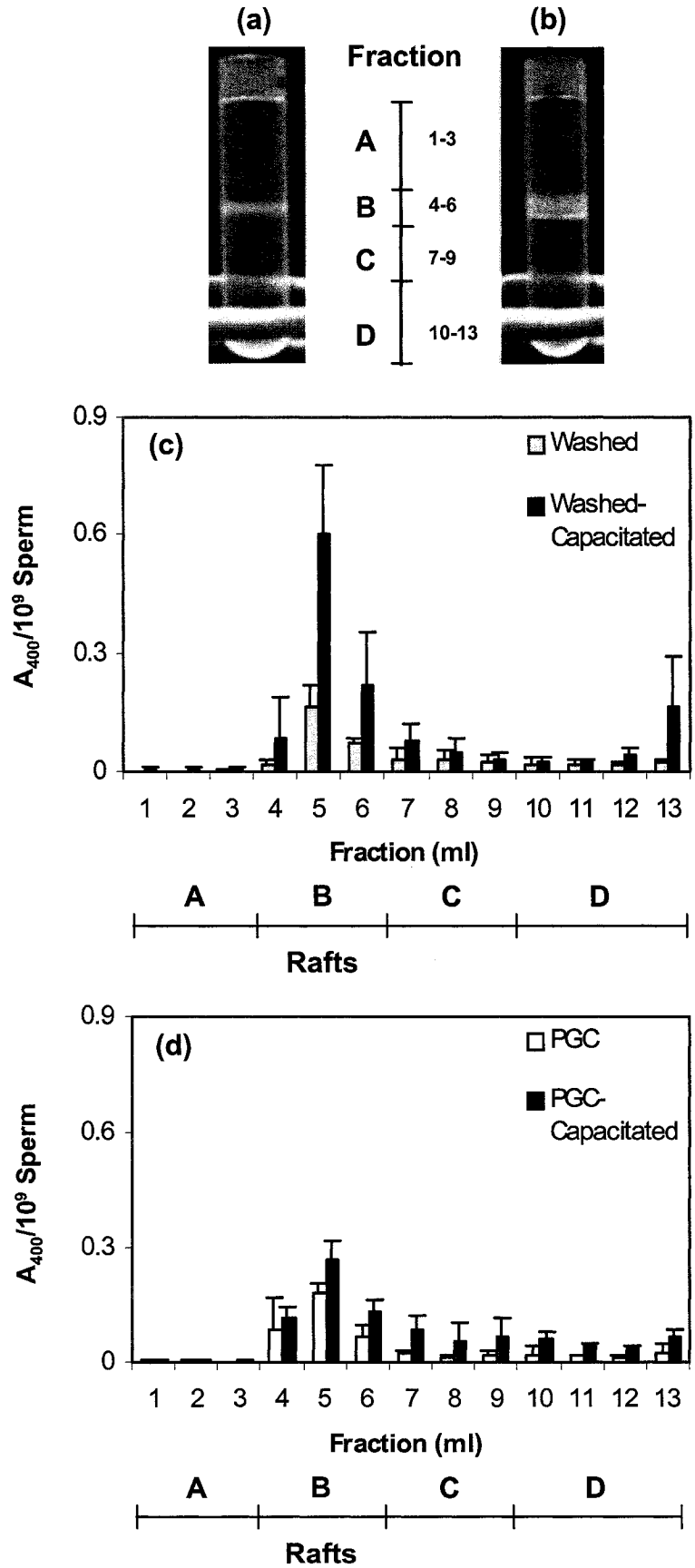
(a)
(b)
Fraction
A
1-3
B
4-6
C
7-9
D
10-13
(c)
Washed
Washed-Capacitated
$A_{400}/10^9$ Sperm
0.9
0.6
0.3
0
1 2 3 4 5 6 7 8 9 10 11 12 13
Fraction (ml)
A
B
C
D
Rafts
(d)
PGC
PGC-Capacitated
$A_{400}/10^9$ Sperm
0.9
0.6
0.3
0
1 2 3 4 5 6 7 8 9 10 11 12 13
Fraction (ml)
A
B
C
D
Rafts

**Figure 3.29.** Characteristics of washed sperm rafts. Distribution of cholesterol and proteins in the 1 ml-fractions/tube obtained following sucrose gradient ultracentrifugation of the Triton X-100 lysate of washed sperm (**a**), and washed-capacitated sperm (**b**), as described in Figure 3.28. The average and standard deviation of values obtained from three different experimental days were shown.

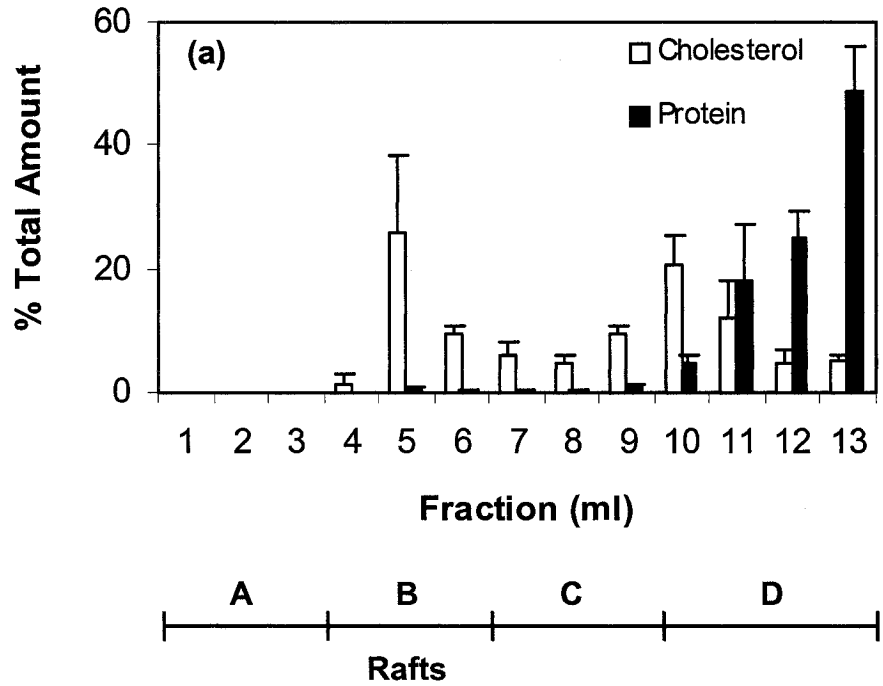
(a)
Cholesterol
Protein
% Total Amount
60
40
20
0
1 2 3 4 5 6 7 8 9 10 11 12 13
Fraction (ml)
A
B
C
D
Rafts

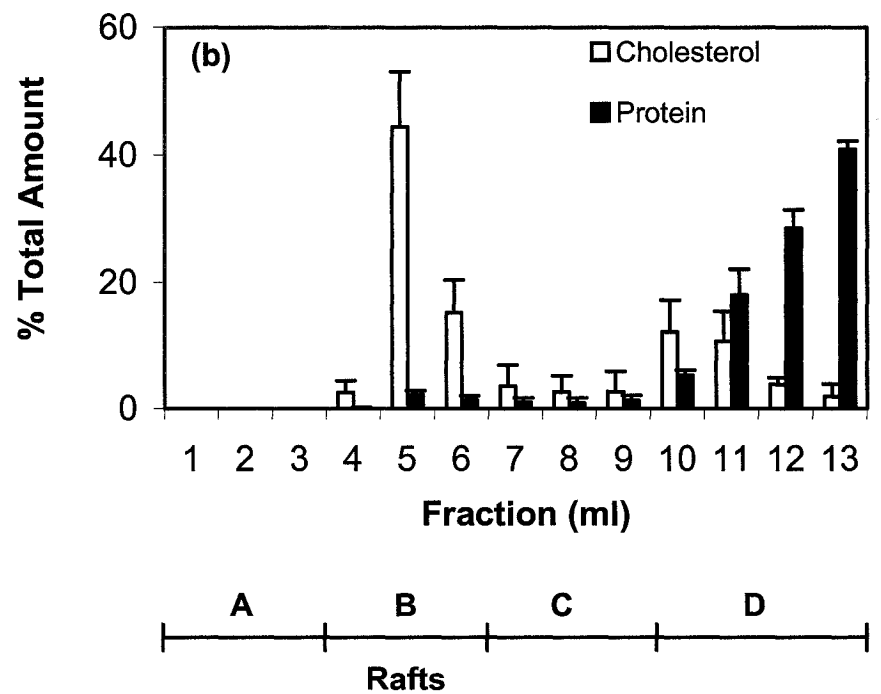
(b)
Cholesterol
Protein
% Total Amount
60
40
20
0
1 2 3 4 5 6 7 8 9 10 11 12 13
Fraction (ml)
A
B
C
D
Rafts

**Figure 3.30.** Characteristics of PGC sperm rafts. Distribution of cholesterol and proteins in the 1 ml-fractions/tube obtained following sucrose gradient ultracentrifugation of the Triton X-100 lysate of PGC sperm (**a**), and PGC-capacitated sperm (**b**), as described in Figure 3.28. The average and standard deviation of values obtained from three different experimental days were shown.

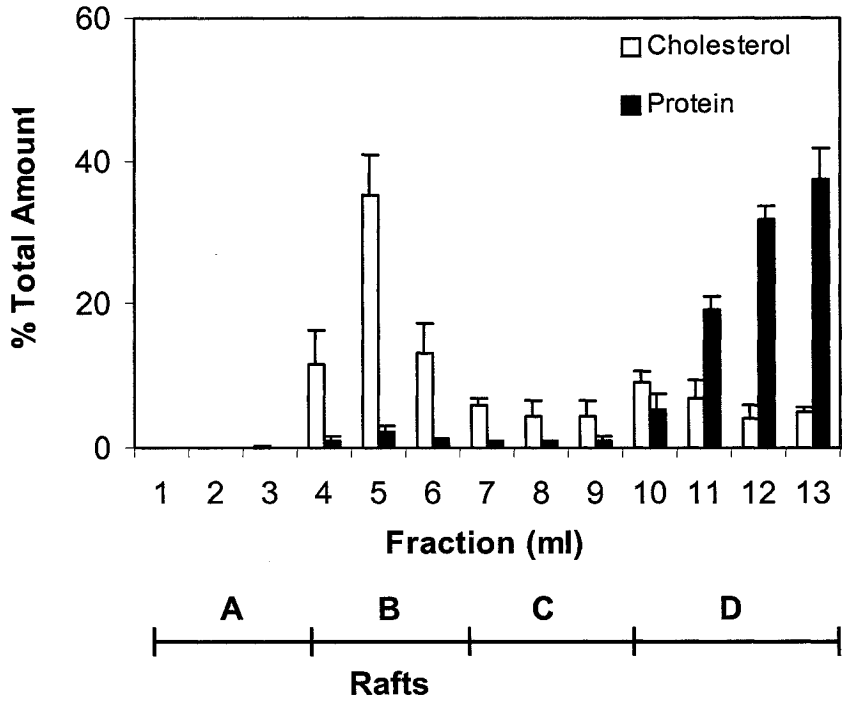
60
40
20
0
% Total Amount
Cholesterol
Protein
1 2 3 4 5 6 7 8 9 10 11 12 13
Fraction (ml)
A
B
C
D
Rafts

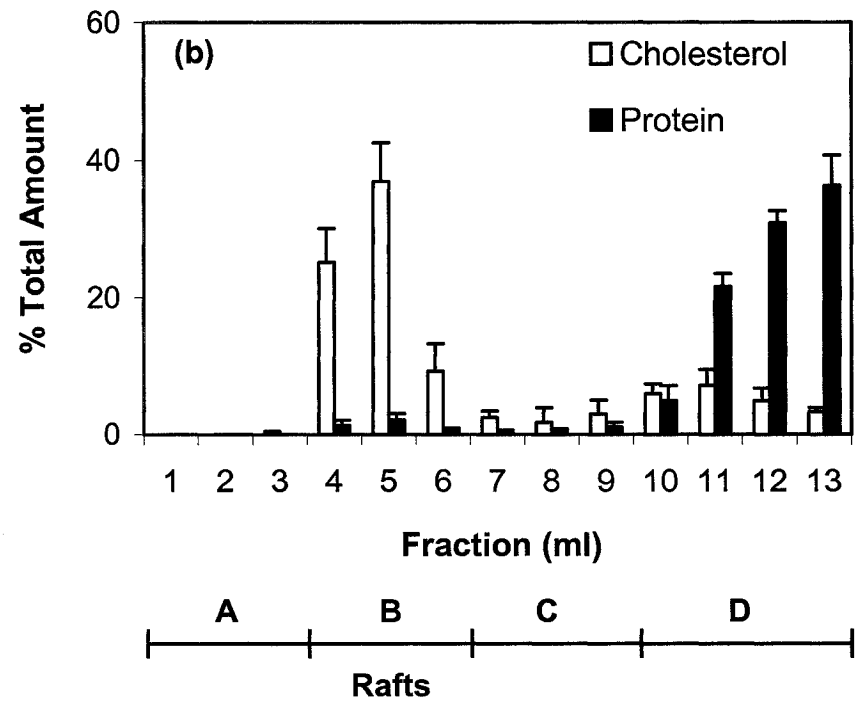
(b)
60
40
20
0
% Total Amount
Cholesterol
Protein
1 2 3 4 5 6 7 8 9 10 11 12 13
Fraction (ml)
A
B
C
D
Rafts

**Figure 3.31.** Light scattering intensity ($A_{400}/10^9$ sperm) and cholesterol levels ($\mu$moles/$10^9$ sperm) of the pooled fractions 4-6 (i.e., rafts) of the Triton X-100 lysate of washed sperm (beige bar) and washed-capacitated sperm (maroon bar) (**A**), and PGC sperm (yellow bar) and PGC-capacitated sperm (green bar) (**B**). The average and standard deviation of values obtained from three different experimental days were shown. $^{*,\times}$ Each denotes significant difference between control and capacitated sperm ($P<0.001$ and 0.05 for $A_{400}$ and cholesterol, respectively, in panels **A** and **B**, as analyzed by Student's *t* test).

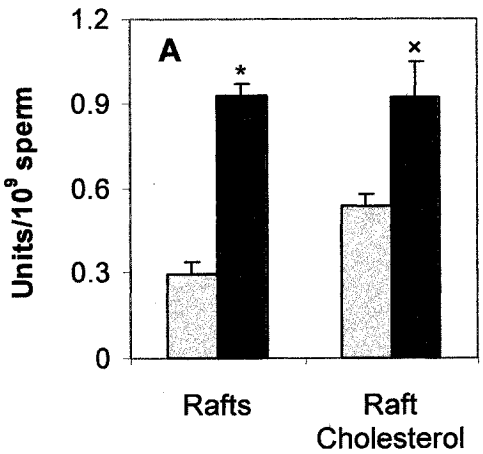
A
1.2
0.9
0.6
0.3
0
Units/10^9 sperm
*
×
Rafts
Raft
Cholesterol

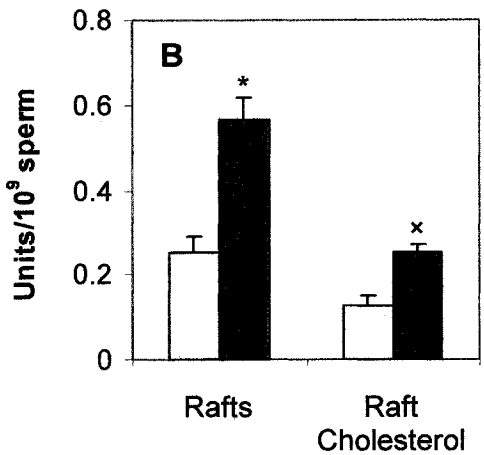
B
0.8
0.6
0.4
0.2
0
Units/10^9 sperm
*
×
Rafts
Raft
Cholesterol

cholesterol in capacitated sperm (31% from washed sperm and 40% from PGC sperm, Figure 3.22), the levels of raft cholesterol increase proportionally with raft amounts in capacitated sperm (Figure 3.31).

### *3.3.3. Characterization of the Lipid Composition of Pig Sperm Rafts*

In rafts, the presence of glycosphingolipids, cholesterol, as well as adhesion and signaling molecules is a universal characteristic of these membrane domains (reviews: Simons and Ikonen, 1997; Simons and Toomre, 2000; Brown and London, 1998a, b, 2000; van der Goot and Harder, 2001). $GM_1$ and $GM_3$ monosialogangliosides, and SGC (a structural analog of SGG) are present in rafts isolated from somatic cells (Iwabuchi *et al.*, 1998a, b; Harder and Simons, 1999) and gametes (Ohta *et al.*, 1999a; Luria *et al.*, 2002; Sato *et al.*, 2002). As shown in Section 3.2, the mammalian male germ cell specific sulfoglycolipid SGG (Murray and Narasimhan, 1990; Ishizuka, 1997), interacts strongly with cholesterol (an integral component of rafts) (Figures 3.20 and 3.21). In addition, both SGG and cholesterol colocalize to the anterior pig sperm head region, at the ZP binding site (Figures 3.24, 3.25). It is therefore likely that SGG is a pig sperm raft component. To validate this hypothesis, the lipid composition of washed, washed-capacitated, PGC and PGC-capacitated pig sperm rafts is characterized by HPTLC. This experiment was carried out by Mr. N. Vuong.

Total lipid profiles of washed, washed-capacitated, PGC, and PGC-capacitated sperm and their corresponding rafts are shown in Figure 3.32. Coomassie blue staining of the HPTLC chromatogram reveals the presence of SGG, cholesterol, DAG, PC, PE and sphingomyelin in all sperm samples and in their corresponding rafts. Significantly, SGG

**Figure 3.32.** Characterization of the lipid composition of sperm and their isolated rafts. HPTLC lipid profiles of control and capacitated sperm (washed and PGC), their isolated rafts (**A**), and sperm tail (**B**). Lipids were visualized following Coomassie blue staining (**A, B**) and orcinol staining (**C**) of the HPTLC chromatogram. The lipid samples were loaded onto the HPTLC plate based on equal amounts of SGG, i.e., 3 μg/sample (**A**) and based on sperm number, i.e., $1x10^6$ sperm (**B, C**). Standards used included SGG, cholesterol, DAG, PE, PC, and sphingomyelin. The HPTLC chromatograms shown were representative of results obtained from three different experimental days. *Abbreviations:* DAG, diacylglycerol; PC, 3-*sn*-glycerophosphorylcholine; PE, 3-*sn*-glycerophosphoryl-ethanolamine; SGG, sulfogalactosylglycerolipid; Stds, standards.

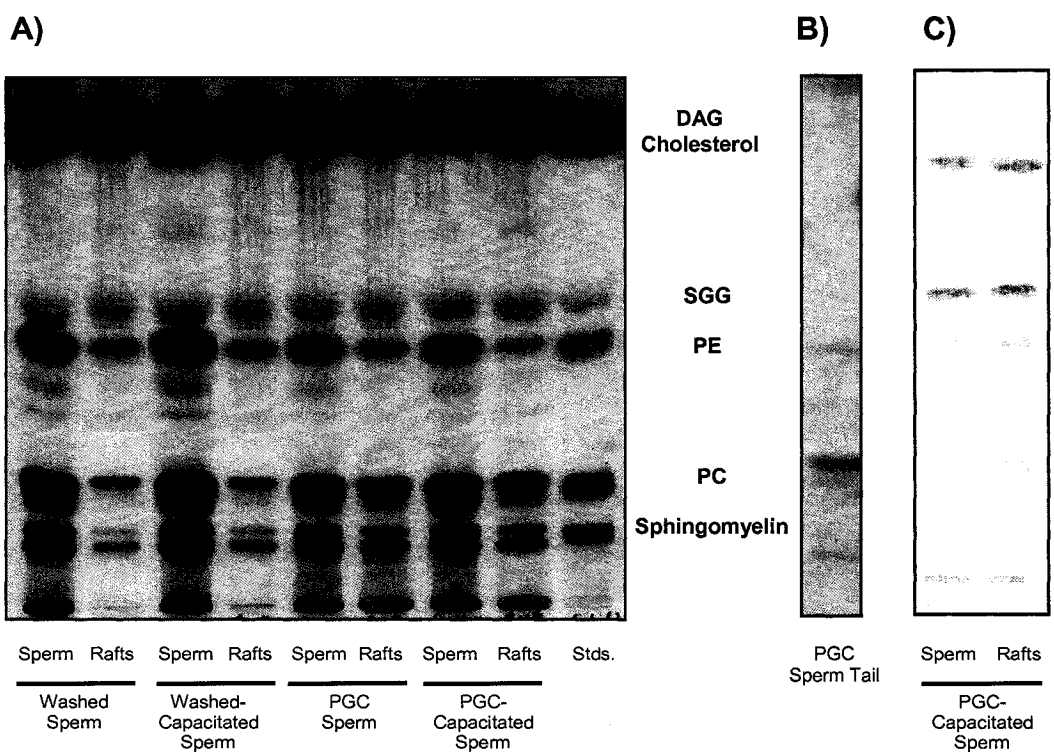
A)
B)
C)
DAG
Cholesterol
SGG
PE
PC
Sphingomyelin
Sperm Rafts Sperm Rafts Sperm Rafts Sperm Rafts Stds.
Washed Sperm
Washed-Capacitated Sperm
PGC Sperm
PGC-Capacitated Sperm
PGC Sperm Tail
Sperm Rafts
PGC-Capacitated Sperm

is absent in the pig sperm tail (Figure 3.32B). Orcinol staining, specific for glycolipids, of another HPTLC chromatogram indicates that SGG is the only glycolipid in both sperm and raft samples (Figure 3.32C). Since the samples are loaded onto the HPTLC plate based on equal amounts of SGG (see analysis in Sections 3.3.4), the illustrated Coomassie blue stained profiles indicate that the ratio of SGG to phospholipids appears higher in all raft samples, compared to their corresponding sperm samples, as visually observed (Figure 3.32A). This suggests that SGG had a higher distribution in the rafts, compared to whole sperm.

### *3.3.4. Distribution of SGG, Cholesterol and Phospholipids*

To further validate the semi-quantitative results from HPTLC, suggesting a higher ratio of SGG to phospholipids in sperm rafts, the major lipid components, i.e., SGG, cholesterol, and total phospholipids, are quantitated in non-capacitated and capacitated sperm rafts (Figure 3.33), and compared with their corresponding whole sperm (Table 3.1). Although the levels of SGG and phospholipids are the same in control and capacitated sperm, higher levels of these lipids are obtained in capacitated sperm rafts, compared with non-capacitated sperm rafts. The same results are also observed with cholesterol, despite its lower content in capacitated whole sperm (Table 3.1). The increases in the amounts of these three raft lipids (SGG, cholesterol and total phospholipids) in the capacitated sample appear to be commensurate with one another. Therefore, the molar ratio of SGG:cholesterol:phospholipids is similar in PGC-capacitated sperm rafts and PGC sperm rafts (i.e., 1.0:2.0:3.4 vs. 1.0:2.2:4.0), and in washed-capacitated sperm rafts and washed sperm rafts (i.e., 1.0:3.6:9.9 vs. 1.0:2.8:12).

**Figure 3.33.** Lipid components of control and capacitated sperm rafts. Levels of cholesterol (white bar), phospholipids (black bar), and SGG (diagonal stripes) in sperm rafts isolated from washed sperm and washed-capacitated sperm (**A**), and PGC sperm and PGC-capacitated sperm (**B**). The average and standard deviation of values obtained from three different experimental days were shown. $^{*, \times, +}$ Each denotes a statistical difference in the lipid value between control and capacitated sperm rafts ($P<0.001$ for cholesterol, and $P<0.01$ for phospholipids and SGG in panels **A** and **B**, as analyzed by Student's *t* test).

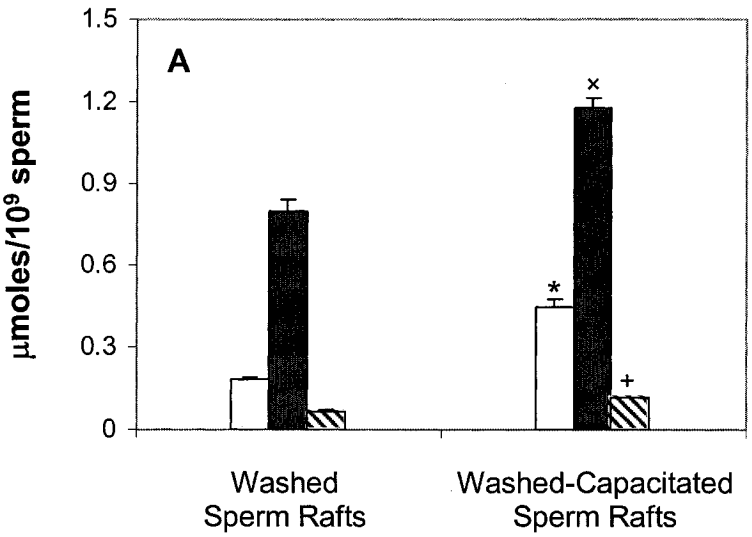
A
1.5
1.2
0.9
0.6
0.3
0
µmoles/10⁹ sperm
*
×
+
Washed
Sperm Rafts
Washed-Capacitated
Sperm Rafts

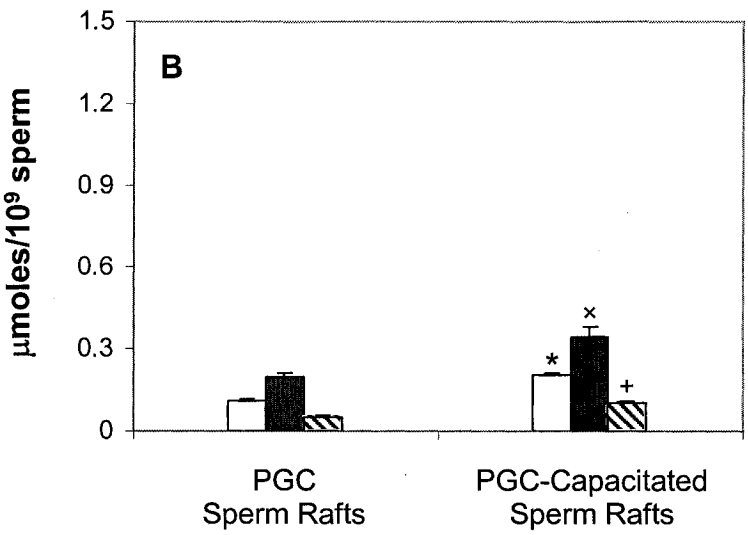
B
1.5
1.2
0.9
0.6
0.3
0
µmoles/10⁹ sperm
*
×
+
PGC
Sperm Rafts
PGC-Capacitated
Sperm Rafts

**Table 3.1. Levels of SGG, Cholesterol and Phospholipids in Whole Sperm and Isolated Sperm Rafts**

| Amounts (μmoles/$10^9$ sperm) | | | | | | | |
|---|---|---|---|---|---|---|---|
| **SGG** | **Chol** | **PLs** | **Total** | **SGG** | **Chol** | **PLs** | **Total** |
| **Washed Sperm** | | | | **PGC Sperm** | | | |
| 0.15 | 0.82 | 2.16 | 3.11 | 0.15 | 0.49 | 1.00 | 1.65 |
| [a] 5% | 26% | 69% | | 9% | 30% | 61% | |
| **Washed Sperm Rafts** | | | | **PGC Sperm Rafts** | | | |
| 0.065 | 0.18 | 0.80 | 1.06 | 0.048 | 0.11 | 0.20 | 0.35 |
| [a] 7% | 18% | 75% | | 14% | 29% | 57% | |
| [b] *44%* | *24%* | *37%* | *34%* | *32%* | *20%* | *20%* | *21%* |
| **Washed-Capacitated Sperm** | | | | **PGC-Capacitated Sperm** | | | |
| 0.15 | 0.55 | 1.89 | 2.65 | 0.14 | 0.27 | 1.01 | 1.44 |
| [a] 6% | 21% | 74% | | 10% | 21% | 69% | |
| **Washed-Capacitated Sperm Rafts** | | | | **PGC-Capacitated Sperm Rafts** | | | |
| 0.12 | 0.44 | 1.18 | 1.71 | 0.10 | 0.20 | 0.34 | 0.64 |
| [a] 7% | 21% | 70% | | 16% | 31% | 53% | |
| [b] *71%* | *73%* | *61%* | *65%* | *71%* | *67%* | *34%* | *44%* |

*Abbreviations: SGG, sulfogalactosylglycerolipid; Chol, cholesterol; PLs, phospholipids.*

[a] Percent of total lipids within whole sperm or sperm rafts.

[b] Percent of that specific lipid in sperm rafts, compared to the same lipid in whole sperm.

Significantly, 32-44% and 71% of total SGG in non-capacitated and capacitated sperm, respectively, is found in the isolated sperm rafts (Table 3.1). Since SGG binds to the ZP (White *et al.*, 2000; Weerachatyanukul *et al.*, 2001; Figure 3.27), the sulfoglycolipid may participate in both the formation of sperm rafts and in sperm raft-ZP binding.

Higher cholesterol and phospholipid levels accumulate in washed sperm rafts, compared with PGC sperm rafts. Moreover, higher raft levels are present in washed capacitated sperm, relative to PGC-capacitated sperm (Figure 3.31). Washed sperm are surrounded by lipid-rich coating vesicles (Tanphaichitr *et al.*, 1988, 1990), which may contribute to their higher cholesterol and phospholipid levels (Table 3.1), as well as to higher raft levels in washed-capacitated sperm, compared with PGC-capacitated sperm.

### *3.3.5. Fatty Acyl Chain Composition of Sperm Raft Phospholipids*

A key feature of raft formation lies in the tight acyl chain packing of lipids. The saturated acyl chains of lipids promote the formation of rafts because they are more extended then the unsaturated acyl chains, and pack well among themselves and with cholesterol (review: Brown and London, 2000). Since SGG is enriched in sperm rafts, and since the sulfoglycolipid forms homogenous bilayers with saturated phospholipids (Figure 3.18), it is likely that sperm raft phospholipids would be enriched in saturated fatty acyl chains. The fatty acyl chain composition of the major sperm raft phospholipids, i.e., PC and PE is analyzed by GC-MS to determine whether sperm rafts are enriched in saturated phospholipid species, similarly to rafts isolated from somatic cells (Stulnig *et al.*, 2001; Rouquette-Jazdanian *et al.*, 2001). This experiment was performed in collaboration with Mr. N. Vuong, and Dr. P. Kumarathasan (Health Canada).

FAME and DMA analyses of PC and PE of non-capacitated and capacitated pig reveal appreciable amounts of unsaturated fatty acyl chains, i.e., >40% of 22:5 and 22:6 (Figure 3.34), in agreement with previous results (pig: Nikolopoulou *et al.*, 1985; Parks and Lynch, 1992; *rat*: Aveldano *et al.*, 1992; *bull, stallion, rooster*: Parks and Lynch, 1992; *human*: Zalata *et al.*, 1998; Conquer *et al.*, 1999; Ollero *et al.*, 2000). The fatty acyl chains of sperm PC/PE also contain saturated species (mainly 16:0). High amounts of DMAs are obtained in pig sperm (Figure 3.34) since the mammalian male germ cell contains a high proportion of plasmalogens (20-40 mole%), compared with somatic cells (Poulos *et al.*, 1973; Parks and Lynch, 1992; Lin *et al.*, 1993; Brouwers *et al.*, 1998).

In contrast, FAME and DMA analyses of PC and PE in rafts of non-capacitated and capacitated sperm reveal that >85% of FAMEs + DMAs in PC and PE of both raft samples are saturated (mainly 16, with a minor amount of 18:0). Only 15% or less of these FAMEs + DMAs existed as 22:5 (Figure 3.34). These results indicate that pig sperm rafts contain significant proportions of saturated fatty acyl chains.

### *3.3.6. Binding of Pig Sperm Rafts to Homologous ZP*

Mouse sperm rafts contain ZP-binding proteins (e.g., GPI-linked PH-20) and egg plasma membrane binding proteins (e.g., fertilin α and cyritestin) (Nishimura *et al.*, 2001). Results reported herein (Figures 3.32, 3.33) also reveal the presence of SGG, another ZP binding molecule (White *et al.*, 2000; Weerachatyanukul *et al.*, 2001), in pig sperm rafts. Therefore, it is pertinent to determine whether the isolated sperm rafts could bind directly to homologous egg ZP (Alexa-430 ZP), and whether this ability is greater in capacitated sperm rafts, compared with non-capacitated sperm rafts.

**Figure 3.34.** FAMEs and DMAs of PC and PE isolated from non-capacitated (**A**) and capacitated sperm (**B**), and from their isolated rafts (**C** & **D**), as analyzed by GC-MS. The average of duplicate samples was shown.

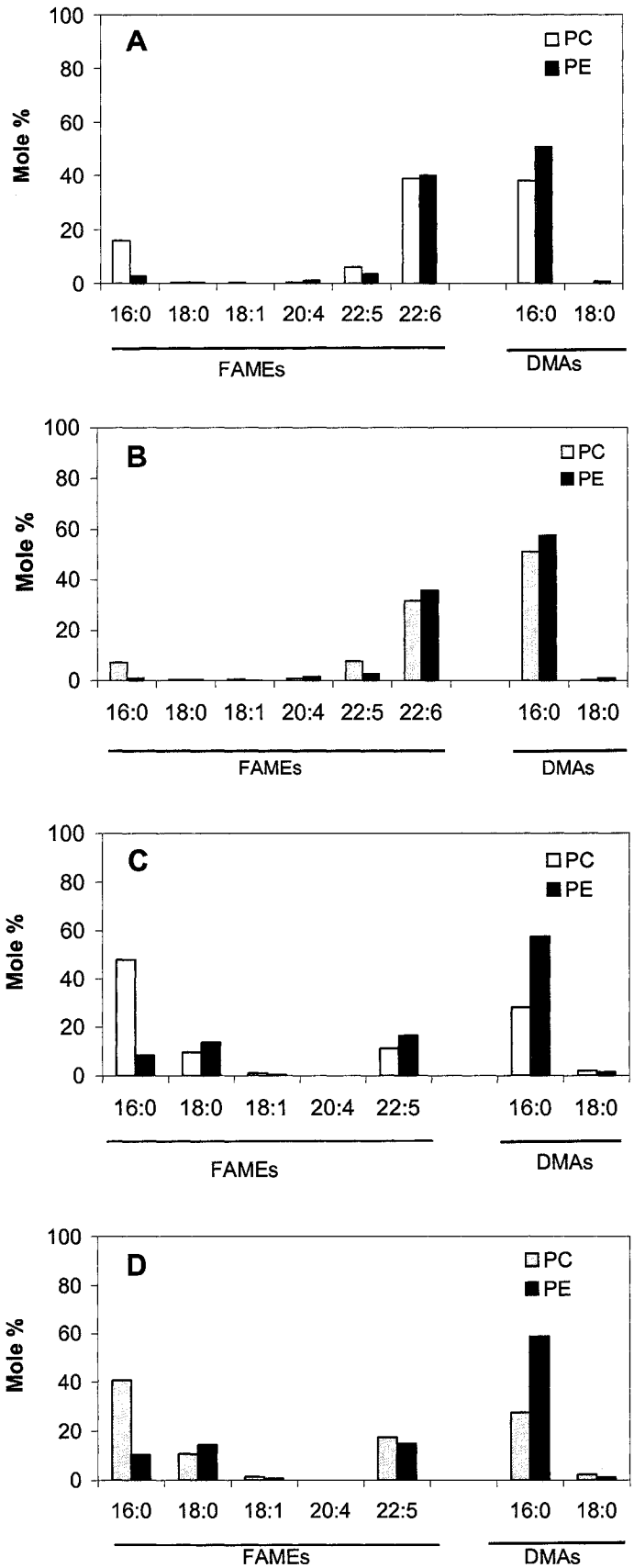
A
PC
PE
Mole %
100
80
60
40
20
0
16:0 18:0 18:1 20:4 22:5 22:6
16:0 18:0
FAMEs
DMAs
B
PC
PE
Mole %
16:0 18:0 18:1 20:4 22:5 22:6
16:0 18:0
FAMEs
DMAs
C
PC
PE
Mole %
16:0 18:0 18:1 20:4 22:5
16:0 18:0
FAMEs
DMAs
D
PC
PE
Mole %
16:0 18:0 18:1 20:4 22:5
16:0 18:0
FAMEs
DMAs

Initially, the binding of Alexa-488 ZP to pig sperm is investigated to determine whether the ZP used in this study (bought from Calbiochem) binds to its receptors on the pig sperm surface, and/or whether the ZP-labeling process interferes with sperm-ZP binding (experiment performed by Dr. K. Chakrabandhu). Sperm-ZP binding induces acrosomal exocytosis, which requires a high concentration of solubilized ZP, i.e., 125 $\mu$g/ml (Berger et al., 1989). Thus, 5 $\mu$g/ml of Alexa-488 ZP is used in our experiment. Alexa-488 ZP binds to live (i.e., negative for PI staining) PGC and PGC-capacitated pig sperm at the head anterior, confined as a thin band over the acrosomal edge (Figure 3.35). These data indicate that the conjugation of Alexa-488 to solubilized pig ZP did not interfere with the ability of the ZP to recognize its sperm surface receptors, and that ZP binding sites are exposed in non-capacitated and capacitated pig sperm. This is consistent with previous results of the same experiment performed by Burkin and Miller (2000), showing no discernable differences in the ZP binding ability of non-capacitated and capacitated pig sperm. However, when the ability of PGC non-capacitated and PGC-capacitated sperm to bind to intact ZP is assessed, higher numbers of PGC-capacitated sperm bound the ZP (experiments performed in our laboratory by Dr. E. Carmona). This observation corroborates a higher capacity of PGC-capacitated sperm to penetrate the ZP and to become acrosome-reacted in situ (Harrison, 1997; Matas et al., 2003). In contrast, the similarity in the binding of solubilized Alexa-488 ZP to PGC and PGC-capacitated sperm, as detected under an epifluorescent microscope, may reflect the possibility that this experimental approach may not be sufficiently quantitative for detecting the inherent differences in the ZP affinity of the two sperm types. These differences may only be detected by a more sensitive approach (e.g., using a spectrofluormeter or flow cytometer).

**Figure 3.35.** Binding of pig sperm to Alexa-488 ZP. PGC sperm (**a, b, c**) and PGC-capacitated (**d, e, f**) sperm were incubated with 5 μg/ml Alexa-488 ZP for 30 min. After washing the unbound fluorescent ZP, sperm were viewed under a Zeiss IM35 epifluorescent microscope. Panels **a, d**: phase contrast micrographs; panels **b, e**: fluorescent micrographs showing the binding of Alexa-488 ZP to the sperm head anterior; panels **c, f**: fluorescent micrographs showing that sperm were viable, as assessed by the lack of PI (0.5 μg/ml) staining. When Alexa-488 ovalbumin was used instead of Alexa-488 ZP, no binding was detected in PGC and PGC-capacitated sperm. Micrographs shown were representative of results obtained from three different experimental days.

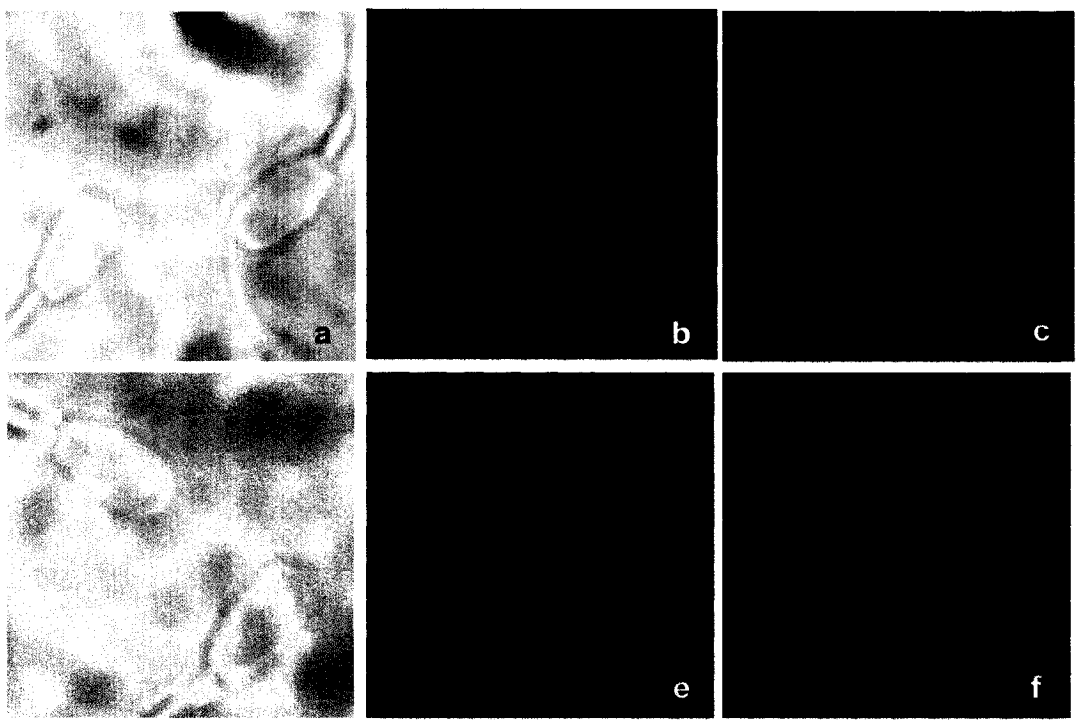
a
b
c
e
f

The binding of sperm rafts to Alexa-430 ZP is studied using a microtiter plate assay. This assay, which requires small amounts of material (0.5 μg of protein/well), has been widely used to assess the ZP-binding ability of pig sperm plasma membrane vesicles (Yurewicz *et al.*, 1993, 1998), as well as the binding ability of sea urchin sperm rafts to homologous egg plasma membrane rafts (Ohta *et al.*, 1999a). In addition, the interaction of rafts, isolated from various cells, with their ligands has been studied using the microtiter plate assay (Iwabuchi *et al.*, 1998b; Iwabuchi *et al.*, 2000; Handa *et al.*, 2000). Equal amounts of raft proteins (0.5 μg) were coated onto each well, since the protein to lipids (i.e., SGG, cholesterol and phospholipids) weight ratio does not change in non-capacitated and capacitated sperm rafts isolated from both washed and PGC sperm (Figure 3.36).

The binding of Alexa-430 ZP to uncoated (i.e., without sperm rafts) plates was less than 1% of total binding, and thus negligible. Figure 3.37 shows that all sperm raft samples exhibit binding ability to Alexa-430 ZP (the data shown represent total binding levels, i.e., before subtraction of non-specific binding of Alexa-430 ZP to sperm rafts, see below). Although washed non-capacitated sperm rafts bind to Alexa-430 ZP, the binding levels increase with ZP concentrations without approaching saturation, atypical of receptor-ligand binding. On the other hand, washed-capacitated sperm rafts, PGC sperm rafts, and PGC-capacitated sperm rafts all bind to Alexa-430 ZP, and the binding levels approach saturation at high ZP concentrations (Figure 3.37). In the set-up binding conditions, three negative controls are used to demonstrate the binding specificity between the ligand (i.e., Alexa-430 ZP) and the receptor (ZP adhesion molecules in sperm rafts).

**Figure 3.36.** Proteins to lipids (SGG, cholesterol, total phospholipids) weight ratio of non-capacitated and capacitated sperm rafts, isolated from washed (**A**) and PGC sperm (**B**). The average and standard deviation of values obtained from three different experimental days were shown.

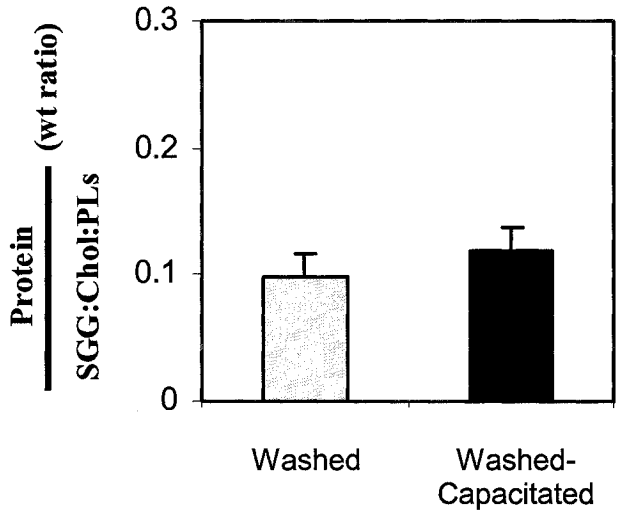
Protein / SGG:Chol:PLs (wt ratio)
0.3
0.2
0.1
0
Washed
Washed-Capacitated

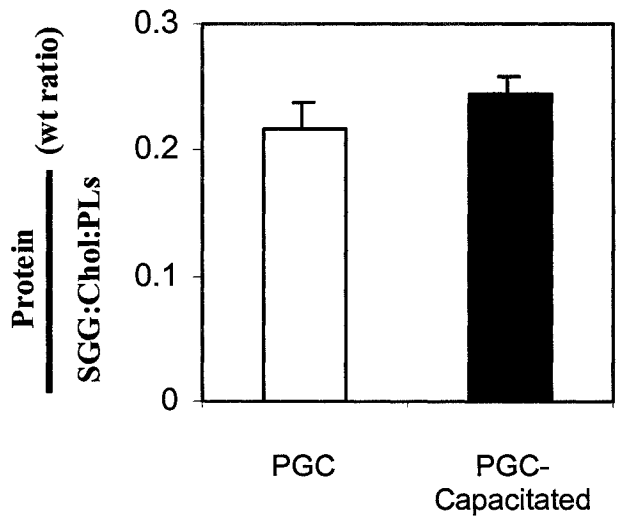
Protein / SGG:Chol:PLs (wt ratio)
0.3
0.2
0.1
0
PGC
PGC-Capacitated

**Figure 3.37.** Binding of pig sperm rafts to homologous ZP. Various concentrations of Alexa-430 ZP were incubated (1 h, room temperature) with washed sperm rafts (○) and washed-capacitated sperm rafts (●) (**A**), and with PGC sperm rafts (×) and PGC-capacitated sperm rafts (◇) (**B**). Low levels of interaction between washed-capacitated sperm rafts (**A**, ▲) or PGC-capacitated sperm rafts (**B**, ⬡) and an inert Alexa-430 protein (i.e., Alexa-430 ovalbumin) were also assessed. In an alternate experiment, PGC-capacitated sperm tail rafts (▽) were used instead of whole sperm rafts for incubation with Alexa-430 ZP (**A**). Non-specific binding of Alexa-430 ZP to washed sperm rafts (□) and washed-capacitated sperm rafts (■) (**A**), and to PGC sperm rafts (+) and PGC-capacitated sperm rafts (◆) (**B**) was assessed in the presence of a 100-fold excess of unlabeled ZP. The Y axis represents the levels of Alexa-430 ZP bound to sperm rafts in the microwells (0.5 μg raft proteins/well), except for the Alexa-430 ovalbumin experiment in which the axis denotes the levels of the bound Alexa-430 ovalbumin. The average and standard deviation of values obtained from three different experimental days were shown, except for the experiments that used a 100-fold excess of unlabeled ZP (□ and ■ in **A**), which were done twice, and the representative data from one experiment were shown.

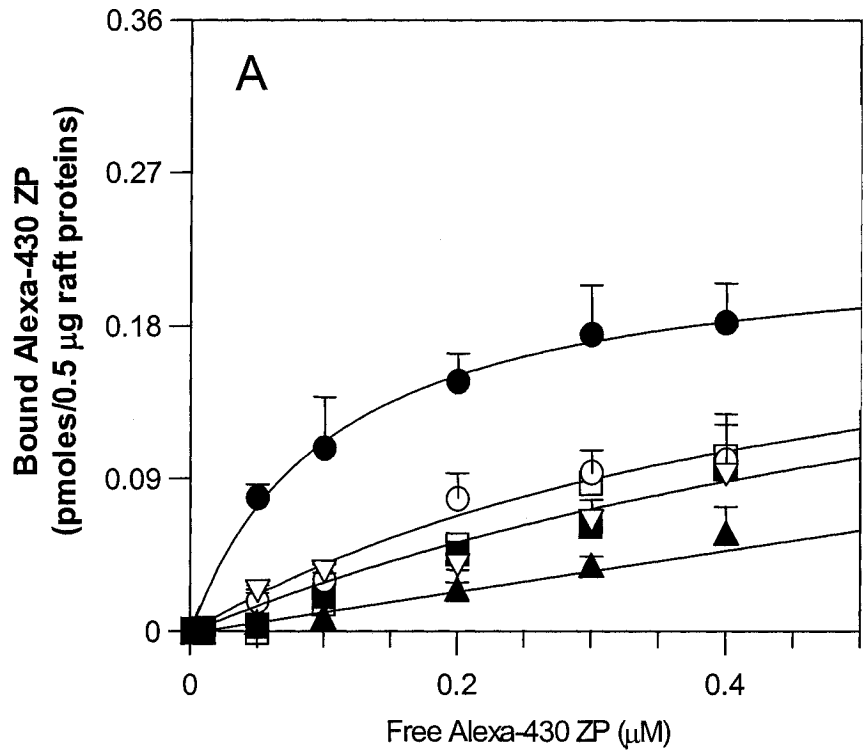
A
0.36
0.27
0.18
0.09
0
0
0.2
0.4
Bound Alexa-430 ZP
(pmoles/0.5 μg raft proteins)
Free Alexa-430 ZP (μM)

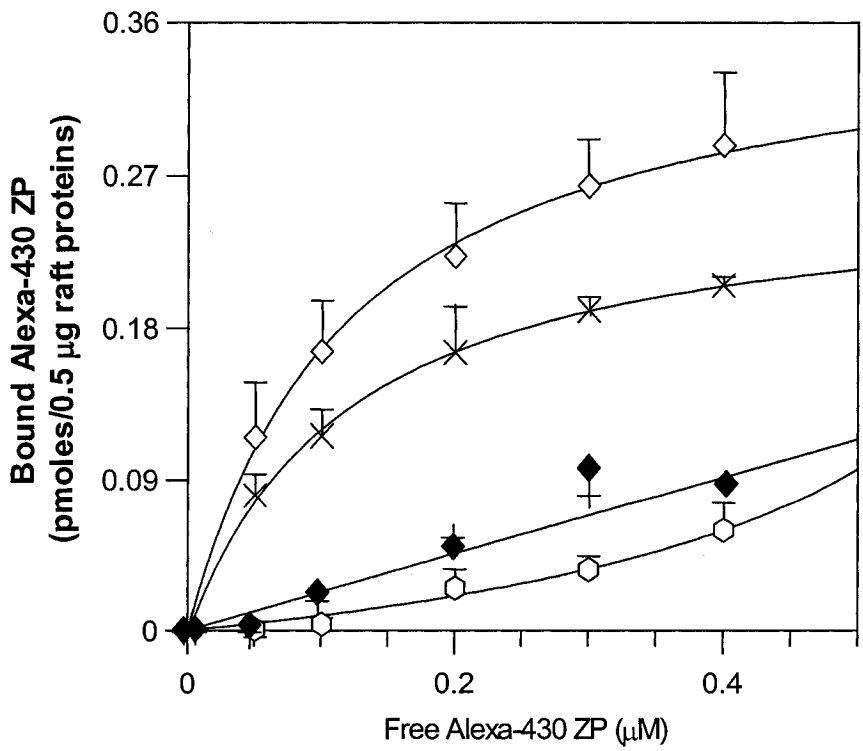
0.36
0.27
0.18
0.09
0
0
0.2
0.4
Bound Alexa-430 ZP
(pmoles/0.5 μg raft proteins)
Free Alexa-430 ZP (μM)

*Binding studies using an irrelevant ligand.* Ovalbumin does not to bind to sperm (Carmona *et al.*, 2002; Tantibhedhyangkul *et al.*, 2002; Bendahmane and Tulsiani, 2003). Thus, Alexa-430 ovalbumin is used as negative control to demonstrate that the binding of Alexa-430 ZP to sperm rafts is a ZP-specific event (Figure 3.37A, B). Alexa-430 ovalbumin exhibits a low binding ability to all sperm raft samples (i.e., isolated from washed, washed-capacitated, PGC and PGC-capacitated sperm), increasing gradually with ovalbumin concentrations without reaching a plateau. This was indicative of non-specific binding of ovalbumin to sperm rafts, thus substantiating the binding specificity of Alexa-430 ZP to sperm rafts.

*Binding studies using the sperm tail.* In my thesis, rafts were isolated from whole sperm, and consist of a mixture of those from the head and tail. While the sperm head is the interaction site of the egg, with the head anterior plasma membrane being the ZP binding site (Chen and Cardullo, 1994; Kerr *et al.*, 2001; Yanagimachi, 1994), the sperm tail houses the motility apparatus and does not bind to the ZP (Eddy and O'Brien, 1994; Yanagimachi, 1994). Thus, rafts isolated from the sperm tail are included in this study to act as negative controls from the receptor aspect. Sperm tail rafts also serve as a negative of control of SGG-containing rafts, since the sperm tail does not contain SGG (Figure 3.32B). Rafts isolated from PGC-capacitated sperm tail, separated from the sperm head by sonication and sucrose gradient ultracentrifugation (Shao *et al.*, 1997), exhibit a low binding ability to Alexa-430 ZP. This binding increased gradually with ZP concentrations without reaching saturation (Figure 3.37A). Although the sperm tail plasma membrane is partially disrupted using this isolation procedure (Shao *et al.*, 1997), these disrupted tail plasma membranes and the tail organelle membranes still should not

have ZP binding ability. Therefore, rafts isolated from these sperm tails can be used as negative controls of whole sperm rafts, which house the ZP binding receptor(s), to validate the functional specificity of sperm rafts in ZP binding.

*Binding studies in the presence of the unlabeled ligand (ZP).* In addition to binding to ZP receptors in sperm rafts, Alexa-430 ZP also binds to non-receptor sites. Therefore, when performing the fluorescently labeled ligand binding experiments, both total binding and non-specific binding are measured to calculate specific (receptor) binding as the difference. Non-specific binding of Alexa-430 ZP to sperm rafts is determined in the presence of 100-fold excess of unlabeled ligand, a ZP concentration that binds to essentially all ZP receptors in sperm rafts. As a result, the unlabeled ZP occupies all receptors in sperm rafts, and Alexa-430 ZP only binds non-specifically. The levels of non-specific binding of Alexa-430 ZP are 60% for washed sperm rafts, 38% for washed-capacitated sperm rafts (Figure 3.37A), 34% for PGC sperm rafts, and 26% for PGC-capacitated sperm rafts (Figure 3.37B). Non-specific binding of Alexa-430 ZP to sperm rafts is higher in washed sperm rafts, compared to PGC sperm rafts. This indicates that the excess amounts of unlabeled ZP effectively competed with Alexa-430 ZP for the ZP receptors in PGC sperm rafts, contrasted to washed sperm rafts. Compared with PGC sperm, washed sperm are surrounded by coating vesicles (Tanphaichitr *et al.*, 1988; 1990). As a result, coating vesicles may contribute to the formation of washed sperm rafts. This may trap Alexa-430 ZP non-specifically, thus contributing to the high levels of non-specific binding of the fluorescently labeled ZP to washed sperm rafts, relative to PGC sperm rafts.

To determine the $K_d$ of sperm raft-ZP binding, only the amount of fluorescently labeled ligand specifically bound to sperm rafts is used, i.e., total binding minus non-specific binding obtained in the presence of a 100-fold excess of unlabeled ZP (Figure 3.38). The $K_d$ of the binding of washed-capacitated sperm rafts to the ZP is lower than that of washed sperm rafts (i.e., 0.063 ± 0.02 μM vs. 0.25 ± 0.24 μM). A lower $K_d$ is also observed for the binding of PGC-capacitated sperm rafts to the ZP, compared to PGC sperm rafts (i.e., 0.056 ± 0.01 μM vs. 0.11 ± 0.03 μM) (Table 3.2). The $K_d$ of capacitated sperm rafts binding to the ZP is in the same range as that described for mouse sperm-ZP binding (0.050-0.070 μM) (Thaler and Cardullo, 1996; Kerr *et al.*, 2001). Capacitated sperm rafts exhibit enhanced ZP binding ability, compared with non-capacitated sperm rafts. These data corroborate the physiology of pig sperm-ZP binding, and confirm the concept that sperm rafts house the ZP binding domains. This concept is further supported by the finding that SGG is enriched in sperm rafts (Table 3.1).

PGC-capacitated sperm rafts exhibited a higher ZP binding ability than washed-capacitated sperm rafts (Figure 3.38). In comparison with washed sperm, Percoll gradient centrifugation generates partially capacitated sperm, devoid of coating vesicles (Tanphaichitr *et al.*, 1988, 1990), which may originate from seminal plasma, previously shown to contain an anti-fertility glycoprotein (Audhya *et al.*, 1987). These coating vesicles may interfere with the function of existing ZP binding molecules in washed-capacitated sperm rafts, relative to PGC-capacitated sperm rafts. The highest ZP binding ability of PGC-capacitated sperm rafts corroborates the higher egg penetration ability of PGC-capacitated sperm, compared with washed sperm (Tanphaichitr *et al.*, 1988; Matas *et al.*, 2003).

**Figure 3.38.** Specific binding of Alexa-430 ZP to washed sperm rafts (○) and washed-capacitated sperm rafts (●) (**A**), and to PGC sperm rafts (×) and PGC-capacitated sperm rafts (◇) (**B**). These specific binding levels were obtained by subtracting non-specific binding levels from total binding levels of Alexa-430 ZP (as described and shown in Figure 3.37). * Denotes significant difference of the levels of ZP binding between control and capacitated sperm rafts, as analyzed by ANOVA ($P<0.05$ for all concentrations).

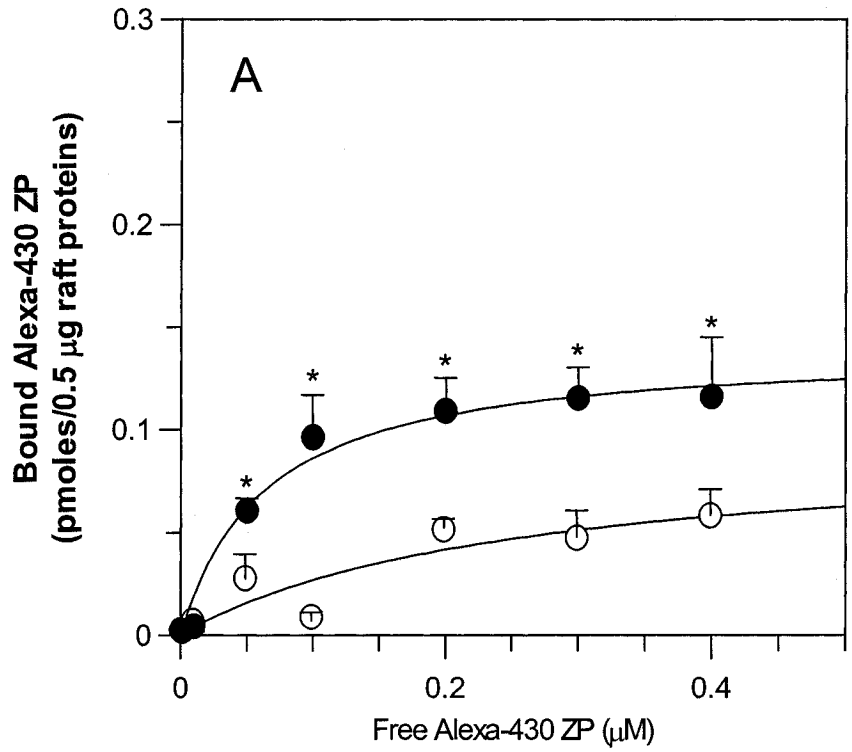
A
Bound Alexa-430 ZP
(pmoles/0.5 µg raft proteins)
0.3
0.2
0.1
0
0
0.2
0.4
Free Alexa-430 ZP (µM)

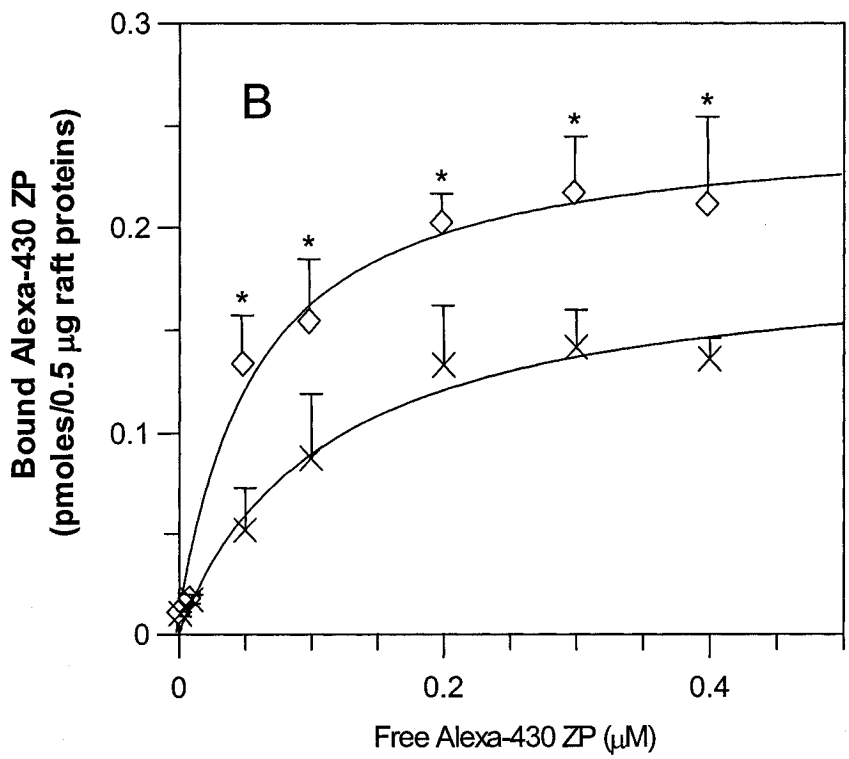
B
Bound Alexa-430 ZP
(pmoles/0.5 µg raft proteins)
0.3
0.2
0.1
0
0
0.2
0.4
Free Alexa-430 ZP (µM)

**Table 3.2. $K_d$ and $B_{max}$ of Rafts-ZP Binding***

| | $B_{max}$ (pmoles/0.5 μg raft proteins) | $K_d$ (μM) |
|---|---|---|
| **Washed Sperm Rafts** | 0.95 ± 0.45 | 0.25 ± 0.24 |
| **Washed-Capacitated Sperm Rafts** | 1.40 ± 0.11 | 0.063 ± 0.02 |
| **PGC Sperm Rafts** | 1.86 ± 0.16 | 0.11 ± 0.03 |
| **PGC-Capacitated Sperm Rafts** | 2.50 ± 0.06 | 0.056 ± 0.02 |

* Parameters were determined by non-linear regression.

Pig ZP3, consisting of ZP3α and ZP3β hetero-oligomers, has been implicated in binding to pig sperm plasma membrane vesicles. The ZP3α moiety may be the major participant in intact pig sperm-ZP binding, although the co-existence of ZP3β is also essential for this interaction (Yurewicz *et al.*, 1993, 1998). If sperm rafts represent the ZP-binding domains on intact sperm, the binding of sperm rafts to ZP would then be dependent on pig ZP3, and primarily on ZP3α. Figure 3.39 depicts representative competition binding curves of Alexa-430 ZP (0.2 μM) to PGC-capacitated sperm rafts, in the presence of excess amounts of unlabeled solubilized pig ZP, ZP3, ZP3α and ZP3β. As expected, total pig ZP, ZP3 and ZP3α competitively inhibits the binding of Alexa-430 ZP to PGC-capacitated sperm rafts with high efficiency. Maximum inhibition is 98% with total ZP and ZP3 (Figure 3.39A), compared to 81% with ZP3α (Figure 3.39B). This is consistent with previous findings revealing that ZP3α binds to sperm (Sacco *et al.*, 1989), as well as isolated sperm plasma membrane vesicles (Yurewicz *et al.*, 1991, 1993). On the other hand, ZP3β exhibits less drastic inhibitory effects (34%) on the binding of Alexa-430 ZP to PGC-capacitated sperm rafts (Figure 3.39B). The inability of ZP3β and ZP3α alone to inhibit the binding of Alexa-430 ZP to PGC-capacitated sperm rafts to the same extent as ZP3 and total ZP indicates that ZP3α-ZP3β heterocomplexes are needed to efficiently inhibit this binding event. Conclusively, these results reveal that capacitated sperm rafts utilize the same ZP receptors as sperm, thus further revealing their physiological significance.

**Figure 3.39.** Competitive Alexa-430 ZP-sperm rafts binding assays showing the dependence of the binding on pig ZP glycoproteins. These experiments involved incubation of capacitated sperm rafts with 0.2 μM Alexa-430-conjugated ZP in the presence of various concentrations (0-4 μM) of solubilized total pig ZP (◆), ZP3 (▲) or ovalbumin (negative control) (■) (**A**), and in the presence of ZP3α (●) and ZP3β (○) (**B**). The levels of Alexa-430 ZP bound to capacitated sperm rafts were expressed as percentages of the values obtained from the Alexa-430 ZP-sperm rafts co-incubates that contained no competitor ligands. The average and standard deviation of values obtained from 3 different experimental days were shown. The sperm rafts-Alexa-430 ZP binding levels at all concentrations of the unlabeled ZP competitor were significantly lower from the control values (denoted by *), as determined by ANOVA ($P<0.05$ for all concentrations).

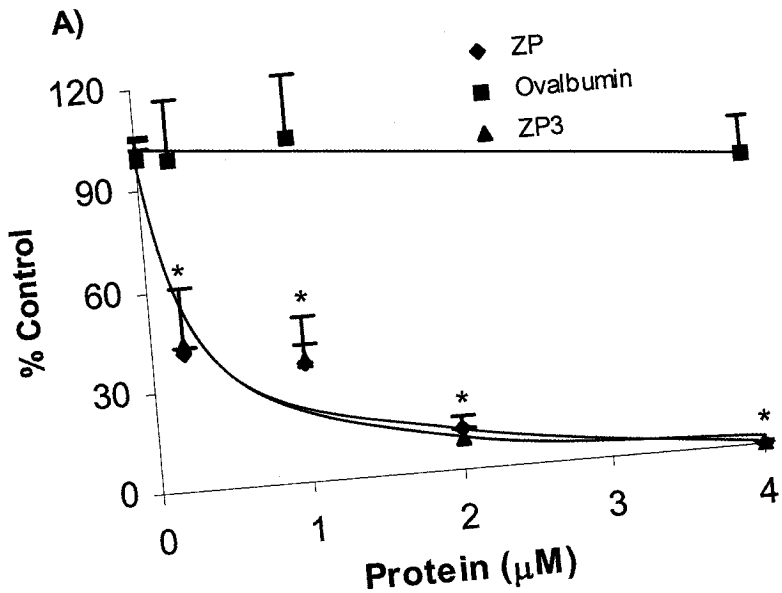
A)
ZP
Ovalbumin
ZP3
120
90
60
30
0
% Control
0
1
2
3
4
Protein (μM)

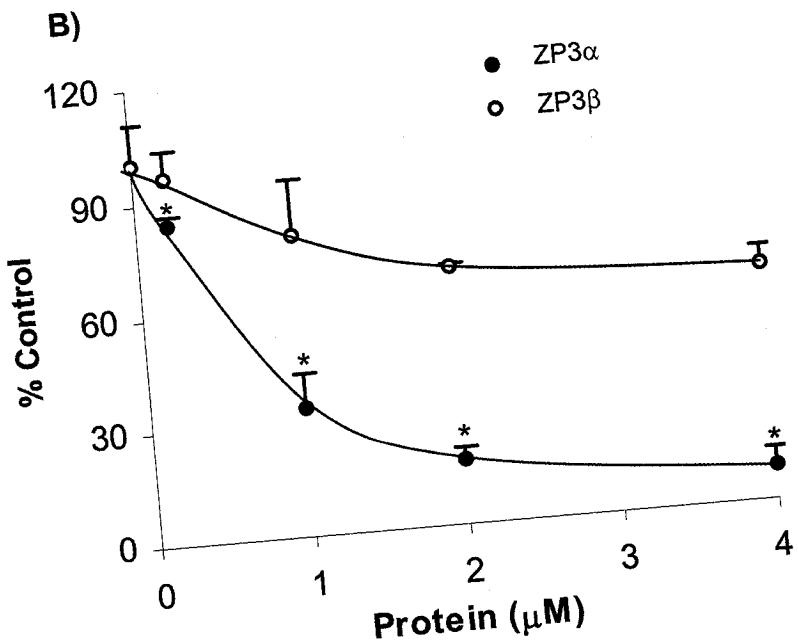
B)
ZP3α
ZP3β
120
90
60
30
0
% Control
0
1
2
3
4
Protein (μM)

### *3.3.7. Contribution of SGG in Capacitated Sperm Rafts to ZP Binding*

SGG localizes to the pig sperm head anterior region (Figure 3.24), i.e., the ZP binding site (Figure 3.35), binds specifically to the pig ZP (Figure 3.27), and the majority of the sulfoglycolipid is found in capacitated sperm rafts (Table 3.1), which exhibit a higher ZP binding ability than non-capacitated sperm rafts (Table 3.2). To elucidate the role of SGG as a sperm raft component in ZP binding, PGC-capacitated sperm rafts, attached to the microtiter well plate, are pretreated with affinity purified anti-SGG IgG, and their binding to Alexa-430 ZP (0.2 μM) is assessed. Pretreatment of capacitated sperm rafts with anti-SGG IgG significantly inhibits the binding of these units to Alexa-430-labeled ZP, in a concentration dependent manner (Figure 3.40A). However, maximal inhibition was ~85% at the antibody concentration of 7.20 μM. In contrast, PRS IgG exerts minimal inhibitory effects on the binding of capacitated sperm rafts to Alexa-430 ZP. These results suggested that SGG in capacitated sperm rafts participates significantly in ZP binding, and corroborate previous findings showing that pretreatment of mouse and human sperm (White *et al.*, 2000; Weerachatyanukul *et al.*, 2001) with anti-SGG IgG markedly reduces ZP binding. To determine whether the inhibition of rafts-ZP binding is due to specific masking of SGG in sperm rafts rather than due to steric hindrance attributed by the bivalent nature of anti-SGG IgG, capacitated sperm rafts are also pretreated with anti-SGG Fab. This pretreatment also reduces the ability of capacitated sperm rafts to bind to Alexa-430 ZP dose dependently, with maximal inhibition accounting for ~47% at 14.4 μM anti-SGG Fab (Figure 3.40B). In contrast, pretreatment of capacitated sperm rafts with PRS Fab, used as negative control, does not affect their ZP binding ability. The degree of inhibition of sperm raft-ZP binding is less pronounced

**Figure 3.40.** Binding of Alexa-430 ZP to PGC-capacitated sperm rafts pretreated with anti-SGG IgG/Fab. Capacitated sperm rafts were pretreated with various concentrations (0-8 μM) of anti-SGG IgG (○) and PRS IgG (▲) (**A**), or (0-16 μM) antiSGG Fab (○) and preimmune rabbit serum Fab (▲) (**B**), and then incubated with 100 μl of 0.2 μM Alexa-430 ZP. The levels of Alexa-430 ZP bound to capacitated sperm rafts were expressed as percentages of the values obtained from the untreated co-incubates of sperm rafts and Alexa-430 ZP.

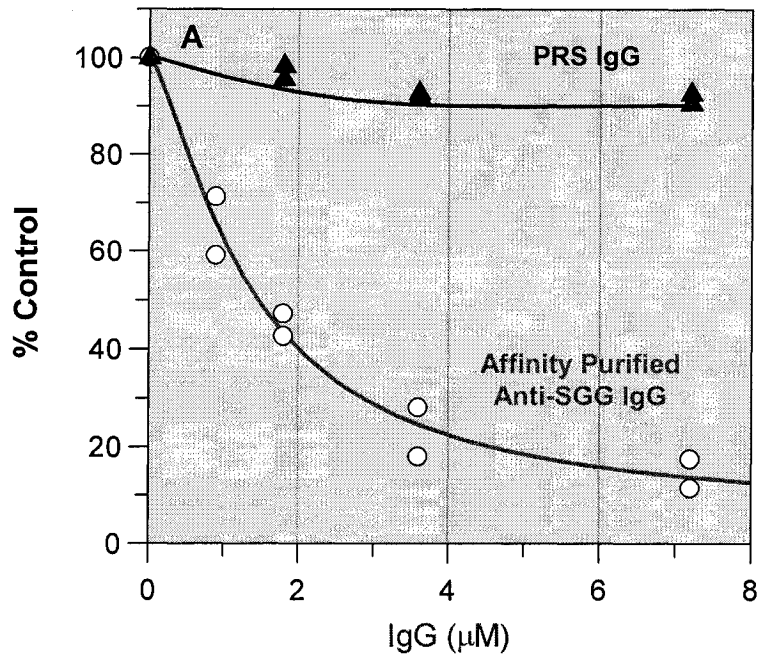
A
PRS IgG
Affinity Purified
Anti-SGG IgG
% Control
IgG (μM)
100
80
60
40
20
0
0
2
4
6
8

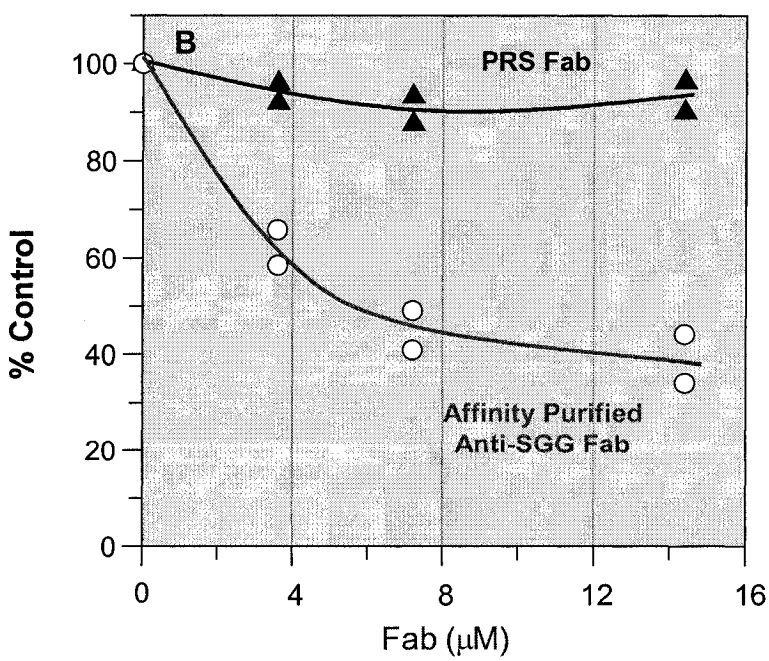
B
PRS Fab
Affinity Purified
Anti-SGG Fab
% Control
Fab (μM)
100
80
60
40
20
0
0
4
8
12
16

with anti-SGG Fab, compared with anti-SGG IgG concentrations of the same antigen-binding valency. At 3.60 μM, 37% inhibition is observed with anti-SGG Fab, relative to 75% inhibition with 1.80 μM anti-SGG IgG. At 7.20 μM, 40% inhibition is observed with anti-SGG Fab, relative to 75% inhibition with 3.60 μM anti-SGG IgG. At 14.4 μM, 47% inhibition is obtained with anti-SGG Fab, relative to 85% inhibition with 7.20 μM anti-SGG IgG. The lower degree of inhibition of the binding of capacitated sperm rafts to Alexa-430 ZP caused by anti-SGG Fab may be due to its lower affinity for SGG, compared with anti-SGG IgG. These results indicate that the inhibition of sperm raft-ZP binding is specific to the masking of SGG molecules in sperm rafts. Conclusively, SGG in sperm rafts is involved in ZP binding.

# CHAPTER FOUR

# DISCUSSION

## 4.1. Biophysical Properties of SGG and Structurally Related Glycolipids

FTIR spectroscopy revealed that SGG, and its structural analogs SGC, NFA-GC, and HFA-GC exhibited complex polymorphic phase behavior, characterized by high phase transition temperatures (Table 4.1), increased conformational order and tight packing of the hydrocarbon chains in the bilayer matrix, and extensive hydrogen bonding networks. The long chain character of the fatty acids, primarily 24:0 and 24:1 (Johnston and Chapman, 1988), combined with the extensive hydrogen bonding capacity of the galactosyl headgroup of NFA-GC and HFA-GC gave rise to extremely high hydrocarbon chain melting temperatures or $T_m$ (80 and 72°C, respectively, Table 4.1 ). Both HFA-GC and NFA-GC consist of an 18:1 sphingosine chain, to which an amide linked fatty acid (24:0 or 24:1) is attached (Ruocco and Shipley, 1986; Attar *et al.*, 1998; O'Brien and Rouser, 1964). This hydrocarbon chain asymmetry may result in the formation of interdigitated HFA-GC and NFA-GC bilayers (Reed and Shipley, 1987). In addition, the carbon-carbon double bond in the sphingosine chain moiety of sphingomyelin is *trans*, and it would not disrupt bilayer packing (Karlsson, 1970; Calhoun and Shipley, 1979). X-ray diffraction reveals that the galactosyl headgroups of NFA-GC are bent almost perpendicular to the hydrocarbon chains. This conformation involves extensive hydrogen bonding between the amide groups and neighboring galactosyl headgroups. The presence of α-hydroxyl group in GC favors a shovel conformation with respect to the hydrocarbon chain axis (Pascher and Sundell, 1977; Nyholm *et al.*, 1990; Bunow and Levin, 1980).

**Table 4.1. The Hydrocarbon Chain Melting Temperatures and Crystal-Like Polymorphs of SGG, SGC, NFA-GC, and HFA-GC Dispersions**

| Glycolipid | Order-Disorder $T_m$ (°C)* | | Crystal-like Polymorphs | |
|---|---|---|---|---|
| | Heating | Cooling | Heating | Cooling |
| **SGG** | 45 | 44 | $L_{cI}$, $L_{cII}$ | $L_{cI}$, $L_{cII}$ |
| **SGC** | 41 | 38 | $L_{c1}$ | $L_{c1}$ |
| **NFA-GC** | 80 | 72 | $L_c1$, $L_c2$ | $L_c3$ |
| **HFA-GC** | 62 | 66 | Gel, $L_cI$ | Gel |

* The $T_m$ values were estimated from the first derivative plots of the $CH_2$ symmetric stretching vibration frequency vs. temperature.

This may disrupt the interdigitated state of the hydrocarbon chains of HFA-GC in the bilayer matrix, thus resulting in a lower $T_m$, relative to NFA-GC. In fact, prevention of hydrocarbon chain interdigitation was previously reported to induce a disordering effect for different PC species (Mason *et al.*, 1981; Huang and Mason, 1986).

The hydrocarbon chain melting of SGC and SGG occurred at lower temperatures, compared to NFA-GC and HFA-GC (Table 4.1). Although SGC has the same hydrocarbon chain composition as its parental glycolipid GC (Ruocco and Shipley, 1986; Attar *et al.*, 1998; O'Brien and Rouser, 1964), the lower $T_m$ of SGC may be attributed to the presence of the sulfate group in the galactosyl moiety of SGC, compared to NFA-GC and HFA-GC. The sulfated galactosyl moiety of SGC and SGG may result in charge repulsion between their negatively charged headgroups, and such a phenomenon would inhibit dense packing of SGC/SGG bilayers. In fact, the higher frequencies of the $CH_2$ symmetric stretching band of SGC (Figure 3.10) and SGG (Figure 3.14), compared with NFA-GC (Figure 3.2) and HFA-GC (Figure 3.6), were indicative of an increased conformational disorder, and presumably less dense/tight packing, of the hydrocarbon chains of SGC/SGG in the bilayer matrix. The hydrocarbon chain melting temperature of SGG was higher than that of SGC (Table 4.1), and this may be attributed to SGG's ability to form interdigitated bilayers (Tupper *et al.*, 1992, 1994). Interdigitation of the hydrocarbon chains of SGG may be partially attributed to the presence of an ether linkage in the *sn*-1 position of the SGG glycerol backbone (Wong and Mantsch, 1988). The ether bond is not as bulky as the ester linkage in most phospholipids, and this will allow interdigitation of individual hydrocarbon chains of opposing leaflets. In addition, both the alkyl and acyl chains of SGG are saturated (mainly 16:0, Tupper *et al.*, 1994; Attar *et*

*al.*, 2000), the extended nature of which will also promote interdigitation. Such a phenomenon may result in strong van der Waals interactions between the hydrocarbon chains of neighboring SGG molecules, thus allowing tighter chain packing in the bilayer plane, compared with SGC. SGC occurs naturally as non-hydroxylated and α-hydroxylated species (Vos *et al.*, 1994; Norton and Cammer, 1984), and the hydroxyl group may increase the hydrogen bonding potential of SGC (Boggs *et al.*, 1988a) and GC (Pascher and Sundell, 1977; Lee *et al.*, 1986). The increased hydrogen bonding interactions between SGC molecules may disrupt the interdigitated state of the hydrocarbon chains of SGC in the bilayer matrix, and thus result in lower $T_m$, relative to SGG.

While both SGG and DPPC have 16:0 hydrocarbon chains, the sulfoglycolipid exhibited higher $T_m$ than DPPC (45 vs. 40°C, Figure 3.18). In addition, SGC, which has the same hydrocarbon chain composition (Ruocco and Shipley, 1986; Attar *et al.*, 1998; O'Brien and Rouser, 1964) as sphingomyelin, also exhibited a higher $T_m$ than sphingomyelin, i.e., 41°C (Figure 3.2) vs. 35°C (Calhoun and Shipley, 1979; Barenholz and Thompson, 1980). Compared with the phosphorylcholine headgroup of DPPC and sphingomyelin, the sulfated galactosyl moiety of SGG/SGC would still engage in interfacial hydrogen bonding. This resulted in the formation of more ordered SGC/SGG bilayer structures, relative to phospholipids of the same hydrocarbon chain length.

Prior to hydrocarbon chain melting and upon subsequent cooling from the chain melted state, SGG, SGC, NFA-GC, and HFA-GC underwent conversions between metastable and stable bilayer structures. These various polymorphs were crystal-like and partially dehydrated, as revealed by the patterns of the ester C=O and amide I band of

SGG and SGC/GC, respectively. The crystal-like bilayers of SGG, SGC, NFA-GC, and HFA-GC were characterized by (*a*) high conformational order and tight packing of the hydrocarbon chains in the bilayer matrix, as well as by (*b*) strong hydrogen bonding networks. Significant amounts of GC are present in myelin rafts, which participate in the assembly of myelin in oligodendrocytes (Simons *et al.*, 2000). The extensive hydrogen bonding interactions of GC with other raft lipids, i.e., cholesterol saturated phospholipids (reviews: Brown and London, 1998b, 2000; Simons and Toomre, 2000), may contribute to the formation of rafts in myelin. In fact, GC and SGC may play a role in adhesion between apposing extracellular surfaces of myelin, and in its stability and function via carbohydrate-carbohydrate mediated interactions (Koshy and Boggs, 1996; Koshy *et al.*, 1999; Boggs *et al.*, 2000). SGC is also a component of sea urchin sperm rafts, which bind to homologous egg plasma membrane rafts (Ohta *et al.*, 1999a, b). However, SGC-containing rafts in sea urchin sperm, compared to GC-containing rafts in myelin, may have increased conformational disorder and less dense/tight packing of the hydrocarbon chains, as well as weaker hydrogen bonding networks due to charge repulsion between the negatively charged sulfated galactosyl headgroups of SGC. This may be advantageous for fusion of the sea urchin sperm plasma membrane with the egg plasma membrane following the initial binding between gametes.

### 4.2. Contribution of SGG to the Formation of Sperm Rafts

As stated above, SGG exhibited strong hydrogen bonding networks among themselves. Furthermore, FTIR spectroscopy revealed that the ester C=O group of SGG engaged in strong hydrogen bonding with the hydroxyl group of cholesterol (Figure 3.20),

an important raft component (reviews: London and Brown, 2000; Simons and Toomre, 2000). SGG also formed homogeneous bilayers with the saturated phospholipids DPPC (Figure 3.18) and DMPC (Attar *et al.*, 2000). On the other hand, both SGG and DPPC showed limited miscibility with PDPC, a polyunsaturated phospholipid present in significant amounts in the sperm plasma membrane (Cooper and Yeung, 1997; Flesch and Gadella, 2000). Significantly, binary mixtures of SGG-cholesterol and DPPC-cholesterol were insoluble in Triton X-100 (Figure 3.21B). Compared with DPPC, SGG liposomes were more prone to Triton X-100 solubilization. At 0.05% Triton X-100, SGG was completely solubilized, whereas 50% of DPPC liposomes still remained insoluble at 1% Triton X-100 (Figure 3.21A). This suggested that SGG-detergent interactions were stronger than SGG-SGG interactions, due to the repulsion between the negatively charged sulfated galactosyl head groups of SGG. Therefore, the Triton X-100 insolubility of SGG induced by cholesterol likely resulted from strong intermolecular hydrogen bonding of the ester C=O group of SGG with the hydroxyl group of cholesterol, as well as from strong van der Waals interactions between the saturated hydrocarbon chains of SGG and cholesterol (planar ring and side chain). Since cholesterol and saturated phospholipids are significant raft components of both somatic and gamete cells (Brown and Rose, 1992; Ohta *et al.*, 1999b; Travis *et al.*, 2001; Stulnig *et al.*, 2001), the inherent properties of SGG described herein suggested that SGG may participate in sperm raft formation.

### 4.3. Properties of Capacitated Sperm Rafts

Cholesterol efflux is an event associated with mammalian sperm capacitation (Flesch and Gadella, 2000; Visconti *et al.*, 2002). Since cholesterol is an important

component of rafts in many cell types (Brown and Rose, 1992; reviews: Brown and London, 1998b; Simons and Ikonen, 2000; Silvius, 2003), the question whether sperm raft levels would change during capacitation needed to be answered. In this thesis, hyperactivated motility (Yanagimachi, 1994), reduced cholesterol levels (Figure 3.22, Flesch *et al.*, 2001) and higher levels of sperm protein tyrosine phosphorylation (Figure 3.23, Tardif *et al.*, 2001, 2003; Flesch *et al.*, 1999; Kalab *et al.*, 1998) confirmed the capacitation status of pig sperm. Although washed-capacitated and PGC-capacitated sperm had lower levels of cholesterol than control sperm (i.e., washed and PGC sperm, respectively), the levels of phospholipids and SGG were similar in control and capacitated sperm, except for the slightly lower phospholipid levels in washed capacitated sperm, relative to washed sperm (Figure 3.22, Table 3.1). Contrary to what we expected, higher levels of isolated rafts were obtained in capacitated sperm, compared with control sperm (Figure 3.31). Nonetheless, the raft lipid components in both capacitated and control sperm were qualitatively similar, i.e., containing cholesterol, saturated phospholipids and SGG (Figures 3.32-3.34). Significantly, ~70% of total sperm SGG and cholesterol was found in the isolated capacitated sperm rafts, consistent with previous finding revealing that significant proportions of glycosphingolipids and cholesterol accumulate in rafts isolated from various cell types (Ohta *et al.*, 1999b; Brown and Rose, 1992; Fra *et al.*, 1994; Prinetti *et al.*, 1999; Iwabuchi *et al.*, 1998b). Therefore, cholesterol may have been released from the non-raft domains of the sperm plasma membrane during capacitation, and this efflux may have caused sperm plasma membrane remodeling (Gadella and Harrison, 2000). This capacitation-induced membrane remodeling may include coalescence and segregation of preexisting sperm rafts, a

phenomenon similar to that observed in Chinese hamster ovary cells and T-cells (Hao *et al.*, 2001; Pierini and Maxfield, 2001; Gomez-Mouton *et al.*, 2001). Concurrently, the recruitment of pertinent lipids (including remaining cholesterol in the sperm plasma membrane) to form more sperm rafts may have been induced by cholesterol efflux.

Rafts from both somatic and gamete cells have been implicated in cell adhesion (Galbiati *et al.*, 2001; Harris and Siu, 2002; Hakomori, 2000; Iwabuchi *et al.*, 1998). In fact, binding of sperm rafts to egg rafts has been preliminarily shown in sea urchins (Ohta *et al.*, 1999a). Furthermore, sialylated gangliosides, lipid components of sea urchin sperm rafts, have an affinity to the 350-kDa SBP present in the sea urchin egg vitelline layer (Maehashi *et al.*, 2003). Proteins involved in ZP and egg plasma membrane binding (GPI-linked PH-20, fertilin α and cyritestin) are also present in mammalian sperm rafts (Nishimura *et al.*, 2001). In this study, we reported that rafts isolated from both control pig sperm and capacitated pig sperm had an ability to bind directly to homologous ZP (Figure 3.38). The binding levels and affinity for the ZP of capacitated sperm rafts were higher (i.e., higher $B_{max}$ and lower $K_d$, Table 3.2) than those of control sperm rafts. This observation corroborated the physiology of pig sperm-ZP binding (Yanagimachi, 1994), with capacitated sperm possessing a higher capacity to penetrate the ZP and to become acrosome reacted *in situ* (Matas *et al.*, 2003;Harrison, 1997). Since both capacitated sperm rafts and control sperm rafts had very similar lipid composition, the higher efficiency of capacitated sperm rafts to bind to the ZP may reflect greater amounts of ZP-binding proteins in these rafts. Moreover, if rafts represent the main ZP-binding microdomains of sperm, the higher levels of rafts in capacitated sperm (Figure 3.31) would contribute to the increased ability of these sperm to interact with the ZP.

Although the sperm rafts used in this binding were prepared from whole sperm, the raft membranes responsible for this ZP binding were likely from the sperm head, the site of ZP binding, since rafts isolated from sperm tails exhibited only background binding to ZP sulfoglycoproteins (Figure 3.37A). Furthermore, we demonstrated that the binding of isolated pig sperm rafts to Alexa-430 ZP was specific, since a parallel incubation of these rafts with Alexa-430 ovalbumin resulted in background interaction with this protein (Figure 3.37A, B). More importantly, the interaction between capacitated sperm rafts and Alexa-430 ZP was competed by purified pig ZP3 sulfoglycoproteins (i.e., the sperm receptors), particularly by its ZP3α component, a major player in sperm binding (Yurewicz *et al.*, 1993, 1998). These results suggested that the mechanism through which sperm rafts interacted with ZP was the same as that employed by intact sperm, and isolated pig sperm rafts may be used as cell free systems to study integrative mechanisms of sperm-ZP interaction and downstream sperm signaling events. Ongoing experiments in the laboratory of Dr. N. Tanphaichitr are geared towards identifying signaling molecules in isolated sperm raft membranes.

Capacitated sperm rafts contain 71% of total sperm SGG (Table 3.1). SGG binds directly to both mouse and human ZP (White et al., 2000;Weerachatyanukul et al., 2001). In this thesis, SGG was localized to the pig sperm head anterior, i.e., the ZP binding site (Figure 3.24). SGG was also involved in binding to the pig ZP. The apparent $K_d$ of SGG-ZP binding was relatively low (0.092 ± 0.011 μM, Figure 3.27), and in the same range as that of sphingolipid-protein interactions (Shimada *et al.*, 1985; Kuziemko *et al.*, 1996). Significantly, SGG contributed to the binding of sperm rafts to the ZP, since pretreatment of capacitated sperm rafts with affinity purified anti-SGG IgG/Fab decreased

sperm raft-ZP binding dose-dependently (Figure 3.40). SGG may bind to the ZP via carbohydrate-carbohydrate mediated interactions and hydrogen bonding between its sulfated galactosyl head group and the ZP glycopeptides. In fact, previous FTIR spectroscopic studies reveal that SGC (SGG's analog) and GC may play a role in adhesion between apposing extracellular surfaces of myelin via carbohydrate-carbohydrate mediated interactions (Koshy and Boggs, 1996; Koshy *et al.*, 1999; Boggs *et al.*, 2000). In addition, hydrogen bonding between $GM_1$ ganglioside and cholera toxin was previously suggested to be the basis of this interaction (Kuziemko *et al.*, 1996). Although carbohydrate-carbohydrate mediated interactions are not as strong as protein-carbohydrate interactions, they may be stabilized by the multiplicity of SGG molecules in sperm rafts. The function of SGG in sperm raft-ZP binding is analogous to the involvement of glycosphingolipids in cell adhesion events (Iwabuchi *et al.*, 1998a, b; Hakomori, 2000a, b), including trout sperm-egg interaction (Yu *et al.*, 2002).

## 4.4. Conclusions

FTIR spectroscopy revealed that SGG may contribute to the formation of sperm rafts by interacting preferentially with cholesterol and saturated phospholipids. SGG-cholesterol complexes were insoluble in Triton X-100, a common property of isolated raft membranes. Rafts were isolated from non-capacitated and capacitated pig sperm, and contained significant proportions of SGG and cholesterol, and saturated phospholipids, compared to whole sperm. Despite cholesterol efflux from the sperm plasma membrane, pig sperm capacitation resulted in the formation of higher levels of rafts. SGG localized to the pig sperm head anterior region, i.e., the ZP binding site, bound specifically to the

pig ZP, and the majority of the sulfoglycolipid was found in capacitated sperm rafts, which bound to fluorescently labeled solubilized ZP with the highest efficiency. SGG may play a dual role in sperm rafts by participating in their formation and sperm rafts-ZP binding.

## 4.5. Scientific Significance and Future Directions

The use of sperm rafts in this study will allow a better understanding of sperm-ZP binding events and sperm signaling in an integrative manner because rafts would represent a platform of molecules involved in the sequential events of fertilization. Compared with whole sperm, the use of sperm rafts is also advantageous, since the binding of rafts to the ZP will not induce subsequent acrosomal exocytosis, which would affect ZP binding. Since cholesterol is a common raft component (reviews: Brown and London, 2000; Simons and Toomre, 2000), and since capacitation is accompanied by cholesterol efflux from the sperm plasma membrane, it was questionable whether rafts would exist in capacitated sperm. If rafts house the ZP binding domains, it was also of interest to determine whether rafts isolated from capacitated sperm exhibit higher ZP affinity than control sperm rafts should also be answered.

Capacitated sperm rafts contained the ZP binding domains. SGG was enriched in sperm rafts, and the mammalian male germ cell specific sulfoglycolipid contributed to the affinity of sperm rafts for the ZP. Since SGG interacted preferentially with raft lipids, i.e., cholesterol and saturated phospholipids, the inherent properties of SGG described herein suggested that SGG participated in sperm raft formation. These dual functions of SGG affirm the significance of glycolipids and rafts in cell adhesion (Hakomori, 2000).

Recently, *Cgt* knockout mice have been generated, and the testis of these mice are depleted of SGG (Fujimoto *et al.*, 2000), with spermatogenesis arrested in the late pachytene stage. Therefore, the significance of SGG as an integral component of rafts isolated from mammalian male germ cells can be revealed if the spermatogenic cells of these *Cgt* knockout mice fail to form rafts following treatment with Triton X-100.

To further validate the biological significance of sperm rafts, future studies can specifically be designed to discern whether sperm rafts also partake in sperm signaling events associated with capacitation and acrosomal exocytosis. Sperm capacitation is not only associated with the exposure of the ZP binding molecules on the sperm surface, but also with the acquisition of sperm hyperactivated motility necessary for sperm to reach the ZP and penetrate this matrix. Therefore, information on the identity of sperm raft components will give insight into (*a*) mechanisms of sperm-ZP interaction, and (*b*) will be pertinent to development of non-hormonal contraceptives based on interference with gamete interaction, as well as based on targeting of molecules involved in the acquisition of sperm hyperactivated motility. Since $PIP_2$ is the precursor of $IP_3$, implicated in the ZP-induced acrosomal exocytosis, its presence in sperm rafts can be detected by the HPTLC overlay-chemiluminescence technique using anti-$PIP_2$ antibody and peroxidase-conjugated secondary antibody as probes. In addition, the protein composition of sperm rafts can be discerned by proteomic analyses. The identification of ZP-binding and signaling proteins (e.g., AS-A, β-galactosyltransferase, PH20, P26, spermadhesin, zonaadhesin, $G_i$ protein, adenylyl cyclase, PLC, and tyrosine phosphorylated proteins), known to be present in whole sperm and/or sperm rafts, can be performed first by immunoblotting. Since actin plays an important role in acrosomal exocytosis, its

existence can be similarly investigated. Increases of some of these proteins may be observed in capacitated sperm rafts, as these units have higher ZP binding ability. To obtain a global picture of how sperm raft proteins change during capacitation, 2-D SDS-PAGE can be performed for these rafts isolated from equal numbers of non-capacitated and capacitated sperm. Protein spots of non-capacitated and capacitated sperm rafts can then be subjected to tryptic digestion and mass spectrometry to identify raft proteins.

Collectively, the understanding of the molecular mechanisms of mammalian sperm rafts-ZP interaction will provide information necessary for the development of male fertility markers and non-hormonal vaginal contraceptives, with fewer systemic side effects compared to oral estrogen birth control pills. Using antibodies/inhibitors generated against a group of ZP binding molecules, concentrated in sperm rafts, should effectively interfere with sperm-egg binding. In addition, compounds that can also prevent sexually transmitted diseases (STD) are the most desirable as vaginal contraceptives. Since pathogenic STD-associated microbials also bind to SGG (Harouse *et al.*, 1991; Gadella *et al.*, 1998; Piomboni and Baccetti, 2000), the use of antibodies/inhibitors generated against SGG and/or other sperm raft-associated molecules may also prevent STD by masking/interfering with the functions SGG in sperm rafts.

## REFERENCES

Ahmed, S.A., Brown, D.A., and London, E. (1997) On the origin of sphingolipid/ cholesterol-rich detergent-insoluble cell membranes: physiological concentrations of cholesterol and sphingolipid induce formation of a detergent-insoluble, liquid-ordered lipid phase in model membranes. Biochemistry *36*, 10944-10954.

Ahnonkitpanit, V., White, D., Suwajanakorn, S., Kan, F., Namking, M., Wells, G., and Tanphaichitr, N. (1999) Role of egg sulfolipid immobilizing protein 1 (SLIP1) on sperm-egg plasma membrane binding. Biology of Reproduction *61*, 749-756.

Aitken, R.J. (1997) Molecular mechanisms regulating human sperm function. Molecular Human Reproduction *3*, 169-173.

Ali, S., Smaby, J.M., Brockman, H.L., and Brown, R.E. (1994) Cholesterol's interfacial interactions with galactosylceramides. Biochemistry *33*, 2900-2906.

Alvarez, J.G., Lopez, I., Touchstone, J.C., and Storey, B.T. (1987) Thin layer chromatography of phospholipid composition in mouse and rabbit spermatozoa. Journal of Liquid Chromatography *10*, 3557-3573.

Alvarez, J.G., Storey, B.T., Hemling, M.L., and Grob, R.L. (1990) High-resolution proton nuclear magnetic resonance characterization of seminolipid from bovine spermatozoa. Journal of Lipid Research *31*, 1073-1081.

Anderson, R.G. (1998) The caveolae membrane system. Annual Review of Biochemistry *67*, 199-225.

Anderson, R.G., and Jacobson, K. (2002) A role for lipid shells in targeting proteins to caveolae, rafts, and other lipid domains. Science *296*, 1821-1825.

Arnoult, C., Cardullo, R.A., Lemos, J.R., and Florman, H.M. (1996) Activation of mouse sperm T-type $Ca^{2+}$ channels by adhesion to the egg zona pellucida. Proceedings of the National Academy of Science USA *93*, 13004-13009.

Attar, M., Wong, P.T.T., Kates, M., Carrier, D., Jaklis, P., and Tanphaichitr, N. (1998) Interaction between sulfogalactosylceramide and dimyristoylphosphatidylcholine increases the orientational fluctuations of the lipid hydrocarbon chains. Chemistry and Physics of Lipids *94*, 228-238.

Attar, M., Kates, M., Bou Khalil, M., Carrier, D., Wong, P.T.T., and Tanphaichitr, N. (2000) A Fourier-transform infrared study of the interaction between germ-cell specific sulfogalactosylglycerolipid and dimyristoylglycerophosphocholine. Chemistry and Physics of Lipids *106*, 101-114.

Audhya, T., Reddy, J., and Zaneveld, L.J. (1987) Purification and partial chemical characterization of a glycoprotein with antifertility activity from human seminal plasma. Biology of Reproduction *36*, 511-521.

Auger, M., Jarrell, H.C., Smith, I.C.P., Wong, P.T., Siminovitch, D.J., and Mantsch, H.H. (1987) Pressure-Induced Exclusion of a Local Anesthetic from Model and Nerve Membranes. Biochemistry *26*, 8513-8516.

Aveldano, M.I., Rotstein, N.P., and Vermouth, N.T. (1992) Occurence of long and very long polyenoic fatty acids of the n-9 series in rat spermatozoa. Lipids *27*, 676-680.

Baldi, E., Luconi, M., Bonaccorsi, L., and Forti, G. (2002) Signal transduction pathways in human spermatozoa. Journal of Reproductive Immunology *53*, 121-131.

Barenholz, Y., and Thompson, T.E. (1980) Sphingomyelins in bilayers and biological membranes. Biochimica *et* Biophysica Acta *604*, 129-158.

Bendahmane, M., and Tulsiani, D.R. (2003) Capacitated acrosome-intact mouse spermatozoa bind to Sepharose beads coated with functional neoglycoproteins. Archives of Biochemistry and Biophysics *415*, 203-212.

Benoff, S. (1993) The role of cholesterol during capacitation of human spermatozoa. Human Reproduction *8*, 2001-2008.

Berditchevski, F. (2001) Complexes of tetraspanins with integrins: more than meets the eye. Journal of Cell Science *114*, 4143-4151.

Berger, T., Davis,A., Wardrip, N.J., and Hedrick, J.L. (1989) Sperm binding to the pig zona pellucida and inhibition of binding by solubilized components of the zona pellucida. Journal of Reproduction and Fertility *86*, 559-565.

Berger, T., Turner, K.O., Meizel, S., and Hedrick, J.L. (1989b) Zona pellucida-induced acrosome reaction in boar sperm. Biology of Reproduction *40*, 525-530.

Blackmore, P.F. (1999) Extragenomic actions of progesterone in human sperm and progesterone metabolites in human platelets. Steroids *64*, 149-156.

Bleil, J.D., and Wassarman, P.M. (1983) Sperm-egg interactions in the mouse: sequence of events and induction of the acrosome reaction by a zona pellucida glycoprotein. Developmental Biology *95*, 317-324.

Bleil, J.D., and Wassarman, P.M. (1988) Galactose at the non-reducing terminus of O-linked oligosaccharides of mouse egg zona pellucida glycoprotein ZP3 is essential for the glycoprotein's sperm receptor activity. Proceedings of the National Academy of Science USA *854*, 6778-6782.

Bleil, J.D., and Wassarman, P.M. (1990) Identification of a ZP3-binding protein on acrosome intact mouse sperm by photoaffinity crosslinking. Proceedings of the National Academy of Science USA *87*, 5563-5567.

Bligh, E.G., and Dyer, W.J. (1959) A rapid method of total lipid estraction and purification. Canadian Journal of Biochemistry and Physiology *31*, 911-917.

Boggs, J.M., Koshy, K.M., and Rangaraj, G. (1984) Effect of fatty acid chain length, fatty acid hydroxylation, and various cations on phase behavior of synthetic cerebroside sulfate. Chemistry and Physics of Lipids *36*, 65-89.

Boggs, J.M., Koshy, K.M., and Rangaraj, G. (1988a) Influence of structural modifications on the phase behavior of semi-synthetic cerebroside sulfate. Biochimica *et* Biophysica Acta *938*, 361-372.

Boggs, J.M., Koshy, K.M., and Rangaraj, G. (1988b) Interdigitated lipid bilayers oflong acyl chain species of cerebroside sulfate. A fatty acid spin label study. Biochimica *et* Biophysica Acta *938*, 373-385.

Boggs, J.M., Menikh, A., and Rangaraj, G. (2000) Trans interactions between galactosylceramide and cerebroside sulfate across apposed bilayers. Biophysical Journal *78*, 874-885.

Bookbinder, L.H., Cheng, A., and Bleil, J.D. (1995) Tissue-and species-specific expression of sp56, a mouse sperm fertilization protein. Science *269*, 86-89.

Bork, P. (1996) Sperm-egg binding protein or proto-oncogene? Science *271*, 1431-1432.

Bosio, A., Binczek, E., and Stoffel, W. (1996) Functional breakdown of the lipid bilayer of the myelin membrane in central and peripheral nervous system by disrupted galacto-cerebroside synthesis. Proceedings of the National Academy of Science USA *93*, 13280-13285.

Bosio, A., Binczek, E., Haupt, W.F., and Stoffel, W. (1998a) Composition and biophysical properties of myelin lipid define the neurological defects in galactocerebroside and sulfatide deficient mice. Journal of Neurochemistry *70*, 308-315.

Bosio, A., Bussow, H., Adam, J., and Stoffel, W. (1998b) Galactosphingolipids and axono-glial interaction in myelin of the central nervouse system. Cell Tissue Research *292*, 199-210.

Bou Khalil, M., Kates, M., and Carrier, D. (2000) FTIR study of the monosialo-ganglioside $GM_1$ in perdeuterated dimyristoylglycerophosphocholine ($DMPC_{d54}$) multilamellar bilayers: spectroscopic evidence of a significant interaction between $Ca^{2+}$ ions and the sialic acid moiety of $GM_1$. Biochemistry *39*, 2980-2988.

Bou Khalil, M., Carrier, D., Wong, P.T.T., and Tanphaichitr, N. (2001) Polymorphic phases of galactocerebrosides: spectroscopic evidence of lamellar crystalline structures. Biochimica *et* Biophysica Acta *1512*, 158-170.

Boue, F., Berube, B., De Lamirande, E., Gagnon, C., and Sullivan, R. (1994) Human sperm-zona pellucida interaction is inhibited by an antiserum against a hamster sperm protein. Biology of Reproduction *51*, 577-587.

Boue, F., and Sullivan, R. (1996) Cases of human infertility are associated with the absence of P34H, an epididymal sperm antigen. Biology of Reproduction *54*, 1018-1024.

Boulanger, J., Huesca, M., Arab, S., and Lingwood, C.A. (1994) Universal method for the facile production of glycolipid/lipid matrices for the affinity purification of binding ligands. Analytical Biochemistry *217*, 1-6.

Boulanger, J., Faulds, D., Eddy, E.M., and Lingwood, C.A. (1995) Members of the 70 kDa heat shock protein family specifically recognize sulfoglycolipids: role in gamete recognition and mycoplasma-related infertility. Journal of Cell Physiology *165*, 7-17.

Braccia, A., Villani, M., Immerdal, L., Niels-Christiansen, L.L., Nystrom, B.T., Hansen, G.H., and Danielsen, E.M. (2003) Microvillar membrane microdomains exist at physiological temperature. Role of galectin-4 as lipid raft stabilizer revealed by "superrafts". Journal of Biological Chemistry *278*, 15679-15684.

Bradford, M.M. (1976) A rapid and sensitive method for the quantitation of microgram quantities of protein utilizing the principle of protein-dye binding. Analytical Biochemistry *72*, 248-254.

Brandon, C.I., Srivastava, P.N., Heusner, G.L., and Fayrer-Hosken, R.A. (1997) Extraction and quantification of acrosin, α-*N*-acetylglucosaminidase, and arylsulfatase-A from equine ejaculated spermatozoa. Journal of Experimental Zoology *279*, 301-308.

Bray, C., Son, J.H., Kumar, P., Harris, J.D., and Meizel, S. (2002) A role for the human sperm glycine receptor/$Cl^-$ channel in the acrosome reaction initiated by recombinant ZP3. Biology of Reproduction *66*, 91-98.

Breitbart, H., and Spungin, B. (1997) The biochemistry of the acrosome reaction. Molecular Human Reproduction *3*, 195-202.

Breitbart, H. (2002a) Intracellular calcium regulation in sperm capacitation and acrosomal reaction. Molecular and Cellular Endocrinology *187*, 139-144.

Breitbart, H. (2002b) Role and regulation of intracellular calcium in acrosomal exocytosis. Journal of Reproductive Immunology *53*, 151-159.

Brewis, I.A., and Wong, C.H. (1999) Gamete recognition: sperm proteins that interact with the egg zona pellucida. Reviews in Reproduction *4*, 135-142.

Brockhausen, I., and Kuhns, W. (1997) Role and metabolism of glycoconjugate sulfation. Trends in Glycoscience and Glycotechnology *9*, 379-398.

Brouwers, J.F., Gadella, B.M., Van Golde, L.M., and Tielens, A.G. (1998) Quantitative analysis of phosphatidylcholine molecular species using HPLC and light scattering detection. Journal of Lipid Research *39*, 344-353.

Brown, D.A., and London, E. (1998a) Functions of lipid rafts in biological membranes. Ann. Rev. Cell Developmental Biology *14*, 111-136.

Brown, D.A., and London, E. (1998b) Structure and origin of ordered lipid domains in biological membranes. Journal of Membrane Biology *164*, 103-114.

Brown, D.A., and London, E. (2000) Structure and function of sphingolipid- and cholesterol-rich membrane rafts. Journal of Biological Chemistry *275*, 17221-17224.

Brown, D.A., and Rose, J.K. (1992) Sorting of GPI-anchored proteins to glycolipid-enriched membrane subdomains during transport to the apical cell surface. Cell *68*, 533-544.

Brown, M.F., and Seelig, J. (1978) Influence of cholesterol on the polar region of phosphatidycholine and phosphatidylethanolamine bilayers. Biochemistry *17*, 381-384.

Bunow, M.R., and Levin, I.W. (1980) Molecular conformations of cerebrosides in bilayers determined by Raman spectroscopy. Biophysical Journal *32*, 1007-1022.

Burkatt, T., Caimi, L., Herschkowitz, N.N., and Wiesmann, U.N. (1983) Metabolism of sulfogalactosyl glycerolipids in the myelinating mouse brain. Developmental Biology *98*, 182-186.

Burkin, H.R., and Miller, D.J. (2000) Zona pellucida protein binding ability of porcine sperm during epididymal maturation and the acrosome reaction. Developmental Biology *222*, 99-109.

Burks, D.J., Carballada, R., Moore, H.D.M., and Saling, P.M. (1995) Interaction of a tyrosine kinase from human sperm with the zona pellucida at fertilization. Science *269*, 83-86.

Calhoun, W.I., and Shipley, G.G. (1979) Fatty acid composition and thermal behavior of natural sphingomyelins. Biochimica *et* Biophysica Acta *555*, 436-441.

Calogero, A.E., Burrello, N., Barone, N., Palermo, I., Grasso, U., and D'Agata, R. (2000) Effects of progesterone on sperm function: mechanisms of action. Human Reproduction *15 Suppl 1*, 28-45.

Cameron, D.G., and Moffatt, D.J. (1987) A generalized approach to derivative spectroscopy. Applied Spectroscopy *41*, 539-544.

Cameron, D.G., Casal, H.L., and Mantsch, H.H. (1980) Characterization of the pretransition in 1,2-dipalmitoyl-*sn*-glycero-3-phosphocholine by Fourier transform infrared spectroscopy. Biochemistry *19*, 3665-3672.

Carmona, E., Weerachatyanukul, W., Soboloff, T., Fluhary, A.L., White, D., Promdee, L., Ekker, M., Berger, T., Buhr, M., and Tanphaichitr, N. (2002a) Arylsulfatase A is present on the pig sperm surface and is involved in sperm-zona pellucida binding. Developmental Biology *247*, 182-196.

Carmona, E., Weerachatyanukul, W., Xu, H., Fluharty, A.L., Anupriwan, A., Shoushtarian, A., Chakrabandhu, K., and Tanphaichitr, N. (2002b) Binding of arylsulfatase A to mouse sperm inhibits gamete interaction and induces the acrosome reaction. Biology of Reproduction *66*, 1820-1827.

Caroni, P. (2001) New EMBO members' review: actin cytoskeleton regulation through modulation of $PI(4,5)P_2$ rafts. Europian Molecular Biology Organization Journal *20*, 4332-4336.

Casal, H.L., and Mantsch, H.H. (1984) Polymorphic phase behaviour of phospholipid membranes studied by infrared spectroscopy. Biochimica *et* Biophysica Acta *779*, 381-401.

Chamberlin, M., and Dean, J. (1990) Human homology of the mouse sperm receptor. Developmental Biology *87*, 6014-6018.

Chapman, D. (1988) Biomembrane structure and function: recent studies and new techniques. Parasitology *96*, S11-S23.

Chen, S., and Cardullo, R. (1994) Characterization and localization of fluorescent zonae pellucidae on mouse sperm. Molecular Biology of the Cell *5*, 224a.

Chen, Y., Cann, M.J., Litvin, T.N., Iourgenko, V., Sinclair, M.L., Levin, L.R., and Buck, J. (2000) Soluble adenylyl cyclase as an evolutionarily conserved bicarbonate sensor. Science *289*, 625-628.

Cheng, C.Y., and Mruk, D.D. (2002) Cell junction dynamics in the testis: Sertoli-germ cell interactions and male contraceptive development. Physiology Reviews *82*, 825-874.

Claas, C., Stipp, C.S., and Hemler, M.E. (2001) Evaluation of prototype transmembrane 4 superfamily protein complexes and their relation to lipid rafts. Journal of Biological Chemistry *276*, 7974-7984.

Coetzee, T., Fujita, N., Dupree, J., Shi, R., Blight, A., Suzuki, K., and Popko, B. (1996) Myelination in the absence of galactocerebroside and sulfatide: normal structure with abnormal function and regional instability. Cell *86*, 209-219.

Coetzee, T., Dupree, J.L., and Popko, B. (1998) Demyelination and altered expression of myelin associated glycoprotein isoforms in the central nervous system of galactolipid deficient mice. Journal of Neuroscience Research *54*, 613-622.

Conquer, J.A., Martin, J.B., Tummon, I., Watson, L., and Tekpetey, F. (1999) Fatty acid analysis of blood serum, seminal plasma and spermatozoa of normozoospermic vs. asthenozoospermic males. Lipids *34*, 793-799.

Cooper, T.G. and Yeung, C.H. (1997) Physiology of sperm maturation and fertilization. In Andrology: Male Reproductive Health and Dysfunction, E.Nieschlag, ed. (Berlin Heidelberg: Springer-Verlag), pp. 61-78.

Cornwall, G.A., Tulsiani, D.R.P., and Orgebin-Crist, M.C. (1991) Inhibition of the mouse sperm surface α-D-mannosidase inhibits sperm-egg binding in vitro. Biology of Reproduction *44*, 913-921.

Crook, S.J., Stewart, R., Boggs, J.M., Vistnes, A.I., and Zalc, B. (1987) Characterization of anti-cerebroside sulfate antisera using a theoretical model to analyze liposome immune lysis data. Molecular Immunology *24*, 1135-1143.

Cross, N.L. (1996) Human seminal plasma prevents sperm from becoming acrosomally responsive to the agonist, progesterone: cholesterol is the major inhibitor. Biology of Reproduction *54*, 138-145.

Cross, N.L. (1998) Role of cholesterol in sperm capacitation. Biology of Reproduction *59*, 7-11.

Cross, N.L. (1999) Effect of methyl-beta-cyclodextrin on the acrosomal responsiveness of human sperm. Molecular Reproduction and Development *53*, 92-98.

Cross, N.L. (2003) Decrease in order of human sperm lipids during capacitation. Biology of Reproduction *69*, 529-534.

Curatolo, W. (1982) Thermal behavior of fractionated and unfractionated bovine brain cerebrosides. Biochemistry *21*, 1761-1764.

Curatolo, W. (1987a) Glycolipid function. Biochimica *et* Biophysica Acta *906*, 137-160.

Curatolo, W. (1987b) The physical properties of glycolipids. Biochimica *et* Biophysica Acta *906*, 111-136.

Curatolo, W., and Jungalwala, F.B. (1985) Phase behavior of galactocerebrosides from bovine brain. Biochemistry *24*, 6608-6613.

Curatolo, W., and Neuringer, L.J. (1986) The effects of cerebrosides on model membrane shape. Journal of Biological Chemistry *261*, 17177-17182.

Darszon, A., Beltran, C., Felix, R., Nishigaki, T., and Trevino, C.L. (2001) Ion transport in sperm signaling. Developmental Biology *240*, 1-14.

Davis, B.K. (1981) Timing of fertilization in mammals: sperm:cholesterol:phospholipid ratio as a determinant of the capacitation interval. Proceedings of the National Academy of Science USA *78*, 7560-7564.

De Blas, G., Michaut, M., Trevino, C.L., Tomes, C.N., Yunes, R., Darszon, A., and Mayorga, L.S. (2002) The intraacrosomal calcium pool plays a direct role in acrosomal exocytosis. Journal of Biological Chemistry *277*, 49326-49331.

De Lamirande, E., Leclerc, P., and Gagnon, C. (1997) Capacitation as a regulatory event that primes spermatozoa for the acrosome reaction and fertilization. Molecular Human Reproduction *3*, 175-194.

Dell, A., Morris, H.R., Easton, R.L., Patankar, M., and Clark, G.F. (1999) The glycobiology of gametes and fertilisation. Biochimica *et* Biophysica Acta *1473*, 196-205.

Demarco, I.A., Espinosa, F., Edwards, J., Sosnik, J., De La Vega-Beltran, J.L., Hockensmith, J.W., Kopf, G.S., Darszon, A., and Visconti, P.E. (2003) Involvement of a Na+/HCO-3 cotransporter in mouse sperm capacitation. Journal of Biological Chemistry *278*, 7001-7009.

Diekman, A.B. (2003) Glycoconjugates in sperm function and gamete interactions: how much sugar does it take to sweet-talk the egg? Cellular and Molecular Life Sciences *60*, 298-308.

Dietrich, C., Bagatolli, L.A., Volovyk, Z.N., Thompson, N.L., Levi, M., Jacobson, K., and Gratton, E. (2001a) Lipid rafts reconstituted in model membranes. Biophysical Journal *80*, 1417-1428.

Dietrich, C., Volvyk, Z.N., Levi, M., Thompson, N.L., and Jacobson, K. (2001b) Partitioning of Thy-1, $GM_1$, and cross-linked phospholipid analogs into lipid rafts reconstituted in supported model membrane monolayers. Proceedings of the National Academy of Science USA *98*, 10642-10647.

Dietrich, C., Yang, B., Fujiwara, T., Kusumi, A., and Jacobson, K. (2002) Relationship of lipid rafts to transient confinement zones detected by single particle tracking. Biophysical Journal *82*, 274-284.

Dong, K.W., Chi, T.F., Juan, Y.W., Chen, C.W., Lin, Z., Xiang, X.Q., Mahoney, M., Gibbons, W.E., and Oehninger, S. (2001) Characterization of the biologic activities of a recombinant human zona pellucida protein 3 expressed in human ovarian teratocarcinoma (PA-1) cells. American Journal of Obstetrics and Gynecology *184*, 835-844.

Dorval, V., Dufour, M., and Leclerc, P. (2002) Regulation of the phosphotyrosine content of human sperm proteins by intracellular $Ca^{2+}$: role of $Ca^{2+}$-adenosine triphosphatases. Biology of Reproduction *67*, 1538-1545.

Dostalova, Z., Calvete, J.J., Sanz, L., and Topfer-Petersen, E. (1995) Boar spermadhesin AWN-1. Oligosaccharide and zona pellucida binding characteristics. Europian Journal of Biochemistry *230*, 329-336.

Drevot, P., Langlet, C., Guo, X.J., Bernard, A.M., Colard, O., Chauvin, J.P., Lasserre, R., and He, H.T. (2002) TCR signal initiation machinery is pre-assembled and activated in a subset of membrane rafts. Europian Molecular Biology Organization Journal *21*, 1899-1908.

Duck-Chong, C.G. (1979) A rapid sensitive method for determining phospholipid phosphorus involving digestion with magnesium nitrate. Lipids *14*, 492-497.

Dudkiewicz, A.B. (1984) Purification of boar acrosomal arylsulfatase A and possible role in the penetration of cumulus cells. Biology of Reproduction *30*, 1005-1014.

Dunbar, B.S., Timmons, T.M., Skinner, S.M., and Prasad, S.V. (2001) Molecular analysis of a carbohydrate antigen involved in the structure and function of zona pellucida glycoproteins. Biology of Reproduction *65*, 951-960.

Dym, M. (1977) The male reproductive system. In Histology, L.Weiss, ed. (New York: McGraw-Hill Book Company), pp. 979-1038.

Easton, R.L., Patankar, M.S., Lattanzio, F.A., Leaven, T.H., Morris, H.R., Clark, G.F., and Dell, A. (2000) Structural analysis of murine zona pellucida glycans. Evidence for the expression of core 2-type O-glycans and the $Sd^a$ antigen. Journal of Biological Chemistry *275*, 7731-7742.

Eddy, E.M., Muller, C.H., and Lingwood, C.A. (1985) Preparation of monoclonal antibody to sulfatoxygalactosylglycerolipid by *in vitro* immunization with a glycolipid-glass conjugate. Journal of Immunological Methods *81*, 137-146.

Eddy, E.M., and O'Brien, D.A. (1994) The spermatozoon. In The Physiology of Reproduction, E.Knobil, ed. (New York: Raven Press), pp. 29-77.

Eddy, E.M., Toshimori, K., and O'Brien, D.A. (2003) Fibrous sheath of mammalian spermatozoa. Microscopy Research and Technique *61*, 103-115.

Edidin, M. (2001) Shrinking patches and slippery rafts: scales of domains in the plasma membrane. Trends in Cell Biology *11*, 492-496.

Edidin, M. (2003) The state of lipid rafts: from model membranes to cells. Annual Review of Biophysics and Biomolecular Structure *4*, 414-418.

Ehrenwald, E., Foote, R.H., and Parks, J.E. (1990) Bovine oviductal fluid components and their potential role in sperm cholesterol efflux. Molecular Reproduction and Development *25*, 195-204.

Faivre-Sarrailh, C., Gauthier, F., Denisenko-Nehrbass, N., Le Bivic, A., Rougon, G., and Girault, J.A. (2000) The glycosylphosphatidyl inositol-anchored adhesion molecule F3/contactin is required for surface transport of paranodin/contactin-associate protein (caspr). Journal of Cell Biology *149*, 491-501.

Ficarro, S., Chertihin, O., Westbrook, V.A., White, F., Jayes, F., Kalab, P., Marto, J.A., Shabanowitz, J., Herr, J.C., Hunt, D.F., and Visconti, P.E. (2003) Phosphoproteome analysis of capacitated human sperm. Evidence of tyrosine phosphorylation of a kinase-anchoring protein 3 and valosin-containing protein/p97 during capacitation. Journal of Biological Chemistry *278*, 11579-11589.

Flesch, F.M., Voorhout, W.F., Colenbrander, B., Van Golde, L.M.G., and Gadella, B.M. (1998) Use of lectins to characterize plasma membrane preparations from boar spermatozoa: a novel technique for monitoring membrane purity and quantity. Biology of Reproduction *59*, 1530-1539.

Flesch, F.M., Colenbrander, B., Van Golde, L.M.G., and Gadella, B.M. (1999) Capacitation induces tyrosine phosphorylation of proteins in the boar sperm plasma membrane. Biochemical and Biophysical Research Communications *262*, 787-792.

Flesch, F.M., and Gadella, B.M. (2000) Dynamics of the mammalian sperm plasma membrane in the process of fertilization. Biochimica *et* Biophysica Acta *1469*, 197-235.

Flesch, F.M., Brouwers, J.F., Nievelstein, P.F., Verkleij, A.J., Van Golde, L.M.G., Colenbrander, B., and Gadella, B.M. (2001a) Bicarbonate stimulated phospholipid scrambling induces cholesterol redistribution and enables cholesterol depletion in the sperm plasma membrane. Journal of Cell Science *114*, 3543-3555.

Flesch, F.M., Wijnand, E., van de Lest, C.H., Colenbrander, B., van Golde, L.M.G., and Gadella, B.M. (2001b) Capacitation dependent activation of tyrosine phosphorylation generates two sperm head plasma membrane proteins with high primary binding affinity for the zona pellucida. Molecular Reproduction and Development *60*,107-415.

Florman, H.M., Tombes, R.M., First, N.L., and Babcock, D.F. (1989) An adhesion-associated agonist from the zona pellucida activates G protein-promoted elevations of internal Ca+2 and pH that mediate mammalian sperm acrosomal exocytosis. Developmental Biology *135*, 133-146.

Forti, G., Baldi, E., Krausz, C., Luconi, M., Bonaccorsi, L., Maggi, M., Bassi, F., and Scarselli, G. (1999) Effects of progesterone on human spermatozoa: clinical implications. Annals of Endocrinology (Paris) *60*, 107-110.

Foster, J.A., Friday, B.B., Maulit, M.T., Blobel, C., Winfrey, V.P., Olson, G.E., Kim, K.S., and Gerton, G.L. (1997) AM67, a secretory component of the guinea pig sperm acrosomal matrix, is related to mouse sperm protein sp56 and the complement component 4-binding proteins. Journal of Biological Chemistry *272*, 12714-12722.

Foster, L.J., De Hoog, C.L., and Mann, M. (2003) Unbiased quantitative proteomics of lipid rafts reveals high specificity for signaling factors. Proceedings of the National Academy of Science USA *100*, 5813-5818.

Fra, A.M., Williamson, E., Simons, K., and Parton, R.G. (1994) Detergent-insoluble glycolipid microdomains in lymphocytes in the absense of caveolae. Journal of Biological Chemistry *269*, 30745-30748.

Fraser, L.R. (1987) Minimum and maximum extracellular Ca+2 requirements during mouse sperm capacitation and fertilization in vitro. Journal of Reproduction and Fertility *81*, 77-89.

Fraser, L.R. (1993) Calcium channels play a pivotal role in the sequence of ionic changes involved in initiation of mouse sperm acrosomal exocytosis. Molecular Reproduction and Development *36*, 368-376.

Fraser, L.R. (1998) Sperm capacitation and acrosome reaction. Human Reproduction *13 Suppl 1*, 9-19.

Fredman, P., Mattsson, L., Andersson, K., Davidsson, P., Ishizuka, I., Jeansson, S., Mansson, J.E., and Svennerholm, L. (1988) Characterization of the binding epitope of a monoclonal antibody to sulphatide. Biochemical Journal *251*, 17-22.

Freeman, E.A., Jani, P., and Millette, C.E. (2002) Expression and potential function of Rho family small G proteins in cells of the mammalian seminiferous epithelium. Cell Communication and Adhesion *9*, 189-204.

Fridriksson, E.K., Shipkova, P.A., Sheets, E.D., Holowka, D., Baird, B., and McLafferty, F.W. (1999) Quantitative analysis of phospholipids in functionally important membrane domains from RBL-2H3 mast cells using tandem high-resolution mass spectrometry. Biochemistry *38*, 8056-8063.

Friedrichson, T., and Kurzchalia, T.V. (1998) Microdomains of GPI-anchored proteins in living cells revealed by crosslinking. Nature *394*, 802-805.

Friend, D. (1982) Plasma-membrane diversity in a highly polarized cell. Journal of Cell Biology *93*, 243-249.

Fujii, T., Kobayashi, T., Honke, K., Gasa, S., Ishikawa, M., Shimizu, T., and Makita, A. (1992) Proteolytic processing of human lysosomal arylsulfatase A. Biochimica *et* Biophysica Acta *1122*, 93-98.

Fujimoto, H., Tadano-Aritomi, K., Tokumasu, A., Ito, K., Hikita, T., Suzuki, K., and Ishizuka, I. (2000) Requirement of seminolipid in spermatogenesis revealed by UDP-galactose:ceramide galactosyltransferase-deficient mice. Journal of Biological Chemistry *275*, 22623-22626.

Fujiwara, T., Ritchie, K., Murakoshi, H., Jacobson, K., and Kusumi, A. (2002) Phospholipids undergo hop diffusion in compartmentalized cell membrane. Journal of Cell Biology *157*, 1071-1081.

Fukami, K., Yoshida, M., Inoue, T., Kurokawa, M., Fissore, R.A., Yoshida, N., Mikoshiba, K., and Takenawa, T. (2003) Phospholipase $C_{\delta 4}$ is required for $Ca^{2+}$ mobilization essential for acrosome reaction in sperm. Journal of Cell Biology *161*, 79-88.

Fukasawa, M., Nishijima, M., and Hanada, K. (1999) Genetic evidence for ATP-dependent endoplasmic reticulum-to-Golgi apparatus trafficking of ceramide for sphingomyelin synthesis in Chinese hamster ovary cells. Journal of Cell Biology *144*, 673-685.

Furimsky, A. (2001) Characterization of the lipid composed of washed and percoll gradient centrifuged epididymal mouse sperm following capacitation. University of Ottawa, Department. of Biochemistry, Microbiology and Immunology (*M.Sc. Thesis*).
Furimsky, A., Vuong, N., Kumarathasan, P., Kates, M., Bou Khalil, M., Weerachatyanukul, W., Xu, H., and Tanphaichitr, N. (2003) Increased distribution of sulfogalactosyglycerolipid and docohexaenoic acid containing phospholipids in mouse Percoll-gradient centrifuged sperm. Biology of Reproduction (*submitted*).

Gadella, B.M., and Harrison, R.A. (2000) The capacitating agent bicarbonate induces protein kinase A-dependent changes in phospholipid transbilayer behavior in the sperm plasma membrane. Development *127*, 2407-2420.

Gadella, B.M., Colenbrander, B., Van Golde, L.M.G., and Lopes-Cardozo, M. (1993) Boar seminal vesicles secrete arylsulfatases into seminal plasma: Evidence that desulfation of seminolipid occurs only after ejaculation. Biology of Reproduction *48*, 483-489.

Gadella, B.M., Gadella, T.W.J., Colenbrander, B., Van Golde, L.M., and Lopes-Cardozo, M. (1994) Visualization and quantification of glycolipid polarity dynamics in the plasma membrane of the mammalian spermatozoon. Journal of Cell Science *107*, 2151-2163.

Gadella, B.M., Hammache, D., Pieroni, G., Colenbrander, B., Van Golde, L.M.G., and Fantini, J. (1998) Glycolipids as potential binding sites for HIV: topology in the sperm plasma membrane in relation to the regulation of membrane fusion. Journal of Reproductive Immunology *41*, 233-253.

Galbiati, F., Razani, B., and Lisanti, M.P. (2001) Emerging themes in lipid rafts and caveolae. Cell *108*, 403-411.

Gao, Z., and Garbers, D.L. (1998) Species diversity in the structure of zonaadhesin, a sperm-specific membrane protein containing multiple cell adhesion molecule-like domains. Journal of Biological Chemistry *273*, 3415-3421.

Garcia, M.A., and Meizel, S. (1999) Progesterone-mediated calcium influx and acrosome reaction of human spermatozoa: pharmacological investigation of T-type calcium channels. Biology of Reproduction *60*, 102-109.

Ge, M., Field, K.A., Aneja, R., Holowka, D., Baird, B., and Freed, J.H. (1999) Electron spin resonance characterization of liquid ordered phase of detergent resistant membranes from RBL-2H3 cells. Biophysical Journal *77*, 925-933.

Gomez-Mouton, C., Abad, J.L., Mira, E., Lacalle, R.A., Gallardo, E., Jimenez-Baranda, S., Illa, I., Bernad, A., Manes, S., and Martinez, A. (2001) Segregation of leading-edge and uropod components into specific lipid rafts during T cell polarization. Proceedings of the National Academy of Science USA *98*, 9642-9647.

Graf, K., Baltes, H., Ahrens, H., Helm, C.A., and Husted, C.A. (2002) Structure of hydroxylated galactocerebrosides from myelin at the air-water interface. Biophysical Journal *82*, 896-907.

Gupta, N., and DeFranco, A.L. (2003) Visualizing lipid raft dynamics and early signaling events during antigen receptor-mediated B-lymphocyte activation. Molecular Biology of the Cell *14*, 432-444.

Haas, N.S., and Shipley, G.G. (1995) Structure and properties of *N*-palmitoleoyl-galactosylsphingosine (cerebroside). Biochimica *et* Biophysica Acta *1240*, 133-141.

Hagmann, J., and Fishman, P.H. (1982) Detergent extraction of cholera toxin and gangliosides from cultured cells and isolated membranes. Biochimica *et* Biophysica Acta *720*, 181-187.

Hakomori, S.I. (1981) Glycosphingolipids in cellular interaction, differentiation, and oncogenesis. Annual Review of Biochemistry *50*, 733-764.

Hakomori, S. (1984) Glycosphingolipids as markers for development and differentiation and as regulators of cell proliferation. Glycosphingolipids as Markers for Development 181-201.

Hakomori, S. (1990) Bifunctional role of glycosphingolipids. Journal of Biological Chemistry *265*, 18713-18716.

Hakomori, S. (2000a) Cell adhesion/recognition and signal transduction through glycosphingolipid microdomain. Glycoconjugate Journal *17*, 143-151.

Hakomori, S. (2000b) Traveling for the glycosphingolipid path. Glycoconjugate Journal *17*, 627-647.

Han, X., Holtzman, M., McKeel, D.W., Jr., Kelley, J., and Morris, J.C. (2002) Substantial sulfatide deficiency and ceramide elevation in very early Alzheimer's disease: potential role in disease pathogenesis. Journal of Neurochemistry *82*, 809-818.

Handa, S., Yamoto, K., Ishizuka, I., Suzuki, A., and Yamakawa, T. (1974) Biosynthesis of seminolipid: Sulfation in vivo and in vitro. Journal of Biochemistry *75*, 77-83.

Handa, K., Kojima, N., and Hakomori, S. (2000) Analysis of glycolipid-dependent cell adhesion based on carbohydrate-carbohydrate interaction. Methods in Enzymology *312*, 447-458.

Hansen, G.H., Immerdal, L., Thorsen, E., Niels-Christiansen, L.L., Nystrom, B.T., Demant, E.J., and Danielsen, E.M. (2001) Lipid rafts exist as stable cholesterol-independent microdomains in the brush border membrane of enterocytes. Journal of Biological Chemistry *276*, 32338-32344.

Hao, M., Mukherjee, S., and Maxfield, F.R. (2001) Cholesterol depletion induces large scale domain segregation in living cell membranes. Proceedings of the National Academy of Science USA *98*, 13072-13077.

Harder, T., Scheiffele, P., Verkade, P., and Simons, K. (1998) Lipid domain structure of the plasma membrane revealed by patching of membrane components. Journal of Cell Biology *141*, 929-942.

Harder, T., and Simons, K. (1999) Clusters of glycolipid and glycosyl-phosphatidylinositol-anchored proteins in lymphoid cells: accumulation of actin regulated by local tyrosine phosphorylation. Europian Journal of Immunology *29*, 556-562.

Hardy, D.M., and Garbers, D.L. (1995) A sperm membrane protein that binds in a species-specific manner to the egg extracellular matrix is homologous to von Willebrand Factor. Journal of Biological Chemistry *270*, 26025-26028.

Harlow, E., and Lane, D. (1988) Antibodies: a laboratory manual. Cold Spring Harbor Symposium (Cold Spring Harbor, NY).

Harouse, J.M., Bhat, S., Spitalnik, S.L., Laughlin, M., Stefano, K., Silberberg, D.H., and Gonzalez-Scarano, F. (1991) Inhibition of entry of HIV-1 in neural cell lines by antibodies against galactosyl ceramide. Science *253*, 320-323.

Harris, J.D., Hibler, D.W., Fontenot, G.K., Hsu, K.T., Yurewicz, E.C., and Sacco, A.G. (1994) Cloning and characterization of zona pellucida genes and cDNAs from a variety of mammalian species: The ZPA, ZPB and ZPC gene families. DNA Sequence *4*, 361-393.

Harris, T.J., and Siu, C.H. (2002) Reciprocal raft-receptor interactions and the assembly of adhesion complexes. BioEssays *24*, 996-1003.

Harrison, R.A. (1997) Sperm plasma membrane characteristics and boar semen fertility. Journal of Reproduction and Fertility Suppl *52*, 195-211.

Harrison, R.A., Mairet, B., and Miller, N.G. (1993) Flow cytometric studies of bicarbonate-mediated Ca2+ influx in boar sperm populations. Molecular Reproduction and Development *35*, 197-208.

Harrison, R.A.P., Ashworth, P.J.C., and Miller, N.G.A. (1996) Bicarbonate/CO2, an effector of capacitation, induces a rapid and reversible change in the lipid architecture of boar sperm plasma membranes. Molecular Reproduction and Development *45*, 378-391.

Harrison, D.A., Carr, D.W., and Meizel, S. (2000) Involvement of protein kinase A and A kinase anchoring protein in the progesterone-initiated human sperm acrosome reaction. Biology of Reproduction *62*, 811-820.

Hart, N.H., Wolenski, J.S., and Donovan, M.J. (1987) Ultrastructural localization of lysosomal enzymes in the egg cortex Brachydanio. Journal of Experimental Zoology *244*, 17-32.

Hedrick, J.L., and Wardrip, N.J. (1986) Isolation of the zona pellucida and purification of its glycoprotein families from pig oocytes. Analytical Biochemistry *157*, 63-70.

Heerklotz, H. (2002) Triton promotes domain formation in lipid raft mixtures. Biophysical Journal *83*, 2693-2701.

Heller, H., Schaefer, M., and Schulten, K. (1993) Molecular dynamics simulation of a bilayer of 200 lipids in the gel and in the liquid crystal phases. Journal of Physical Chemistry *97*, 8343-8360.

Hermo, L., Badran, H., and Andonian, S. (2002) The structural organization and functins of the epithelium of the vas deferens. In The Epididymis: From Molecules to Clinical Practice, B.Robaire, ed. (New York: Kluwer Academic/Plenum Publishers), pp. 233-250.

Ho, H.C., and Suarez, S.S. (2001) Hyperactivation of mammalian spermatozoa: function and regulation. Reproduction *122*, 519-526.

Ho, H.C., and Suarez, S.S. (2003) Characterization of the intracellular calcium store at the base of the sperm flagellum that regulates hyperactivated motility. Biology of Reproduction *68*, 1590-1596.

Hoessli, D., and Rungger-Brandle, E. (1985) Association of specific cell-surface glycoproteins with a triton X-100-resistant complex of plasma membrane proteins isolated from T-lymphoma cells (P1798). Exp. Cell Res. *156*, 239-250.

Holowka, D., Sheets, E.D., and Baird, B. (2000) Interactions between FcεRI and lipid raft components are regulated by the actin cytoskeleton. Journal of Cell Science *113 (Pt 6)*, 1009-1019.

Holub, B.J., and Watson, S.P. (1996) Methods for measuring agonist-induced phospholipid metabolism in intact human platelets. In Platelets: A Practical Approach, S.P.Watson, ed. (New York: Oxford University Press), pp. 235-257.

Honda, A., Yamagata, K., Sugiura, S., Watanabe, K., and Baba, T. (2002) A mouse serine protease TESP5 is selectively included into lipid rafts of sperm membrane presumably as a glycosylphosphatidylinositol-anchored protein. Journal of Biological Chemistry *277*, 16976-16984.

Honke, K., Yamane, M., Ishii, A., Kobayashi, T., and Makita, A. (1996) Purification and characterization of 3'-phosphoadenosine-5'-phosphosulfate: GalCer sulfotransferase from human renal cancer cells. Journal of Biochemistry *119*, 421-427.

Honke, K., Tsuda, M., Hirahara, Y., Ishii, A., Makita, A., and Wada, Y. (1997) Molecular cloning and expression of cDNA encoding human 3'-phosphoadenylyl-sulfate:galactosylceramide 3'-sulfotransferase. Journal of Biological Chemistry *272*, 4864-4868.

Honke, K., Hirahara, Y., Dupree, J., Suzuki, K., Popko, B., Fukushima, K., Fukushima, J., Nagasawa, T., Yoshida, N., Wada, Y., and Taniguchi, N. (2002) Paranodal junction formation and spermatogenesis require sulfoglycolipids. Proceedings of the National Academy of Science USA *99*, 4227-4232.

Hooper, N.M. and Turner, A.J. (1988) Ectoenzymes of the kidney microvillar membrane. Differential solubilization by detergents can predict a glycosyl-phosphatidylinositol membrane anchor. Biochemical Journal *250*, 865-869.

Horejsi, V. (2003) The roles of membrane microdomains (rafts) in T cell activation. Immunological Reviews *191*, 148-164.

Hsu, L.H., Narasimhan, R., and Levine, M. (1983) Studies of the biosynthesis and metabolism of rat testicular galactoglycerolipids. Canadian Journal of Biochemistry and Cell Biology *61*, 1272-1281.

Huang, C.H., and Mason, J.T. (1986) Structure and properties of mixed-chain phospholipid assemblies. Biochimica *et* Biophysica Acta *864*, 423-470.

Ipsen, J.H., Karlstrom, G., Mouritsen, O.G., Wennerstrom, H., and Zuckermann, M.J. (1987) Phase equilibria in the phosphatidylcholine-cholesterol system. Biochimica *et* Biophysica Acta *905*, 162-172.

Ishizuka, I. (1997) Chemistry and functional distribution of sulfoglycolipids. Progress in Lipid Research *36*, 245-319.

Ishizuka, I., Suzuki, M., and Yamakawa, T. (1973) Isolation and characterization of a novel sulfoglycolipid, seminolipid, from boar testis and spermatozoa. Journal of Biochemistry *73*, 77-87.

Iwabuchi, K., Handa, K., and Hakomori, S. (1998a) Separation of "glycosphingolipid signaling domain" from caveolin-containing membrane fraction in mouse melanoma B16 cells and its role in cell adhesion coupled with signaling. Journal of Biological Chemistry *273*, 33766-33773.

Iwabuchi, K., Yamamura, S., Prinetti, A., Handa, K., and Hakomori, S. (1998b) $GM_3$-enriched microdomain involved in cell adhesion and signal transduction through carbohydrate-carbohydrate interaction in mouse melanoma B16 cells. Journal of Biological Chemistry *273*, 9130-9138.

Iwabuchi, K., Zhang, Y., Handa, K., Withers, D.A., Sinay, P., and Hakomori, S. (2000) Reconstitution of membranes simulating "glycosignaling domain" and their susceptibility to lyso-GM3. Journal of Biological Chemistry *275*, 15174-15181.

Jackson, M., Johnston, D.S., and Chapman, D. (1988) Differential scanning calorimetric and Fourier transform infrared spectroscopic investigations of cerebroside polymorphism. Biochimica *et* Biophysica Acta *944*, 497-506.

Jacobson, K., and Dietrich, C. (1999) Looking at lipid rafts? Trends in Cell Biology *9*, 87-91.

Janes, P.W., Ley, S.C., and Magee, A.I. (1999) Aggregation of lipid rafts accompanies signaling via the T cell antigen receptor. Journal of Cell Biology *147*, 447-461.

Johnston, D.S., and Chapman, D. (1988) The properties of brain galactocereborside monolayers. Biochimica *et* Biophysica Acta *937*, 10-22.

Jungnickel, M.K., Marrero, H., Birnbaumer, L., Lemos, J.R., and Florman, H.M. (2001) Trp2 regulates entry of Ca2+ into mouse sperm triggered by egg ZP3. Nature Cell Biology *3*, 499-502.

Kalab, P., Visconti, P., Leclerc, P., and Kopf, G.S. (1994) p95, the major phosphotyrosine-containing protein in mouse spermatozoa, is a hexokinase with unique properties. Journal of Biological Chemistry *269*, 3810-3817.

Kalab, P., Peknicova, J., Geussova, G., and Moos, J. (1998) Regulation of protein tyrosine phosphorylation in boar sperm through a cAMP-dependent pathway. Molecular Reproduction and Development *51*, 304-314.

Karlsson, K.A., Samuelsson, B.E., and Steen, G.O. (1974) The lipid composition and $Na^+/K^+$-dependent adenosine-triphosphatase activity of the salt (nasal) gland of eider duck and herring gull: A role for sulphatides in sodium-ion transport. Europian Journal of Biochemistry *46*, 243-258.

Kasahara, K., Watanabe, K., Takeuchi, K., Kaneko, H., Oohira, A., Yamamoto, T., and Sanai, Y. (2000) Involvement of gangliosides in glycosylphosphatidylinositol-anchored neuronal cell adhesion molecule TAG-1 signaling in lipid rafts. Journal of Biological Chemistry *275*, 34701-34709.

Kates, M. (1986) Technique of lipidology: isolation, analysis and identification of lipids. In Laboratory Techniques in Biochemistry and Molecular Biology, R.H.Burdon, ed. (New York: Elsevier), pp. 100-278.

Kates, M. (1990) In Glycolipids, Phosphoglycolipids, and Sulfoglycolipids, M.Kates, ed. (New York: Plenum Press).

Kaul, G., Singh, S., Gandhi, K.K., and Anand, S.R. (1997) Calcium requirement and time course of capacitation of goat spermatozoa assessed by chlorotetracycline assay. Andrologia *29*, 243-251.

Kean, E.L. (1968) Rapid, sensitive spectrophotometric method for quantitative determination of sulfatides. Journal of Lipid Research *9*, 319-327.

Kenworthy, A.K., Petranova, N., and Edidin, M. (2000) High-resoluion FRET microscopy of cholera toxin B-subunit and GP1-anchored proteins in cell plasma membranes. Molecular Biology of the Cell *11*, 1645-1655.

Kerr, C.L., Hanna, W., Shaper, J.H., and Wright, W.W. (2001) Fluorescently-labeled murine ZP3 and ZP2 glycoproteins bind to distinct sites on sperm in a calcium-, capacitation-. and maturation-dependent manner. Biology of Reproduction *64 Suppl. 1*, 276.

Kerr, C.L., Hanna, W.F., Shaper, J.H., and Wright, W.W. (2002) Characterization of zona pellucida glycoprotein 3 (ZP3) and ZP2 binding sites on acrosome-intact mouse sperm. Biology of Reproduction *66*, 1585-1595.

Kilsdonk, E.P., Yancey, P.G., Stoudt, G.W., Bangerter, F.W., Johnson, W.J., Phillips, M.C., and Rothblat, G.H. (1995) Cellular cholesterol efflux mediated by cyclodextrins. Journal of Biological Chemistry *270*, 17250-17256.

Kim, K.S., Foster, J.A., and Gerton, G.L. (2001) Differential release of guinea pig sperm acrosomal components during exocytosis. Biology of Reproduction *64*, 148-156.

King, G.J., and Macpherson, J.W. (1973) A comparison of two methods for boar semen collection. Journal of Animal Science *36*, 563-565.

Kirkman-Brown, J.C., Punt, E.L., Barratt, C.L., and Publicover, S.J. (2002) Zona pellucida and progesterone-induced $Ca^{2+}$ signaling and acrosome reaction in human spermatozoa. Journal of Andrology *23*, 306-315.

Knapp, A., Kornblatt, M.J., Schachter, H., and Murray, R.K. (1973) Studies on the biosynthesis of testicular sulfoglycerogalactolipid: Demonstration of a golgi-associated sulfotransferase activity. Biochemical and Biophysical Research Communications *55*, 179-186.

Kornblatt, M.J. (1979) Synthesis and turnover of sulfogalactoglycerolipid, a membrane lipid, during spermatogenesis. Canadian Journal of Biochemistry *57*, 255-258.

Kornblatt, M.J., Schachter, H., and Murray, R.K. (1972) Partial characterization of a novel glycerogalactolipid from rat testis. Biochemical and Biophysical Research Communications *48*, 1489-1494.

Kornblatt, M.J., Knapp, A., Levine, M., Schachter, H., and Murray, R.K. (1974) Studies on the structure and formation during spermatogenesis of the sulfoglycerogalactolipid of rat testis. Canadian Journal of Biochemistry *52*, 689-697.

Koshy, K.M. and Boggs, J.M. (1996) Investigation of the calcium-mediated association between the carbohydrate head groups of galactosylceramide and galactosylceramide $I^3$ sulfate by electrospray ionization mass spectrometry. Journal of Biological Chemistry *271*, 3496-3499.

Koshy, K.M., Wang, J., and Boggs, J.M. (1999) Divalent cation-mediated interaction between cerebroside sulfate and cerebrosides: an investigation of the effect of structural variations of lipids by electrospray ionization mass spectrometry. Biophysical Journal *77*, 306.

Kubler, E., Dohlman, H.G., and Lisanti, M.P. (1996) Identification of Triton X-100 insoluble membrane domains in the yeast Saccharomyces cerevisae. Lipid requirements for targeting of heterotrimeric G-protein subunits. Journal of Biological Chemistry *271*, 32975-32980.

Kulkarni, V.S., Anderson, W.H., and Brown, R.E. (1995) Bilayer nanotubes and helical ribbons fromed by hydrated galactosylceramides: acyl chain and head group effects. Biophysical Journal *69*, 1976-1986.

Kulkarni, V.S., and Brown, R.E. (1998) Thermotropic behavior of galactosylceramides with cis-monoenoic fatty acyl chains. Biochimica *et* Biophysica Acta *1372*, 347-358.

Kulkarni, V.S., Boggs, J.M., and Brown, R.E. (1999) Modulation of nanotube formation by structural modifications of sphingolipids. Biophysical Journal *77*, 319-330.

Kushi, Y., Arita, M., Ishizuka, I., Kasama, T., Fredman, P., and Handa, S. (1996) Sulfatide is expressed in both erythrocytes and platelets of bovine origin. Biochimica *et* Biophysica Acta *1304*, 254-262.

Kuziemko GM, Stroh M, and Stevens RC. (1996) Cholera toxin binding affinity and specificity for gangliosides determined by surface plasmon resonance. Biochemistry *35*, 6375-6384.

Laemmli, U.K. (1970) Cleavage of structural proteins during the assembly of the head of bacteriophage T4. Nature *227*, 680-685.

Lalumière, G., Bleau, G., Chapdelaine, A., and Roberts, K. (1976) Cholesteryl sulfate and sterol sulfatase in the human reproductive tract. Steroids *27*, 247-260.

Langlais, J., and Roberts, K.D. (1985) A molecular membrane model of sperm capacitation and the acrosome reaction of mammalian spermatozoa. Gamete Research *12*, 183-224.

Langlais, J., Kan, F.W.K., Granger, L., Raymond, L., Bleau, G., and Roberts, K.D. (1988) Identification of sterol acceptors that stimulate cholesterol efflux from human spermatozoa during in vitro capacitation. Gamete Research *20*, 185-201.

Langlet, C., Bernard, A.M., Drevot, P., and He, H.T. (2000) Membrane rafts and signaling by the multichain immune recognition receptors. Current Opinion in Immunology *12*, 250-255.

Larsson, D., and Karlsson, D.A. (1972) Molecular arrangements in glycosphingolipids. Chemistry and Physics of Lipids *8*, 152-179.

Law, H., Itkonnen, O., and Lingwood, C.A. (1988) Sulfogalactolipid binding protein SLIP 1: A conserved function for a conserved protein. Journal of Cell Physiology *137*, 462-468.

Leclerc, P., and Goupil, S. (2002) Regulation of the human sperm tyrosine kinase c-yes. Activation by cyclic adenosine 3', 5'-monophosphate and inhibition by $Ca^{2+}$. Biology of Reproduction *67*, 301-307.

Leclerc, P., and Kopf, G.S. (1995) Mouse sperm adenylyl cyclase: general properties and regulation by the zona pellucida. Biology of Reproduction *52*, 1227-1233.

Leclerc, P. and Kopf, G.S. (1999) Evidence for the role of heterotrimeric guanine nucleotide-binding regulatory proteins in the regulation of the mouse sperm adenylyl cyclase by the egg's zona pellucida. Journal of Andrology *20*, 126-134.

Lee, D.C., Miller, I.R., and Chapman, D. (1986) An infrared spectroscopic study of metastable and stable forms of hydrated cerebroside bilayers. Biochimica *et* Biophysica Acta *859*, 266-270.

Letts, P.J., Hunt, R.C., Shirley, M.A., Pinteric, L., and Schachter, H. (1978) Late spermatocytes from immature rat testis: Isolation, electron microscopy, lectin agglutin ability and capacity for glycoprotein and sulfogalactoglycerolipid biosynthesis. Biochimica *et* Biophysica Acta *541*, 59-75.

Lewis, R.N.A.H., and McElhaney, R.N. (1990) Subgel phases of *n*-saturated diacylphosphatidylcholines: A Fourier-transform infrared spectroscopic study. Biochemistry *29*, 7946-7953.

Lewis, R.N.A.H., and McElhaney, R.N. (1993) Calorimetric and spectroscopic studies of the polymorphic phase behavior of a homologous series of *n*-saturated 1, 2-diacyl phosphatidylethanolamines. Biophysical Journal *64*, 1081-1096.

Lewis, R.N., and McElhaney, R.N. (2000) Calorimetric and spectroscopic studies of the thermotropic phase behavior of lipid bilayer model membranes composed of a homologous series of linear saturated phosphatidylserines. Biophysical Journal *79*, 2043-2055.

Lewis, R.N.A.H., Mannock, D.A., McElhaney, R.N., Wong, P.T.T., and Mantsch, H.H. (1990) Physical properties of glycosyldiacylglycerols: an infrared spectroscopic study of the gel phase polymorphism of 1, 2-di-*O*-acyl-3-*O*-(α-D-glucopyranosyl)-*sn*-glycerols. Biochemistry *29*, 8933-8943.

Lewis, R.N.A.H., McElhaney, R.N., Monck, M.A., and Cullis, P.R. (1994) Studies of highly asymmetric mixed-chain diacyl phosphatidylcholines that form mixed-interdigitated gel phases: Fourier transform infrared and $^{2}H$ NMR spectroscopic studies of hydrocarbon chain conformation and orientational order in the liquid-crystalline state. Biophysical Journal *67*, 197-207.

Leyton, L., and Saling, P. (1989) 95 kd sperm proteins bind ZP3 and serve as tyrosine kinase substrates in response to zona binding. Cell *57*, 1123-1130.

Leyton, L., LeGuen, P., Bunch, D., and Saling, P. (1992) Regulation of mouse gamete interaction by a sperm tyrosine kinase. Proceedings of the National Academy of Science USA *89*, 11692-11695.

Liang, L.F., and Dean, J. (1993) Oocyte development: molecular biology of the zona pellucida. Vitamins and Hormones *47*, 115-159.

Lin, D.S., Connor, W.E., Wolf, D.P., Neuringer, M., and Hachey, D.L. (1993) Unique lipids of primate spermatozoa: desmosterol and docosahexaenoic acid. Journal of Lipid Research *34*, 491-499.

Lindwasser, O.W., and Resh, M.D. (2002) Myristoylation as a target for inhibiting HIV assembly: unsaturated fatty acids block viral budding. Proceedings of the National Academy of Science USA *99*, 13037-13042.

Lingwood, C.A. (1981) Localization of sulfatoxygalactosylacylalkylglycerol at the surface of rat testicular germinal cells by immunocytochemical techniques: pH dependence of a nonimmunological reaction between immunoglobulin and germinal cells. Journal of Cell Biology *89*, 621-630.

Lingwood, C.A., Hay, G., and Schachter, H. (1981) Tissue distribution of sulfolipids in the rat. Restricted location of sulfatoxygalactosylacylalkylglycerol. Canadian Journal of Biochemistry *59*, 556-563.

Lingwood, C.A. (1985a) Protein-glycolipid interactions during spermatogenesis. Binding of specific germ cell proteins to sulfatoxygalactosylacylalkylglycerol, the major glycolipid of mammalian male germ cells. Canadian Journal of Biochemistry and Cell Biology *63*, 1077-1085.

Lingwood, C.A. (1985b) Timing of sulfogalactolipid biosynthesis in the rat testis studied by tissue autoradiography. Journal of Cell Science *75*, 329-338.

Lingwood, C.A. (1986) Colocalization of sulfogalactosylacylalkylglycerol (SGG) and its binding protein during spermatogenesis and sperm maturation. Topology of SGG defines

a new testicular germ cell membrane domain. Biochemistry and Cell Biology *64*, 984-992.

Lingwood, C.A., Murray, R.K., and Schachter, H. (1980) The preparation of rabbit antiserum specific for mammalian testicular sulfogalactoglycerolipid. Journal of Immunology *124*, 769-774.

Lingwood, C., Schramayr, S., and Quinn, P. (1990) Male germ cell specific sulfo-galactoglycerolipid is recognized and degraded by mycoplasmas associated with male infertility. Journal of Cell Physiology *142*, 170-176.

Lingwood, C.A., and Nutikka, A. (1991) Studies on the spermatogenic sulfogalactolipid binding protein SLIP1. Journal of Cell Physiology *146*, 258-263.

Lisanti, M.P., Caras, I.W., Davitz, M.A., and Rodriguez-Boulan, E. (1989) A glycophospholipid membrane anchor acts as an apical targeting signal in polarized epithelial cells. Journal of Cell Biology *109*, 2145-2156.

London, E., and Brown, D.A. (2000) Insolubility of lipids in Triton X-100: physical origin and relationship to sphingolipid/cholesterol membrane domains (rafts) Biochimica *et* Biophysica Acta *1508*, 182-195.

Lu, Q., and Shur, B.D. (1997) Sperm from α1,4-galactosyltransferase-null mice are refractory to ZP3-induced acrosome reactions and penetrate the zona pellucida poorly. Development *124*, 4121-4131.

Lukatela, G., Krauss, N., Theis, K., Selmer, T., Gieselmann, V., von Figura, K., and Saenger, W. (1998) Crystal structure of human arylsulfatase A: the aldehyde function and the metal ion at the active site suggest a novel mechanism for sulfate ester hydrolysis. Biochemistry *37*, 3654-3664.

Luria, A., Vegelyte-Avery, V., Stith, B., Tsvetkova, N.M., Wolkers, W.F., Crowe, J.H., Tablin, F., and Nuccitelli, R. (2002) Detergent-free domain isolated from *Xenopus* egg plasma membrane with properties similar to those of detergent-resistant membranes. Biochemistry *41*, 13189-13197.

Maehashi, E., Sato, C., Ohta, K., Harada, Y., Matsuda, T., Hirohashi, N., Lennarz, W.J., and Kitajima, K. (2003) Identification of the sea urchin 350-kDa sperm-binding protein as a new sialic acid-binding lectin that belongs to the heat shock protein 110 family: implication of its binding to gangliosides in sperm lipid rafts in fertilization. Journal of Biological Chemistry *278*, 42050-42057.

McMullen, T.P., Wong, B.C., Tham, E.L., Lewis, R.N., and McElhaney, R.N. (1996) Differential scanning calorimetric study of the interaction of cholesterol with the major lipids of the Acholeplasma laidlawii B membrane. Biochemistry *35*, 16789-16798.

Mahfoud, R., Garmy, N., Maresca, M., Yahi, N., Puigserver, A., and Fantini, J. (2002) Identification of a common sphingolipid-binding domain in Alzheimer, prion, and HIV-1 proteins. Journal of Biological Chemistry *277*, 11292-11296.

Mannock, D.A., McElhaney, R.N., Harper, P.E., and Gruner, S.M. (1994) Differential scanning calorimetry and x-ray diffraction studies of the thermotropic phase behavior of the diastereomeric di-tetradecyl-α-D-galactosyl glycerols and their mixtures. Biophysical Journal *66*, 734-740.

Mantsch, H.H., Cameron, D.G., Tremblay, P., and Kates, M. (1982) Phosphatidyl-sulfocholine bilayers: An infrared spectroscopic characterization of the polymorphic phase behaviour. Biochimica *et* Biophysica Acta *689*, 63-72.

Mantsch, H.H., and McElhaney, R.N. (1991) Phospholipid phase transitions in model and biological membranes as studied by infrared spectroscopy. Chemistry and Physics of Lipids *57*, 213-226.

Marsh, D. (1991) General features of phospholipid phase transitions. Chemistry and Physics of Lipids *57*, 109-120.

Mason, J.T., Huang, C., and Biltonen, R.L. (1981) Calorimetric investigations of saturated mixed chain phosphatidylcholine bilayer dispersions. Biochemistry *20*, 6086-6092.

Matas, C., Coy, P., Romar, R., Marco, M., Gadea, J., and Ruiz, S. (2003) Effect of sperm preparation method on in vitro fertilization in pigs. Reproduction *125*, 133-141.

Mayer, L.D., Hope, M.J., Cullis, P.R., Janoff, A.S. (1985) Solute distributions and trapping efficiencies observed in freeze-thawed multilamellar vesicles. Biochimica *et* Biophysica Acta *817*, 193-196.

Mayor, S., and Maxfield, F.R. (1995) Insolubility and redistribution of GPI-anchored proteins at the cell surface after detergent treatment. Molecular Biology of the Cell *6*, 929-944.

McConville, M.J., and Ferguson, M.A. (1993) The structure, biosynthesis and function of glycosylated phosphatidylinositols in the parasitic protozoa and higher eukaryotes. Biochemical Journal *294 (Pt 2)*, 305-324.

McMullen, T.P.W., Lewis, R.N.A.H., and McElhaney, R.N. (1994) Comparative differential scanning calorimetric and FTIR and $^{31}$P-NMR spectroscopic studies of the effects of cholesterol and androstenol on the thermotropic phase behavior and organization of phosphatidylcholine bilayers. Biophysical Journal *66*, 741-752.

McMullen, T.P.W., Lewis, R.N.A.H., and McElhaney, R.N. (1999) Calorimetric and spectroscopic studies of the effects of cholesterol on the thermotropic phase behavior and organization of a homologous series of linear saturated phosphatidylethanolamine bilayers. Biochimica *et* Biophysica Acta *1416*, 119-134.

McMullen, T.P.W., Lewis, R.N.A.H., and McElhaney, R.N. (2000) Differential scanning calorimetric and Fourer transform infrared spectroscopic studies of the effects of cholesterol on the thermotropic phase behavior and organization of a homologous series of linear saturated phosphatidylserine bilayer membranes. Biophysical Journal *79*, 2056-2065.

Meizel, S. (1997) Amino acid neurotransmitter receptor/chloride channels of mammalian sperm and the acrosome reaction. Biology of Reproduction *56*, 569-574.

Melendrez, C.S., Meizel, S., and Berger, T. (1994) Comparison of the ability of progesterone and heat solubilized porcine zona pellucida to initiate the porcine sperm acrosome reaction in vitro. Molecular Reproduction and Development *39*, 433-438.

Menikh, A., Nyholm, P.G., and Boggs, J.M. (1997) Characterization of the interaction of $Ca^{2+}$ with hydroxy and non-hydroxy fatty acid species of cerebroside sulfate by Fourier transform spectroscopy and molecular modeling. Biochemistry *36*, 3438-3447.

Miller, D.J., Macek, M.B., and Shur, B.D. (1992a) Complementarity between sperm surface α-1,4-galactosyltransferase and egg-coat ZP3 mediates sperm-egg binding. Nature *357*, 589-593.

Miller, D., Brough, S., and Harbi, O. (1992b) Characterization and cellular distribution of human spermatozoal heat shock proteins. Human Reproduction *7*, 637-645.

Moffatt, D.J., Kauppinen, J.K., Cameron, D.G., Mantsch, H.H., and Jones, R.N. (1986) Computer programs for infrared spectrophotometry. N. R. C. C. Bulletin *18*, 23.

Moffett, S., Brown, D.A., and Linder, M.E. (2000) Lipid-dependent targeting of G proteins into rafts. Journal of Biological Chemistry *275*, 2191-2198.

Morell, P., and Radin, N.S. (1969) Synthesis of cerebroside by brain from uridine diphosphate galactose and ceramide containing hydroxy fatty acid. Biochemistry *8*, 506-512.

Moreno, R.D., Bustamante, E., Schatten, G., and Barros, C. (2002) Inhibition of mouse in vitro fertilization by an antibody against a unique 18-amino acid domain in the polysulfate-binding domain of proacrosin/acrosin. Fertility and Sterility *77*, 812-817.

Mori, T., Guo, M.W., Sato, E., Baba, T., Takasaki, S., and Mori, E. (2000) Molecular and immunological approaches to mammalian fertilization. Journal of Reproductive Immunology *47*, 139-158.

Moss, S.B., and Gerton, G.L. (2001) A-kinase anchor proteins in endocrine systems and reproduction. Trends in Endocrinology and Metabolism *12*, 434-440.

Muller, E., Giehl, A., Schwarzmann, G., Sandhoff, K., and Blume, A. (1996) Oriented 1,2-dimyristoyl-*sn*-glycero-3-phosphorylcholine/ganglioside membranes: a Fourier transform infrared attenuated total reflection spectroscopic study. Band assignments;

orientational, hydrational, and phase behavior, and effects of $Ca^{2+}$ binding. Biophysical Journal *71*, 1400-1421.

Murase, T., and Roldan, E.R. (1996) Progesterone and the zona pellucida activate different transducing pathways in the sequence of events leading to diacylglycerol generation during mouse sperm acrosomal exocytosis. Biochemical Journal *320 (Pt 3)*, 1017-1023.

Murray, R.K., and Narasimhan, R. (1990) Glycoglycerolipids of animal tissues. In Glycolipids, Phosphoglycolipids, and Sulfoglycolipids, M.Kates, ed. (New York: Plenum Press), pp. 321-361.

Myles, D.G., and Primakoff, P. (1997) Why did the sperm cross the cumulus? To get to the oocyte. Functions of the sperm surface proteins PH-20 and fertilin in arriving at, and fusing with, the egg. Biology of Reproduction *56*, 320-327.

Naaby-Hansen, S., Wolkowicz, M.J., Klotz, K., Bush, L.A., Westbrook, V.A., Shibahara, H., Shetty, J., Coonrod, S.A., Reddi, P.P., Shannon, J., Kinter, M., Sherman, N.E., Fox, J., Flickinger, C.J., and Herr, J.C. (2001) Co-localization of the inositol 1,4,5-trisphosphate receptor and calreticulin in the equatorial segment and in membrane bounded vesicles in the cytoplasmic droplet of human spermatozoa. Molecular Human Reproduction *7*, 923-933.

Naaby-Hansen, S., Mandal, A., Wolkowicz, M.J., Sen, B., Westbrook, V.A., Shetty, J., Coonrod, S.A., Klotz, K.L., Kim, Y.H., Bush, L.A., Flickinger, C.J., and Herr, J.C. (2002) CABYR, a novel calcium-binding tyrosine phosphorylation-regulated fibrous sheath protein involved in capacitation. Developmental Biology *242*, 236-254.

Nabet, A., Boggs, J.M., and Pézolet, M. (1996) Study by infrared spectroscopy of the interdigitation of C26:0 cerebroside sulfate into phosphatidyl choline bilayers. Biochemistry *35*, 6674-6683.

Nakamura, K., and Handa, S. (1984) Coomassie brilliant blue staining of lipids on thin-layer plates. Analytical Biochemistry *142*, 406-410.

Nakano, M., and Yonezawa, N. (2001) Localization of sperm ligand carbohydrate chains in pig zona pellucida glycoproteins. Cells Tissues Organs *168*, 65-75.

Nichols, B.J., Kenworthy, A.K., Polishchuk, R.S., Lodge, R., Roberts, T.H., Hirschberg, K., Phair, R.D., and Lippincott-Schwartz, J. (2001) Rapid cycling of lipid raft markers between the cell surface and Golgi complex. Journal of Cell Biology *153*, 529-541.

Nikolopoulou, M., Soucek, D., and Vary, J. (1985) Changes in the lipid content of boar sperm plasma membranes during epididymal maturation. Biochimica *et* Biophysica Acta *815*, 486-498.

Nishimura, H., Cho, C., Branciforte, D.R., Myles, D.G., and Primakoff, P. (2001) Analysis of loss of adhesive function in sperm lacking cyritestin or fertilin α. Developmental Biology *233*, 204-213.

Noguchi, S., Hatanaka, Y., Tobita, T., and Nakano, M. (1992) Structural analysis of the N-linked carbohydrate chains of the 55-kDa glycoprotein family (PZP3) from porcine zona pellucida. Europian Journal of Biochemistry *204*, 1089-1100.

Norton, W.T., and Cammer, W. (1984) Isolation and characterization of myelin. In Myelin, P.Morell, ed. (New York: Plenum Press), pp. 147-195.

Nyholm, P., Pascher, I., and Sundell, S. (1990) The effect of hydrogen bonds on the conformation of glycosphingolipids. Methylated and unmethylated cerebroside studied by X-ray single crystal analysis and model calculations. Chemistry and Physics of Lipids *52*, 1-10.

O'Brien, J.S. and Rouser, G. (1964) The fatty acid composition of brain sphingolipids: sphingmyelin, ceramide, cerebroside, and cerebroside sulfate. Journal of Lipid Research *5*, 339-342.

O'Toole, C.M., Roldan, E.R., and Fraser, L.R. (1996) Protein kinase C activation during progesterone-stimulated acrosomal exocytosis in human spermatozoa. Molecular Human Reproduction *2*, 921-927.

Oehninger, S. (2001) Molecular basis of human sperm-zona pellucida interaction. Cells Tissues Organs *168*, 58-64.

Ohler, B., Revenko, I., and Husted, C. (2001) Atomic force microscopy of nonhydroxy galactocerebroside nanotubes and their self-assembly at the air-water interface, with applications to myelin. Journal of Structural Biology *133*, 1-9.

Ohta, K., Sato, C., Matsuda, T., Norohashi, N., Lennarz, W.J., and Kitajima, K. (1999a) Egg receptor for sperm binds to gangliosides in the low-density detergent-insoluble membrane (LD-DIM) domain of the sperm surface. Possible involvement of the LD-DIM in sperm-egg binding coupled with signal transduction during fertilization. Glycoconj. J. *16*, S63.

Ohta, K., Sato, C., Matsuda, T., Toriyama, M., Lennarz, W., and Kitajima, K. (1999b) Isolation and characterization of low density detergent-insoluble membrane (LD-DIM) fraction from sea urchin sperm. Biochemical and Biophysical Research Communications *258*, 616-623.

Ohta, K., Sato, C., Matsuda, T., Toriyama, M., Vacquier, V.D., Lennarz, W.J., and Kitajima, K. (2000) Colocalization of receptor and transducer proteins in the glycosphingolipid-enriched, low density, detergent-insoluble membrane fraction of sea urchin sperm. Glycoconj. J. *17*, 205-214.

Ollero, M., Powers, R.D., and Alvarez, J.G. (2000) Variation of docosahexaenoic acid content in subsets of human spermatozoa at different stages of maturation: implications for sperm lipoperoxidative damage. Molecular Reproduction and Development *55*, 326-334.

Ono, A., and Freed, E.O. (2001) Plasma membrane rafts play a critical role in HIV-1 assembly and release. Proceedings of the National Academy of Science USA *98*, 13925-13930.

Ostermeyer, A.G., Beckrich, B.T., Ivarson, K.A., Grove, K.E., and Brown, D.A. (1999) Glycosphingolipids are not essential for formation of detergent-resistant membrane rafts in melanoma cells. Journal of Biological Chemistry *274*, 34459-34466.

Pancake, S.J., Holt, G.D., Mellouk, S., and Hoffman, S.L. (1993) Malaria sporozoites and circumsporozoite protein bind sulfated glycans: carbohydrate binding properties predicted from sequence homologies with other lectins. Parasitologia *35*, 77-80.

Parks, J.E., and Lynch, D.V. (1992) Lipid composition and thermotropic phase behavior of boar, bull, stallion, and rooster sperm membranes. Cryobiology *29*, 255-266.

Pascher, I. (1976) Molecular arrangements in sphingolipids conformation and hydrogen bonding of ceramide and their implication on membrane stability and permeability. Biochimica *et* Biophysica Acta *455*, 433-451.

Pascher, I., and Sundell, S. (1977) Molecular arrangements in sphingolipids. The crystal structure of cerebroside. Chemistry and Physics of Lipids *20*, 175-191.

Patrat, C., Serres, C., and Jouannet, P. (2000) The acrosome reaction in human spermatozoa. Biology of the Cell *92*, 255-266.

Pernber, Z., Molander-Melin, M., Berthold, C.H., Hansson, E., and Fredman, P. (2002) Expression of the myelin and oligodendrocyte progenitor marker sulfatide in neurons and astrocytes of adult rat brain. Journal of Neuroscience Research *69*, 86-93.

Pierini, L., and Maxfield, F.R. (2001) Flotillas of lipid rafts fore and aft. Proceedings of the National Academy of Science USA *98*, 9471-9473.

Pike L.J. (2003) Lipid rafts: bringing order to chaos. Journal of Lipid Resesearch *44*, 655-667.

Piomboni, P., and Baccetti, B. (2000) Spermatozoon as a vehicle for HIV-1 and other viruses: a review. Molecular Reproduction and Development *56 Suppl. 2*, 238-242.

Poulos, A., Darin-Bennett, A., and White, I.G. (1973) The phospholipid-bound fatty acids and aldehydes of mammalian spermatozoa. Comparative Biochemistry and Physiology *46*, 541-549.

Pralle, A., Keller, P., Florin, E.L., Simons, K., and Horber, J.K.H. (2000) Sphingolipid-cholesterol rafts diffuse as small entities in the plasma membrane of mammalian cells. Journal of Cell Biology *148*, 997-1007.

Prasad, S.V., Skinner, S.M., Carino, C., Wang, N., Cartwright, J., and Dunbar, B.S. (2000) Structure and function of the proteins of the mammalian zona pellucida. Cells Tissues Organs *166*, 148-164.

Primakoff, P., and Myles, D.G. (2002) Penetration, adhesion, and fusion in mammalian sperm-egg interaction. Science *296*, 2183-2185.

Prinetti, A., Iwabuchi, K., and Hakomori, S. (1999) Glycosphingolipid-enriched signaling domain in mouse neuroblastoma Neuro2a cells. Mechanism of ganglioside-dependent neuritogenesis. Journal of Biological Chemistry *274*, 20916-20924.

Pursel, V.G., and Johnson, L.A. (1975) Freezing of boar spermatozoa: fertilizing capacity with concentrated semen and a new thawing procedure. Journal of Animal Science *40*, 99-102.

Reed, R.A., and Shipley, G.G. (1987) Structure and metastability of *N*-lignoceryl-galactosylsphingosine (cerebroside) bilayers. Biochimica *et* Biophysica Acta *896*, 153-164.

Reed, R.A., and Shipley, G.G. (1989) Effect of chain unsaturation on the structure and thermotropic properties of galactocerebrosides. Biophysical Journal *55*, 281-292.

Reis, O., Winter, R., and Zerda, T.W. (1996) The effect of high external pressure on DPPC-cholesterol multilamellar vesicles: a pressure-tuning Fourier-transform infrared spectroscopy study. Biochimica *et* Biophysica Acta *1279*, 5-16.

Richardson, R.T., and O'Rand, M.G. (1994) Cloning and sequencing of cDNAs for rabbit preproacrosin and a novel preproacrosin-related cDNA. Biochimica *et* Biophysica Acta *1219*, 215-218.

Richardson, R.T., Yamasaki, N., and O'Rand, M.G. (1994) Sequence of a rabbit sperm zona pellucida binding protein and localization during the acrosome reaction. Developmental Biology *165*, 688-701.

Rietveld, A., and Simons, K. (1998) The differential miscibility of lipids as the basis for the formation of functional membrane rafts. Biochimica *et* Biophysica Acta *1376*, 467-479.

Rietveld, A., Neutz, S., Simons, K., and Eaton, S. (1999) Association of sterol- and glycosylphosphatidylinositol-linked proteins with *Drosophila* raft lipid microdomains. Journal of Biological Chemistry *274*, 12049-12054.

Riffo, M.S., and Parraga, M. (1996) Study of the acrosome reaction and the fertilizing ability of hamster epididymal cauda spermatozoa treated with antibodies against

phospholipase $A_2$ and/or lysophosphatidylcholine. Journal of Experimental Zoology *275*, 459-468.

Roberts, D.D., and Ginsburg, V. (1988) Sulfated glycolipis and cell adhesion. Archives of Biochemistry and Biophysics *267*, 405-415.

Rock, P., Allietta, M., Young, J.W., Thompson, T.E., and Tillack, T.W. (1990) Organization of glycosphingolipids in phosphatidylcholine bilayers: use of antibody molecules and Fab fragments as morphologic markers. Biochemistry *29*, 8484-8490.

Rodgers, W., and Zavzavadjian, J. (2001) Glycolipid-enriched membrane domains are assembled into membrane patches by associating with the actin cytoskeleton. Experimental Cell Research *267*, 173-183.

Roldan, E.R., and Vazquez, J.M. (1996) Bicarbonate/$C0_2$ induces rapid activation of phospholipase A2 and renders boar spermatozoa capable of undergoing acrosomal exocytosis in response to progesterone. Federation of European Biochemical Societies Letters *396*, 227-232.

Roldan, E.R.S., Murase, T., and Shi, Q. (1994) Exocytosis in spermatozoa in response to progesterone and zona pellucida. Science *266*, 1578-1581.

Rouquette-Jazdanian, A.K., Pelassy, C., Breittmayer, J.P., Cousin, J.L., and Aussel, C. (2002) Metabolic labelling of membrane microdomains/rafts in Jurkat cells indicates the presence of glycerophospholipids implicated in signal transduction by the CD3 T-cell receptor. Biochemical Journal *363*, 645-655.

Ruknudin, A. (1989) Cytochemical study of intracellular calcium in hamster spermatozoa during the acrosome reaction. Gamete Research *22*, 375-384.

Ruocco, M.J., Atkinson, D., Small, D.M., Skarjune, R.P., Oldfield, E., and Shipley, G.G. (1981) X-ray diffraction and calorimetric study of anhydrous and hydrated *N*-palmitoylgalactosylsphingosine (cerebroside). Biochemistry *20*, 5957-5966.

Ruocco, M.J., and Shipley, G.G. (1986) Thermal and structural behavior of natural cerebroside 3-sulfate in bilayer membranes. Biochimica *et* Biophysica Acta *859*, 246-256.

Sacco, A.G., Yurewicz, E.C., Subramanian, M.G., and Matzat, P.D. (1989) Porcine zona pellucida: association of sperm receptor activity with the α-glycoprotein component of the $M_r$ 55,000 family. Biology of Reproduction *41*, 523-532.

Sakac, D., Zachos, M., and Lingwood, C.A. (1992) Purification of the testicular galactolipid: 3'-phosphoadenosine 5'-phosphosulfate sulfotransferase. Journal of Biological Chemistry *267*, 1655-1659.

Saling, P.M., Wolf, D.P., and Storey, B.T. (1978) Calcium-dependent binding of mouse epididymal spermatozoa to the zona pellucida. Developmental Biology *65*, 515-525.

Sankaram, M.B., and Thompson, T.E. (1990) Interaction of cholesterol with various glycerophospholipids and sphingomyelin. Biochemistry *29*, 10670-10675.

Sankaram, M.B., and Thompson, T.E. (1991) Cholesterol-induced fluid-phase immiscibility in membranes. Proceedings of the National Academy of Science USA *88*, 8686-8690.

Sato, K., Iwasaki, T., Ogawa, K., Konishi, M., Tokmakov, A.A., and Fukami, Y. (2002) Low-density detergent-insoluble membrane of *Xenopus* eggs: subcellular microdomain for tyrosine kinase signaling in fertilization. Development *129*, 885-896.

Saxena, K., Duclos, R.I., Zimmermann, P., Schmidt, R.R., and Shipley, G.G. (1999) Structure and properties of totally synthetic galacto- and gluco-cerebrosides. Journal of Lipid Research *40*, 839-849.

Schierau, A., Dietz, F., Lange, H., Schestag, F., Parastar, A., and Gieselmann, V. (1999) Interaction of arylsulfatase A with UDP-*N*-acetylglucosamine:lysosomal enzyme-*N*-acetylglucosamine-1-phosphotransferase. Journal of Biological Chemistry *274*, 3651-3658.

Schlegel, A., and Lisanti, M.P. (2001) The caveolin triad: caveolae biogenesis, cholesterol trafficking, and signal transduction. Cytokine Growth Factor Reviews *12*, 41-51.

Schroeder, R., London, E., and Brown, D. (1994) Interactions between saturated acyl chains confer detergent resistance on lipids and glycosylphosphatidylinositol (GPI)-anchored proteins: GPI-anchored proteins in liposomes and cells show similar behavior. Proceedings of the National Academy of Science USA *91*, 12130-12134.

Schroeder, R.J., Ahmed, S.N., Zhu, Y., London, E., and Brown, D.A. (1998) Cholesterol and sphingolipid enhance the Triton X-100 insolubility of glycosylphosphatidylinositol-anchored proteins by promoting the formation of detergent-insoluble ordered membrane domains. Journal of Biological Chemistry *273*, 1150-1157.

Schutz, G.J., Kada, G., Pastushenko, V., and Schindler, H. (2000) Properties of lipid microdomains in a muscle cell membrane visualized by single molecule microscopy. Europian Molecular Biology Organization Journal. *19*, 892-901.

Sen, A., Williams, W.P., and Quinn, P.J. (1981) The structure and thermotropic properties of pure 1,2-diacylgalactosylglycerols in aqueous systems. Biochimica *et* Biophysica Acta *663*, 380-389.

Sen, A., Hui, S.W., Mannock, D.A., Lewis, R.N.A.H., and McElhaney, R.N. (1990) Physical properties of glycosyldiacylglycerols. 2. X-ray diffraction studies of a homologous series of 1,2-di-*O*-acyl-3-*O*-(α-D-glucopyranosyl)-*sn*-glycerols. Biochemistry *29*, 7799-7804.

Shah, J., Atienza, J.M., Duclos, R.I., Rawlings, A.V., Dong, Z., and Shipley, G.G. (1995) Structural and thermotropic properties of synthetic C16:0 (palmitoyl) ceramide: effect of hydration. Journal of Lipid Research *36*, 1936-1944.

Shao, X., Tarnasky, H.A., Schalles, U., Oko, R., and van der Hoorn, F.A. (1997) Interactional cloning of the 84-kDa major outer dense fiber protein Odf84. Leucine zippers mediate associations of Odf84 and Odf27. Journal of Biological Chemistry *272*, 6105-6113.

Sharpe, R.M. (1994) Regulation of spermatogenesis. In The Physiology of Reproduction, E.Knobil, ed. (New York: Raven Press Ltd.), pp. 1363-1434.

Sheets, E.D., Lee, G.M., Simson, R., and Jacobson, K. (1997) Transient confinement of a glycosylphosphatidylinositol-anchored protein in the plasma membrane. Biochemistry *36*, 12449-12458.

Shi, Q.X. and Roldan, E.R. (1995) Bicarbonate/$CO_2$ is not required for zona pellucida- or progesterone-induced acrosomal exocytosis of mouse spermatozoa but is essential for capacitation. Biology of Reproduction *52*, 540-546.

Shimada, T., Kato, H., Maeda, H., and Iwanaga, S. (1985) Interaction of factor XII, high-molecular-weight (HMW) kininogen and prekallikrein with sulfatide: analysis by fluorescence polarization. Journal of Biochemistry *97*, 1637-1644.

Shinitzky, M. (1984) Physiology of Membrane Fluidity. (Boca Raton, Florida: CRC Press, Inc.).

Shirley, M.A., and Schachter, H. (1980) Enrichment of sulfogalactosylalkylacylglycerol in a plasma membrane fraction from adult rat testis. Canadian Journal of Biochemistry *58*, 1230-1239.

Shur, B.D., Evans, S., and Lu, Q. (1998) Cell surface galactosyltransferase: current issues. Glycoconjugate Journal *15*, 537-548.

Silvius, J.R. (1992) Cholesterol modulation of lipid intermixing in phospholipid and glycosphingolipid mixtures. Evaluation using fluorescent lipid probes and brominated lipid quenchers. Biochemistry *31*, 3398-3408.

Silvius, J.R. (2003) Role of cholesterol in lipid raft formation: lessons from lipid model systems. Biochimica *et* Biophysica Acta *1610*, 174-183.

Silvius, J.R., del Giudice, D., and Lafleur, M. (1996) Cholesterol at different bilayer concentrations can promote or antagonize lateral segregation of phospholipids of differing acyl chain length. Biochemistry *35*, 15198-15208.

Simons, K., and Ikonen, E. (1997) Functional rafts in cell membranes. Nature *387*, 569-572.

Simons, K., and Toomre, D. (2000) Lipid rafts and signal transduction. Nature Reviews Molecular Cell Biology *1*, 31-39.

Simons, K., and van Meer, G. (1988) Lipid sorting in epithelial cells. Biochemistry *1988*, 27.

Singer, S.J., and Nicolson, G.L. (1972) The fluid mosaic model of the structure of cell membranes. Science *175*, 720-731.

Smart, E.J., Graf, G.A., McNiven, M.A., Sessa, W.C., Engelman, J.A., Scherer, P.E., Okamoto, T., and Lisanti, M.P. (1999) Caveolins, liquid-ordered domains, and signal transduction. Molecular and Cellular Biology *19*, 7289-7304.

Spiegel, S., Kassis, S., Wilchek, M., and Fishman, P.H. (1984) Direct visualization of redistribution and capping of fluorescent gangliosides on lymphocytes. Journal of Cell Biology *99*, 1575-1581.

Spiegel, S., Blumenthal, R., Fishman, P.H., and Handler, J.S. (1985) Gangliosides do not move from apical to basolateral plasma membrane in cultured epithelial cells. Biochimica *et* Biophysica Acta *821*, 310-318.

Stein, R.S., and Sutherland, G.B.B.M. (1953) Interaction of methylene deformation frequencies of paraffin crystals. Journal of Chemistry and Physics *21*, 370-371.

Stein, R.S., and Sutherland, G.B.B.M. (1954) Effect of intermolecular interactions between CH frequencies on the infrared spectra of N-paraffins and polythene. Journal of Chemistry and Physics *22*, 1993-1999.

Stevenson, C.C., Rich, N.H., and Boggs, J.M. (1992) Raman spectroscopic study of semisynthetic species of cerebroside sulfate: two types of hydrocarbon chain interdigitation. Biochemistry *31*, 1875-1881.

Stulnig, T.M., Huber, J., Leitinger, N., Imre, E.M., Angelisova, P., Nowotny, P., and Waldhausl, W. (2001) Polyunsaturated eicosapentaenoic acid displaces proteins from membrane rafts by altering raft lipid composition. Journal of Biological Chemistry *276*, 37335-37340.

Suarez, S., Varosi, S.M., and Dai, X. (1993) Intracellular calcium increases with hyperactivation intact, moving hamster sperm and oscillates with the flagellar beat cycle. Cell Biology *90*, 4660-4664.

Suarez, S.S. (1996) Hyperactivated motility in sperm. Journal of Andrology *17*, 331-335.

Suarez, S.S., and Ho, H.C. (2003) Hyperactivation of mammalian sperm. Cellular and Molecular Biology *49*, 351-356.

Subczynski, W.K., and Kusumi, A. (2003) Dynamics of raft molecules in the cell and artificial membranes: approaches by pulse EPR spin labeling and single molecule optical microscopy. Biochimica *et* Biophysica Acta *1610*, 231-243.

Sugkraroek, P., Kates, M., Leader, A., and Tanphaichitr, N. (1991) Levels of cholesterol and phospholipids in freshly ejaculated sperm and Percoll-gradient-pelletted sperm from fertile and unexplained infertile men. Fertility and Sterility *55*, 820-827.

Suzuki, A., Ishizuka, I., Ueta, N., and Yamakawa, T. (1973). Isolation and characterization of seminolipd (1-*O*-Alkyl-2-*O*-Acyl-3-[3'-sulfogalactosyl] glycerol) from guinea pig testis and incorporation of $^{35}$S-sulfate into seminolipid in sliced testis. Japan Journal of Experimental Medicine *43*, 435-442.

Suzuki, Y., Toda, Y., Tamatani, T., Watanabe, T., Suzuki, T., Nakao, T., Murase, K., Kiso, M., Hasegawa, A., Tadano-Aritomi, K., Ishizuka, I., and Miyasaka, M. (1993) Sulfated glycolipids are ligands for a lymphocyte homing receptor, L-selectin (LECAM-1), binding epitope in sulfated sugar chain. Biochemical and Biophysical Research Communications *190*, 426-434.

Suzuki, K., Sanematsu, F., Fujiwara, T., Edidin, M., and Kusumi, A. (2001) A GPI-anchored membrane protein, CD59, frequently visits/forms rafts in signaling: a single molecule study. Biophysical Journal *80*, 252a.

Svennerholm, L., and Stallberg-Stenhagen, S. (1968) Changes in the fatty acid composition of cerebrosides and sulfatides of human nervous tissue with age. Journal of Lipid Research *9*, 215-225.

Takasaki, S., Mori, E., and Mori, T. (1999) Structures of sugar chains included in mammalian zona pellucida glycoproteins and their potential roles in sperm-egg interaction. Biochimica *et* Biophysica Acta *1473*, 206-215.

Talbot, P., Shur, B.D., and Myles, D.G. (2003) Cell adhesion and fertilization: steps in oocyte transport, sperm-zona pellucida interactions, and sperm-egg fusion. Biology of Reproduction *68*, 1-9.

Tanphaichitr, N., Millette, C.F., Agulnick, A., and Fitzgerald, L.M. (1988) Egg-penetration ability and structural properties of human sperm prepared by Percoll-gradient centrifugation. Gamete Research *20*, 67-81.

Tanphaichitr, N., Smith, J., and Kates, M. (1990) Levels of sulfogalactosylglycerolipid in capacitated motile and immotile mouse sperm. Biochemistry and Cell Biology *68*, 528-535.

Tanphaichitr, N., Smith, J., Mongkolsirikieart, S., Gradil, C., and Lingwood, C. (1993) Role of a gamete specific sulfoglycolipid-immobilizing protein on mouse sperm-egg binding. Developmental Biology *156*, 164-175.

Tanphaichitr, N., Zheng, Y., Kates, M., Abdullah, N., and Chan, A. (1996) Cholesterol and phospholipid levels of washed and Percoll-gradient centrifuged mouse sperm: Presence of lipids possessing inhibitory effects on sperm motility. Molecular Reproduction and Development *43*, 187-195.

Tanphaichitr, N., Moase, C., Taylor, T., Surewicz, K., Hansen, C., Namking, M., Bérubé, B., Kamolvarin, N., Lingwood, C.A., Sullivan, R., Rattanachaiyanont, M., and White, D. (1998a) Isolation of antiSLIP1-reactive boar sperm P68/62 and its binding to mammalian zona pellucida. Molecular Reproduction and Development *49*, 203-216.

Tanphaichitr, N., Taylor, T., White, D., Rattanachaiyanont, M., and Moase, C. (1998b) Arylsulfatase-A is a component of boar sperm SLIP1 (P68) and may be involved in sperm-zona pellucida binding. Biology of Reproduction *58 Suppl.*, 158a.

Tanphaichitr, N., White, D., Taylor, T., Attar, M., Rattanachaiyanont, M., and Kates, M. (1999) Role of male germ-cell specific sulfogalactosylglycerolipid (SGG) and its binding protein, SLIP1, in mammalian sperm-egg interaction. In The Male Gamete: From Basic Knowledge to Clinical Applications, C.Gagnon, ed. (Vienna, IL: Cache Press), pp. 227-235.

Tanphaichitr, N., Haebe, J., Leader, A., Carmona, E., Harris, J.D., da Silva, S.M., Antunes, T.T., Chakrabandhu, K., and Léveillé, M.C. (2003a) Towards a more precise assay of sperm function in egg binding. Journal of Obstetrics and Gynaecology Canada *25*, 461-470.

Tanphaichitr, N., Bou Khalil, M., Weerachatyanukul, W., Kates, M., Xu, H., Carmona, E., Attar, M., and Carrier, D. (2003b) Physiological and biophysical properties of male germ cell sulfogalactosylglycerolipid. In Lipid Metabolism and Male Fertility, S.De Vriese, ed. (Champaign, IL: AOCS Press).

Tantibhedhyangkul, J., Weerachatyanukul, W., Carmona, E., Xu, H., Anupriwan, A., Michaud, D., and Tanphaichitr, N. (2002) Role of sperm sufrace arylsulfatase A in mouse sperm-zona pellucida binding. Biology of Reproduction *67*, 212-219.

Tardif, S., Dubé, C., Chevalier, S., and Bailey, J.L. (2001) Capacitation is associated with tyrosine phosphorylation and tyrosine kinase-like activity of pig sperm proteins. Biology of Reproduction *65*, 784-792.

Tardif, S., Dubé, C., and Bailey, J.L. (2003) Porcine sperm capacitation and tyrosine kinase activity are dependent on bicarbonate and calcium but protein tyrosine phosphorylation is only associated with calcium. Biology of Reproduction *68*, 207-213.

Tate, M.W., Eikenberry, E.F., Turner, D.C., Shyamsunder, E., and Gruner, S.M. (1991) Nonbilayer phases of membrane lipids. Chemistry and Physics of Lipids *57*, 147-164.

Thaler, C.D., and Cardullo, R.A. (1996) The initial interaction between mouse sperm and the zona pellucida is a complex binding event. Journal of Biological Chemistry *271*, 23289-23297.

Thompson, T.E., and Tillack, T.W. (1985) Organization of glycosphingolipids in bilayers and plasma membranes of mammalian cells. Annual Review of Biophysics and Biophysical Chemistry *14*, 361-386.

Towbin, H., and Gordon, J. (1984) Immunoblotting and dot immunobinding-current status and outlook. Journal of Immunological Methods *72*, 313-340.

Travis, A.J., Merdiushev, T., Vargas, L.A., Jones, B.H., Purdon, M.A., Nipper, R.W., and Galatioto, J. (2001) Expression and localizaiton of caveolin-1, and the presence of membrane rafts, in mouse and Guinea pig spermatozoa. Developmental Biology *240*, 599-610.

Trevino, C.L., Serrano, C., Beltran, C., Felix, R., and Darszon, A. (2001) Identification of mouse trp homologs and lipid rafts from spermatogenic cells and sperm. Federation of European Biochemical Societies Letters *509*, 119-125.

Tsuji, Y., Fukuda, H., Iuchi, A., Ishizuka, I., and Isojima, S. (1992) Sperm immobilizing antibodies react to the 3-O-sulfated galactose residue of seminolipid on human sperm. Journal of Reproductive Immunology *22*, 225-236.

Tulsiani, D.R.P., Abou-Hailaa, A., Loeser, C.R., and Pereira, B.M.J. (1998) The biological and functional significance of the sperm acrosome and acrosomal enzymes in mammalian fertilization. Experimental Cell Research *240*, 151-164.

Tulsiani, D.R.P., and Abou-Haila, A. (2001) Mammalian sperm molecules that are potentially important in interaction with female genital tract and egg vestments. Zygote *9*, 51-69.

Tupper, S., Wong, P.T.T., and Tanphaichitr, N. (1992) Binding of $Ca^{2+}$ to sulfogalactosylceramide and the sequential effects on the lipid dynamics. Biochemistry *31*, 11902-11907.

Tupper, S., Wong, P.T.T., Kates, M., and Tanphaichitr, N. (1994) Interaction of divalent cations with germ cell specific sulfogalactosylglycerolipid and the effects on lipid chain dynamics. Biochemistry *33*, 13250-13258.

Umemura, J., Cameron, D.G., and Mantsch, H.H. (1980) A Fourier-transform infrared spectroscopic study of the molecular interaction of cholesterol with 1,2-dipalmitoyl-*sn*-glycero-3-phosphocholine. Biochimica *et* Biophysica Acta *602*, 32-44.

Valensin, S., Paccani, S.R., Ulivieri, C., Mercati, D., Pacini, S., Patrussi, L., Hirst, T., Lupetti, P., and Baldari, C.T. (2002) F-actin dynamics control segregation of the TCR signaling cascade to clustered lipid rafts. Europian Journal of Immunology *32*, 435-446.

van der Goot, F.G., and Harder, T. (2001) Raft membrane domains: from a liquid-ordered membrane phase to a site of pathogen attack. Seminars in Immunology *13*, 89-97.

Van Duin, M., Polman, J.E.M., De Breet, I.T.M., Van Ginneken, K., Bunschoten, H., Grootenhuis, A., Brindle, J., and Aitken, R.J. (1994) Recombinant human zona pellucida protein ZP3 produced by chinese hamster ovary cells induces the human sperm acrosome reaction and promotes sperm-egg fusion. Biology of Reproduction *51*, 607-617.

van Meer, G., and Simons, K. (1982) Viruses budding from either the apical or the basolateral plasma membrane domain of MDCK cells have unique phospholipid compositions. Europian Molecular Biology Organization Journal *1*, 847-852.

van Meer, G. and Simons, K. (1986) The function of tight junctions in maintaining differences in lipid composition between the apical and the basolateral cell surface domains of MDCK cells. Europian Molecular Biology Organization Journal *5*, 1455-1464.

van Meer, G., Stelzer, E.H.K., Wijnaendts-van-Resandt, R.W., and Simons, K. (1987) Sorting of sphingolipids in epithelial (Mardin-Darby canine kidney) cells. Journal of Cell Biology *105*, 1623-1635.

van Meer, G. (1989) Lipid traffic in animal cells. Annual Review of Cell Biology *5*, 247-275.

van Meer, G. (2000) Cellular organelles: how lipids get there, and back. Trends in Cell Biology *10*, 550-552.

van Meer, G., and Lisman, Q. (2002) Sphingolipid transport: rafts and translocators. Journal of Biological Chemistry *277*, 25855-25858.

Varma, R., and Mayor, S. (1998) GPI-anchored proteins are organized in submicron domains at the cell surface. Nature *394*, 798-801.

Visconti, P.E. and Kopf, G.S. (1998) Regulation of protein phosphorylation during sperm capacitation. Biology of Reproduction *59*, 1-6.

Visconti, P.E., Bailey, J.L., Moore, G.D., Pan, D., Olds-Clarke, P., and Kopf, G.S. (1995a) Capacitation of mouse spermatozoa. I. Correlation between the capacitation state and protein tyrosine phosphorylation. Development *121*, 1129-1137.

Visconti, P.E., Moore, G.D., Bailey, J.L., Leclerc, P., Connors, S.A., Pan, D., Olds-Clarke, P., and Kopf, G.S. (1995b) Capacitation of mouse spermatozoa. II. Protein tyrosine phosphorylation and capacitation are regulated by a cAMP-dependent pathway. Development *121*, 1139-1150.

Visconti, P.E., Johnson, L.R., Oyaski, M., Fornes, M., Moss, S.B., Gerton, G.L., and Kopf, G.S. (1997) Regulation, localization, and anchoring of protein kinase A subunits during mouse sperm capacitation. Developmental Biology *192*, 351-363.

Visconti, P.E., Galantino-Homer, H., Ning, X., Moore, G.D., Valenzuela, J.P., Jorgez, C.J., Alvarez, J.G., and Kopf, G.S. (1999a) Cholesterol efflux-mediated signal

transduction in mammalian sperm. beta-cyclodextrins initiate transmembrane signaling leading to an increase in protein tyrosine phosphorylation and capacitation. Journal of Biological Chemistry *274*, 3235-3242.

Visconti, P.E., Ning, X., Fornes, M.W., Alvarez, J.G., Stein, P., Connors, S.A., and Kopf, G.S. (1999b) Cholesterol efflux-mediated signal transductin in mammalian sperm: cholesterol release signals an increase in protein tyrosine phosphorylation during mouse sperm capacitation. Developmental Biology *214*, 429-443.

Visconti, P.E., Westbrook, V.A., Chertihin, O., Demarco, I., Sleight, S., and Diekman, A.B. (2002) Novel signaling pathways involved in sperm acquisition of fertilizing capacity. Journal of Reproduction and Immunology *53*, 133-150.

Vist, M.R., and Davis, J.H. (1990) Phase equilibiria of cholesterol/dipalmitoyl-phosphatidylcholine mixtures: nuclear magnetic resonance and differential scanning calorimetry. Biochemistry *29*, 451-464.

Vos, J.P., Lopes-Cardozo, M.G., and Gadella, B.M. (1994) Metabolic and functional aspects of sulfogalactolipids. Biochimica *et* Biophysica Acta *1211*, 125-149.

Walensky, L.D., and Snyder, S.H. (1995) Inositol 1,4,5-triphosphate receptors selectively localized to the acrosomes of mammalian sperm. Journal of Cell Biology *130*, 857-869.

Wang, T.Y, and Silvius, J.R. (2000) Different sphingolipids show differential partitioning into sphingolipid/cholesterol-rich domains in lipid bilayers. Biophysical Journal *79*, 1478-1489.

Wang, T.Y., Leventis, R., and Silvius, J.R. (2000) Fluorescence-based evaluation of the partitioning of lipids and lipidated peptides into liquid-ordered lipid microdomains: a model for molecular partitioning into "lipid rafts". Biophysical Journal *79*, 919-933.

Wang, T.Y., and Silvius, J.R. (2001) Cholesterol does not induce segregation of liquid-ordered domains in bilayers modeling the inner leaflet of the plasma membrane. Biophysical Journal *81*, 2762-2773.

Wang TY, Leventis R, and Silvius, J.R. (2001) Partitioning of lipidated peptide sequences into liquid-ordered lipid domains in model and biological membranes. Biochemistry *40*, 13031-13040.

Ward, C., and Kopf, G. (1993) Molecular events mediating sperm activation. Developmental Biology *158*, 9-34.

Wassarman, P. (1988) Zona pellucida glycoproteins. Annual Review of Biochemistry *57*, 415-442.

Wassarman, P.M. (1999) Mammalian fertilization: molecular aspects of gamete adhesion, exocytosis, and fusion. Cell *96*, 175-183.

Wassarman, P.M. and Litscher, E.S. (2001) Towards the molecular basis of sperm and egg interaction during mammalian fertilization. Cells Tissues Organs *168*, 36-45.

Weerachatyanukul, W., Rattanachaiyanont, M., Carmona, E., Furimsky, A., Mai, A., Shoushtarian, A., Sirichotiyakul, S., Ballakier, H., Leader, A., and Tanphaichitr, N. (2001) Sulfogalactosylglycerolipid is involved in human gamete interaction. Molecular Reproduction and Development *60(4)*, 569-578.

Weerachatyanukul, W., Xu, H., Anupriwan, A., Carmona, E., Wade, M., Hermo, L., da Silva, S.M., Rippstein, P., Sobhon, P., Sretarugsa, P., and Tanphaichitr, N. (2003) Acquisition of arylsulfatase A (AS-A) onto the mouse sperm surface during epididymal transit. Biology of Reproduction (*provisionally accepted*).

White, D., Weerachatyanukul, W., Gadella, B., Kamolvarin, N., Attar, M., and Tanphaichitr, N. (2000) Role of sperm sulfogalactosylglycerolipid in mouse sperm-zona pellucida binding. Biology of Reproduction *63*, 147-155.

Wolf, D., Hagopian, S., and Ishijima, S. (1986) Changes in sperm plasma membrane lipid diffusibility after hyperactivation during in vitro capacitation in the mouse. Journal of Cell Biology *102*, 1372-1377.

Wolf, D.E., Maynard, V.M., McKinnon, C.A., and Melchior, D.L. (1990) Lipid domains in the ram sperm plasma membrane demonstrated by differential scanning calorimetry. Proceedings of the National Academy of Science USA *87*, 6893-6896.

Wolf, A.A., Fujinaga, Y., and Lencer, W.I. (2002) Uncoupling of the cholera toxin-$GM_1$ ganglioside receptor complex from endocytosis, retrograde Golgi trafficking, and downstream signal transduction by depletion of membrane cholesterol. Journal of Biological Chemistry *277*, 16249-16256.

Wong, P.T.T. and Mantsch, H.H. (1988) High-pressure infrared spectroscopic evidence of water binding sites in 1,2-diacylphospholipids. Chemistry and Physics of Lipids *46*, 213-224.

Wong, P.T.T., Siminovitch, D.J., and Mantsch, H.H. (1988) Structure and properties of model membranes: New knowledge from high-pressure vibrational spectroscopy. Biochimica *et* Biophysica Acta *947*, 139-171.

Wong, P.T.T. (1994) Pressure induced correlation field splitting if vibrational modes: Structural and dynamic properties in lipid bilayers and biomembranes. Biophysical Journal *66*, 1505-1514.

Xu, X., and London, E. (2000) The effect of sterol structure on membrane lipid domains reveals how cholesterol can induce lipid domain formation. Biochemistry *39*, 843-849.

Xu, X., Bittman, R., Duportail, G., Heissler, D., Vilcheze, C., and London, E. (2001) Effect of the structure of natural sterols and sphingolipids on the formation of ordered sphingolipid/sterol domains (rafts). Journal of Biological Chemistry *276*, 33540-33546.

Yamaji, A., Sekizawa, Y., Emoto, K., Sakuraba, H., Inoue, K., Kobayashi, H., and Umeda, M. (1998) Lysenin, a novel sphingomyelin-specific binding protein. Journal of Biological Chemistry *273*, 5300-5306.

Yamamura, S., Handa, K., and Hakomori, S.I. (1997) A close association of $GM_3$ with c-Src and Rho in $GM_3$-enriched microdomains at the B16 melanoma cell surface membrane: a preliminary note. Biochemical and Biophysical Research Communications *236*, 218-222.

Yanagimachi, R. (1994) Mammalian fertilization. In The Physiology of Reproduction, E.Knobil, ed. (New York: Raven Press Ltd.), pp. 189-317.

Yancey, P.G., Rodrigueza, W.V., Kilsdonk, E.P., Stoudt, G.W., Johnson, W.J., Phillips, M.C., and Rothblat, G.H. (1996) Cellular cholesterol efflux mediated by cyclodextrins. Demonstration Of kinetic pools and mechanism of efflux. Journal of Biological Chemistry *271*, 16026-16034.

Yonezawa, N., Aoki, H., Hatanaka, Y., and Nakano, M. (1995a) Involvement of N-linked carbohydrate chains of pig zona pellucida in sperm-egg binding. Europian Journal of Biochemistry *233*, 35-41.

Yonezawa, N., Hatanaka, Y., Takeyama, H., and Nakano, M. (1995b) Binding of pig sperm receptor in the zona pellucida to the boar sperm acrosome. Journal of Reproduction and Fertility *103*, 1-8.

Yoshinaga, K. and Toshimori, K. (2003) Organization and modifications of sperm acrosomal molecules during spermatogenesis and epididymal maturation. Microscopy Research and Technique *61*, 39-45.

Yu, S., Kojima, N., Hakomori, S.I., Kudo, S., Inoue, S., and Inoue, Y. (2002) Binding of rainbow trout sperm to egg is mediated by strong carbohydrate-to-carbohydrate interaction between (KDN)$GM_3$ (deaminated neuraminyl ganglioside) and $Gg_3$-like epitope. Proceedings of the National Academy of Science USA *99*, 2854-2859.

Yuan, Y.Y., Chen, W.Y., Shi, Q.X., Mao, L.Z., Yu, S.Q., Fang, X., and Roldan, E.R. (2003) Zona pellucida induces activation of phospholipase $A_2$ during acrosomal exocytosis in Guinea pig spermatozoa. Biology of Reproduction *68*, 904-913.

Yurewicz, E.C., Sacco, A.G., and Subramanian, M.G. (1987) Structural characterization of the $M_r$ 55,000 antigen (ZP3) of porcine oocyte zona pellucida. Journal of Biological Chemistry *262*, 564-571.

Yurewicz, E.C., Pack, B.A., and Sacco, A.G. (1991) Isolation, composition, and biological activity of sugar chains of porcine oocyte zona pellucida 55K glycoproteins. Molecular Reproduction and Development *30*, 126-134.

Yurewicz, E.C., Pack, B.A., Armant, D.R., and Sacco, A.G. (1993) Porcine zona pellucida ZP3α glycoprotein mediates binding of the biotin-labeled $M_r$ 55,000 family (ZP3) to boar sperm membrane vesicles. Molecular Reproduction and Development *36*, 382-389.

Yurewicz, E.C., Sacco, A.G., Gupta, S.K., Xu, N., and Gage, D.A. (1998) Hetero-oligomerization-dependent binding of pig oocyte zona pellucida glycoproteins ZPB and ZPC to boar sperm membrane vesicles. Journal of Biological Chemistry *273*, 7488-7494.

Zalata, A.A., Christophe, A.B., Depuydt, C.E., Schoonjans, F., and Comhaire, F.H. (1998) The fatty acid composition of phospholipids of spermatozoa from infertile patients. Molecular Human Reproduction *4*, 111-118.

Zalc, B., Jacque, C., Radin, N.S., and Dupouey, P. (1977) Immunogenicity of sulfatide. Immunochemistry *14*, 775-779.

Zeng, Y., Clark, E.N., and Florman, H.M. (1995) Sperm membrane potential: hyperpolarization during capacitation regulates zona pellucida-dependent acrosomal secretion. Developmental Biology *171*, 554-563.

Zhang, Y.P., Lewis, R.N.A.H., and McElhaney, R.N. (1997) Calorimetric and spectroscopic studies of the thermotropic phase behavior of the n-saturated 1,2-diacylphosphatidylglycerols. Biophysical Journal *72*, 779-793.

Zhuang, M., Oltean, D.I., Gomez, I., Pullikuth, A.K., Soberon, M., Bravo, A., and Gill, S.S. (2002) Heliothis virescens and Manduca sexta lipid rafts are involved in Cry1A toxin binding to the midgut epithelium and subsequent pore formation. Journal of Biological Chemistry *277*, 13863-13872.

# APPENDIX ONE

# FOURIER TRANSFORM INFRARED SPECTROSCOPY

## A1.1. Fourier Transform Infrared Spectroscopy

FTIR spectroscopy has been extensively used to monitor the molecular vibrations of individual structural groups of biological molecules (Wong *et al.*, 1988), and to gain insight into the biophysical properties of lipid bilayers (Tupper *et al.*, 1992; Tupper *et al.*, 1994; Nabet *et al.*, 1996; Attar *et al.*, 1998; Attar *et al.*, 2000; Bou Khalil *et al.*, 2000; McMullen *et al.*, 1994; McMullen *et al.*, 1999; McMullen *et al.*, 2000) and intact membranes and living cells (Auger *et al.*, 1987). Generally, the FTIR spectrum reflects the contribution of many structural groups, and different spectral regions have been used to probe lipid-lipid, lipid-protein and protein-protein interactions, as well as to assess the secondary structure of proteins. However, the subsequent sections will summarize the use of FTIR spectroscopy to discern the conformational and dynamic properties of membrane lipids.

### *A1.1.1. Conformational Order of Lipids*

The $CH_2$ symmetric stretching vibration of lipids provides a useful means to monitor the dynamics and molecular order of their hydrocarbon chains. The $CH_2$ symmetric (~2850 $cm^{-1}$) and anti-symmetric (~2920 $cm^{-1}$) stretching modes are sensitive to temperature. Notably, the $CH_2$ symmetric stretching band is usually monitored as a function of temperature because interference of the terminal $CH_3$ symmetric and

antisymmetric stretching vibration is minimal in this region of the spectrum (Mantsch and McElhaney, 1991). The $CH_2$ symmetric stretching band is related to the average number of *gauche* conformers in a system. Thus, when the hydrocarbon chains of lipids are in the all-*trans* conformation, i.e., in the gel phase, the methylene groups absorb at 2850 $cm^{-1}$. As temperature increases, lipids undergo a transition from the gel to the liquid-crystalline phase due to the introduction of *gauche* conformers. Consequently, the $CH_2$ symmetric stretching vibration shifts to higher absorption frequencies (Mantsch and McElhaney, 1991; Umemura *et al.*, 1980) and is broadened (Nabet *et al.*, 1996). Specifically, changes in bandwidths are related to variations in the rates of libarational motion of the hydrocarbon chains (Cameron *et al.*, 1980; Umemura *et al.*, 1980; Mantsch and McElhaney, 1991).

### *A1.1.2. Interfacial Hydrogen Bonding and Lipid-Lipid Interactions*

One of the most important properties of lipids, other than their amphiphilic nature, is their ability to interact with each other via intermolecular hydrogen bonding. At the interfacial region of the bilayer, the C=O stretching vibrations have been monitored to probe the sphingosine or glycerol-acyl chain interface (Mantsch and McElhaney, 1991). The degree of interfacial hydrogen bonding can be assessed by examining the amide I (1600-1680 $cm^{-1}$), and ester C=O (1700-1780 $cm^{-1}$) stretching modes (Kates, 1986). Wong and Mantsch (1988) showed that the frequencies of these two modes decrease proportionally with the degree of their hydrogen bonding to proton donating groups, due to the elongation of the C=O bonds. As a consequence, the amide I band of

glycosphingolipids (Nabet *et al.*, 1996; Attar *et al.*, 1998; Bou Khalil *et al.*, 2000, 2001) and the ester C=O band of SGG and phospholipids (Attar *et al.*, 2000) are used to monitor interfacial hydrogen bonding. Moreover, the patterns of the ester C=O stretching vibration are also used to assess the physical state or the polymorphic phase behavior of lipids (Lewis and McElhaney, 1993; Zhang *et al.*, 1993, 1997; McMullen *et al.*, 1994, 1999, 2000; Attar *et al.*, 2000).

### *A1.1.3. Packing of the Hydrocarbon Chains*

It has been demonstrated that the conformational disorder, orientational fluctuations, and the torsion/twisting motions of methylene chains in lipid bilayers can be ordered and dampened by external pressure (Wong, 1994). As a result, pressure tuning FTIR spectroscopy has been used to evaluate the dynamic properties of lipid bilayers. The methylene bending mode absorption band (1450-1490 $cm^{-1}$) is usually used for this purpose, since it is sensitive to structural differences in hydrocarbon chain packing (Stein and Sutherland, 1953, 1954). As pressure increases, interactions, which are normally weak at ambient pressure, increase in magnitude and become detectable in the spectrum. The applied pressure reorients the hydrocarbon chains and reduces the number of *gauche* conformers along the acyl chains, which results in increased order, and thus increased intermolecular interactions (Reis *et al.*, 1996). Increasing pressure also induces correlation field splitting of the $CH_2$ bending frequency, and the pressure at which this splitting is initially observed is directly related to membrane fluidity (Wong *et al.*, 1988; Wong, 1994).

### *A1.1.4. Interaction of Sulfoglycolipids and Phospholipids with Cations*

Infrared bands characteristic of the sulfate group of sulfoglycolipids and the phosphate group of phospholipids, occur between 1000 and 1300 $cm^{-1}$ (Kates, 1986). The frequency of the asymmetric phosphate stretching vibration varies between 1200 and 1270 $cm^{-1}$, depending on the hydrogen bonding strength. These infrared bands exhibit a complex profile in this region, which is attributable to contributions from many vibrations, including the C-N, C-O and C-C stretching modes, as well as the $CH_2$ twisting and wagging modes (Casal and Mantsch, 1984). This spectroscopic region has been studied in $H_2O$ instead of $^2H_2O$ to avoid interference from the bending mode of deuterated water near 1200 $cm^{-1}$. The sulfate band of SGG and SGC (Tupper *et al.*, 1992, 1994), and the phosphate band of phospholipids (Muller *et al.*, 1996; Bou Khalil *et al.*, 2000) have been used to study their interaction with divalent cations of biological significance.

Lipid bilayers of controled composition have been extensively used to gain insight into biological membranes. The application of spectroscopic techniques, including FTIR spectroscopy, to lipid bilayers continues to be essential to elucidate the physico-chemical interactions, which give rise to the unique and diverse properties of biological membranes.

# APPENDIX TWO

## ZONAE PELLUCIDAE SULFOGLYCOPROTEINS

### A2.1. Isolation of Pig Ovary ZP

Pig ZP was kindly provided by Dr. T. Berger (University of California, Davis, CA, USA). Briefly, the follicles of frozen pig ovaries were ruptured using an apparatus consisting of two wheels of ganged razor blades submerged in isolation buffer (10 mM sodium phosphate, pH 7.4, 125 mM sodium chloride, 3 mM sodium citrate, 2 mM EDTA, 3 mM sodium azide). ZP-intact oocytes were separated from debris by multiple sievings through nylon screens of different mesh sizes, as previously described. Subsequently, the oocytes were gently homogenized in a Potter-Elvehjem homogenizer using the isolation buffer described above. The ZP was collected on a 41 μm screen, extensively washed with the isolation buffer, and briefly rinsed with deionized water to remover excess buffer salts, lyophilized, and stored at -20°C (Hedrick and Wardrip, 1986).

Pig ZP3 (55 kDa, consisting of ZP3α and ZP3β), and partially deglycosylated ZP3α (46 kDa) and ZP3β (42 kDa) were produced as previously described (Yurewicz *et al.*, 1998), and kindly provided by Dr. E. Yurewicz (Wayne State University, Detroit, MI). Briefly, ZP3α and ZP3β were separated by reverse phase high performance liquid chromatography (HPLC) following pretreatment with endo-*β*-galactosidase. The ZP3β glycoprotein ($M_r$ 41,000 following endo-*β*-galactosidase digestion) elutes first and appears homogeneous on SDS gels. The ZP3α glycoprotein ($M_r$ 44,000 following endo-*β*-galactosidase digestion) follows and contains 5-10% of ZP3β contaminant (Yurewicz

*et al.*, 1987). ZP3α was purified by size exclusion chromatography to produce a preparation depleted of residual ZP3β. Five subfractions of ZP3α were collected from the column, and concentrated by ultrafiltration. The protein composition of the pooled fractions was examined by SDS-PAGE and immunoblotting. Coomassie blue staining revealed the purified ZP3α sulfoglycoprotein as a predominant (>95%) 44 kDa band (Yurewicz *et al.*, 1998).